Use Of Magnetic Resonance Imaging In Radical Prostate Radiotherapy

A thesis submitted to The University of Manchester for the degree of Doctor of Medicine in the Faculty of Biology Medicine and Health

Andrew J. McPartlin

2016

School of Medical Sciences

Contents

List of figures

List of tables

Glossary

AATH	Adiabatic Approximated to Tissue Homogeneity
ADC	Apparent Diffusion Co-efficient
AIF	Arterial Input Function
AJCC	American Joint Committee on Cancer
AUC	Area Under the Curve
BED	Biological Equivalent Dose
BF	Biochemical Failure
BFS	Biochemical Failure Free Survival
BPH	Benign Prostatic Hypertrophy
CRT	Conformal Radiotherapy
CRUK	Cancer Research UK
CTCAE	Common Terminology Criteria for Adverse Events
CTV	Clinical Tumour Volume
DCE	Dynamic Contrast Enhancement
DE-EBRT	Dose Escalated External Beam Radiotherapy
DIL	Dominant Intra-Prostatic Lesion
DR	Deformable Registration
DRE	Digital Rectal Exam
DSS	Disease Specific Survival
DWI	Diffusion weighted Imaging
EBRT	External Beam Radiotherapy
EQD2	Equivalent Dose in two Gray per fraction
ERC	Endo-Rectal Coil
ESTRO	European Society for Therapeutic Radiology and Oncology
ESUR	European Society of Urogenital Radiology
FEM	Finite Element Methods
FSH	Follicle Stimulating Hormone
GI	Gastro-Intestinal
GS	Gleason Score
GTV	Gross Tumour Volume
GU	Genito-Urinary
Gy	Gray
HDR	High Dose Rate
HR	High Risk
HT	Hormone Therapy
IB-EBRT	Integrated Boost External Beam Radiotherapy
IJCC	International Union for Cancer Control
IMRT	Intensity Modulated Radiotherapy
IR	Intermediate Risk
ISMRM	International Society for Magnetic Resonance in Medicine
kV	Kilo voltage
LDR	Low Dose Rate
LH	Luteinising Hormone
LHRH	Luteinising Hormone Releasing Hormone
LINAC	Linear Accelerator
MP-MRI	Multi-Parametric Magnetic Resonance Imaging

MRS	Magnetic Resonance Spectroscopy
MU	Monitor Units
NA-HT	Neo-adjuvant Hormone Therapy
NTCP	Normal Tissue Complication Probability
OAR	Organs At Risk
PDW	Proton Density Weighted
PET-CT	Positron Emission Tomography CT
PFS	Progression Free Survival
PIRADS	Prostate Imaging, Reporting and Data System
PSA	Prostate Specific Antigen
PSA-DT	Prostate Specific Antigen Doubling Time
PTV	Planning Target Volume
PZ	Peripheral Zone
RF	Radio Frequency
RP	Radical Prostatectomy
RT	Radiotherapy
RTOG	Radiation Therapy Oncology Group
T	Tesla
T1W	T1 Weighted
T2W	T2 Weighted
TCP	Tumour Control Probability
TE	Echo Time
TPS	Thin Plate Spines
TR	Repetition Time
TRUS	Trans-Rectal Ultra-Sound
TURP	Trans-Urethral Resection of Prostate
TZ	Transition Zone
VMAT	Volumetric Modulated Arc Therapy

Abstract

The University of Manchester
Andrew McPartlin June 2016

Use of Magnetic Resonance Imaging in Radical Prostate Radiotherapy

Purpose: To assess (1) the potential benefit that MRI may bring to prostate radiotherapy planning and delivery; (2) a method of improving registration of MRI and CT imaging to aid the RT planning workflow; (3) the role of in-bore MRI guided biopsy in informing management; (4) dosimetric outcome and toxicity of an integrated High Dose Rate (HDR-B) or Volumetric Modulated Arc Therapy (VMAT-IB) boost to the area of dominant disease within the prostate; (5) whether a predictive response can be identified measuring changes in Diffusion Weighted Imaging (DWI) and Dynamic Contrast Enhancement (DCE) during prostate RT after neo-adjuvant HT (NA-HT); (6) the necessity of hormone therapy (HT) with dose escalated radiotherapy (DE-RT) for intermediate risk prostate cancer.

Methods: (1) Perform a systematic review of literature pertaining to MRI and image guided radiotherapy; (2) compare registration accuracy, based on displacement of fiducial markers or degree of overlap of segmented prostate measured by Dice Similarity Coefficient (DSC), of MRI and CT for 14 patients after conventional operator driven visual matching and then an additional registration step using interstitial points identified on high quality volumetric CT (HQVCT); (3) assess the predictive power of in-bore MRI guided biopsy of areas with suspicious appearance on multi-parametric MRI by comparing biopsy accuracy to histological findings and repeat biopsy results for 42 PIRADS 4-5 lesions in 31 men; (4) analyse patients treated in a prospective study receiving standard radiotherapy to the prostate plus a HDR-B (20 patients) or VMAT-IB (26) to a total dose of 250 Gy BED to assess acute and late toxicity and dosimetric variation between the two methods; (5) prospectively recruit 15 patient who have received NA-HT and perform DWI and DCE before, during and after completion of radiotherapy to look for significant changes in values in normal and malignant tissue which may predict for ultimate outcome; (6) Assess clinical outcome for patients receiving 75.6 – 78 Gy +/- bicalutamide.

Results: (1) The review has quantified uncertainties in treatment delivery and the degree that the addition of MRI may mitigate this; (2) point based registration of CT and MRI imaging after visual registration achieved a significant reduction in fiducial marker displacement and a significant increase in DSC; (3) seven lesions targeted by in-bore MR guided biopsy had non-significant or negative results, most with biopsy needle deflected to the target periphery with four confirmed false negative on repeat biopsy; (4) with a median follow up of 12 months acute and late toxicity was similar after either treatment with HDR-B delivering a significantly higher dose to a proportion of the gross tumour volume (GTV) but with significantly lower minimum dose to the planned target volume (PTV); (5) tumour DWI values during RT after NA-HT were not found to significantly alter, DCE was found to vary significantly during treatment and initial changes correlated with changes in DWI; (6) the addition of bicalutamide did not significantly improve biochemical control or overall survival.

Conclusions: (1) Routine use of MRI will to improve radiotherapy planning and delivery; (2) repeat point based registration using interstitial points has the potential to improve visual CT and MRI registration; (3) an in-bore MRI guided biopsy has little value in informing a decision to offer focal therapy to an MRI identified PIRADS 4-5 lesion due to its high false negative rate; (4) with limited follow up HDR-B and VMAT-IB appear safe methods of focal dose escalation although with significant dosimetric variations;(5) early changes in DWI and DCE during RT after NA-HT appear to correlate, longer follow up will assess their prognostic value; (6) A benefit of HT combined with DE-RT was not shown in this study.

Declaration

No portion of the work referred to in this thesis has been submitted in support of an application for another degree or qualification of this of any other university of other institute of learning.

Copyright Statement

Choice of Alternative Format

This thesis is the product of various projects assessing the use of MR imaging in various aspects of radical prostate radiotherapy. Each project, although related through an over-arching theme, stands as an independent piece of research. The studies have all been performed with the intention of ultimately being published in peer reviewed journals, so that the results contained may inform the practice of the uro-oncology community.

As a consequence the thesis is submitted in alternate format. Each project is written up as a separate chapter in the style of a scientific article. Some chapters have been accepted for publication at the time of submission; others are in the editorial process or will be submitted in near future. Additional information on previous work related to choice of methodology which would not usually be contained within a published work is contained in the relevant section of the introduction

The conclusions from the projects described in Chapters 2- 6 are then drawn together in Chapter 7: *Discussion* with a summary of their implications and the future work that might arise. In chapter 8:Appendix A a supplementary piece of work reporting on the efficacy of hormone therapy with dose escalated radiotherapy in intermediate risk prostate cancer is reported, which has implications for MRI techniques described in chapter 6.

Chapter 1: Introduction

1.1 Prostate Cancer

1.1.1 *Introduction*

Prostate cancer is the second most common cancer in men worldwide and is responsible for around a quarter of a million deaths a year (Jemal et al., 2011). It was the most common cancer, excluding superficial skin cancers, in the UK in 2011, with 41736 new diagnoses and 10793 deaths from the disease (CRUK, 2016). Although often perceived as indolent in nature, it is one of the commonest causes of cancer related death amongst men albeit usually following a long disease course. Of those diagnosed with the disease in the UK 81.4% were living five years after diagnosis in the period 2005-2009. The incidence of the disease, within the UK and globally, has substantially increased over the recent past.in part as a result of an aging population and due to asymptomatic detection through screening prostate specific antigen (PSA) tests and trans-urethral resection of prostate (TURP) tissue to treat benign prostatic hypertrophy (Bray et al., 2010). As a result the challenge of treatment of this disease is increasing, with significant public health and financial implications (Zou et al., 2004).

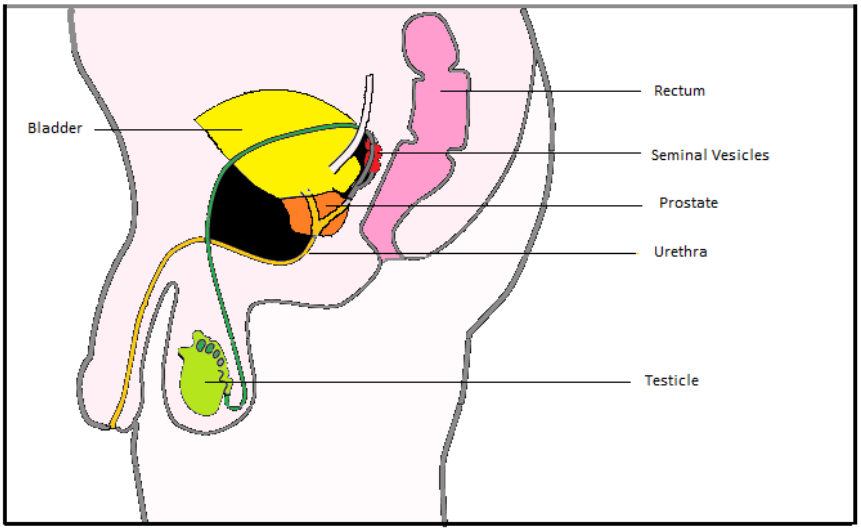

Figure 1-1: Gross anatomy of the pelvis

1.1.2 *Anatomy*

The prostate is a gland situated beneath the bladder, surrounding the exiting urethra (Figure 1-1). It is the largest accessory gland in the human body and typically weighs between 20-40 grams with average dimensions of 3 x 4 x 2 cm. It is comprised of around 70% glandular and 30% fibromuscular tissue. Drainage from prostate, vas deferens and seminal vesicles occurs into the prostatic urethra and makes up the constituents of semen. It has the gross appearance of an inverted pyramid with the base of the gland superior and apex its inferior surface. It is connected to

the pubic bone by the pubo-prostate ligaments and rests on the levator-ani fascia. The prostate is surrounded by a true capsule, consisting of a thin layer of connective tissue at the periphery of the gland and a pseudo-capsule of fibrous tissue which fuses with the levator fascia. At the 5 and 7 'o clock position when viewed coronally, neurovascular bundles travel and innervate the prostate at apex and base (Lee et al., 2011).

The prostate can be described in anatomical and histological terms with some overlap of meaning (Figure 1-2). It divides into three histological zones:

- Peripheral: The posterolateral portion of gland, representing approximately 70% of the prostate volume, is the origin of the majority of prostate cancers. It is formed from embryological mesodermal tissue.
- Central: The cone shaped region surrounding the ejaculatory ducts. It makes up around 25% of the volume of the prostate. It is likely formed from the embryological Wolffian duct.
- Transition: Around 5% of the prostate volume, it is formed from the embryological endodermal tissue. In younger men this zone is small however it enlarges with age and compresses the central zone due to the benign process of benign prostatic hyperplasia (BPH).

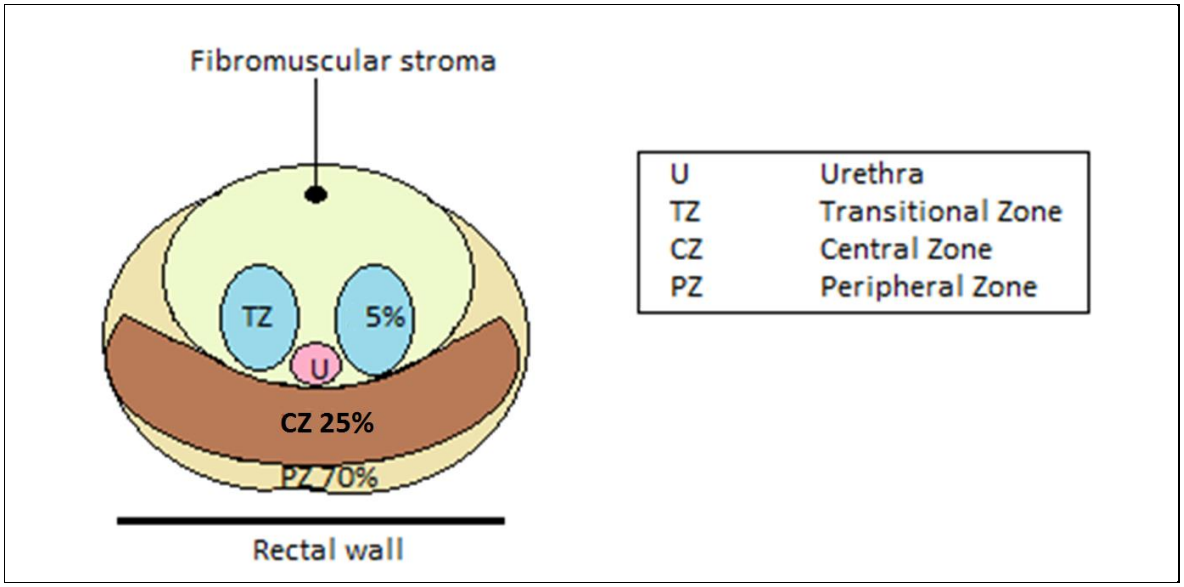

Figure 1-2: Anatomy of the prostate gland with approximate percentage of disease occurring within each zone

The prostate can also further be described anatomically in lobes:

- Anterior lobe: The gland lying in front of urethra, it is comprised entirely of fibromuscular tissue and is devoid of any glandular structures.
- Median lobe: The cone shaped portion of gland situated between the two ejaculatory ducts and the urethra.
- Lateral lobes: This is made up of left and right lobes which form the main mass of the gland and are continuous posteriorly.

- Posterior lobe: This is an occasionally used term for the posterior-medial aspect of the lateral lobes. It is palpated on rectal exam.

1.1.3 *Epidemiology*

Despite the prevalence of prostate cancer and significant research into its aetiology and treatments there is still much that is unknown about its pathogenesis. There is little UK wide geographic variation in the incidence of prostate cancer but marked alterations between ethnic groups. Within the UK age-standardised incidence per 100000 is between 121-248 for black males, 96-100 for white males and 29-61 for Asian males (CRUK. and UK, 2009). This is similar to data from the United Stated showing an incidence per 100000 of 228.5 for black males and 144.9 for white males (Saman et al., 2014). Regardless of ethnic group prostate cancer is predominantly a disease of the elderly with incidence rising sharply over the age of 50 (Figure 1-3) (CRUK, 2016). Autopsy studies have shown this incidence continues to increase as men age, with identified evidence of occult disease in around three quarters of men over the age of 80 (Haas et al., 2008).

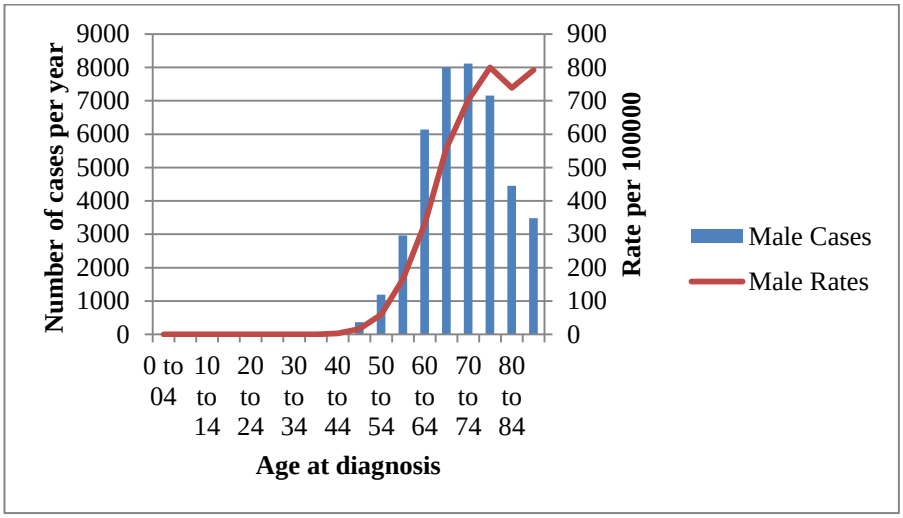

Figure 1-3: Prevalence and incidence of prostate cancer by age in United Kingdom 2011-2013(Cancer Research UK figures)

1.1.4 *Diagnosis*

Prostate cancer is in general a slow growing, indolent disease. It may be present for many years before local symptoms of obstruction of urinary flow due to disease, mass effect or local invasion occur. Diagnosis is complicated by the prevalence of benign prostatic hypertrophy in the aging male population which will cause symptoms of urinary frequency, urgency, nocturia and hesitancy that maybe indistinguishable from those caused by an enlarging tumour. As disease progresses sufferers may complain of pain due to mass effect from an enlarging tumour, local invasion of other structures or bone pain from metastatic disease.

The historical diagnosis of prostate cancer was made via a suggestive clinical history and subsequent digital rectal exam (DRE) of the prostate to identify nodules or increased hardness followed by biopsy to confirm diagnosis. Only disease of sufficient volume, and in the correct anatomical location to be palpable was likely be diagnosed. Diagnosis was transformed by the

discovery of PSA in the 1980's. PSA is a peptidase secreted by epithelial cells of the prostate gland, playing a role in liquefying semen. Its serum levels are increased in the presence of prostate cancer and other benign prostatic conditions such as prostatitis or benign prostatic hypertrophy. It also naturally rises in concentration as age increases (Oesterling et al., 1993) (Table 1-1). As such it is an imperfect test for prostate disease, with high sensitivity (it is likely to detect people with disease) but less specificity (it will identify a large number of people incorrectly who do not have the disease). More widespread use of PSA testing has resulted in stage migration at diagnosis with disease being picked up earlier and reducing incidence of advanced pathology at presentation. Two large trials, one performed in the United States and one in Europe, have generated conflicting results of its benefit as a screening tool to improve outcome for prostate cancer sufferers (Schroder et al., 2009; Andriole et al., 2009).

Table 1-1: Normal PSA level by age

	Age (years)			
	<50	**50-59**	**60-69**	**>70**
Concentration ng/ml (95^{th} centile)	2.5	3.5	4.5	6.5

Taken from (Oesterling et al., 1993)

DRE also remains a diagnostic tool although having low sensitivity and a low positive predictive value in patients with lower PSA results (Schröder et al., 1998). For patients with a positive DRE or raised PSA, unless metastatic disease is suspected, NICE guidance suggests the results are discussed with the patient, in combination with consideration of comorbidities and risk factors(NICE, 2014). After explaining the relative risks and benefits a decision is then taken whether to proceed to random trans-rectal ultrasound (TRUS) guided biopsies of the prostate to look for histological evidence of disease. This procedure generally involves placing an ultrasound probe in the rectum, allowing identification of the prostate but not routinely of small volume disease. Random core samples are then taken via the rectal wall of the prostate gland. These are assessed for evidence of malignant tissue and, if present, for the number and volume of cores containing disease and its histological appearance. The appearance is graded using the Gleason score (GS) (Table 1-2). For patients who have negative TRUS a multi-parametric MRI, discussed subsequently, should be considered to determine whether a repeat biopsy is needed (NICE, 2014).

Table 1-2: Gleason score

Gleason Score	**Microscopic appearance**
1	Resembles normal tissue
2	Larger glands with increased stroma
3	Cells have begun to invade or infiltrate surrounding tissue
4	Few recognisable glands, many cells invading surrounding tissue in clumps
5	Few/no glands, sheets of cells throughout surrounding tissue

For tissue to be considered malignant on needle biopsy it must be at least GS 3 in appearance. The primary grade is assigned to the dominant pattern, which must be greater than 50% of the total seen, and secondary grade to the next most frequent which must be >5% of the total seen.

Increasingly a tertiary component is also reported if a small component of more aggressive disease is seen. It can be reported in a number of ways such as the total score (sum of primary and secondary grades) or modified score (primary, secondary and tertiary, with overall score obtained from combining primary and tertiary) (Fine et al., 2012). The overall score for malignant disease is the sum of two scores, giving a result between 6 and 10 with increasing score representing more aggressive disease. Limitations in this scoring system have been demonstrated with variation in inter-pathologist scoring of samples, and variable correlation with post prostatectomy specimens (Nguyen et al., 2004; King and Long, 2000).

1.1.5 *Staging*

Staging of prostate cancer is performed using the TNM system developed by the American Joint Committee on Cancer (AJCC) and International Union for Cancer Control (IUCC) ((Edge, 2010)). It provides information on the extent of the primary tumour (T), involvement of lymph nodes (N) and spread of distant metastases (M) (Table 1-3). Information is obtained from clinical examination, trans-rectal ultra-sound (TRUS) guided biopsies and, when concerns are present about the likelihood of more advanced disease, cross sectional imaging.

Table 1-3: 7th edition of the TNM staging system for Prostate Cancer (2010)

Tumour	
TX	Primary tumour cannot be assessed
T0	No evidence of primary tumour
T1	Clinically in-apparent tumour (for example incidental finding at TURP)
T1a	Incidental finding in ≤5% resected tissue
T1b	Incidental finding in >5% of resected tissue
T1c	Identified by needle biopsy (i.e. for raised PSA)
T2	Tumour confined to prostate
T2a	Involves ≤half of one lobe
T2b	Involves >half of one lobe
T2c	Involves both lobes
T3	Extends through prostate capsule
T3a	Extra capsular extension
T3b	Invasion of seminal vesicle(s)
T4	Invades adjacent structures
Nodes	
NX	Regional nodes not assessed
N0	No regional lymph node metastases
N1	Metastases in regional lymph node(s)
Metastases	
M0	No distant Metastases
M1	Distant metastases
M1a	Non-regional lymph node(s)
M1b	Bone(s)
M1c	Other site(s)
PSA = Prostate specific antigen, TURP = Trans-urethral resection of prostate	

1.1.6 *Carcinogenesis*

The histological subtype of over 95% of prostate malignancy is adenocarcinoma. Rarer subtypes including transitional cell, carcino-sarcoma, basal cell carcinoma, lymphoma or small cell cancer will not be considered further here.

Prostatic adenocarcinoma falls into two separate entities; around 15% is hereditary disease usually occurring under the age of 55 and the remainder is sporadic disease occurring in more elderly patients. Genome-wide association studies have identified multiple low penetrance loci which can act summatively to increase the risk of disease (Eeles et al., 2014). This is supported by the fact that the risk of developing disease is approximately double that of the general population in those who have a previously diagnosed first degree relative (Goldgar et al., 1994). This risk is higher with multiple first degree relatives or relatives affected at an early age. A study of 44788 twin pairs suggests as much as 42% of the risk of developing disease may be inherited (Lichtenstein et al., 2000). Certain single site mutations, such as those in BRCA1 and BRCA2, have also been demonstrated to significantly increase the incidence of disease (Leongamornlert et al., 2012).

The development of sporadic disease involves various events such as dysregulation of tumour oncogenes and tumour suppressing genes but the precise molecular events involved in prostate neoplastic initiation and progression remain poorly understood. It has been suggested that exposure to certain foodstuffs such as animal fats may increase, and others such as tomatoes and soy possibly reduce, the risk of disease although evidence for this is inconclusive (Sinha et al., 2009; Zu et al., 2014). There is also good observational evidence for a contribution from as yet not fully understood environmental and lifestyle factors through analysis of variations in incidence within migrant populations (Lee et al., 2007).

1.1.7 *Prognostic factors*

The prognosis of prostate cancer differs greatly between individuals due to variable disease behaviour and metastatic risk. The number of patients diagnosed with early stage disease has increased greatly, largely due to the use of screening PSA testing. Many of these asymptomatic diagnoses would have remained otherwise undetected through the patient's lifetime. The challenge facing clinicians is to decide whether disease will ultimately affect life expectancy or become symptomatic without treatment. Management decisions need to consider the likelihood of progression to metastatic, fatal disease, within a patient's lifetime. This risk is stratified using information on the stage of disease, the PSA at presentation and the histological appearance to divide patients into prognostic categories (D'Amico et al., 1998). Further prognostication based on number of biopsy cores containing disease and the presence of >50% disease in any core may also be factored into treatment decisions (Freedland et al., 2003). In the United Kingdom stratification as outlined by the National Institute of Health and Care Excellence (NICE) is routinely used (Cancer, 2014) (Table 1-4).

Multiple pre-treatment predictive models based on these three prognostic factors have been proposed (Capitanio et al., 2010). Historically the most commonly used are Partin tables, predicting

for stage of disease, and the Kattan nomogram predicting the 5-year likelihood of biochemical relapse after radiotherapy (Eifler et al., 2013b; Kattan et al., 2000).

Table 1-4: National Institute of Health and Care Excellence prognostic classification scheme

Low risk	Intermediate risk	High Risk
T1-T2a and GS≤6 and PSA≤10	T2b-c and/or GS=7 and/or PSA >10-20	≥T3a or PSA>20 or GS 8-10
GS = Gleason score, PSA = Prostate specific antigen		

Risk stratification is combined with information on a patient's age and fitness to guide intervention. Due to imperfect stratification criteria, patients who would die with, rather than from, their disease can be over-treated and other patients with a more aggressive tumour who may be under-treated do not receive appropriate definitive therapy.

1.1.8 *Treatment*

Treatment offered is based upon initial risk stratification of disease, with differing modalities of active surveillance, radical prostatectomy, or radiotherapy with or without hormone therapy offered accordingly. The different strategies are discussed below and summarised.

1.1.8.1 Active Surveillance

Active surveillance is used in early, low risk disease to defer definitive treatment, and potential associated side-effects. Treatment is offered before disease progresses to have an unacceptable risk of dissemination. The objective is to avoid, or at least postpone treatment related complications for men whose disease may never require intervention. Active surveillance differs from "watchful waiting" in that definitive treatment is intended to be offered at some point if required, rather than palliation on symptomatic progression. There are no randomised data comparing active surveillance with immediate definitive treatment but it appears to be safe if a patient is kept on close supervision, monitoring PSA levels and repeating TRUS biopsies at 12-18 months to look for evidence of disease progression. The ongoing UK ProtecT trial has completed recruitment randomising patients between active treatment and active surveillance and, it is hoped, will report later this year (Lane et al., 2010). A previous retrospective series looking at outcome for patients treated with watchful waiting in the era before routine PSA testing found 27% of GS 6 patients, 45% of GS 7 and 66% GS 8-10 died of prostate cancer within 20 years, justifying the concern about the appropriateness of deferring treatment in more histologically aggressive disease (Albertsen et al., 2005). With earlier detection via PSA screening and active treatment when indicated the contemporary 20 year mortality for GS 6 disease is significantly lower than identified in this series. A more recent study of 993 patients with low (79%) or intermediate risk (21%) disease, followed for a median of 6.4 years, found prostate cancer specific survival of 94.3% at 15 years (Klotz et al., 2015). Of the 28 patients who developed metastasis only two did not have GS ≥7 before developing disseminated disease.

The requirement for repeated PSA checks and biopsies on active surveillance can induce a level of patient anxiety which some find intolerable. One method of deciding suitability for active

surveillance is the Epstein criteria; life expectancy less than 10-15 years, PSA density < 0.15 (PSA/prostate volume) and GS ≤6 with <3 cores containing disease and ≤50% involvement of any core (Epstein et al., 1994).

These criteria have been shown to have accuracy in contemporary series of between 76-84% at predicting low risk disease, with up to 92% having organ confined disease (Jeldres et al., 2008; Bastian et al., 2004). Further information to aid the stratification of low risk disease can be achieved through the use of axial imaging. The use of functional MRI to give information on likely disease behaviour is becoming an increasing component of decisions about a patient's suitability for active surveillance, and is discussed in detail below. NICE guidelines currently recommended that it be considered at baseline in patients being offered active surveillance(Graham et al., 2014). As a final consideration, it has also been suggested that patients with a PSA doubling time (PSHT) < 2 years may not be appropriate candidates for active surveillance whilst those with PSHT > 4 years have excellent outcomes, even when active intervention is required (Ali et al., 2007).

1.1.8.2 Radiotherapy

External beam radiotherapy (EBRT) directs high energy photon beams at malignant tissues to induce cell death and tumour shrinkage or resolution. Photons are generated within a linear accelerator (Linac) and shaped into a beam to treat precisely a target within the body (Figure 1-4). As a first step the linear accelerator uses microwaves to accelerate electrons, negatively charged sub-atomic particles, produced from an electron gun, giving them additional energy. These electrons are steered using magnets into a metal target. As the electrons decelerate by hitting other particles within the target they give off energy as photons, through the process of *bremsstrahlung* (braking radiation). These photons are targeted through the gantry of the linac towards the planned treatment site (Figure 1-5). The gantry is able to rotate through 360º and can give treatment from any position in this arc.

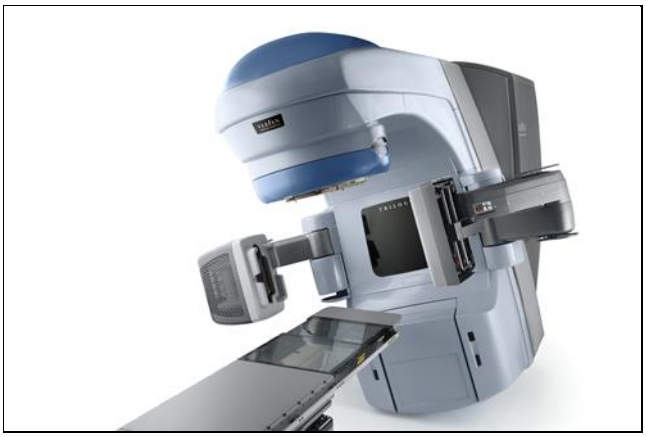

Figure 1-4: Linear Accelerator (commercial image)

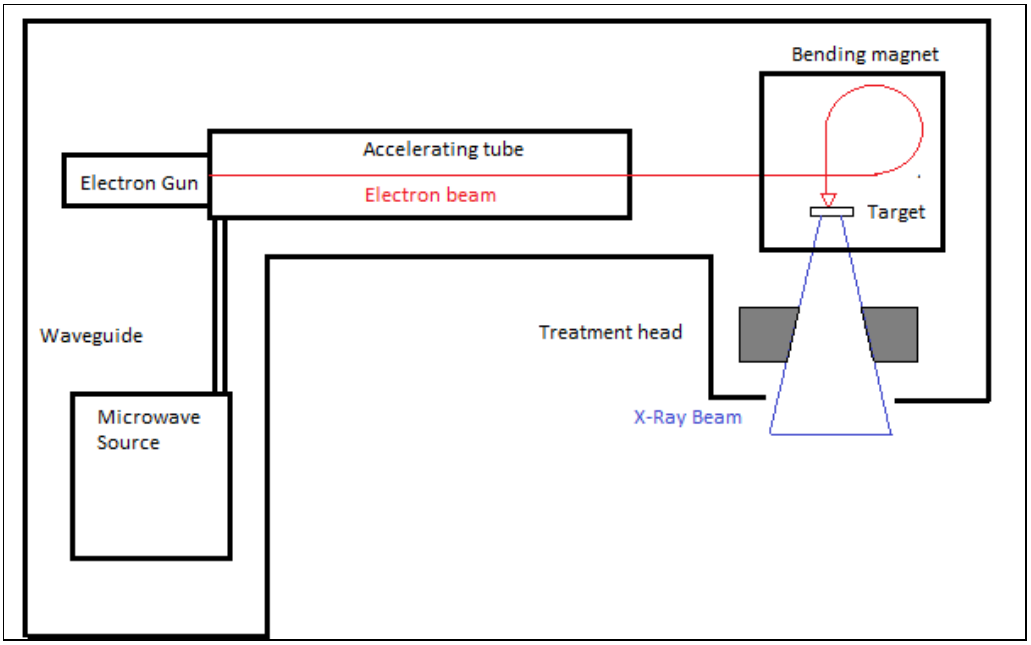

Figure 1-5: Schematic of a linac

Photons distribute their energy when they strike another structure. The probability of this happening is a product of the amount of material the photon has travelled through and the speed at which it is travelling. Photon speed is a product of its energy and therefore different energy beams have different dose/depth characteristics and distribute their energy at different depths. The effect of photons on cells is either via direct interaction with cellular DNA or, more commonly, indirectly through production of free radicals via ionisation of water molecules which then cause DNA damage. DNA is a double stranded structure and damage can occur as either single or, less commonly, double strand breaks. Unless DNA damage can be repaired a cell is likely to die by apoptosis or necrosis when it attempts to divide. Cellular mechanism for repairing single strand breaks are more efficient and therefore failed repair and cell death is more likely after a double strand break.

Malignant cells have, as a necessary part of their development, deficient repair mechanisms. As a consequence they are more sensitive to radiation damage and more likely to undergo cell death after exposure. This characteristic is exploited by radiotherapy being given in small daily treatments, termed fractions, over a number of weeks. In the time between each fraction normal tissue is able to undergo repair whilst malignant tissue is less likely to do so. In addition cells are more sensitive to radiation at various points in the cell cycle and spreading the dose increases the chances of sensitivity to treatment. Finally, as the tumour responds and shrinks the remaining diseased tissue becomes increasingly oxygenated and radiation sensitive. These benefits of fractionation are counteracted by an increased cell turnover within a tumour that begins to occur during treatment, meaning that an increasing proportion of each daily dose is required to counter the effects of this repopulation. An optimal fractionation regimen balances these opposing factors. The dose per fraction is measured in Gray (Gy), which is the amount of radiation required to distribute one joule of energy per kilogram of matter. The prescribed dose per fraction varies depending on the tumour type being treated but is usually between 1.8-3 Gy for standard

fractionation, although there is increasing experience in the use of carefully targeted higher doses per fraction, termed stereotactic body radiotherapy (SBRT).

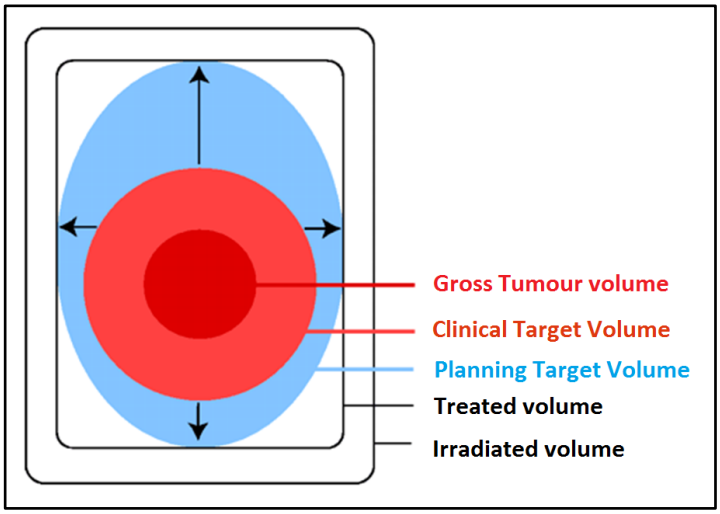

Figure 1-6: Planning volumes for radiotherapy

External beam radiotherapy (EBRT) is prescribed to a given target volume following the guidelines laid down in ICRU 50 (Chavaudra and Bridier, 2001). Within this schema the visible tumour is defined as the gross tumour volume (GTV). A margin is then applied for potential microscopic extension as a clinical target volume (CTV). Lastly, account must be taken of potential errors in positioning the patient each day for treatment and for tumour movement with a further expansion to create the planning target volume (PTV) (Figure 1-6). Because of limitations of treatment technique the volume receiving the prescribed dose may vary from the PTV and is termed the treated volume. Finally the irradiated volume is the tissue volume receiving a dose that is considered significant in relation to normal tissue tolerance.

In practice this involves manually delineating the tumour to be treated, termed contouring or segmenting, and then applying prescribed expansions to create the CTV and PTV, dependent on tumour site and location. The entire prostate gland, with or without seminal vesicle inclusion, is conventionally contoured as CTV when planning EBRT due to issues of disease identification within the gland and concerns regarding its multifocal nature. Whether to include a proportion of seminal vesicle is decided upon by risk stratification of the tumour based on PSA level, Gleeson score and stage. It has been shown that the probability of occult seminal vesicle involvement predictably increases for higher risk disease necessitating its inclusion in these patients (Eifler et al., 2013a). This is then expanded to form a PTV, dependent on local policy and ability to account for treatment uncertainties.

The use of definitive EBRT has become a standard treatment modality, given with the intent of providing a sufficient dose to kill disease within the prostate whilst minimising radiation effects on surrounding tissues. Large single centre series reported encouraging control of disease following EBRT, particularly in early stage malignancy and it became an accepted standard of care (Shipley

et al., 1999). The effectiveness of radiation was however limited by the dose which could be safely delivered to the prostate without unacceptable toxicities.

Toxicity associated with EBRT is primarily due to early and late effects on the bladder and rectum. These symptoms may include urgency, increased frequency, bleeding, diarrhoea, incontinence, erectile dysfunction and rarely more severe effects such as bowel perforation or bone damage. Some degree of long term toxicity following radiotherapy is common; for example erectile impairment is experienced by around half of men(van der Wielen et al., 2007); moderate chronic genito-urinary (GU) symptoms occur in around 15% and severe symptoms in around 3% (Zelefsky et al., 2008a); mild to moderate gastro-intestinal (GI) symptoms are experienced chronically in around 20-25% of patients and more severe symptoms in around 10%(Giordano et al., 2006; Kim et al., 2011); severe complications such as fistula formation or stricture occur in <0.5%.

Improved EBRT techniques, such as 3-D conformal radiotherapy (3-D CRT) have allowed increasingly conformal treatment with sculpting of dose distribution and sharper drop off beyond the target volume. As a consequence the dose received by nearby structures, such as bladder and rectum, is reduced. Higher doses can therefore be given to the tumour without increasing associated toxicity. The maximum tolerable prostate treatment dose using 2D-radiotherapy techniques was previously limited to around 70 Gy (Pilepich et al., 1987). The use of 3D-CRT has achieved a significant reduction in radiation induced proctitis and rectal bleeding when delivering a dose of 64 Gy to the prostate (Dearnaley et al., 1999). Subsequently a safe escalation to ≥ 74 Gy was shown to be possible in multiple trials. Improved biochemical progression free survival has been demonstrated, although this has not translated to improved overall survival in randomised studies (Table 1-5). This benefit has been shown in all risk groups but appears greatest in those with intermediate or high risk disease (Al-Mamgani et al., 2010).

Dose escalation studies show that even with these improvements in EBRT technique there is a trend towards significant increases in rectal and urinary symptoms following dose escalation. An improved toxicity profile may be seen with dose escalation using more modern and conformal Intensity Modulated Radiotherapy (IMRT) planning instead of 3D-CRT. A recent comparison of late toxicity from two Dutch studies treating to 78 Gy using IMRT or 3D-CRT found a reduction in late ≥ G2 GI, but not genito-urinary (GU), complications with the use of IMRT (Wortel et al., 2016) . The use of IMRT with optimal image guidance in selected patients appears potentially capable of keeping toxicity within traditionally accepted levels even with further dose escalation above 80 Gy; one study treating to 86.4 Gy using IMRT found ≥G2 late GU and GI toxicities of 21.1% and 4.4% (Spratt et al., 2013).

Table 1-5: Effect of dose escalated radiotherapy to the prostate

Author	Pts	Risk group	Dose	HT	Outcome	Radiotherapy/toxicity
(Kuban et al., 2008)	301	20% LR 46% IR 34% HR	70 vs 78Gy	Nil	50 vs 73% PFS (p<0.05) 78vs79% OS @ 10 years	4 field RTOG-LENT modified ≥G2 GI 13 vs 26% NS ≥G2 GU 8 vs 13% NS
(Zietman et al., 2010)	393	59% LR 37% IR 4% HR	70.2vs 79.2Gy	Nil	68 vs 85% PFS (p<0.05) 78vs83% OS @ 8.9 years	Conformal, RTOG ≥G2 GI 13 vs 24% NS ≥G2 GU 25 vs 29% NS
(Beckendorf et al., 2004)	306	72% IR 28% HR	70 vs 80Gy	Nil	68 vs 76 % PFS (p=0.09) 92 vs 92% OS @ 5 years	Conformal LENT-SOMA ≥2 GI 20 vs 27% NS ≥2 GU 17 vs 27% (p<0.05)
(Creak et al., 2013)	126	53% HR	64 vs 74Gy	3-6/12 NA/A	45vs49% PFS 56 vs 63% OS @ 13.7 years (Non-significant)	Conformal RTOG ≥G2 GI 11 vs 23% (p<0.05) ≥2 GU 11 vs 18% NS
(Heemsbergen et al., 2014)	664	18% LR 27% IR 55% HR	68 vs 78Gy	21% received up to 3 years, of these 87% HR	47 Vs 54% PFS(p<0.05) , no benefit in LR 69 vs 69% OS @ 9 years	Conformal, RTOG/EORTC ≥G2 GI 27 vs 32% NS ≥G2 GU 39 vs 41% NS
(Dearnaley et al., 2014)	843	19% LR 38% IR 43% HR	64 vs 74Gy	3-6/12 NA/A	43 vs 55% PFS (p<0.05) 71 vs 71% OS @ 10years	Conformal LENT-SOMA @ 5 years ≥G2 GI bleed 26 vs 43% HR 1.55
A = Adjuvant, GI = Gastro-intestinal, GU = Genito-urinary, HR = High risk, IR = Intermediate risk, LR = Low risk, NA = Neo-adjuvant, OS = Overall survival, PFS = Progression free survival						

EBRT alone has been shown to offer excellent outcome for low risk disease with relapse free and cause specific survival rates at seven years of 90% and 99% respectively in one large retrospective series (Zelefsky et al., 2008c). Due to the generally indolent nature of disease in this group it is hard to prove a definite benefit from treatment and curative therapy or active surveillance is considered appropriate.

For more advanced disease the results after EBRT, in the pre-dose escalation era, have been more disappointing with around 40% of intermediate risk patients suffering biochemical failure within 5 years and only around one in five patient with T3-4 tumours free of disease 10 years after treatment (Zietman et al., 1995; D'Amico et al., 1998). As a consequence its use in combination with systemic agents has been investigated.

1.1.8.3 Radiotherapy and Androgen Deprivation Therapy

Radiotherapy acts synergistically with androgen deprivation hormone therapy (HT) to treat prostate cancer and the combination can improve clinical outcome (Zietman et al., 1997b). The objective of androgen suppression can be achieved in two possible ways. One method is through administering hyper-normal levels of luteinising hormone releasing hormone (LHRH), causing suppression of secretion of follicle-stimulating hormone (FSH) and luteinising hormone (LH) from the pituitary gland which would usually stimulate production of testosterone in the testes. Alternatively anti-androgen drugs act as competitive inhibitors of testosterone receptors, blocking the sites at which it would normally act. The exact mechanism of synergy of androgen suppression with radiotherapy is uncertain, but it may have an effect as a radio-sensitiser and as a treatment for occult micro-metastatic disease (Wo and Zietman, 2008). It also causes a reduction in prostate volume which may improve radiotherapy response by increasing blood flow through the remaining gland and reducing areas of radio-resistant hypoxia (Whittington et al., 1999). Tumour response to HT causes suppression of PSA levels in almost all patients. HT does have associated side effects however causing hot flushes for many users, reduced libido and energy levels, cardiovascular complications and bone thinning. For this reason the treatment period is kept to the minimum required. HT is usually commenced prior to EBRT for between 3-6 months and continued for up to 3 years after it is completed depending on the initial disease characteristics.

For low risk prostate disease the addition of HT does not appear to offer an improvement in outcome over EBRT alone. This has been demonstrated in sub-group analysis from multiple studies and as such the potential side effects of hormone treatment are not justified (Jones et al., 2011).

With intermediate and high risk disease a survival benefit from combined treatment has been demonstrated, although the duration of HT required to maximise this benefit is less defined (D'Amico et al., 2008). A total of two to three years of HT appears to offer improved survival for higher risk patients compared to a shorter course of four to six months (Bolla et al., 2009; Horwitz et al., 2008). In intermediate risk patients however there appears to be no additional benefit from prolonged hormone therapy with studies showing no effect from additional therapy over shorter peri-radiotherapy hormone treatment (Pisansky et al., 2015). Combination therapy in intermediate risk disease was associated was one series with a 10 year biochemical failure rate of 28% and a decrease in 10 year disease specific mortality from 8% to 4% compared with radiotherapy alone (Jones et al., 2011).

These studies of combination therapy involved relatively modest total doses of EBRT. The benefit in biochemical control achieved by dose escalation raised the question of whether the addition of HT in this setting was of required. The DART 01/05 study has confirmed a survival benefit from two years vs four months HT with dose escalated radiotherapy for high risk disease (Zapatero et al., 2015). The lack of randomised data showing an improved outcome from the combination of HT and dose escalated EBRT in intermediate risk disease has caused some clinicians to argue patients should not be unnecessarily exposed to the side effects of HT. An alternative viewpoint would be

that the previously described studies of dose escalated radiotherapy did not use what would now be considered optimal HT. Given that it has been demonstrated that extended HT offers a survival advantage in intermediate and high risk disease some of the improvement in outcome demonstrated from dose escalation may be a mitigation of sub-optimal combination treatment.

This area of contention has recently begun to be addressed with the publication of modern prospective randomised data of the benefit of the addition of HT to dose escalated radiotherapy (Bolla et al., 2016). The necessity of combination therapy is of significance to future studies of further dose escalation utilising MRI.

1.1.8.4 Radical prostatectomy

Radical prostatectomy (RP) is used to treat localised prostate cancer, surgically removing all prostate tissue via a laparoscopic or open approach. Following this procedure, since the entire prostate has been removed, PSA levels should become undetectable, although not all men with detectable levels after surgery will require further therapy. Even if histologically clear margins are obtained there is a risk of relapse either due to small amounts of residual tissue or the presence of undetectable micro-metastatic disease at the time of surgery. RP has potential side-effects, particularly a risk of urinary incontinence and impotence due to damage to the neurovascular bundles running alongside the prostate gland. Symptoms of urinary incontinence may be present in more than 25% of patients after a year and be considered a significant problem in 5-10% (Sanda et al., 2008). The loss of erectile function is almost inevitable if nerve damage occurs during surgery and, even if this is avoided, it is more likely if sexual function prior to surgery is impaired.

For early, localised disease the reported results for freedom from biochemical relapse and local relapse at 10 years are excellent, achieving 82% and 97% respectively following RP in one large series, with a prostate specific mortality of 1% at 15 years (Mullins et al., 2012; Boorjian et al., 2008). However as previously noted active surveillance in this risk group can also achieve excellent results, questioning the need for early definitive therapy. For intermediate risk disease freedom from biochemical relapse is impaired, falling to approximately 65% at 10 years, but it is still considered an appropriate management strategy. For high risk disease, by contrast, the risk of treatment failure following surgery has traditionally been felt to be too high to justify it as a treatment approach. The role of surgery in actually improving this survival figure in high risk disease is marginal having a modest at best effect in two recent prospective randomised phase III trials, PIVOT and SPCG-4 (Wilt et al., 2012; Bill-Axelson et al., 2011). The PIVOT trial included 157 patients with high risk disease of whom 80 underwent RP and found a 6.7% statistically non-significant increase in overall survival compared to observation. SPCG-4 demonstrated in a cohort of 695 patients randomly assigned to observation or surgery a reduction in risk of death from prostate cancer at 15 years from 20.7% to 14.6% in those undergoing RP but did not stratify for high risk disease. It found those with pT3 disease identified at surgery had a seven times greater risk of death from prostate cancer and suggested adjuvant treatment may be required in this setting. This would imply that surgery may not be an appropriate approach in these high risk patients.

1.1.8.5 Radiotherapy vs radical prostatectomy

No prospective randomised trial comparing the two radical approaches has been completed. Various retrospective series have been published with differing results and all with limitations in terms of the treatment patients received, equivalence of patient cohorts or the primary end point. In low risk disease large, non-randomised studies have demonstrated a survival benefit to RP over EBRT or BT but not in prostate cancer specific mortality, suggesting a potential selection bias (Zumsteg and Zelefsky, 2013). In high risk disease equivalence issues between comparative cohorts persist. For example a combined analysis from the Mayo Clinic and Fox Chase Cancer Centre of 1238 patients receiving RP and 344 receiving EBRT +HT found equivalent 10 year cancer specific survival of 92% (Boorjian et al., 2011). However 253 men received salvage EBRT following RP and 415 received salvage HT. In addition patients receiving RP were younger with earlier stage disease, and average radiotherapy doses of 72 Gy would be considered sub-optimal care. A retrospective comparison of RP vs. dose escalated EBRT in Afro-Caribbean men showed improved outcomes for all risk groups from EBRT plus HT if indicated (Schreiber et al., 2014b).

Overall the choice of treatment, particularly in early and intermediate risk disease, therefore has to be made after careful consideration of the patient's best interests and wishes and the likely side effects profile. A long term follow up of 1655 patients found more urinary symptoms and erectile dysfunction following surgery while bowel symptoms occurred more commonly after radiotherapy; however these differences had lost statistical significance by 15 years post treatment (Resnick et al., 2013). In low and intermediate disease patients will generally be offered both treatment options with assumed equivalence but differing side effects profile. In high risk disease, in the UK, radiotherapy with hormone treatment is the preferred approach.

1.1.8.6 Salvage therapy

In high risk patients adjuvant EBRT following surgery can be offered based on adverse pathological features. There are prospective randomised trial data supporting the use of adjuvant radiotherapy in patients with confirmed T3 disease or, particularly, those with positive surgical margins (Bolla et al., 2012). There is no evidence that surgery followed by radiotherapy confers any survival benefit over radiotherapy alone. An alternative approach is delayed salvage EBRT once a patient suffers biochemical relapse following surgery. Biochemical relapse is most commonly defined using the American Urological Association criteria as two sequential PSA results with a level >0.2 ng/ml (Cookson et al., 2007). This is likely to indicate residual malignant tissue, although not necessarily representing disease from which the patient will develop symptoms. Delaying intervention avoids over treating men who will not recur and reduces those exposed to potential side effects of increased rectal bleeding, incontinence and urethral stricture. There is mixed evidence of EBRT in this setting improving overall survival but it does appear to be effective for controlling local relapse. Factors associated with improved PFS include a negative surgical margin, early stage disease, low presenting GS, a low PSA level at recurrence and a long interval from surgery to relapse (Briganti et al., 2014). The chances of achieving progression free survival at six years are improved by treating when PSA levels are low, improving from 18% when treating with PSA>1.5ng/ml to 48% if

PSA<0.5ng/ml in one study (Stephenson et al., 2007). The merit of up front versus delayed radiotherapy post-operatively in those with high risk features is being addressed in ongoing randomised phase III trials. Emerging evidence suggests a role for hormone therapy in addition to RT in this setting (Shipley et al.; Carrie et al.).

1.2 Improving radiotherapy delivery

1.2.1 *Developments and limitations in conventional radiotherapy planning*

Over the past twenty years the increasing use of 3D-CT planning scans, 3D conformal radiotherapy (3D-CRT) and then IMRT have increased the conformality of radiation therapy. Dose may be closely matched to the intended treatment volume with a sharp dose gradient outside of the target allowing safe dose escalation. This steep fall off reduces doses to nearby organs at risk (OARs) but necessitates accurate identification of disease to prevent a geographical miss. The routine use of CT imaging for planning has arisen due to benefits of ease of access and short scanning times, good spatial and reasonable anatomical delineation, particularly at bone/soft tissue or air/soft tissue interfaces, and lack of geometric distortion. Crucially it also provides information on electron density of tissues allowing for application of radiation attenuation and distribution algorithms to treatment plans. Without allowance for this, over or under dosing of tumour and normal structures would occur.

1.2.2 *Limitations of CT planning*

The use of CT planning has limitations, particularly in regard to image reconstruction, differentiation of soft tissue structures and the unavoidable associated radiation exposure. 3D images are generated from a series of 2D axial images obtained through processing information on attenuation of kV photons as they pass though the body before hitting an x-ray sensor. The information between each slice of data is interpolated in the 3D construction (Figure 1-7). Resolution of imaging is dependent on slice thickness with a reduction in the accuracy of volume estimation as slice thickness and distance between slices is increased (Disler et al., 1994). In addition within a slice the signal from a small area of high density can appear indistinguishable from a larger area of lower density potentially leading to a “partial voluming” effect with inaccurate estimation between slices leading to errors in tissue reconstruction (Figure 1-8). Metal implants can completely attenuate signal, leading to significant artefacts in the reconstructed image. This is a particular problem in the pelvis when hip implants are present.

In addition CT imaging provides poor differentiation between adjacent soft tissue structures of similar electron density. It has previously been demonstrated that the limitations of CT imaging cause significant variability of inter-operator delineation of various cancers (Nijkamp et al., 2012; Caldwell et al., 2001; Hurkmans et al., 2001; Van de Steene et al., 2002). This variability may be mitigated with explicit contouring guidelines, suggesting that image quality itself is not the only factor affecting delineation reproducibility(Geets et al., 2005).

For prostate radiotherapy planning inter-operator reproducibility is a particular problem at its apex and the posterior aspect adjacent to the seminal vesicles due to poor CT differentiation of tissue structures at these sites. Previous studies have shown that there may be variation in delineation of these areas with potential for under-treatment of prostatic tissue or over-treatment of surrounding organs at risk. For example in a study of five experienced radiotherapists differences of up to 1cm in the cranio-caudal extent of the contoured prostate and seminal vesicles and 0.7cm at the anterior of the prostate were seen (Fiorino et al., 1998b).

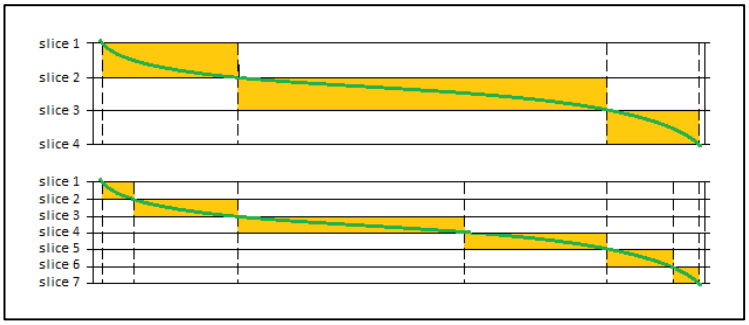

Figure 1-7**: **Effect of slice thickness on image resolution

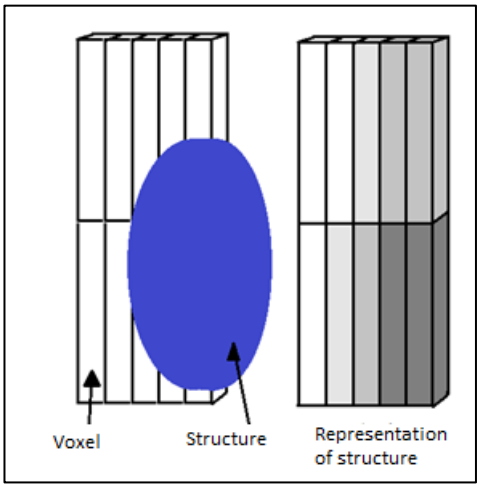

Figure 1-8: Partial voluming effect

Another group found significant differences between the prostate and seminal vesicle PTV contours of three radiation oncologists with consistent tendencies from each, i.e. they tended to be always larger or smaller, reflecting in part an issue with image quality (Cazzaniga et al., 1998a). In contrast this variation was not seen in a study of clinicians given explicit contouring guidelines which found only minor differences in GTV volume (Rasch et al., 1999b). Despite the improvement guidelines appeared to achieve variation in delineation cannot be entirely eliminated by improved knowledge; even within an expert study group it has been demonstrated that in 70% of images contoured there was disagreement about which axial CT slice represented the prostate apex (Cox et al., 1994). In addition similar contour volumes do not necessarily mean accurate contouring. The CT delineation of six radiation oncologists has been compared with photographic anatomical images with the contoured prostate found on average to be 30% larger that the true gland but only included 84% of its volume (Gao et al., 2007). The study found the posterior portions of the

prostate were always missed and anterior normal tissue always included The majority of prostate carcinoma arises within the posterior peripheral zone and effective dosing of this region therefore has important implications for treatment outcome (McNeal, 1992).

In summary the findings of these studies reflect the limitations of CT imaging for prostate radiotherapy planning which can only be partially mitigated by operator expertise.

1.3 Addition of MR to planning

Given these issues with tumour identification on CT and its potential detrimental effect on treatment planning, methods to reduce error have been assessed. Magnetic Resonance (MR) imaging is one particular area of interest given its superior ability to differentiate soft tissue structures.

1.3.1 *Introduction to MR imaging*

1.3.1.1 Concepts

Protons within atoms have spin and a positive charge and therefore produce a small intrinsic magnetic field. Water and fat are the source of protons in the human body. At the quantum level spin can be up or down and is usually randomly distributed within a tissue, summing to zero. A quantum description of the effect of a magnetic field on protons is complex and a classical description more intuitive. Described in this way placing a proton in a magnetic field will cause spin to align in an almost parallel or almost anti-parallel direction with the field. A slight excess will align in the positive direction as it is a lower energy state, creating a net magnetisation in the direction of the magnetic field B0, described as the z-direction. This is indistinguishable from the far larger extrinsic magnetic field. The excess is proportional to the strength of the magnetic field, the stronger the magnet, the more excess and the higher signal to noise ratio. Within a voxel on an MR scan, approximately 2x2x5mm in volume, there are around 6 million billion protons.

Protons wobble, or precess, around the axis of the external B0 field at a frequency directly proportional to its strength, defined by the Larmor equation.

$$\omega 0 = \gamma B0$$

where: $\omega 0$ = angular frequency of precession of protons in external magnetic field (MHz)

γ = proportionality constant (gyromagnetic ratio)

B0 = magnetic field strength (T)

If a radio frequency (RF) pulse is applied at the resonant frequency protons will absorb this energy and move to a higher energy state. The absorbed energy causes the net magnetisation to spiral away from the z-axis. The net magnetisation vector rotation is proportional to the duration of the RF pulse. The component of magnetisation in the x-y plane is perpendicular to the extrinsic magnetic field and can be detected.

1.3.1.2 T1 and T2 relaxation

After the RF pulse ends the absorbed energy is lost and the magnetisation vector begins to return to its original orientation in two independent processes called spin-lattice and spin-spin relaxation. Recovery of magnetisation along the z-axis has a characteristic time constant T1, representing the time at which 63% of recovery has occurred. In this process energy is given off into the surrounding tissue called the lattice and is termed the spin-lattice relaxation. T1 time varies in different tissues being generally short in fat, mid-range in water based tissues and longest in fluids.

Decay in the transverse plane is controlled by spin-spin relaxation and is given the notation T2. In this process protons which are briefly in phase following the RF signal immediately begin to de-phase as a result of the variable influence of the magnetic fields of surrounding protons. This causes a change in precession rates and a loss of phase coherence, described as spin-spin interaction, reducing transverse signal at the T2 relaxation rate. T2 is the time after excitation when this transverse signal has reduced by 63%.The T2 relaxation time in a tissue is always shorter than T1. T2 relaxation is a property of a tissue but is accelerated by inhomogeneities in the extrinsic magnetic field and susceptibility effects due to the variable magnetisation of different tissues in a magnetic field. The combined effect of these processes gives the apparent relaxation time, given the notation T2*.

1.3.1.3 TE, TR, Spin Echo, and Gradient Echo

A period of time after a RF pulse is delivered the resulting transverse magnetisation is measured. This is termed the time to echo (TE). Further excitation RF pulses are delivered as part of an imaging sequence with the time to repetition given the notation TR.

By varying TR and TE in different sequences it is possible to obtain T1 weighted (T1W), T2 weighted (T2W) and proton density weighted (PDW), images. Because these characteristics can vary greatly between soft tissue structures of similar electron density MRI is able to differentiate these tissues far more clearly than CT imaging. This clarity can be exploited to allow more accurate identification of areas of interest for radiotherapy planning.

Table 1-6:Effect of choice of repetition time (TR) and time to echo (TE) for conventional spin echo sequences

TR	TE	
	Short (<40 ms)	Long (>75 ms)
Short (<750 ms)	T_1-weighted	Not useful
Long (>1500 ms)	PD-weighted	T_2-weighted
Ms, millisecond; TE, Time to echo; TR, Repetition time		

The most basic sequence used in MRI is the spin echo (SE). This starts with a 90^o pulse, causing the net magnetisation vector to spiral down into the x-y plane. By varying TE and TR, weighting of images can be achieved as shown in Table 1-6. A 180^o RF pulse is applied while T2 decay is occurring, causing de-phasing protons to re-phase and allowing a second, slightly lowered maximum signal to form at which time an echo is taken. The 180^o pulse removes T2* effects and

allows T2w images to be formed. Acquisition is relatively slow as the time to full relaxation after a 90^o RF pulse, required for T2 weighted images, is long and consequently so are TR, TE and overall image acquisition time.A standard spin echo pulse sequence is shown in Figure 1-9 and includes slice selecting, phase encoding and frequency encoding gradients which allow localisation of signal at TE.

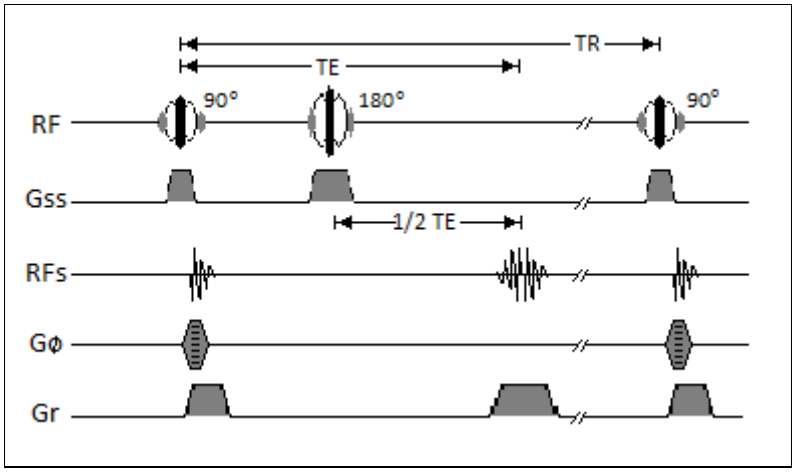

Figure 1-9: The basic spin echo pulse sequence (RF_t, Radiofrequency pulse; G_{ss}, Slice selecting gradient; RF_s, Radiofrequency signal; G_ϕ, Phase encoding gradient; G_R, Frequency encoding gradient)

Alternatively a gradient echo (GE) sequence usually starts with a smaller RF pulse and produces a flip angle of $<90^o$. Only a proportion of the net magnetisation vector is moved away from the z-axis meaning full T1 relaxation occurs faster. This allows shorter TR and TE times and quicker image acquisition. By varying the flip angle the degree of T1 weighting is improved at higher flip angles. After the RF pulse a gradient pulse is given which de-phases and then a second opposite gradient pulse is given which rephases the signal with an echo taken at TE. In GE sequences T2* decay occurs.

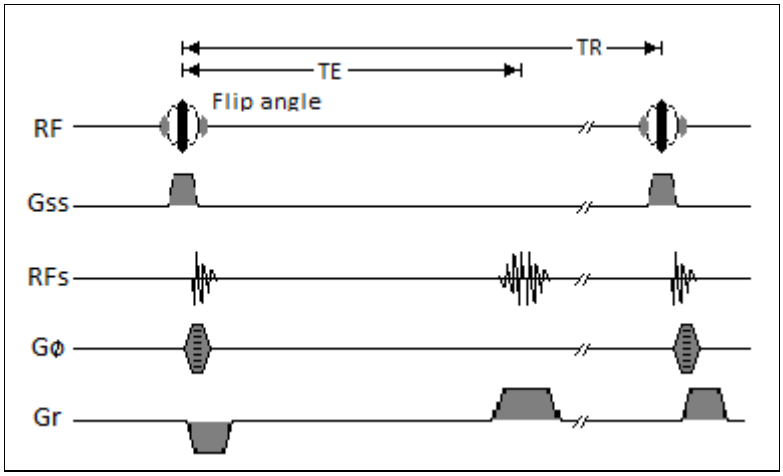

Figure 1-10: The basic gradient echo pulse sequence (RF, Radiofrequency pulse; Gss, Slice selecting gradient; RFs, Radiofrequency signal; G_ϕ, Phase encoding gradient; Gr, Frequency encoding gradient)

1.3.1.4 Comparison of MR and CT based planning

Anatomical MRI of the prostate is generally performed using T2W imaging which can have high spatial resolution and differentiate between the low signal central gland and high signal peripheral zone of the prostate. This differentiation can become more challenging as men age with benign prostatic hypertrophy affecting the appearance of the transition zone, increasing its size and compressing the remainder of the gland. The improved visualisation of MRI has clinical implications; multiple studies have demonstrated a reduction in volume of contoured prostate when MR imaging is used to provide addition information for planning, and a reduction in inter-observer delineation variation(Villeirs et al., 2005)(Table 1-7). The MR delineated prostate volume has been shown to correlate well with post prostatectomy specimens.(Sosna et al., 2003; Jeong et al., 2008).

This decrease in volume permitted by MR imaging reduces delivered radiation dose to the rectum during treatment, thereby potentially reducing its associated toxicity. When using 3-D conformal radiotherapy and prescribing a dose of 78 Gy to the prostate, MR planning might allow for a further increase of up to 7 Gy to the PTV for the same rectal wall dose with potential benefit of dose escalation for tumour control probability (Steenbakkers et al., 2003). Although metallic hip replacements degrade the image quality of both MR and CT it has been demonstrated that identification of the prostate is less impaired on MR imaging (Charnley et al., 2005). This further limits the accuracy of delineation of soft tissue structures on CT imaging and provides an additional rationale for the use of MRI in prostate planning.

A final area of potential benefit is the ability of MR imaging to identify areas of high density malignant tissue within the prostate, providing the potential for targeted dose escalation.

Table 1-7: Benefit of MR vs. CT imaging on prostate contouring

Author	Pts	MR sequence and slice thickness	Image fusion	p-value	% reduction in volume with MR vs CT + Area of largest discrepancy	Reduction in mean rectal dose
(Roach Iii et al., 1996)	10	?T ?coil T1W+ T2W 4-6mm	Nil	0.0004	23% Posterior (7mm) Apex (4.5mm)	7mm increased distance from target to rectal wall
(Kagawa et al., 1997)	22	1T Pelvic array T2W 4mm	Bony anatomy	0.0001	19% Apex (5mm) Base	N/A
(Rasch et al., 1999a)	54	?T ?coil PD +T2W 6mm	Bony anatomy	>0.005	30% Base (8mm) Apex (6mm)	Increased distance from target to rectal wall
(Debois et al., 1999)	10	1.5T ?coil T2W 5mm	MI fusion	0.004	28% Apex	23.8% reduction in volume receiving 80% dose
(Sannazzari et al., 2002)	8	1 T Pelvic array T2W 3mm, 3mm gap	Fiducial markers	<0.01	25% Apex (5mm) A-P (5mm)	Spare 10% of rectal volume
(Villeirs et al., 2005)	13	1 T Pelvic array T2W 5mm, 0mm gap	Nil	<0.05	7% Apex	N/A
(Jackson et al., 2007b)	11	1.5 T Pelvic array T2W 3D	Bony anatomy	0.009	12%	4-6% reduction in volume receiving 45-65Gy
(Hentschel et al., 2011a)	294	1.5 T Pelvic array T1W+T2W 3mm	Eclipse automated fusion	<0.001	35% Superior and inferior	N/A
(Tanaka et al., 2011a)	39	1.5T ?coil T2W 3mm	Automated fusion	>0.05	31% Apex	18% reduction in mean dose to rectum
PD= proton density, Pts=patients, T = Tesla, T1W=T1 weighted, T2W=T2 weighted,						

1.3.2 *Dose escalation- necessity of whole prostate boost*

A prescribed radiation dose is given with the objective of achieving a satisfactory likelihood of local control of disease while keeping the risk of complications within acceptable levels. Dose escalation improves the likelihood of disease control but for prostate therapy is limited by the proximity of the anterior rectal wall and bladder. Even using highly conformal techniques such as IMRT it is impossible to spare this entirely while delivering a prescribed dose to the PTV. Reducing the expansion margin from CTV to PTV posteriorly can spare the rectum but carries a clinical risk. As the rectum fills and empties the prostate moves significantly in the anterior and posterior direction. This motion may be sufficient to move the prostate outside of a reduced PTV volume for a proportion on treatment delivery and would risk under-dosing of the posterior prostate.

The CTV usually includes the entire prostate due to the concerns about likely multifocal disease and the presence of cancer representing a field change effect. Over half of patients are found to have multi-focal disease following RP and around 85% of specimens also contain areas of pre-malignant prostatic intraepithelial neoplasia (PIN) (Qian et al., 1997; Villers et al., 1992). However it

has also been shown that local relapse following EBRT is most likely to occur at the site of original disease. Twelve patients who had experienced an intra-prostatic recurrence appeared, on the basis semi-quantitative analysis using clinical examination and imaging, to have recurred within the initial tumour volume (Cellini et al., 2002a). Eight patients treated with salvage RP for local relapse after EBRT all had clinically significant recurrences at the site of primary disease (Pucar et al., 2007). Finally nine patients who had unequivocal dominant tumour on pre-treatment evaluation eight were found two years post EBRT to have recurrent disease within the same location confirmed on biopsy (Arrayeh et al., 2012). In addition to these findings there is emerging evidence that even in multi-focal disease the dominant lesion by size criteria may be the only one with malignant potential although this remains contentious (Karavitakis et al., 2011; Schmidt et al., 2006). The presence of a dominant nodule within the prostate may be predictive for biochemical failure following treatment (Noguchi et al., 2003).

Given these findings a means of delivering selective dose escalation of radiotherapy to a small area of the prostate with highest disease density, rather than the entire gland, is a logical and attractive concept to reduce radiation dose to surrounding structures and associated treatment related toxicity.

1.3.3 *Improved disease identification with Multi-parametric MR*

In addition to improving accuracy of prostate delineation MRI has the potential to identify regions of high disease density within the gland. Meta-analysis of 10 studies correlating T2W imaging to whole mount histology showed a wide range of reported sensitivity for detecting disease within the peripheral zone between 37-96% (Kirkham et al., 2006). This large range may in part be due to the differing restrictions on size considered significant by various studies and differing reporting requirements. The two largest studies included, representing 60% of patients imaged, found sensitivities of 60% and 62%. In the transition zone T2W performs less effectively with one series showing 78 of 79 tumours <0.5 ml in size could not be identified (Ellis et al., 1994). Standard MRI is not therefore sufficient to allow confident identification of intra-prostatic disease for focal therapy and alternative imaging approaches are needed.

In addition to providing information on the relative PD, T1 and T2 characteristics of tissues MRI is increasingly being used to assess functional characteristics. This can achieved, for example, through the use of diffusion weighted imaging (DWI), dynamic contrast enhanced MRI (DCE) and MR spectroscopy (MRS).

1.3.3.1 Diffusion Weighted Imaging

The amount of free water in tissues varies according to its cellularity and cell membrane integrity. Water molecules move due to Brownian motion. This motion, or diffusion, is limited by tissue structures and is measured by DWI. By applying a series of magnetic gradients, characterised by their B-values, a profile can be obtained for a given tissue providing an indication of how freely water can diffuse. These magnetic gradients are applied in pairs; the first de-phases the proton spins and the second re-phases if no net movement has occurred. If net movement has occurred

then signal attenuation results. This attenuation is affected by the strength of the diffusion gradients and time between them. B-values are a measure of the diffusion gradient applied and usually range from 0-1000 sec/mm^2. There have been recent reports suggesting that the use of "ultra-high" values may improve diagnostic accuracy, although the evidence is conflicting (Kim et al., 2010; Kitajima et al., 2012; Ueno et al., 2013). Healthy prostatic tissue will allow less restricted diffusion and therefore be highly attenuated and appear dark on high b-value DWI. Malignant tissue by contrast is more densely packed and will restrict fluid motion, appearing bright (Issa, 2002). High T2 signal will also contribute to brightness, in a process independent of diffusion restriction, termed "shine through", which may confound image interpretation.

Apparent Diffusion Coefficient (ADC) is calculated by linear regression from two or more b-value images allowing removal of this "shine through" effect. The appearance of ADC is reversed from DWI with areas of restricted diffusion appearing dark. The use of DWI/ADC imaging in combination with T1W and T2W has been shown to improve the accuracy of staging and planning of targeted biopsies with sensitivity of up to 88% and specificity of 84% on meta-analysis (Delongchamps et al., 2011; Wu et al., 2012b). ADC values show a correlation with tumour aggressiveness and may be used to predict disease behaviour (Hambrock et al., 2012). It is however affected by the heterogeneity of benign prostate tissue which limits its ability to identify small tumours and therefore needs to be used in combination with other modalities (Borren et al., 2013). There is also overlap of ADC values for normal tissue and prostate cancer preventing a single threshold for malignancy.

1.3.3.2 Dynamic Contrast Enhanced MRI

DCE-MRI represents a measure of vascular perfusion and permeability within a structure. It is assessed by the administration of a gadolinium based contrast agent with speed of enhancement and washout measured. The relationship between signal intensity and contrast agent concentration is non-linear and a conversion using T1 relaxation is required for a quantitative analysis. The signal intensity over time has characteristic appearances in different structures (Figure 1-11). Enhancement following a type 1 pattern is usually benign tissue, whilst type 2 is suspicious but not definitive for disease. Neo-angiogenesis within tumours with disorganised, permeable vessels typically increases speed of enhancement and washout (type 3). Within a lesion all three types may be seen. The data generated can be analysed to look at various semi-quantitative parameters such as the area under the curve or initial slope gradient. Pharmacokinetic models can be fitted to the enhancement data to obtain quantitative parameters. Many have quantified K^{trans} which represents the transfer of gadolinium into and out of the vasculature (Tofts et al., 1999). This is however a combination of two independent variables, tissue permeability and perfusion. Alternatively these factors can be calculated separately by applying the adiabatic approximation to the tissue homogeneity model (AATH) model (St Lawrence and Lee, 1998). The AATH model requires the use of additional parameters however which may also in turn lead to reduced precision in estimates of perfusion and permeability.

DCE-MRI is effective at detecting prostatic cancer; in one series detecting 92.9% of clinically important prostate cancers (Hara et al., 2005). The use of DCE-MRI in addition to DWI and T2W for detection of prostate malignancy is recommended by current European Society of Urogenital Radiology (ESUR) guidelines (Barentsz et al., 2012a). Although the evidence for an additive benefit is mixed, combining DCE-MRI with other sequences reduces the risk of mistaking prostatitis or BPH for cancer (de Rooij et al., 2014a). DCE-MRI results are dependent on arterial flow, described in the arterial input function (AIF), which can be challenging to measure accurately. This affects the repeatability of results and contributes to the large variations found in the measure of K^{trans} in various studies by up to a factor of x10 in normal prostate tissues (van der Heide et al., 2011).

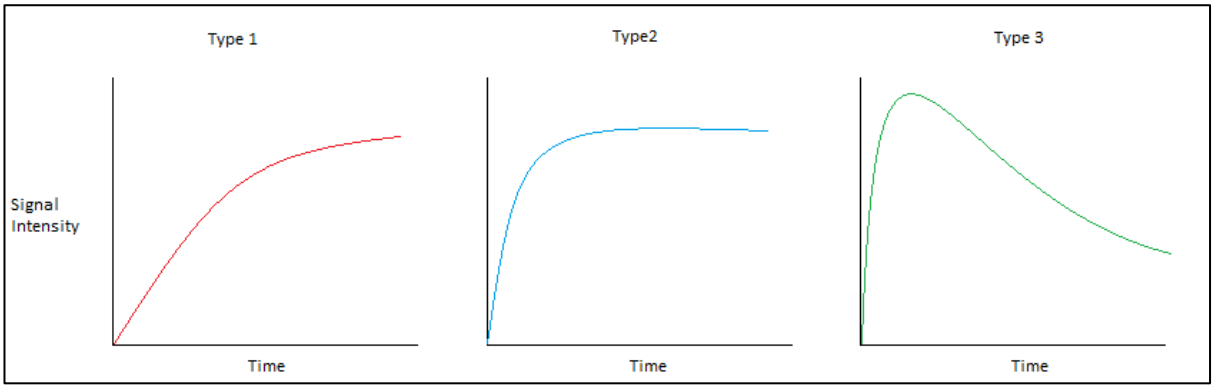

Figure 1-11: Enhancement patterns with DCE-MRI

1.3.3.3 Magnetic Resonance Spectroscopic imaging

The final functional technique most commonly reported in prostate imaging is magnetic resonance spectroscopy (MRS). This exploits the fact normal prostate tissue is an effective producer of citrate but much less so of choline. Within tumour, due to high cell turnover, the choline levels are increased affecting the choline: citrate ratio (Verma et al., 2010). The metabolic concentrations can be analysed using MRS imaging to look for characteristic peaks suggestive of pathology. The ratio is also affected by other conditions such as BPH and it must therefore be used in conjuncture with anatomical imaging. It is a challenging imaging technique requiring expertise and time and is not therefore routinely practiced.

1.3.4 *PI-RADS*

It is only is the last few years that a consensus as to what should be considered malignant based on the finding of multi-parametric (mp)–MRI has been agreed. A consensus document was published in 2011 following a meeting of 16 European prostate cancer experts which proposed a 5 point subjective Likert scale to assign the probability of malignancy and concluded that it should be possible to exclude disease of Gleason ≥ 3+4 and size ≥ 0.2 cm^3 in the transition and peripheral zone (Dickinson et al., 2011). Subsequently in 2012 ESUR published the PI-RADS guidance on the role of MP-MRI (Barentsz et al., 2012b). This scoring system is a narrative description with potential for varying interpretation but provides an accepted schema for all to follow (*Table 1-8* and Table 1-9). Subsequent publications have attempted to provide a visual scale to place alongside it (Figure 1-12).

Table 1-8: Definition of total score according to modalities used (taken from (Rothke et al., 2013))

PI-RADS Classification	**Definition**	**Total score T2+DWI+DCE**	**Total score T2+DWI+DCE+MRS**
1	Highly likely benign	3-4	4-5
2	Likely benign	5-6	6-8
3	Indeterminate	7-9	9-12
4	Likely malignant	10-12	13-16
5	Highly likely malignant	13-15	17-20
DCE= Dynamic contrast enhancement DWI= Diffusion weighted imaging MRS= Magnetic resonance spectroscopy			

Table 1-9: PI-RADS scoring system for prostate cancer detection using MP-MRI

Score	**Criteria**
1	Clinically disease is highly unlikely to be present
2	Clinically significant disease is unlikely to be present
3	Clinically significant disease is equivocal
4	Clinically significant disease is likely to be present
5	Clinically significant disease is highly likely to be present
T2W for peripheral zone	
1	Uniform high signal intensity (SI)
2	Linear wedge shaped or geographical areas of lower SI, not usually well demarcated
3	Intermediate appearances
4	Discrete, homogeneous low signal focus/mass confined to prostate
5	Discrete homogeneous low signal intensity focus with invasive behaviour or mass effect or broad (>1.5cm) contact with surface
T2W for transition zone	
1	Heterogeneous TZ adenoma with well-defined margins
2	Areas of more homogeneous low SI, well marginated, originating from TZ/BPH
3	Intermediate appearances
4	Areas of more homogeneous low SI, ill defined. “erased charcoal sign”
5	4 with involved AFS or anterior horn of PZ, usually lenticular
DWI-MRI	
1	No reduction in ADC compared with normal glandular tissue. No increase SI on high B value (≥800)
2	Diffuse hyper SI on ≥b 800 image with low ADC, no focal features, linear or geographical features allowed
3	Intermediate appearance
4	Focal area(s) of reduced ADC but iso-intense SI on high b-value images (≥800)
5	Focal are/mass of hyper SI ion high b-value images (≥800) with reduced ADC
DCE-MRI	
1	Type 1 enhancement curve
2	Type 2 enhancement curve
3	Type 3 enhancement curve
+1	Focal enhancing lesion with curve type 2-3
+1	For asymmetric lesion or lesion in an unusual place with curve type 2-3
MRS-MRI	**Choline +creatine/citrate ratio**
1	PZ ≤0.44 CG ≤0.52
2	PZ 044-0.58 CG 0.52-0.66
3	PZ 0.58-0.72 CG 0.66-0.80
4	PZ 0.72-0.86 CG 0.8-0.94
5	PZ >0.86 CG >0.94
ADC= Apparent diffusion coefficient, AFS = Anterior fibromuscular stroma, BPH= Benign prostatic hypertrophy, CG = Central gland, TZ = Transition zone,	

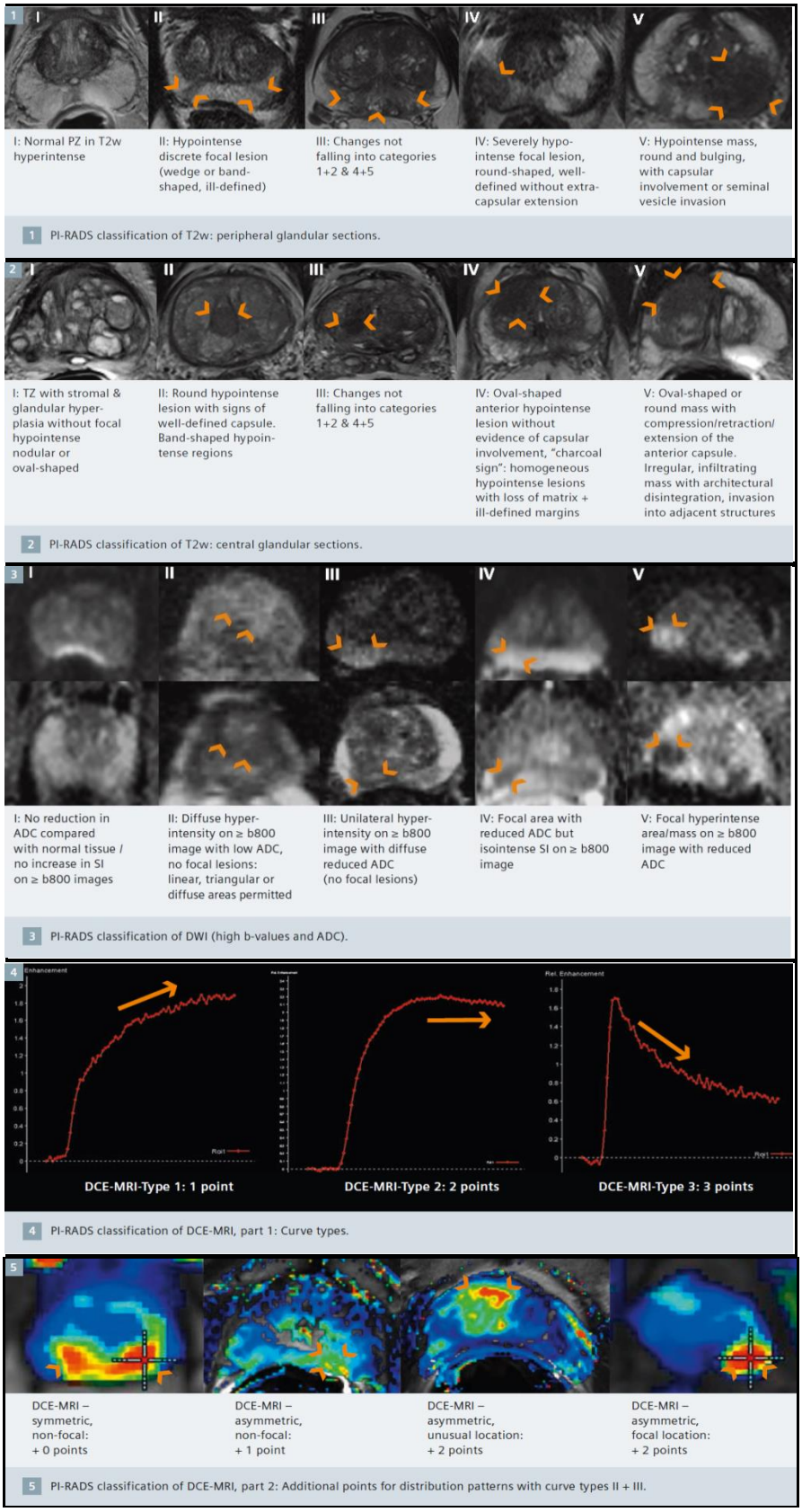

Figure 1-12: Visual representation of PI-RAD scale

The PI-RADS scoring system has been validated, with the sensitivity and specificity of a positive scan finding dictated by the minimum score that is considered to represent disease; in one study considering all PIRADS 2-5 lesions as malignant gave MP-MRI a sensitivity of 98% and specificity

of 37% compared with 47 % and 97% when only considering PIRADS 5 (Grey et al., 2015). The administration of antispasmodics prior to imaging to reduce motion artefact is recommended by some to reduce motion artefact due to bowel movement but not considered essential(Wagner et al., 2010). Comparison of Likert type and PI-RADS scales have shown no significant difference in their performance in identifying disease although with less experienced operators the subjective Likert scale performs less well. This suggests that to allow comparison between studies PI-RADS should be adopted (Rosenkrantz et al., 2013).

PI-RADS V2.0 has recently been published. It removes the use of MRS and downgrades the role of DCE due to its lack of value when T2W and DWI imaging is of diagnostic quality. In the peripheral zone DWI is used predominantly to assign the PIRADS score, with DCE-MRI used to further categorise intermediate DWI signal, whilst in the central transition zone T2w images are used, with DWI playing a secondary role for intermediate scoring disease (Figure 1-13). The grading of DCE signal appearance has also been clarified. The new scoring system still requires testing and validation for specific research and clinical applications.

Peripheral Zone (PZ)

DWI	T2W	DCE	PIRADS
1	Any*	Any	1
2	Any	Any	2
3	Any	-	3
		+	4
4	Any	Any	4
5	Any	Any	5

Transition Zone (TZ)

T2W	DWI	DCE	PIRADS
1	Any	Any	1
2	Any	Any	2
3	≤4	Any	3
	5	Any	4
4	Any	Any	4
5	Any	Any	5

Figure 1-13: PI-RADS v2 grading system

1.3.5 *Clinical application of multi-parametric MRI*

1.3.5.1 Diagnosis and staging of disease

The use of PSA testing, digital rectal exam and TRUS biopsies as a diagnostic tool are imperfect with over diagnosis of early, non-relevant disease. Studies have shown up to half of cancers will be missed by initial prostate biopsies; these have a false negative rate of up to 30% (Djavan et al., 2001). Due to its anatomical location, approaching the prostate via the anterior rectal wall makes sampling the anterior of the gland challenging. MR localisation of prostate cancer is more accurate that DRE and biopsy (Mullerad et al., 2005). It has been shown that tumour size on MRI is a more significant predictor of metastatic failure than the conventional prognostic indicators of PSA, Gleason score, percentage of positive core biopsies or risk category (Joseph et al., 2009b). Patients with a tumour volume >1cc on MRI in that series experienced biochemical failure in 60% of cases compared to only 16% of the remainder.

Used pre-biopsy, or following an initial negative result, MP-MRI helps target biopsies and identify higher grade disease (Moore et al., 2013b). It has been shown that MRS ratios and mean ADC correlate with histology and this information can be used to help guide management towards treatment or active surveillance where appropriate (Zakian et al., 2005; Hambrock et al., 2011; Westphalen et al., 2011). MP-MRI is also recommended as part of an active surveillance program for appropriate patients allowing identification of poor prognostic features such as high grade or size (Johnson et al., 2014). It may improve the staging of disease in combination with conventional T2W MRI, and is recommended in current ESUR guidelines to improve treatment planning for intermediate risk disease (Barentsz et al., 2012b).

1.3.5.2 Benefit of functional MR in identifying prostate cancer

Numerous studies have looked at correlations between pre-treatment MP-MRI imaging and histo-pathological findings after radical prostatectomy. These have shown a significant improvement in identification of disease in comparison to conventional MRI, despite being performed in the pre PI-RADS era (Table 1-10). The variation in imaging techniques used, analytical approach and findings makes overall conclusions hard to form however generally DWI appears to be of more value than DCE but their use in combination may improve performance. Meta-analysis of seven studies, assessing the value to the addition of DWI to T2W, for imaging prostate cancer found the combination increased sensitivity and specificity for detection of disease from 0.62 and 0.77 to 0.72 and 0.81 (Wu et al., 2012a). There was significant heterogeneity of results between studies perhaps due to no attempt being made to correct for tumour location since TZ disease is more challenging to identify. A further meta-analysis of seven studies assessing the role of DWI and DCE with T2W showed an overall sensitivity of 0.74 and specificity of 0.88, however again marked heterogeneity between studies was found although sub-groups were more consistent (de Rooij et al., 2014b). The role of MRS remains unclear. This has not yet been assessed in a meta-analysis and its role in individual studies is of limited importance. Its limited spatial resolution reduces its value in defining the volume of disease.

Mechanical variation of the appearance of post prostatectomy specimens may induce a degree of variation in the correlation with MP-MRI identified disease and there is as yet no accepted standard way of processing specimens. The accuracy of contoured intra-prostatic disease, required for planning of focal boost therapies, appears to be improved more by the addition of DWI than other function sequences (Isebaert et al., 2013; Mazaheri et al., 2009).

All these studies are limited by the lack of consensus when they were carried out as to what represents malignant disease on functional imaging and the use of multiple grading systems. In future the use of a generally accepted scoring system should improve the homogeneity of reported outcomes. A study comparing the contouring of five radiation oncologists following teaching in the MRI appearances of prostate cancer, although not using PI-RADS, showed good agreement on T2W and DCE-MRI and moderate agreement on DWI (Rischke et al., 2013). Analysis of the differences showed inadequate comparison of functional and anatomical sequences and lack of

awareness of non-specific findings. Both would suggest that appropriate training could mitigate the effects.

The use of 3 T, or 1.5 T scanners with ERC, is recommended by various guidelines due to their improved signal to noise ratio, although there is not yet strong evidence for this translating to a clinical benefit (Muller et al., 2014). Further, the expert consensus is that MP-MRI is of sufficient quality to allow focal treatments of prostate lesions.

Table 1-10: Accuracy of MP-MRI in identifying histological whole mount confirmed prostate cancer

Author	Pts	Sequence	Prostate examined and average tumour size if known	Sensitivity	Specificity	Comments
(Villers et al., 2006)	24	?T T2W, DCE	Whole gland Disease >0.5cm^3	0.9	0.88	-
(Haider et al., 2007)	49	ERC 1.5T T2W, DWI	Whole gland 60%>0.13cm^2	0.81	0.84	DWI improved T2W sensitivity, particularly in PZ (A(z) 0.89 vs 0.81)
(Scheenen et al., 2007)	45	3T T2W, MRS	Whole gland	0.78 PZ 0.72 TZ	0.81 PZ 0.62TZ	-
(Yoshizako et al., 2008)	23	1.5T T2W 5mm, DCE+DWI	TZ zone only	0.69	0.94	Combination increased sensitivity
(Schmuecking et al., 2009)	67	1.5T T2W 3mm, DCE +MRS	Whole gland	0.82DCE 0.68 MRS	0.89 DCE 0.67 MRS	Combination not assessed Cut off 3mm for DCE
(Puech et al., 2009)	83	1.5T T2W 4mm, DCE	Whole gland Mean 0.76cm^2	0.86	0.94	for disease >0.5ml
(Mazaheri et al., 2009)	42	ERC 1.5T T2W, ADC	PZ only	0.82 ADC1 0.95 ADC2	0.85 ADC1 0.65ADC2	ADC1 =0.0014mm^2/sec ADC2=0.0016mm^2/sec
(Turkbey et al., 2010)	70	ERC 3T T2W, DCE, MRS	Whole gland	0.73 T2W	0.89 T2W	Combination of images most effective 80% PPV for PZ
(Delongchamps et al., 2011)	57	ERC 1.5T DCE+DWI	Whole gland 83% >0.7mm	0.8 PZ 0.53 TZ	0.97 PZ 0.83 TZ	Combination significantly improves sensitivity specificity in PZ not in TZ
(Osugi et al., 2013)	37	1.5T T2W, DCE+DWI	Whole gland >5mm	0.31 T2W 0.37 DCE 0.71 ADC	-	ADC significantly more sensitive (71.4% in PZ, 89.7% TZ), combining no benefit
(Isebaert et al., 2013)	75	1.5T T2W 3mm, DCE+DWI	Whole gland Median 3.4cm^3	0.58	0.84	Combination of three modalities improved sensitivity DW most accurate for size
(Le et al., 2014)	122	DCE+DWI	Whole Mount	0.47	-	0.8 sensitivity for DIL
(Russo et al., 2015)	115	1.5T T2W 3mm DCE + DWI	Whole Mount	0.91 PZ 0.83 TZ	- -	Gleason score ≥6 or size > 0.5ml considered significant
ADC=Apparent diffusion co-efficient, DCE= Dynamic contrast enhancement, DIL=Dominant intra-prostatic lesion, DWI= Diffusion weighted imaging, ERC=Endo-rectal coil, MRS=Magnetic resonance spectroscopy, Pts=Patients, PZ=Peripheral zone, T=Tesla, T2W=T2 weighted, TZ=Transition zone						

Table 1-10: Outcome of multi-parametric MRI guided focal boost to dominant intra-prostatic lesion							
(Crook et al., 2014)	25 Treatment	3T DWI, DCE, T2w	Nil	Registered	46+25 HDR (46+20HDR)	0mm	Met dose constraints
(Sundahl et al., 2016)	225 Treatment	1.5T DWI, DCE, MRS	94%	Rigid Registration	82 (78)	0mm	≥ G2 GI 20 ≥ G2 GU 45
(Gomez-Iturriaga et al., 2016)	15 Treatment	1.5T, body coil, DWI, DCE, MRS	27%	Rigid registration MRI/USS	37.5+18.7HDR (37.5 + 15)	0mm	≥ G2 GI 13 ≥ G2 GU 20
DCE=Dynamic contrast enhancement, DWI=Diffusion weighted imaging, ERC- Endo-rectal coil, FT- flat top scanner, HT = Hormone therapy, Int=intermediate, MRS=Magnetic resonance spectroscopy, MU-Monitor units, NTCP-normal tissue complication probability, post-tx- MR imaging performed after neo-adjuvant HT, pre-tx- MR scan performed before neo-adjuvant HT, Pts=patients, T=Tesla, T2W=T2 weighted							

1.3.5.3 Using MP-MRI to guide a focal dose boost to the dominant intra-prostatic lesion

Based on these encouraging findings of improved sensitivity and specificity for identifying and localising disease using MP-MRI, multiple groups have carried out planning studies or limited trials of focal dose boosts to the dominant intra-prostatic lesion (DIL) (Table 1-11).

These studies show the feasibility of this approach although with caveats. Given that it has been demonstrated that the whole prostate can be boosted with IMRT to 78-86.4 Gy with clinically acceptable toxicity then the small preliminary patient IMRT study by Singh and the stereotactic treatment by Mirabel, boosting significantly beyond this, may provide the most clinically relevant data (Miralbell et al., 2010a; Singh et al., 2007; Zelefsky et al., 2011). Work modelling local control of prostate cancer using data on prostate hypoxia levels suggests most tumours containing hypoxic cells may not be cured at doses of 80 Gy in conventional 2 Gy per fraction, and therefore dose escalation beyond this may be required (Nahum et al., 2003). The median dose boost to optimise tumour control probability for intermediate and high risk prostatic lesions has been calculated to be in the range 94-116 Gy, (Azzeroni et al., 2013). This is equivalent to a biological effective dose (BED) of 215-270 Gy assuming prostate tumour α/β 1.5 Gy (BED represents a relative effectiveness of a radiation treatment, accounting for a tumours inherent radio-sensitivity and allows comparison of different fractionation regimes; α/β is a measure of a tissues inherent radiosensitivity to different radiotherapy fractionations). This is supported by evidence in the literature of a dose response up to 200-210 Gy BED (Crook et al., 2011; Stone et al., 2010; Martinez et al., 2011). Of interest in this context is the recently published ASCEND-RT study showing a significant BFS benefit from a LDR whole gland boost to 115 Gy over conventional DE-EBRT to 78Gy (Rodda et al.). One planning exercise on 42 patients found it possible to keep OAR doses within tolerance in 50% of plans whilst giving an IMRT boost of 151.2 Gy to the DIL plus a 3 mm margin, suggesting there is potential for significant further dose escalation, although increased toxicity would be a concern (Housri et al., 2011). Encouragingly the studies boosting to doses ≥90 Gy reported early toxicity similar to historic levels from studies of dose escalation to the whole gland, although longer follow up is required to assess for late effects.

On the basis of studies successfully demonstrating acceptable toxicity from focal boosts ongoing trials using this therapeutic approach are currently recruiting. The largest is the multicentre phase III FLAME study which is aiming to recruit 566 patients to receive 77 Gy in 35 fractions +/-95 Gy integrated boost to DIL (Lips et al., 2011). It is powered to look for a benefit in biochemical failure rate at 5-years from DIL boosting and its toxicity data are awaited. The Princess Margaret Cancer Centre, Toronto, is carrying out a single centre phase II study aiming to treat 80 patients with 76Gy in 38 fractions plus an integrated 95 Gy boost or 10 Gy HDR brachytherapy boost (Chung and Menard, 2016). It is investigating local control rates at three years after treatment with repeat biopsies and secondary endpoints of toxicity and dosimetry.

Table 1-11: Outcome of multi-parametric MRI guided focal boost to dominant intra-prostatic lesion

Author	Pts	MR imaging	HT	Image fusion	Dose to DIL (dose PTV)Gy	Margin/ XRT	Comment/Acute toxicity
(Pickett et al., 1999)	1 Planning	?coil ?T ?FT MRS	Nil	Rigid bony anatomy	90 (70)	0mm 3D-CRT	Reduced rectal dose
(Xia et al., 2001)	1 Planning	?coil ?T ?FT MRS	Nil	Rigid	90 (75.6)	0mm IMRT	Within dose constraints
(De Meerleer et al., 2005)	15 Treatment	1.5T FT ERC T2W pre HT	18/7 HT in 8/15	Manual comparison	78.3 (76.9)	0mm IMRT	Dose gradient due to proximity rectum, no significant toxicity
(van Lin et al., 2006)	5 Planning	1.5T Not FT ERC DCE+MRS	Nil	Seed rigid	90 (70)	0mm IMRT	Reduced modelled rectal wall complication
(Singh et al., 2007)	3 (from 3) Treatment	3T ?FT ERC DCE, MRS	Nil	Rigid	94.5 (75.6)	3mm IMRT	No significant toxicity
(Fonteyne et al., 2008)	118 (from 230 assessed) Treatment	1.5T FT Pelvic coil 52 MRS 66 T2W Pre-HT	If int/ high risk	Off line	82 (78) 81 (78) (MRS detected)	8mm IMRT	No increased acute toxicity
(Miralbell et al., 2010a)	50 Treatment	?T ?FT ERC T2W Pre-HT	66% 6-30/12	Registered	Up to ≥100 (64)	3mm IMRT	50% ≥G2 GU 8%≥G2 GI
(Ippolito et al., 2012)	40 Treatment	1.5T ?FT ERC pre-HT	100% 2-3/12	Nil	80(72)	5mm within prostate + 1cm/8mm IMRT	9.55% ≥G2 GU 13.3% ≥G2 GI
(Onal et al., 2014)	15 Planning study	1.5T ?FT DCE, ADC, MRS	Unknown	Rigid	86 (76)	4mm IMRT vs VMAT	IMRT dose more homogeneous and higher to bladder. Low rectum dose significantly increased with both. VMAT less MU
(Riches et al., 2014)	23 Planning study	1.5T FT ERC DCE, DWI, MRS pre-HT 1.5T pelvic,T2W post-HT	100% 3/12	Non-rigid correcting for ERC, rigid to CT using Seeds	82 (74)	2mm	Decreased dose to rectum and bladder. Improved NTCP
(Schild et al., 2014)	78 Treatment	1.5T DWI, DCE T2W	41%	Registered	83 (77.4)	0mm	≥ G2 GI 19 ≥ G2 GU 53

DCE=Dynamic contrast enhancement, DWI=Diffusion weighted imaging, ERC- Endo-rectal coil, FT- flat top scanner, HT = Hormone therapy, Int=intermediate, MRS=Magnetic resonance spectroscopy, MU-Monitor units, NTCP-normal tissue complication probability, post-tx- MR imaging performed after neo-adjuvant HT, pre-tx- MR scan performed before neo-adjuvant HT, Pts=patients, T=Tesla, T2W=T2 weighted

The studies discussed previously have all delivered treatment using IMRT with or without a HDR boost. Newer approaches are possible such as volumetric modulated arc therapy (VMAT), treating patients in one or two continuous rotations of the gantry head rather than from multiple fixed positions. This technique is faster and, compared with IMRT, may be capable of boosting an intra-prostatic lesion whilst keeping OAR doses within tolerance in more clinical cases whilst reducing total radiation delivery (Shaffer et al., 2009; Onal et al., 2014).

Either a VMAT integrated boost (VMAT-IB) or an additional HDR boost (HDR-B) are acceptable methods to intensity therapy. The relative efficacy and toxicity of either approach has not been directly assessed.

1.3.5.3.1 *Technical Issues with summation dosimetry of HDR-B*

Reporting of rectal dosi0metry after combination EBRT with HDR boost has been addressed in multiple publications. The general approach to this has been to consider the HDR boost in isolation, assuming EBRT to be relatively uniform between patients (Hashimoto et al., 2015; Akimoto et al., 2006) or to consider the rectum to be uniformly irradiated by the EBRT dose when summing the two treatments (Okamoto et al., 2012). Both approaches are imperfect. Although the HDR dose to critical structures may be a significant contributor to late effect it is known that EBRT dose also influences outcome. Previously a correlation has been shown between rectal bleeding and anorectal V55-66 and between stool frequency and mean anorectal dose (Peeters et al., 2006; Michalski et al., 2010). Both of these parameters will be influenced by the rectal EBRT DVH.

It is possible to create dosimetric distribution maps for the HDR and EBRT which can be converted into EQD2 and summed giving a three dimensional representation of the combined treatment dose and allowing generation of DVH tables. Linear addition of dose matrices is recommended by the GEC-ESTRO working group for cervical cancer treatment planning, assigning a homogeneous EBRT dose (for example all patients prescribed 45 Gy would be considered to have a uniform EQD2 of 43.2 Gy to OAR) (Potter et al., 2006). This does not however account for deformation of anatomy between treatments.

The use of deformable registration to fuse images containing dynamic structures, accounting for variation in their shape and volume between imaging, is well established (Maintz and Viergever, 1998). Once a deformation vector field (DVF) is generated it can then also be applied to a dose grid located in the same Cartesian coordinates. It has been shown, applying this method to pelvic planning CT for cervical cancer patients receiving a HDR boost, that there is a significant variation between deformed D2cc and uniform dose D2cc to OAR (Kim et al., 2014). Using deformable dose summation three out of ten patients were shown to exceed OAR dose constraints which were met with GEC-ESTRO recommended methods. The deformable registration of rectal contours from EBRT and HDR CT imaging for prostate treatment has also been explored with a view to future dosimetric analysis and been shown to improve over rigid registration (Moulton et al., 2015).

The effect of deformation of dose in comparison to summation of rigid dose fields, rather than homogeneous EBRT dose, has not been assessed. The delivery of an MRI guided HDR boost

requires the insertion of an endo rectal coil at the time of treatment. This distorts rectal architecture and can change the proximity of rectal wall and prostate. When performing dosimetric analysis of EBRT with HDR-B this change in proximity would mean that summation of the dose matrixes of both therapies, converted to EQD2, and applied to OAR delineated on the CT planning scan may misestimate the dose received by the anterior rectal wall. To accurately correlate delivered dose and subsequent toxicity the effect of this deformation should be assessed.

1.3.5.3.2 *Conversion of dose*

The summation of dose from two radiotherapy treatments requires them to be converted into equivalent fractionation regimes. By way of an example 45 Gy delivered in one fraction is likely to be uniformly fatal, while 45 Gy given in 25 fractions is a commonly used and well tolerated treatment. The differing effects of fraction size can be accounted for by converting any dose into its 2 Gy per fraction equivalent (EQD2), using the formula:

$$EQD2 = D(d + \alpha/\beta)/(2+ \alpha/\beta)$$

Where D = Total dose

d = Dose per fraction

α/β= a measure of the relative radio-sensitivity of a tissue to differing fractionations

The value for α/β is obtained by observation of delivered dose and subsequent outcome and as such has changed over time for different tissues as new data becomes available.

The α/β for many tumours is around 10 Gy however for prostate cancer it has been found to be significantly lower, somewhere between 1.5 – 3 Gy, with recent analysis supporting a value of towards the lower end of this range(Brenner et al., 2002). The α/β ratio for rectal late effects appears to be 3-5 Gy (Michalski et al., 2010; Brenner, 2004).

When applying the EQD2 formula any value within these ranges could reasonably be used. An attractive option is to choose an α/β of 3 Gy for both rectum and prostate; this permits the same correction to be applied to the entire dose grid when converting to EQD2 and a single summation procedure to be performed. The calculated EQD2 of a HDR-B is reduced by using an α/β ratio of 1.5 Gy in place of 3 Gy. This should be considered in analysis of the dosimetric outcome of this therapy.

1.3.5.3.3 *Effect of Androgen Deprivation Therapy on disease identification*

No reported results have made allowance for the potential for variable response to HT when targeting an area of disease within the prostate for focal dose escalation. MP-MRI has been performed prior to any hormone therapy in all cases due to concerns about detectability of disease following treatment. It has been demonstrated through DCE-MRI that HT induces a dramatic reduction in prostate vasculature (Alonzi et al., 2011). Within 4 weeks of starting treatment blood volume and flow within the prostate reduce by 83% and 79% respectively and by 3 months significant increases in T2* relaxation occur. The reduction in volume and vascularity makes tumour detection more challenging after hormone therapy but changes in DCE-MRI appearance

have been proposed as a marker of response to HT to monitor for resistance and guide disease management (Barrett et al., 2012). An appreciation of the changes in prostate appearance following > 3 months HT with significantly higher diffusion and lower perfusion of prostate tumour has meant MP-MRI routinely being performed prior to HT for tumour delineation. It has been suggested that imaging post HT is unreliable for this role. This may not necessarily be the case; one study of 21 patients found after a course of HT 18 still had an identifiable suspicious lesion (Groenendaal et al., 2012b). Another found no significant difference between pre and post HT ADC values, except in the ratio of tumour to peripheral gland results, with ADC able to differentiate between tumour and benign tissue in this location (Riches SF, 2007).

Imaging post HT is attractive in that it may allow for identification of disease that is resistant to hormone therapy and that may benefit most from a focal RT boost. Animal studies show that androgen responsive tumours with a >50% volume reduction following HT are significantly more likely to be eradicated by radiation (Zietman et al., 1997a). Therefore focal boosts may be most beneficially directed towards tumours with a lower volume reduction following HT. In addition radiotherapy will be given to a post HT prostate. If there has been a disproportionate reduction in tumour volume relative to the remaining gland, conceivably due it increased vascularisation, then the dominant lesion boost will be administered to an unnecessarily large volume using pre HT MP-MRI even if correcting for overall gland shrinkage with image registration. Any intra-treatment MP-MRI will by necessity be post HT for some intermediate and all high risk disease and therefore an effective way of interpreting imaging in this setting has clinical relevance. Further the recommended combination of T2W, DCE plus DWI for disease identification was used in only one cohort in the above studies to identify the DIL post HT. This combination would be expected to improve sensitivity and specificity based on previously discussed results.

MP-MRI is unable to precisely define the extent of an identified disease. Differing MRI techniques can show apparently conflicting information with limited areas of overlap (Groenendaal et al., 2010b). Using MP-MRI and applying a common margin of 5mm to identified tumour encompassed on average 85-100% of histologically confirmed disease (Groenendaal et al., 2010a). An expansion margin this large would risk delivering dose escalation to an unnecessarily large volume. An alternative solution is to assign a GTV boost to areas of overlap and high certainty with areas of less certainty encompassed within a lower dose CTV margin, or even more complicated methods to vary dose dependent on calculated probability of disease (Groenendaal et al., 2012a; Langer et al., 2009).

1.3.5.3.4 *Benefit of Androgen Deprivation Therapy with focal dominant lesion boosts*

The use of hormone therapy with dose escalation to a dominant lesion is variable. A large proportion of patients treated on studies of focal escalation have had intermediate risk disease. Their localised tumours with lower likelihood of disseminated disease make them good candidates for intensified local therapy. Whether HT should be offered to intermediate risk disease receiving a targeted boost is unclear with limited data available from EBRT trials (Table 1-12). Two studies have reported prospective results. The EORTC 22991 study randomized 819 men with intermediate or high risk disease to 70-78 Gy with or without six months concomitant and adjuvant hormone therapy. 74.8% of those enrolled had intermediate risk and 24.8% high risk disease.

Table 1-12: Summary of published outcomes for intermediate risk prostate cancer receiving dose escalated external beam radiotherapy with or without hormone therapy

	Study type	**No. patients**	**Proportion intermediate**	**Treatment**	**Proportion receiving HT**	**BFS (HT vs no HT)**	**Conclusion**
(Ciezki et al., 2004)	Retrospective	237	100% IR	Median 78Gy +/-median 6/12 HT	59%	84 vs 81% (p=0.6) @ 5 years	No benefit
(dubray et al., 2011a)	Prospective	377	100% IR	80 Gy +/- 4/12 HT	47%	97 vs 91% (p = 0.04) @ 3 years	Benefit
(Krauss et al., 2011)	Retrospective	365	100% IR	Median 79.6 Gy +/- median 6/12 HT	20%	89.2 vs 86.2% (p = 0.59) @ 4 years	No benefit
(Valicenti et al., 2011)	Retrospective	291	100% IR	Median 79/77.4 Gy +/-	25%	77 vs 82% (p > 0.05) @ 5 years	No benefit
(Bian et al., 2012)	Retrospective	636	48% F-IR 52% U-IR	>75Gy +/- median 6/12 HT	40% F-IR 66% U-IR	F-IR 97.4 vs 96.3% (p = 0.874) U-IR 92.9 vs 81.6% (p=0.009) @ 5 years	Benefit only in U-IR
(Castle et al., 2013)	Retrospective	418	62% F-IR 38% U-IR	75.6-78Gy +/- <=6/12 HT	28% F-IR 56% U-IR	F-IR 95 vs 94% (p=0.8546) U-IR 94 vs 74% (p=0.005) @ 5 years	Benefit only in U-IR
(Zumsteg et al., 2013b)	Retrospective	710	100% IR	>=81 Gy +/- median 6/12 HT	50%	80 vs 67.5% (p = 0.003) @ 10 years	Benefit
(Schreiber et al., 2014a)	Retrospective	203	100% IR	>=75.6Gy +/-median 6/12 HT	21%	89.2 vs 76.7% (p = 0.02) @ 6 years	Benefit
(Bolla et al., 2016)	Prospective	819	74.8% IR 24.8% HR	70-78 Gy +/- 6/12 HT	50%	Significantly reduced @ 7.2 years	Benefit
HT = Androgen Deprivation Therapy, BFS = Biochemical failure free survival, F-IR = Favourable intermediate, HT = Hormone Therapy, U-IR = Unfavourable intermediate,							

After 7.2 years the addition of hormones had a significant beneficial effect on BFS and clinical PFS with hazard ratios of 0.53 and 0.63 respectively (Bolla et al., 2016). Analysis of the GETUG 14 study randomizing 377 patients with intermediate risk disease to 80Gy to prostate plus 46Gy to seminal vesicles with or without 4 months HT showed BFS of 97% and 91% (p=0.04) respectively at three years follow up (dubray et al., 2011a).

Retrospective data are available from several series, with conflicting results. Analysis of outcome for 710 intermediate risk patients treated with ≥ 81Gy (mean 83.4Gy) DE-EBRT at Memorial Sloan-Kettering Cancer Centre from 1992-2005 showed a benefit from HT with BFS of 80% and 67.5% (p = 0.003) at 10 years for those who did or did not receive HT (Zumsteg et al., 2013b). Another retrospective analysis looked at 203 intermediate risk patients treated from 2003-2010 who received ≥75.6 Gy with or without a median of six months HT (Schreiber et al., 2014a). Radiotherapy alone was received by 79% of patients with BFS at six years, 89.2% and 76.7% (p = 0.02), favouring those receiving additional HT. A review of 2000 patients receiving varying doses of EBRT also found that doses ≥ 81 Gy and the use of HT were associated with improved outcome in intermediate and high risk patients (Zelefsky et al., 2011).

In contrast other retrospective studies have failed to identify any benefit. A retrospective series of 365 intermediate risk patients receiving a median dose of 79.6Gy EBRT to isocentre found no significant benefit in BFS at 4 years, 89.2% vs 86.2%, from the addition of HT for a median of 6 months (Krauss et al., 2011). Of note only 73 patients received HT and those who did had worse disease characteristics. An analysis on 883 patients enrolled on RTOG 9406, a phase I-II dose escalation study, whose mean PTV dose exceeded 73.8 Gy, found no benefit to HT for any risk group from Cox proportion hazards regression modelling although BFS improvement approached significance in high risk disease (Valicenti et al., 2011). This study had 291 intermediate patients of whom 74 received HT for not longer than 6 months before EBRT. A third analysis of 237 intermediate patients receiving a median of 78 Gy with or without a median 6 months HT showed a non-significant five year BFS increase from 81% to 84% (p=0.6) from the addition of hormones (Ciezki et al., 2004)

Finally two studies have looked at the effect of sub-classification. In the first disease was retrospectively classified as favourable or unfavourable in 636 patients with intermediate risk disease treated to >75Gy with or without an average of 6 months HT at MD Anderson (Bian et al., 2012). A significant benefit in five year BFS from the addition of an LHRH agonist, increasing from 81.61% to 92.9% (p = 0.009), was seen only in those with unfavourable disease, which was identified using recursive partition analysis as primary Gleason 4 or ≥50% positive cores and no moderate or severe comorbidity. For those with favourable-intermediate disease BFS was 97.4% vs 96.3% (p = 0.874). Another retrospective study reviewed 418 patients receiving 75.6-78Gy with or without up to 6 months HT (Castle et al., 2013). Again a BFS benefit from the addition of HT was only seen in unfavourable-intermediate disease, defined from recursive partition analysis as Gleason (4+3) or T2c disease, with an improvement from 74 to 94% at five years. These results must be interpreted with caution as neither stratification has been prospectively validated.

Further work assessing the benefit of HT with DE-RT for stratified intermediate risk disease is therefore of interest. Although various criteria to sub-classify intermediate risk disease have been proposed that by Zelefsky et al (primary Gleason pattern 4, percentage of positive biopsies ≥ 50% or ≥ 2 intermediate risk factors) has subsequently been validated from a prospective cohort by Keane et al at providing merit for its use in other groups (Keane et al., 2014; Zumsteg et al., 2013a).

Given the degree of uncertainty of benefit from the addition of HT to whole gland dose escalation it is even more challenging to have certainty of role with a focal ultra-escalated boost. Any potential clinical improvement has to be considered against the additional difficulty in the identification of disease that HT administration may introduce and the associated morbidity.

1.3.6 *Confirmation of disease by targeted biopsy*

MP-MRI is the optimal imaging modality for identification of significant cancer within the prostate (Weinreb et al., 2016). Despite this there remains a risk of false negative or positive findings; one meta-analysis of studies of PIRADS v1 scored MP-MRI, all using differing definitions of significant disease, found an overall sensitivity of 0.78 (85% CI 0.70-0.84) and specificity of 0.79 (95% CI 0.68 – 0.86) (Hamoen et al., 2015). This is of concern when planning dose escalation based on MP-MRI and is a rational for a targeted biopsy to confirm the presence of localised significant disease prior to delivery of a focal boost. The positive predictive power of a pre-biopsy MP-MRI for subsequent discovery of any disease is increased with lesions with higher PIRADS scores (Futterer et al., 2015). There is limited data on the likelihood of disease within a particular lesion seen on MP-MRI but the positive predictive power for a PIRADS 4/5 lesion appears high. In one series assessing MP-MRI accuracy using subsequent whole mount prostatectomy specimens PIRADSv1 4-5 lesions had a positive predictive value of representing disease of 96% and 98% respectively while others have also shown PIRADSv2 4 lesions to have PPV 96% (Delongchamps et al., 2015b; Baur et al., 2014).

MRI guided biopsy can be performed with trans-rectal US or MRI with samples taken using a trans-rectal or perineal approach, either in-bore or outside of the magnet (Marks et al., 2013; Robertson et al., 2013). MR and US imaging may be combined using visual registration- the operator has a recent MP-MRI image available on separate screen to use in combination with real time US- or the images may be fused and viewed on one display. Visual registration may be challenging, and is dependent on the real time identification of landmarks to allow information from the MR image to be accurately matched to the US. This method may be inferior to fusion of MR and US images at detecting cancer, although a recent meta-analysis found no significant difference (Delongchamps et al., 2013; Schoots et al., 2015). It has been shown in a randomized study that no significant benefit is obtained from trans-rectal biopsies performed with MR-US guidance biopsy plus systematic TRUS biopsy compared with in-bore MR guided biopsy alone, despite requiring significantly more biopsy samples and speaking to the value of in-bore MR guidance (Arsov et al., 2015). Trans-perineal biopsy have also been shown to improve detection and reduce false negative results in comparison with a trans-rectal approach (Chang et al., 2013). The trans-perineal

approach reduces the risk of post-biopsy sepsis and can effectively target anterior gland disease but requires general anaesthesia (Lange et al., 2009; Satoh et al., 2005; Merrick et al., 2008).

The use of in-bore MR guided biopsies allows for visualisation of the target lesion and confirmation of accurate needle deployment. The technique was first reported in 2001 but has had limited subsequent data published on its efficacy (Hata et al., 2001). A recent report demonstrated its efficacy and safety in detecting cancer in patients with positive MP-MRI findings but no information on correlation of biopsy findings and initial imaging characteristics or accuracy of targeting was provided (Penzkofer et al., 2015). It has been demonstrated in one study that out of bore trans-rectal MR-US fusion targeted biopsies yield significant disease in 86% and 93% of PIRADS 4 and 5 lesions targeted but that a benign biopsy has a negative predictive value (NPV) of only 29% and 25% for each grade respectively (Delongchamps et al., 2015b). Despite this multiple studies have used MR-guided biopsy as the standard against which PIRAD classification sensitivity and specificity is assessed (Schimmoller et al., 2013) (Baur et al., 2014).

Given the high PPV that PIRADS 4/5 lesions appear to achieve, the low NPV of targeted biopsies calls into question their value prior to focal dose escalation. It is of interest whether in-bore MR-guided trans-perineal biopsies can improve on this NPV, as failing to dose escalate following a negative result may otherwise carry a high risk of not treating an area of significant disease. Of particular interest is assessment of the mechanism of negative targeted biopsies; whether this is due to inaccurate targeting or a product of imaging misrepresenting the true tumour location. By performing in-bore biopsy imaging can be taken pre- and post-procedure to confirm accurate sampling and correlation to histology. It would seem possible that even with MR-guidance biopsies, particularly from the base of the prostate may be deflected from their intended target.

The growing interest in MRI-targeted biopsy has been hindered by variation in reporting of participants, technique and definition of disease. For example a fraction of Gleason 6 disease identified in a targeted PIRADSv2 5 lesion can be reported as positive but is likely to represent incidental biopsy of a satellite lesion than the disease targeted and may not be clinically significant. For that reason the Standards of Reporting for MRI-targeted Biopsy Studies (START) has been established (Moore et al., 2013a). In particular a definition of significant disease is required but there is not a present consensus on what this is. Various combinations of disease grade and/or core involvement proposed and are considered acceptable for reporting (Epstein et al., 1994; Goto et al., 1996; Ahmed et al., 2011).

1.3.7 *Evaluating disease response during radiotherapy*

An attractive area for research is whether changes in function parameters during EBRT are predictive. These may allow identification of patients who would benefit from an escalation of delivered dose, due to a high risk of disease recurrence, accepting a potential increased risk of treatment related toxicity. The use of ADC as an early clinical marker of treatment response has a role in high grade glioma and may be applicable to other sites. Changes in diffusion properties three weeks after completing treatment for diffuse malignant glioma have been found to predict for response at ten weeks and time to relapse (Hamstra et al., 2005). In rectal cancer post chemo-radiotherapy ADC levels appear significantly higher in complete responders, potentially avoiding

surgery in selected cases (Kim et al., 2009b). It has also been shown in rectal cancer that a low pre-treatment ADC, and significant treatment induced changes, predicts for a better response to chemo-radiotherapy (Lambrecht et al., 2012). This may reflect an increased necrotic component with associated areas of hypoxia in those with high pre-treatment ADC, likely to cause radio-resistance. Work has also been carried out with squamous cell carcinoma of the head and neck, showing an association between ADC elevation at one week and prognosis (Kim et al., 2009a).

It has been demonstrated that the ADC within the prostate is related to cell density and is reduced in malignant tissue relative to the normal gland (Zelhof et al., 2009). Further there appears to be an inverse relationship between Gleason score and mean ADC (Vargas et al., 2011). Both of these phenomena are likely to represent the increased density of more aggressive disease disrupting water diffusion. Multiple studies have also demonstrated a relationship between changes in ADC and administration of systemic agents. For example it has been shown that changes in perfusion of xeno-grafted prostate disease, but not normal tissue, following administration of the tyrosine kinase inhibitor sorafenib, are sufficient to induce detectable changes in ADC, which significantly correlate with cell apoptosis (Cyran et al., 2012). Following HT ADC has also been demonstrated to rise, likely a consequence of induced cell shrinkage, atrophy and apoptosis, with associated marked reduction in tumour volume, density and capsule penetration (Bullock et al., 2002; Hotker et al., 2015).

Data on changes in functional imaging of the prostate during and after radiotherapy has been published by multiple studies (Table 1-13). Radiotherapy induces an increase in tumour ADC during and post treatment with peak values consistently seen on post treatment imaging. This may be due to a reduction in the cell density of disease following treatment and disruption of its architecture. In the one study with a conflicting result of ADC falling slightly between week six and eight of treatment there is no post treatment value to confirm a continued fall and it may be this represents artefact in the context of the other studies findings (Foltz et al., 2013). By contrast normal tissue values appear to fall slightly following treatment presumably due to fibrosis. Post treatment there is no significant difference in ADC of tumour and surrounding normal stroma. No studies have assessed ADC changes in a high risk disease cohort. Patients with high grade disease may be particularly likely to benefit from identification of poor response during therapy. These patients should, on the basis of available evidence, receive HT prior to radiotherapy. Whether ADC can identify changes during radiotherapy in such a patient cohort has not yet been addressed. The available evidence would suggest a rise in the ADC of tumour following neo-adjuvant HT (NA-HT) would reduce any variation with surrounding normal tissue, making disease identification challenging at the time of RT. Having pre-HT imaging to guide identification would be of value. Changes in prostate tumour ADC during RT are also likely to be attenuated.

DCE-MRI has been shown to have predictive for administration of systemic agents. DCE-MRI changes in perfusion of xeno-grafted prostate disease, but not normal tissue, following administration of the tyrosine kinase inhibitor sorafenib are detectable and significantly correlate with cell apoptosis (Cyran et al., 2012).Other work has looked at changes in DCE parameters before and post prostate radiotherapy, predominantly in the context of identifying recurrent disease. Two studies looked at changes through treatment. Kershaw et al studied 20 patients, performing a

baseline DCE scan, using a 1.5 T scanner, and a repeat 12-17 months after completing radiotherapy (Kershaw et al., 2008). All patients received neo-adjuvant ADT following the initial scan. Significant changes were found following treatment with reduction in tumour blood flow and permeability. It is impossible to comment how much of this is due to ADT. Subsequently Franiel et al imaged 6 patients with a 1.5T scanner and ERC before, at the end of radiotherapy and twice subsequently (Franiel et al., 2009). The cohort were found to have an increase in tumour perfusion immediately after treatment which then declined significantly over the next year. The extraction co-efficient was found to fall initially before rising to pre-treatment levels at the end of one year. Unpublished work by Foltz et al, imaging 25 patients fortnightly through 8 weeks of treatment using a 1.5 T scanner, found increases in Toft kinetic parameters from week 2 (personal communication). Extra-vascular volume appeared to correlate with radiotherapy effects. No scans were taken following completion of treatment. These studies show that changes in DCE characteristics do occur with radiotherapy and suggest that these may start to occur early in treatment. As for DWI imaging the work is limited by the lack of data on the effects of radiotherapy on patients receiving ADT, who would be a target for future dose escalation.

Functional imaging performed during therapy would see largest changes towards the end of treatment; imaging at around three quarters of the way through therapy might allow identification of prognostic changes, if present, whilst allowing for treatment intensification by extending therapy or adding a focal boost if felt indicated. ADC rises continue after completion of RT, although for how long is unclear and repeat imaging in the months after RT completion might be most likely to identify changes following combination therapy which predict for ultimate outcome.

Overall this is an area requiring further exploratory work. It is known that changes occur within the prostate during treatment but these have not yet been successfully correlating this with outcome. One study has shown significantly lower post RT ADC values in those who ultimately relapse (Liu et al., 2014a). This could inform surveillance strategies and early salvage therapies but not initial treatment intensification to prevent relapse.

Table 1-13: Changes in DWI during and after radiotherapy treatment

	Pts Av GS Av PSA	MR sequence	ADC ($x10^{-3}mm^2/s$) tumour						Comment
			pre tx	After 25% of tx	After 50% of tx	After 75% of tx	End tx	post tx	
(Takayama et al., 2008)	9 GS 7 PSA10.6	1.5T b=0,700	1.07	-	-	-	-	1-9m post 1.41 P<0.01	Malignant ADC significantly lower than benign pre-tx. Difference disappeared post tx
(Song et al., 2010)	49 GS 7 PSA 43	3T b=0,1000	1.0	-	-	-	-	1-5m post 1.61 p<0.05	Malignant ADC significantly lower than benign pre-tx. Difference disappeared post tx
(Park et al., 2012b)	8 GS 6 PSA 9	3T b=0,100,1000	0.86	1.03 P=0.005	1.15	-	-	1m post 1.26 P<0.001	Malignant ADC significantly lower than benign pre-tx. Difference disappeared post tx
(Iraha et al., 2012)	14 GS 7 PSA 31.4 (0.7 post HT)	1.5T B=0,800,200	0.76	-	-	-	-	NS 1.02 P = 0.001	Received HT prior to RT. 14 of 44 patients with persistent disease post HT assessed
(Foltz et al., 2013)	17 GS 7 PSA 7.8	1.5T b=0,600 b=0,1200	1.13 0.85	1.21 0.90	1.24 0.91	1.30 0.97 (P=0.013)	1.28 0.91	- -	Maximum change in tumour at 6/52 (p = 0.013), in whole gland at 2/52
(Decker et al.)	13 GS 7 PSA 13	3T b=0,800 b=50,800	1.06 1.0	-	1.23 1.16	-	1.28 1.21	3m post 1.41 1.34 p<0.01	Malignant ADC significantly lower than benign pre-tx. Difference disappeared post tx. Changes more marked higher grade, easily identified disease
(Liu et al., 2014b)	78 G 7 PSA > 20	3 T B= 0,800	1.04	-	-	-	-	1-4m post 1.45 P < 0.001	Significantly higher rise is patients not recurring (p < 0.001)
ADC=Average diffusion co-efficient, Av=average, GS=Gleason score, m=months, Pts=Patients, T=Tesla, tx=treatment									

1.4 Medical Image registration and fusion

Conventional RT planning requires CT imaging to provide information on electron density, allowing for calculation of radiation attenuation and dosimetry. For effective integration of MRI into the planning process identified structures of interest, such as the DIL, must be accurately transferred to the CT image which can be achieved in various ways. The most straightforward is to display the two data sets alongside one another with a human operator comparing relevant slices of data but it is challenging to ensure matching images are being compared. Alternatively the two images can be combined as a single output, which has been shown to improve delineation of critical structures (Panigrahy et al., 2000).

The combining of two independent sets of images, with variations in scale, orientation and appearance provides significant challenges for accuracy and reproducibility. The objective of any approach is to achieve a final transformation that most accurately represents the area of interest. Integration of two images requires two steps; an initial registration whereby the images are brought into spatial alignment and a subsequent fusion to allow their integrated display (van den Elsen et al., 1993).

The most straightforward approach to image registration is to perform different imaging sequences in the same Cartesian coordinates by calibrating two scans, allowing for non-image based registration. This is not generally possible with CT and MR imaging, which are performed on different machines at different times. In future with the potential development of combined MR-CT linacs this may become a more common solution (Sjoerd and Bas, 2014).

When Cartesian coordinates are not matched an alternative approach is to base registration of image sets upon extrinsic objects introduced into the image. For registration optimisation the imaging protocols should be matched. Conventionally CT imaging is performed with the patient lying on a flat couch while MRI scanners have couch with a slight transverse curve due to its narrow bore. This can cause changes in patient positioning. A temporary flat top can be added to the MRI couch, reducing the clearance in bore slightly, which improves reproducibility between the two images, aiding registration. Extrinsic objects can be invasive, such as a stereotactic frame for imaging of the brain, or non-invasive with potentially less accuracy, such as skin markers. They are designed to be visible to all imaging modalities and allow for quick, accurate orientation and registration of images. Regardless of approach, it is prospective and must be planned prior to any imaging occurring.

Neither matching of Cartesian coordinates of the use of extrinsic marker can provide information on alterations of internal structure between images, i.e. movement of organs. The fixation of extrinsic markers can also be potentially intrusive for the patient.

By contrast intrinsic objects allow for the internal movement of structures by using a set of landmarks within the imaged anatomy, segmentation of structures or analysing information on image intensity contained within voxel properties. Point based registration uses landmarks that are identifiable anatomical points or areas of geometrical distinction such as corners, bifurcations and edges. More complex intrinsic registration methods may be surface or voxel base and are not

discussed further. The identification of landmarks generally requires some user input, preventing a fully automated process. Once landmarks are identified they generally allow for rigid or semi-deformable transformations and can be combined with other deformable registration processes to prevent large mis-matches and increase speed. An optimisation algorithm can be iteratively applied during a transformation to minimise distance between marker points to give a best fit registration(Besl and McKay, 1992). For accurate deformable registration, good initial registration is required to bring appropriate points into close alignment. Any significant variation can propagate marked errors into the registration process.

CT imaging is unable to routinely identify interstitial prostate anatomy which may be seen on MRI. Consequently the use of shared anatomical points prostate within the prostate to guide registration of the image sets is problematic. To overcome this issue gold seeds have commonly been implanted into the prostate to act as fiducial markers. These are visible on CT and MRI and provide common points to guide accurate rigid registration during planning imaging. They can be easily identified on imaging performed during treatment to assist image guided radiotherapy (IGRT) (Parker et al., 2003).

The insertion of fiducial markers risks morbidity however, with a recent series finding the procedure causing uro-sepsis in around 1 in 13 patients and around 1 in 40 required hospital admission for treatment (Loh et al., 2015). The routine use of fiducial markers for treatment set up has ceased in some centres as a consequence and alternative methods of registering MR and CT images in their absence is of interest.

1.4.1 *Assessment of registration accuracy*

For comparison of registration techniques a method of assessing accuracy is required. If common points are identified then the distance between these once registration is complete is one such method. For this approach a minimum of three shared points, either anatomical points or fiducial markers, are required to localise a structure's orientation in three dimensional space. The distance between mutual points on two registered image sets can be reported in various ways to assess registration accuracy. For example if the mutual points furthest apart after registration have most clinical significance, then the root mean squared error will emphasise these data points. This is calculated by the summing the square of the distance between mutual points then dividing by the number of distances measured and taking the square root of the answer. Alternatively if outliers from the average displacement would skew interpretation, for example the displacement of one set of mutual points may be far worse than others for unexplained technical reasons that do not reflect the overall registration accuracy, then the mean absolute error will be less influenced by this variation. The mean absolute error is calculated by summing all of the distances and then dividing this by the number of distances measured.

When using fiducial markers for assessing registration accuracy their centroid can be taken as the mutual point and the minimum root mean squared distance between them on the two image sets represents optimal registration. Alternatively the fiducial markers can be segmented and converted into a surface model using planning software and registration of the surfaces that minimises the root mean square distances using an automated iterative closest point method can be performed.

This has been demonstrated to significantly improve upon registration using fiducial marker centroids and therefore most closely represents optimal matching against which to compare registration techniques (Huisman et al., 2005).

If common points are not available then the agreement of the delineated outline of the organ of interest on each image set can be assessed. This delineation may be performed automatically but will usually require operator input. Assessment of correlation may be measured using various metrics depending on which errors are of most concern. For example the Hausdorrf metric measures the furthest distance between sets of points and is therefore sensitive at detecting fidelity of shape between structures which may have small volume (Huttenlocher et al., 1993). Alternatively overlapping ratio measures, such as the Tanimoto Coefficient (TC) or Dice Similarity Coefficient (DSC), are sensitive to translational errors but relatively insensitive to changes in volume or shape (Crum et al., 2006). For rigid registration of a structure which has not changed in shape or volume between the two image sets these are both widely used options. Both TC and DSC range between 0, no overlap, to 1, complete overlap and are related by:

$$DSC = 2TC/(TC + 1)$$

Such that they are equal at the extremes (0,1) and DSC > TC between these values. Both are used in the literature although DSC is more commonly reported and therefore can provide some comparable metric between different studies. DSC has demonstrated efficacy as a summary measure of spatial overlap of manual prostate segmentation (Zou et al., 2004)

1.5 Summary, hypotheses and aims

MRI improves prostate identification and allows for a reduction in the volume of delineated GTV and subsequent dose delivered to nearby OAR (Table 1-7). Large quantities of data regarding the likely benefits of MRI for planning and IGRT have been collected over the last two decades. MRI will soon be increasingly incorporated into routine imaging during therapy and IGRT with the development of commercial MR-Linac solutions (Lagendijk et al., 2014). The implications of this for practice are as yet unclear. A review of available published data would help to inform carefully considered future studies.

To be effectively used in combination MR and CT images must be accurately registered in 3-D space. This registration can be performed based upon interstitial points, usually inserted fiducial markers, which can also be used to validate registration accuracy. Conventional CT imaging does not appear to offer sufficient resolution to allow differentiation of interstitial structures for this purpose. Novel image acquisition strategies may permit this and remove the need for fiducial markers insertion with associated potential morbidity (Catton and Alasti, 2016).

Randomised trials of dose escalation in treatment of prostate cancer up to 74-80 Gy have shown improvements in biochemical free survival (Table 1-5). Prospective studies have not shown an improved overall survival advantage but this is suggested by retrospective analysis (Kalbasi et al., 2015). This failure to demonstrate a survival advantage may in part be due to sub-optimal HT use.

Dose escalation of radiotherapy to the prostate beyond 80 Gy is limited by additional toxicity to surrounding organs at risk, in particular the rectum and bladder. The use of IMRT and optimal IGRT has allowed some groups to safely escalate EBRT to 86.4 Gy (Zelefsky et al., 2011). Early malignant changes may be treated effectively with 64 Gy but a tumourcidal dose for a resistant focus of disease may be significantly in excess of 80 Gy, possibly ≥ 96 Gy (Nahum et al., 2003). It has been shown that relapse is most likely to occur at the site of original disease (Cellini et al., 2002b). Multiple planning studies and small treatment groups have demonstrated the feasibility of giving an additional boost to a dominant area of disease although no group has reported late toxicity for patients receiving an IMRT focal boost to greater than 80 Gy.

The use of MRI in the planning process improves visualisation of the prostate, reduces treatment volumes and consequently reduces the dose of radiation received by nearby organs at risk (Table 1-7). Its use should reduce further associated toxicity from dose escalation. The use of VMAT in place of IMRT is faster, further reduces dose to OAR and reduces overall exposure to radiation. Biopsy of an identified lesion prior to dose escalation to confirm the presence of malignancy has merit but appears to carry a significant risk of a false negative finding (Delongchamps et al., 2015b). The effectiveness of in-bore MR-guided trans-perineal biopsies in this setting has not been reported.

Preliminary work has been performed looking at changes in MP-MRI during a course of radiotherapy. This has been carried out with the ultimate aim of identifying patients who are responding poorly to treatment in order to permit selected treatment intensification. Given the already excellent outcomes in low risk cancer it is likely this intensification may be most beneficial in some intermediate and high risk disease. All high risk and most intermediate patients currently receive NA-HT as standard therapy and therefore changes in MP-MRI following NA-HT are of clinical interest; no group has yet assessed MP-MRI changes during RT for this patient group. HT has been shown to improve overall survival for patients receiving radiotherapy and is routinely recommended for patients receiving dose escalated radiotherapy for high risk disease. The evidence for its use in intermediate disease is conflicting (Table 1-12). Available evidence suggests a biochemical relapse free survival benefit from its addition. No survival benefit has yet been demonstrated, although this may be seen with longer follow up.

This thesis tests the hypotheses that:

- MR and CT image registration can be improved after visual registration using interstitial prostate structures.
- In-bore MRI guided biopsy of high PIRADS score lesions prior to focal dose escalation does not have clinical utility.
- A focal boost of 214 -270 Gy BED is possible without unacceptable toxicity.
- Changes in functional parameters of malignant prostate tissue during RT after a course of NA-HT are predictive for subsequent clinical outcome.

- The addition of hormone therapy to dose escalated radiotherapy improves clinical outcome and combination therapy should be considered in studies of a focal dose to the DIL.

Testing of these hypotheses supports the over-arching purpose of the thesis is to investigate the role of MRI to facilitate improved radical prostate radiotherapy through improved treatment planning, delivery, and adaptive radiotherapy by assessment of response to radiotherapy. In chapter 2 current available data on prostate motion and set up uncertainty during radiotherapy is collated to provide a resource for rationalised treatment planning with evidence based margin expansions. The role of MRI in improved radiotherapy delivery systems, particularly as part of an integrated MRI-Linac is discussed and potential future developments hypothesised. In chapter 3 the challenges of integrating MRI into a CT based work flow system are addressed; the issues of image registration are discussed and a novel method of CT/MRI registration based upon interstitial prostate structures is investigated. As previously discussed MRI allows for identification of areas of high disease burden within the prostate and Chapter 4 builds upon this looking at the implication of having combined MR/CT imaging to plan treatment delivery, in particular whether lesions with high risk features on MP-MRI require confirmatory in-bore MRI guided biopsy before targeting for treatment intensification. The implications of a focal dose escalation, delivered as a HDR or integrated VMAT boost, are addressed in Chapter 5 with the dosimetric outcome of these two approaches in a cohort of patients and the associated acute and early late toxicity analysed with differences between the two techniques investigated and discussed. Finally the possible role of MRI in future adaptive prostate radiotherapy is considered; the ability of MP-MRI, performed during a course of radiotherapy, to predict for ultimate outcome is assessed in Chapter 6. In particular its ability to perform this role in a group of patient receiving NA-HT, a standard treatment in higher risk patients that may however impair MP-MRI tissue differentiation, is investigated for the first time. Additionally the necessity of the use of NA-HT in intermediate risk disease is assessed through analysis of the long term outcomes of a randomised study of the benefit of bicalutamide to dose escalated radiotherapy and is reported in appendix A. The implications of NA-HT use on the effectiveness of MP-MR to predict treatment response are discussed and recommendations for future practice made.

The specific aims of this thesis are:

- To collate previously published data on the use of MRI for prostate radiotherapy and to analyse its potential role in future studies for the MR-Linac.
- To determine whether registration of MR and CT images for prostate radiotherapy planning can be performed effectively without patients having to undergo invasive fiducial markers insertion, instead using prostate interstitial structures identified on novel CT imaging techniques for registration.
- To assess the positive and negative predictive power of in-bore trans-perineal MR-guided biopsies of the area of dominant disease in patients with known prostate cancer and it's utility for deciding eligibility for dose escalation.

- To review a cohort of patients receiving a focal prostate boost to greater than 250 Gy BED using HDR brachytherapy or a VMAT integrated boost. To assess dosimetry and associated toxicity following each approach.
- To quantify changes in DWI and DCE characteristics of malignant and benign prostate tissue during a course of radiotherapy, following neo-adjuvant HT.

The results of these separate chapters are then reviewed in Chapter 7 and the implications for the use of MRI in radical prostate radiotherapy discussed. Future directions for research and likely developments in future treatment are expanded upon, providing a blueprint of the future role MRI may play in this setting.

Chapter 2: MRI-guided prostate adaptive radiotherapy – a systematic review

McPartlin AJ, Li XA, Kershaw LE, Heide U, Kerkmeijer L, Lawton C, Mahmood U MD, Pos F, van As N, van Herk M, Vesprini D, van der Voort van Zyp J, Tree A, Choudhury A PhD

2.1 Introduction and contribution of authors

This article is written to provide a resource for future rationalised radiotherapy delivery utilising MR technology. It provides in one place for the first time a record of inter and intra fraction prostate motion recorded from modern studies, and reports in detail on studies using MRI to collate data. It is hoped this will permit evidence based decisions on expansion margins for future radiotherapy studies with the intention of minimising treatment volumes while avoiding the risk of detriment to ultimate outcome. It will also inform future studies employing MRI of the likely potential benefits to IGRT.

The concept of a review of the role of MRI in prostate radiotherapy was raised by the MR-Linac consortium. I devised the format of the review article, selected the search terms for a systematic literature review and performed the literature search, reviewed all abstracts and then appropriate whole articles. I independently wrote the entire article, excepting sections 2.10 and 2.11 which were written with significant input from XA Li. I selected illustrations and the format and content of all tables. A Tree and A Choudhury gave primary feedback on the format of the article suggesting revisions. The content of all tables was proofed by LE Kershaw. The entire MR-Linac group provided feedback on the final format article. I submitted the article for publication and made revisions as requested by the editorial team. It was ultimately accepted for publication in The Radiotherapy and Oncology (McPartlin et al., 2016c).

2.2 Abstract

Dose escalated radiotherapy improves outcomes for men with prostate cancer. A plateau for benefit from dose escalation using EBRT may not have been reached for some patients with higher risk disease. The use of increasingly conformal techniques, such as step and shoot IMRT or more recently VMAT has allowed treatment intensification to be achieved while minimizing associated increases in toxicity to surrounding normal structures. To support further safe dose escalation, the uncertainties in the treatment target position will need be minimised using optimal planning and image-guided radiotherapy (IGRT). In particular the increasing usage of profoundly hypo-fractionated stereotactic therapy is predicated on the ability to confidently direct treatment precisely to the intended target for the duration of each treatment.

This article reviews published studies on the influences of varies types of motion on daily prostate position and how these may be mitigated to improve IGRT in future. In particular the role that MRI has played in the generation of data is discussed and the potential role of the MR-linac in next-generation IGRT is discussed.

2.3 Search strategy and selection criteria

References for this review were identified through PubMed with the search terms “prostate”, “adaptive”, “radiation”, “radiotherapy”, “motion”, “MRI”, “MR”. The literature review was performed between June and September 2015. The titles/abstracts were screened and full text copies of all potentially relevant studies obtained. References within identified papers were reviewed for relevance. A final reference list was generated on the basis of originality and relevance to the scope of this review.

2.4 Introduction

Randomised trials have demonstrated that dose escalated radiotherapy improves outcomes for men with prostate cancer (Kalbasi et al., 2015). The use of increasingly conformal techniques, such as step and shoot IMRT or more recently VMAT has allowed this to be achieved while minimizing associated increases in toxicity to surrounding normal structures (Wortel et al., 2015). The accuracy of any radiotherapy delivery is however limited by multiple factors: organ delineation, set up error and inter-/intra-fraction organ motion, rotation and deformation (Kupelian and Meyer, 2011). A plateau for benefit from dose escalation using EBRT may not have been reached for some higher risk prostate cancers (Eade et al., 2007). To allow further safe dose escalation, the uncertainties in the treatment target must be mitigated using optimal planning and image-guided radiotherapy (IGRT). In particular the increasing usage of profoundly hypo-fractionated stereotactic therapy is predicated on the ability to confidently direct treatment precisely to the intended target for the duration of each treatment (Nicolae et al., 2015).

Much work has been carried out over the past 20 years quantifying the degree of prostate motion, rotation and deformation that occurs during a course of radiotherapy, allowing rationalization of treatment margins based on expansion “recipes” (van Herk, 2004). The use of increasingly sophisticated real time imaging has enabled monitoring of the prostate and OAR’s through treatment delivery and has provided extensive data on their behaviour. MRI, with its unrivalled soft

tissue delineation, has contributed to this data but has not, as yet, emerged as a routine part of daily radiotherapy delivery. The long anticipated arrival of a fully integrated MR-Linac may change this (Lagendijk et al., 2008).

The ideal scenario is to guide prostate radiotherapy with MR imaging, identifying the prostate in real time while delivering radiation. Two systems (ViewRay and the Elekta MR Linac) hope to demonstrate improvement in patient outcomes with this technique.

This article reviews data on target uncertainties when treating prostate cancer and in particular the work performed using MRI. Available techniques to reduce this uncertainty, and the potential benefits an MR-Linac may offer for IGRT are discussed. These data underpin the clinical work which will be undertaken on the MR-Linac to establish its utility in treating localized prostate cancer.

2.5 Non-MR Studies of inter- and intra-fractional prostate motion

The prostate experiences inter- and intra-fractional motion during a course of radiotherapy, as reported from an extensive body of work carried out over the past twenty years (Figure 2-1). A comprehensive review of early studies indicates that the inter-fraction motion appears to have a standard deviation (SD) of around 1 – 4 mm, with one study finding motion with SD as high as 7.3 mm (Byrne, 2005).

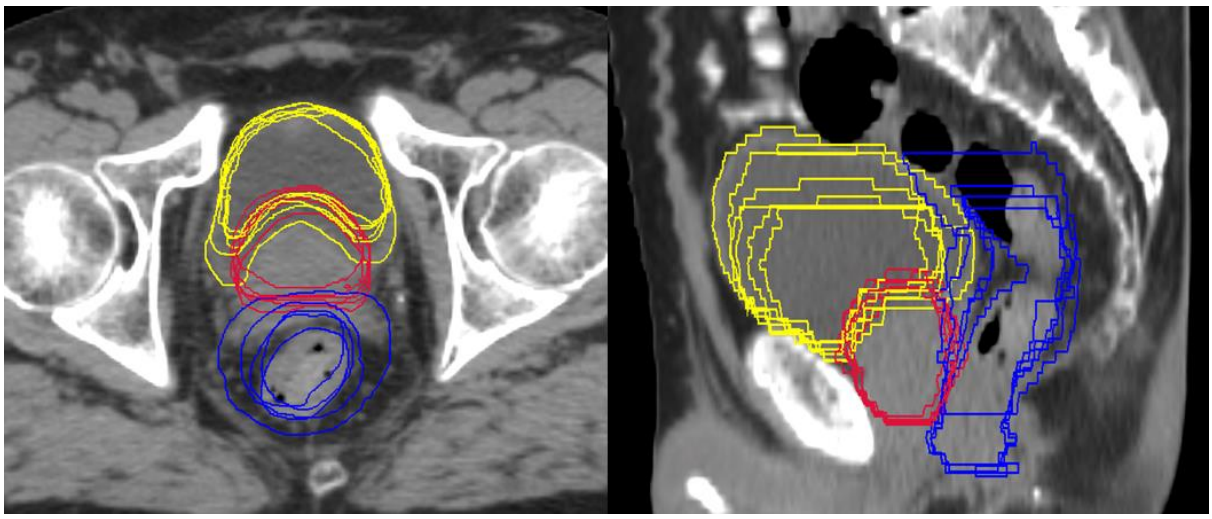

Figure 2-1: Prostate, rectum and bladder contoured on multiple CT images throughout treatment and overlaid to show inter-fraction motion

With increasing use of IMRT and consequently increased treatment duration, the significance of intra-fractional motion has grown, with appreciable variation being demonstrated (Nederveen et al., 2002; Aubry et al., 2004; Letourneau et al., 2005; Huang et al., 2002; Schallenkamp et al., 2005; Kitamura et al., 2002). A minority of patients experience more pronounced changes, as illustrated in a series of 427 patients assessed using fiducial markers and portal imaging, with motion > 3mm in 28% of treatment fractions over a ten minute period (Kotte et al., 2007).

Multiple modalities been used to demonstrate that two general types of intra-fraction motion are seen: non-resolving slow drift, predominantly in the posterior direction due to rectal changes, and

sudden transient motion, largely in the superior and anterior direction, likely a result of peristaltic visceral motion (Butler et al., 2013; Tanyi et al., 2010; Langen et al., 2008; Nederveen et al., 2002). Constant assessment also identifies greater intra-fraction motion; one study using Calypso 4-D tracking of 7738 records in 200 patients over 12 minutes showed the percentage of fractions with prostate shift >2 ,3, 5, and 7 mm for > 30 seconds was 56.8%, 27.2%, 4.6% and 0.7% (Tong et al., 2015). For the worst 10 patients, 5% of the total, these percentages increased to 91.3%, 72.4%, 36.3% and 6%. Cohorts of patients assessed using multiple continuous imaging techniques have also found significant proportions experiencing movements >2-5mm, demonstrating the consistency of this finding within differing imaging modalities (Shimizu et al., 2011; Daly et al., 2012; Polat et al., 2008; Xie et al., 2008). Intra-fraction motion has generally been found to be patient specific and predominantly random, although this has been challenged (Adamson and Wu, 2010; Ballhausen et al., 2015; Kron et al., 2010). The observation that initial systematic intra-fraction changes can be predictive for subsequent movement may provide some guidance to likely behaviour during therapy (Mutanga et al., 2012; Quon et al., 2012; Lin et al., 2013).

Numerous studies have quantified the systematic and random components of inter- and intra-fraction motion to allow application of margin expansion formulas (Table 2-1,Table 2-2).

2.6 MR studies of inter and intra-fraction motion

The superb soft-tissue contrast and continuous imaging capability of MRI have allowed for confident assessment of inter- and intra- fraction prostate and OAR motion (Padhani et al., 1999; Mah et al., 2002; Villeirs et al., 2004; Ghilezan et al., 2005; Nichol et al., 2007; Heijmink et al., 2009; Dinkel et al., 2011; Ogino et al., 2011; Terashima et al., 2013; Gill et al., 2014; Kerkhof et al., 2008; Vargas et al., 2010).

The first work with MRI to quantify prostatic motion used axial cine-MRI on 55 patients to evaluate intra-fraction motion of the rectum and prostate centre of mass every 10 seconds over a 6-7 minute period, representative of a radiotherapy treatment delivery time. This identified a median anterior shift of 4.2mm, which in 16% of patients was >5mm (Padhani et al., 1999). A subsequent study using sagittal and axial cine-MR over 9 minutes, sampling at 20 second intervals, for 42 patients identified displacement with SD 2.9mm, 1.5mm and 3.4mm in the AP, LR and SI plane (Mah et al., 2002). The prostate was identified as tending to return to its original position after large displacements of up to 12 mm, motion which would be missed with pre and post treatment imaging alone (Ghilezan et al., 2005). This motion appeared to increase through the course of treatment, perhaps as a consequence of radiation induced toxicity

Table 2-1: Inter-fraction systematic and random motion

Author	Pt no. (fractions analysed)	Imaging	Inter-fraction motion SD (mm)						Registration	Preparation
			Systematic motion			Random motion				
			AP	LR	SI	AP	LR	SI		
(Zelefsky et al., 1999a)	50 (200)	CT	2.4	0.6	2.7	1.6	0.5	2.0	Bone	Prone, fleet enema at planning, empty bladder, immobilisation device
(Stroom et al., 1999)	15 (60)	CT	2.5	0.5	2.7	2.8	0.6	2.5	Bone	Foot and knee support Laxative prior to planning, 1 litre fluid 1 hour prior to scans
(Hoogeman et al., 2005)	19 (209)	CT	2.7	0.3	2.1	2.4	0.4	2.1	Bone	Empty rectum, 250ml fluid 1 hour prior
(Schallenkamp et al., 2005)	20 (798)	MV EPID + FM	2.5	2.0	1.9	3.5	1.6	2.0	Bone	Vacuum cradle
(de Boer et al., 2005)	15 (255)	MV EPID + FM	2.1	0.8	2.0	1.9	0.7	1.2	Bone	Laxative prior to sim, full bladder
(Litzenberg et al., 2006)	11 (-)	EM	1.5	2.2	3.0	5.2	3.4	3.3	Skin markers	Foot and knee support
(Van den Heuvel et al., 2006)	10 (270)	MV EPID + FM	3.6	3.4	3.9	5.7	5.7	2.7	Skin markers	Alpha cradle
(O'Daniel et al., 2006)	10 (243)	CT	3.9	1.6	3.4	3.6	2.5	2.0	Skin markers	Empty rectum, full bladder at simulation
(Soete et al., 2007)	12 (120)	kV EPID + FM	4.3	1.3	4.2	2.8	1.6	2.3	Bone	Head and knee support
(van der Heide et al., 2007)	453 (15855)	MV EPID + FM	4.8	2.2	2.9	3.5	2.0	2.3	Skin markers	Knee, cushion. Bladder emptied 15 minutes prior to radiotherapy
(McNair et al., 2008)	30 (408)	MV EPID + FM	2.5	1.3	1.9	3.1	2.2	2.2	Bone	Ankle/knee support, partially full bladder, empty rectum no prep
(Beltran et al., 2008)	40 (1532)	MV EPID + FM	3.5	0.9	3.0	2.8	1.2	2.0	Bone	Not specified
(Fiorino et al., 2008)	21 (522)	CBCT	0.3	0.2	0.2	1.0	0.6	0.7	Bone	Leg immobilisation, rectal enema + gas catheter, 250ml fluid 30 minutes prior
(Bylund et al., 2008)	24 (984)	CBCT	2.0	0.7	1.0	2.9	2.0	2.1	Mutual information algorithm	No bladder/bowel prep
(Frank et al., 2008)	15 (369)	CT	4.1	0.9	2.9	1.3	0.5	0.6	Bone	Vac-lok bag, enema at sim, 590ml fluid 30 min prior
(Mutanga et al., 2008)	10 (-)	MV/kV EPID	2.9	1.7	4.1	3.2	1.6	2.7	Skin markers	Not specified
(Nijkamp et al., 2008)	20 (116)	CBCT	1.8	0.5	1.7	1.9	0.5	1.5	Bone	Empty rectum, 250ml fluid 1 hour prior, dietary advice
(Tanyi et al., 2010)	14 (546)	EM	3.4	0.5	2.9	2.5	0.4	2.3	Bone	Not specified
(Su et al., 2011; Mayyas et al., 2013)	17 (476)	EM	4.7	2.3	3.4	3.5	3.7	2.7	Skin markers	Not specified
(Mayyas et al., 2013)	27 (1100)	CBCT	3.0	2.4	2.7	3.2	2.5	2.2	Skin markers	Empty rectum, partially full bladder
		BAT US	3.3	2.8	3.5	4.1	3.6	3.8		
		kV EPID	3.4	2.6	3.1	2.9	2.4	2.0		
(Oh et al., 2014)	17 (546)	CBCT	1.1	1.6	1.9	1.8	2.8	2.4	Skin markers	Knee support, ERB, full bladder
(Oehler et al., 2014)	20 (172)	CBCT	1.9	0.6	1.7	1.9	0.9	1.7	Bone	Leg immobilisation, empty rectum with ERB, empty bladder
		kV EPID	1.8	0.8	1.4	2.0	0.9	2.3		

CBCT, Cone Beam CT; FM, Fiducial Marker; EM, Electromagnetic transponder

Table 2-2: Intra-fraction systematic and random prostate motion

Author	Pt no. (fractions analysed)	Imaging	Intra-fraction motion SD (mm)						Treatment time	Preparation
			Systematic motion			Random motion				
			AP	LR	SI	AP	LR	SI		
(Beltran et al., 2008)	40 (1532)	MV EPID + FM	0.9	0.6	1.0	1.8	1.3	1.2	2 min	Not specified
(Li et al., 2013a)	105 (775)	EM	0.5	0.2	0.4	1.1	0.5	1.0	3 min	Not specified
(Aubry et al., 2004)	18 (282)	MV EPID + FM	0.7	0.2	0.4	1.4	0.8	1.0	<5 min	Full bladder, empty rectum
(Li et al., 2013a)	105 (775)	EM	0.6	0.3	0.5	1.2	0.5	1.1	5 min	Not specified
(Choi et al., 2015)	12 (336)	kV EPID + FM	0.3	0.2	0.4	0.6	0.3	0.5	5 min	Ankle immobilisation, enema
(Oehler et al., 2014)	20 (52)	CBCT + FM	1.4	0.9	1.4	1.6	1.0	1.4	3-6 min	Leg immobilisation, empty rectum with ERB, empty bladder
(Kotte et al., 2007)	427 (11426)	MV EPID + FM	0.6	0.3	0.5	0.9	0.4	0.9	5-7 min	Knee support, empty rectum
(Kron et al., 2010)	184 (5778)	kV EPID + FM	0.8	0.5	0.7	1.2	0.8	1.2	< 6 min	Not specified
(Soete et al., 2007)	12 (120)	MV EPID + FM	0.8	1.3	1.1	1.6	1.4	2.4	7.5 min	Head and knee support
(Kron et al., 2010)	184 (5778)	kV EPID + FM	0.9	0.6	0.8	1.2	0.8	1.1	6-9 min	Not specified
(Su et al., 2011)	17 (467)	EM	0.6	0.3	0.5	1.9	0.7	1.4	8 min	Not specified
(Litzenberg et al., 2006)	11 (-)	EM	2.2	0.7	2.6	0.8	0.2	1.2	8 min	Ankle/knee support, no rectal/bladder prep
(Tanyi et al., 2010)	14 (1638)	EM	0.5	0.3	0.7	1.4	0.8	1.3	8-16 min	Not specified
(Kron et al., 2010)	184 (5778)	kV EPID + FM	1.3	1.1	1.3	1.3	0.7	1.2	> 9 min	Not specified
(Mutanga et al., 2012)	108 (2894)	MV EPID + FM	1.1	-	1.0	1.2	-	1.1	11 min	Headrest/knee support, void bladder 30 minutes prior, laxative at planning
(Li et al., 2009)	105 (775)	EM	0.8	0.3	0.8	1.6	0.7	1.4	10-20 min	Not specified
(Badakhshi et al., 2013)	13 (427)	kV EPID + FM	0.5	2.0	2.1	1.4	2.2	2.6	14.2 min	Empty rectum + full bladder, head and knee support, foot restraint
(Mayyas et al., 2013)	19 (-)	EM	1.3	0.6	1.5	2.6	1.4	2.4	20-30 min	Empty rectum, partially full bladder
(Quon et al., 2012)	53 (265)	MV EPID + FM	1.4	0.2	1.2	2.4	1.3	2.0	Time not specified	Vac-lok bag, full bladder, empty rectum

CBCT, Cone Beam CT; EM, Electromagnetic transponder; EPID, Electronic portal imaging device; FM, Fiducial marker

More recently intra-fraction prostate motion has been assessed by imaging 47 patients with prostate cancer after instructions to remove rectal gas (Ogino et al., 2011). Eleven points of interest were determined on axial and sagittal cine-MRI slices and monitored over a total of ten minutes. Displacement was more marked at the base of prostate than apex, likely a result of distal tethering, with mean of means SI and AP displacements of 0.41 mm and 0.86 mm for the former and 0.26 mm and 0.32 mm for the latter.

Continuous MRI has been able to demonstrate that intra-fraction motion increases with treatment time. A study using an open bore MR-scanner for a total of 68 sagittal cine-MRI sequences demonstrated an increasing displacement in the AP and SI planes during treatment with SD of 0.57 mm and 0.41 mm in the first two minutes increasing to 1.44 mm and 0.91 mm in minutes two to four(Vargas et al., 2010) . This increase in motion appears to occur predominantly in the first few minutes of treatment with another study using cine-MRI over 12-15 minutes finding motion at 3, 5, 10 and 15 minutes of 1mm, 1.3 mm, 2.1 mm and 1.9 mm in the AP plane and 0.7 mm, 1.8 mm, 1.5 mm and 1.6 mm in the SI plane (Gill et al., 2014).

The increasing intra-fractional motion seen initially over time shows the potential benefit of shortened treatments associated with VMAT compared to that with IMRT. Other studies using non-MR based imaging have also shown this increase and that it is the strongest predictor of observed displacements (Langen et al., 2008; Shelton et al., 2011; Cramer et al., 2013; Mansson Haska et al., 2008; Xie et al., 2008; Reggiori et al., 2011; Kron et al., 2010; Curtis et al., 2013). These increasing movements can contribute 1-2mm to the required PTV margin (Mansson Haska et al., 2008; Steiner et al., 2013). Shortened treatment times, such as those achievable by VMAT, have been shown to achieve a marked reduction in the SD of intra-fraction motion (Shelton et al., 2011; Li et al., 2013a; Tong et al., 2015).

Stereotactic radiotherapy is challenging both due to the potential increase in treatment time compared to conventional VMAT and the implications of a geographical miss for even a single fraction. The necessity to avoid this obliges caution in margin reduction although it has been shown using Cyberknife that repeat imaging every 60 -180 seconds may be sufficient to allow correction for the increased prostate motion of longer treatments (van de Water et al., 2014). Even with regular repeat imaging 6-dimensional correction for rotation and translation is required if margins as small as 3mm are to be achievable.

2.7 Deformation and rotation

Many studies of prostatic motion have assumed rigid motion of the prostate. Analyses of prostate changes have shown this to be a simplification although the degree of deformation identified has varied substantially. For example a study comparing the contoured prostate to an average CTV on 8-12 CT images for 19 patients matched for rotation and translation found “real” shape variation, correcting for inter-observer variation, of 1.6 mm at the SV tip and 0.9 mm at the posterior prostate (Deurloo et al., 2005). Another group used three repeat CT scans with prostate and SV contoured and matched to a planning CT and non-rigidly registered to represent deformation (van der Wielen et al., 2008). Deformation of the prostate was small (≤ 1 mm) while the deformation of SV was up to 2.6 mm SD posteriorly. More marked variation has been suggested; a study

matching 200 cone beam CT (CBCT) images for ten patients to planning CT images using B-spline-based deformable registration identified a much larger deformation of the prostate, most marked in the anterior direction with a maximum of 10 mm, 5 mm and 3 mm in 1%, 17% and 76% of cases (Mayyas et al., 2014). Again SV deformation was larger, with changes in the posterior direction of >5 mm and >3 mm in 7.5% and 44.9% of cases. For this analysis three clinicians delineated contours which were averaged in an attempt to reduce error however the SD of the mean centre of mass of the contours was up to 2.2 mm. It may therefore be that the inferior CBCT image quality, limiting contouring accuracy, contributed to the larger changes identified.

MRI, which may mitigate delineation errors associated with CT imaging, has also been used to assess deformation. A study of 10 patients using sagittal and axial cine MRI of the prostate to assess changes in the volume of contoured prostate over six minutes found similar results to those obtained using CT imaging with a deformation with a SD 1.7 mm in the AP plane shown (Khoo et al., 2002). Interestingly it has been suggested through tracking points of movement in sagittal MRI that deformation is only seen with a full rectum, and is most marked at the level of mid-prostate (Ghilezan et al., 2005).

The cause of deformation is due both to mass effect from surrounding structures and as a consequence of treatment itself with the prostate being shown to change in volume during radiotherapy. For example 25 patients underwent MRI pre-radiation and at one time point during therapy to assess prostate motion and deformation through treatment (Nichol et al., 2007). Scans were compared using finite element modelling aligned on the centroid of three fiducial markers. An increase in prostate volume by up to 34% was seen in those scanned early in treatment whilst a decrease of up to 24% was seen later in the course. The degree of shrinkage seen over a course of radiotherapy is affected by the use of neo-adjuvant hormone therapy and pre-treatment volume but may be generally of the order of 10-15% (Frank et al., 2010; Roeske et al., 1995; Tinger et al., 1998; Kasaova et al., 2011). This has implications for further development of MR-guided radiation, which can account for the intra-fraction motion described above, but would need further technical developments to adapt for deformation.

The effect of systematic and random inter-fraction rotations on prostate motion has been assessed by various groups using CT, kV and MVCT or EM imaging. These rotations predominate in the sagittal plane and appear to correlate with rectal filling; this moves the prostate in the AP direction, causing rotation due to apex tethering (Boda-Heggemann et al., 2007). The differing bowel preparations employed by various groups may affect rectal volumes and contribute to the variation in degree of rotation identified.

Intra-fractional rotation has been less well characterised and although appearing smaller, it remains relevant (table 3). A study using continuous kV imaging with fiducial markers during the treatment of 10 patients with prostate cancer found for 35% of treatment time the prostate rotated more than 5° around the lateral axis (Huang et al., 2015). These intra-fraction rotations may be clinically significant. For example even with daily translations the intra-fraction rotation during RT can cause significant under-dosing, and margins of 3mm may be required to account for rotations of up to 5°

(van de Water et al., 2014; Amro et al., 2013). The significance of prostatic rotation is only likely to increase as treatment margins further reduce.

2.8 Relative motion of prostate and seminal vesicles

In high risk disease the likelihood of occult involvement of the SV is increased (Eifler et al., 2013a). It is therefore generally necessary to include this area in the intended CTV for radiotherapy planning. The base of the SV is the region most likely to harbour occult disease, with one pathological series finding disease 2cm beyond this in only 1% of all patients (Kestin et al., 2002). This area must therefore be prioritised to receive the full prescribed dose. CT imaging has demonstrated that the SV tips undergo greater inter-fraction movement than the base and consequently larger expansion margins are required if it is clinically necessary to treat its entirety (Stenmark et al., 2012; Mak et al., 2012) .

It has been shown that the SV and prostate can behave independently making appropriate expansions to PTV challenging (Deurloo et al., 2005; Oehler et al., 2014; Fleshner et al., 1999). The SV volume may vary by as much as 100% during a course of radiotherapy and experience significant independent deformation (Roeske et al., 1995; Fleshner et al., 1999). Inter-fraction SV motion appears more significant than that of the prostate gland with a SD in the order of 2.9 – 7.3 mm, 1.9 - 3.1 mm and 2.1 - 5.5 mm in the AP, LR and SI planes (Dawson et al., 1998; Tinger et al., 1998; Zelefsky et al., 1999b; Liang et al., 2009; Mak et al., 2012; Frank et al., 2008). Despite direct tumour invasion reducing SV mobility, this motion may remain considerable (van der Burgt et al., 2015).

Allowing for intra-fractional motion is also problematic. Overall intra-fractional displacement of the SV appears greater than for the prostate and increases over time. In one series using cine-MRI it was found that for 95 % of the images SV centroid movement at 3, 5, 10 and 15 minutes was 4.7 mm, 5.8 mm, 6.5 mm and 7.2 mm respectively in the SI plane and 4.0 mm, 4.5 mm, 6.5 mm and 7.0 mm in the AP plane (Gill et al., 2014). The correlation between prostate and SV intra-fraction movement was shown to vary greatly with no relationship between the two for most patients

The lack of correlation between prostate and SV inter- and intra-fractional motion has implications for the use of prostate tracking devices, such as calypso transponders, when simultaneously treating the SV. Caution must be employed when considering reducing treatment margins on the basis of an assumed confidence about exact CTV location.

2.9 Contributing factors to prostate motion

2.9.1 *Rectal and bladder volumes*

Rectal distension is a major contributor to, and correlates with, prostate motion (Figure 2-1). This likely relationship was identified in some of the earliest prostate motion analyses (Ten Haken et al., 1991; Schild et al., 1993) and subsequent studies have confirmed this association particularly in relation to AP translation and rotation around the prostate apex (Crook et al., 1995; van Herk et al., 1995; Ghilezan et al., 2005; Mah et al., 2002; Padhani et al., 1999; Adamson and Wu, 2009).

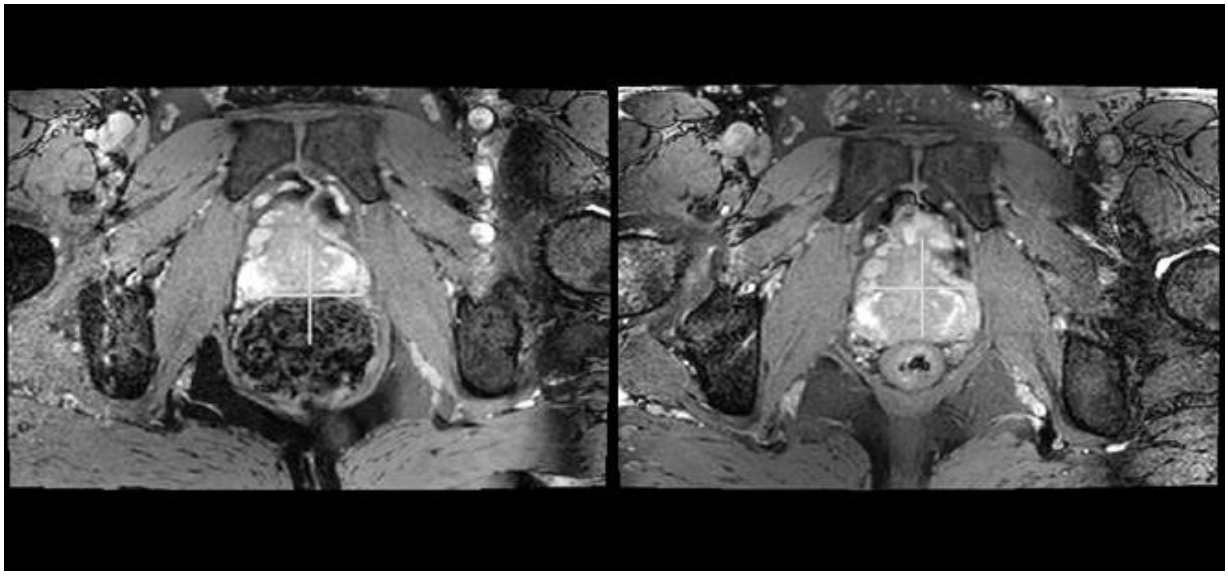

Figure 2-2: MRI at same level of prostate with full and empty rectum, demonstrating rectal induced distortion

This relationship has also been demonstrated with MRI. A small study of seven patients measured the prostate midpoint relative to bony anatomy on pre and post treatment MRI and found variation in rectal filling that correlated strongly with anterior displacement and a lesser correlation between bladder filling and superior motion (Villeirs et al., 2004). A larger study of 42 patients used cine-MRI scans every nine seconds for nine minutes at baseline without any bowel preparation, before CT planning with bowel preparation and at a random point during RT with bowel preparation (Nichol et al., 2007). This demonstrated rectal gas and stool to be responsible for 74% of identified > 3mm prostate motion. Despite this voiding prior to imaging and bowel preparation did not significantly reduce intra-fraction motion.

Rectal diameter may have a threshold above which its effect on prostate motion becomes more significant. It has been suggested that maximum rectal diameters above 3.5 - 4.5 cm or mean cross sectional areas ≥ 9.5 cm^2 at planning imaging are predictive of significant variation in rectal size and prostate position during therapy (Pinkawa et al., 2006b; Oates et al., 2015; Engels et al., 2009b).

The increased motion associated with initial large rectal volumes may also negatively influence treatment outcome. In one series of 127 patients those with a mean rectal cross sectional area greater than the group average of 11.2cm^2 at the time of planning experienced greater biochemical failure rates (HR 3.89) and more toxicity from treatment (de Crevoisier et al., 2005). Another study examined outcomes for 549 patients, stratified by anorectal volumes ≥90cm^3 at time of planning CT, and found that in patients with a risk of SV involvement >25% those with a larger rectal volume had a 15% reduction in freedom from failure at five years (p=0.01) (Heemsbergen et al., 2007).

Various approaches such as diet modification, bowel regimens (enemas, laxatives, etc.) and immobilizing endo-rectal balloons have been used in an attempt to reduce rectal variation. The evidence for efficacy of these techniques is mixed and a recent systematic review concluded that it

was impossible to recommend one particular interventional strategy with further prospective studies required (McNair et al., 2014). The use of effective daily image guidance may mitigate any effects of initial rectal distension.

Although the potential effect of rectal volume on prostate motion appears clear, the effects of changes in bladder volume appear at most to be minimal. Various studies have provided some limited evidence suggesting a weak relationship between the two (Melian et al., 1997; Zelefsky et al., 1999b; Villeirs et al., 2004; Adamson and Wu, 2009) but other groups have failed to find any association (Pinkawa et al., 2006a; Beard et al., 1996; Antolak et al., 1998; Moiseenko et al., 2007). It would therefore seem likely that simple bladder filling protocols are sufficient to minimise any bladder volume effects. However, for prone patients or patients with restricted abdominal movement, e.g. due to MR coils, bladder filling may affect prostate motion and such setups should be avoided.

2.9.2 *Target delineation*

Inter- and intra- operator variation in target delineation, particularly at the SV and apex, can be significant (Oehler et al., 2014; Fiorino et al., 1998a; Cazzaniga et al., 1998b). This is in part due to poor soft tissue definition on CT imaging making identification of the boundaries of the prostate challenging. It is known that CT delineated prostates are routinely larger than the true anatomical site. One study comparing the CT delineation by six radiation oncologists with photographic anatomical images found that the contoured prostate was on average 30% larger that the true gland but only included 84% of its volume, such that posterior portions were always missed and anterior normal tissue always included (Gao et al., 2007). MRI provides better distinction between adjacent soft tissue structures and has been shown to be superior at identifying the prostate apex, SV and posterior border (Figure 2-3**)**. Multiple studies have demonstrated a reduction in volume of contoured prostate, of between 30-35% in the three largest series, when MRI is used to provide addition information for planning (Rasch et al., 1999a; Hentschel et al., 2011b; Tanaka et al., 2011b). These reductions are primarily due to reduced variation at the superior and inferior extent of the prostate and translate into reductions in delivered dose to the rectum (Sannazzari et al., 2002; Jackson et al., 2007a; Debois et al., 1999; Tanaka et al., 2011b). This improved soft tissue visualisation on MRI has also been shown to reduce intra- and inter-observer variation in prostate contouring (Figure 2-4) (Rasch et al., 1999a; Parker et al., 2003). Using MRI in combination with an education program it may be possible to reduce this inter-observer variation further (Khoo et al., 2012). A final benefit from use of MRI for prostate delineation comes from the reduced metal artefact degradation from prosthetic hips which may significantly affect CT imaging and subsequent contour consistency (Rosewall et al., 2009). Good correspondence with MR imaging and prostatectomy specimens has been shown with a correlation coefficient of up to 0.86 (Sosna et al., 2003; Jeong et al., 2008).

Therefore it appears MR-based contouring of the prostate can be done more consistently and with higher fidelity than CT, leading to reduced treatment volumes and radiation to surrounding structures.

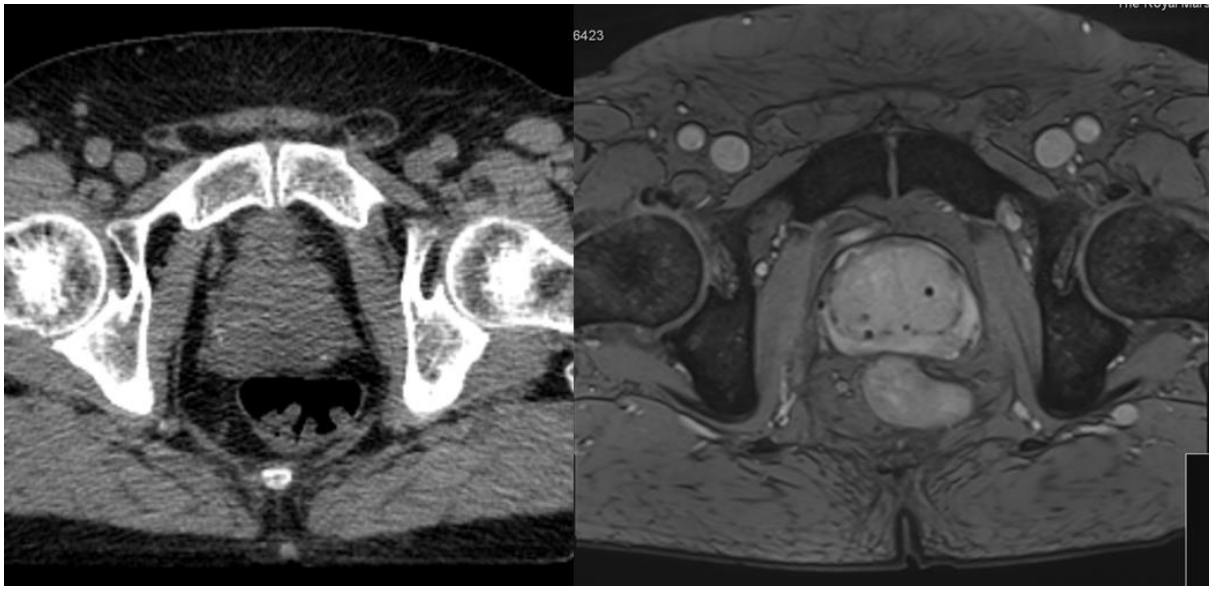

Figure 2-3: Comparison of fidelity using MR or CT imaging

Recently work has focused on the use of multi-parametric (MP) MR to identify areas of high grade tumour within the prostate gland (Barentsz et al., 2016). Confident identification provides the potential to focus dose intensification to this region, which may be the most likely site of ultimate disease recurrence (Cellini et al., 2002a). MPMR guided targeted dose escalation is the subject of the ongoing phase III FLAME study and results are awaited with interest (Lips et al., 2011). It has been shown that the dominant lesion within the prostate can be reliably identified on MP-MRI but as yet data on how this region may be affected by prostatic deformation during therapy is scarce and requires future work (Steenbergen et al., 2015). In a study using collimator adjustments to account for prostate rotations, patients with and without focal boost were equally sensitive to rotations, indicating a limited effect of prostate rotations on boost dose (de Boer et al., 2015).

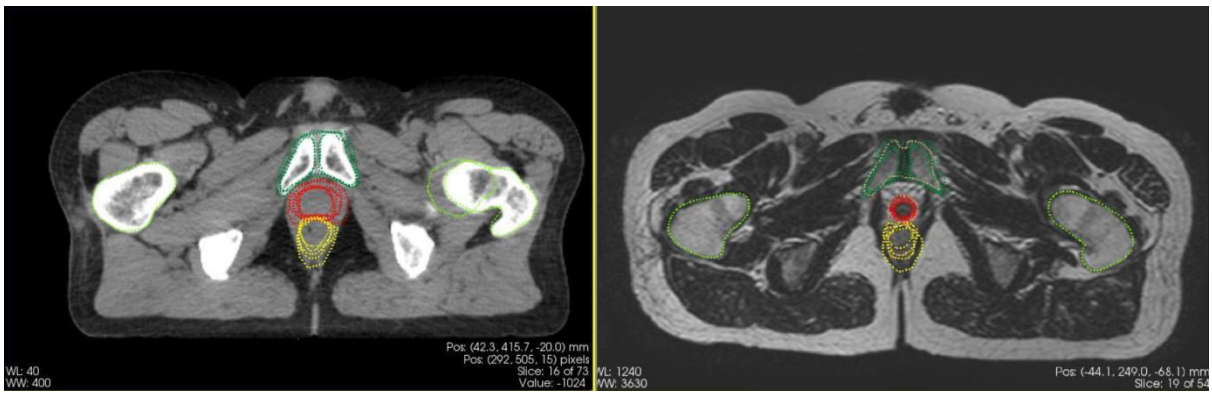

Figure 2-4: Comparison of contouring consistency for operators using MR or CT imaging (unpublished study)

2.10 Adaptive radiotherapy for inter-fraction motion

The current standard practice to manage inter-fraction variations is to use IGRT by repositioning the patient based on the rigid-body registration of the planning image and the image of the day acquired just before treatment, followed by delivery of the original (unchanged) plan. IGRT addresses the translational motions, including set-up errors, but cannot completely account for the

organ deformation, rotation, and independent motion between different organs. The ideal method to fully account for the inter-fractional variations is to adapt the treatment plan based on the anatomy of the day. Such adaptive planning process may be performed in an online or offline manner (Yan et al., 2005; LI, 2011). The offline adaptive process, i.e. using the information from previous treatments to provide feedback for future deliveries, has been used to correct systematic, predictable variations (Yan et al., 2000; Birkner et al., 2003; Nijkamp et al., 2008).

Online adaptive radiotherapy (ART), on the other hand, is capable of addressing both systematic and random variations and is the most effective strategy for precisely irradiating concurrent targets that move independently. Online planning must be fast enough to be completed within a few minutes while the patient is lying on the table waiting for treatment. Although such fast planning is generally challenging using conventional planning technologies, adaptive re-planning does not need to start completely from scratch. For example, it can start with an initial plan fully optimized from the planning images for the same patient and adapt for the anatomy of the day ('warm start' optimization). Technologies to facilitate this, such as the quality of in-room imaging, image registration and segmentation, plan optimization algorithm and computing hardware, are advancing significantly and rapidly. For example, integration of diagnostic-quality MRI in the treatment room, graphic-processing unit (GPU) accelerated auto-segmentation and dose calculation, rapid plan modification algorithms, and plan adaptation based on previous knowledge or a previously-created plan library are among the technology advances that can speed up adaptive planning significantly. In particular, among a number of online planning algorithms (Court et al., 2005; Mohan et al., 2005; Ahunbay et al., 2008; Ludlum et al., 2007), an online adaptive planning scheme (Ahunbay et al., 2008) has been developed that features two distinct steps: a) segment aperture morphing (SAM), and b) segment weight optimization (SWO), and has been used for prostate cancer (Ahunbay et al., 2010). It has been demonstrated that the online SAM+SWO scheme can adequately account for all inter-fraction variations and can be completed within 10 minutes for prostate RT (Ahunbay et al., 2010). Alternative techniques for ART of prostate cancer are reported (Qin et al., 2015; Stanley et al., 2015; Li et al., 2013b; Park et al., 2012a) and reviewed previously (Ghilezan et al., 2010; Li et al., 2014).

With online ART, a CTV-PTV margin can reach as low as 3 mm, depending mainly on intra-fraction variations. Such a small margin would be highly desirable to reduce treatment-related toxicities and/or to allow dose escalation. Online ART is particularly important for hypo-fractionated RT or SBRT where the penalty of a geographical miss and/or over dosing of normal tissue for a single fraction is significant. However, with such small margins, target definition accuracy becomes much more critical to avoid the risk of compromising clinical outcome (Engels et al., 2009a).

2.11 MRI-guided adaptive radiotherapy for inter- and intra-fractional motions

The high soft tissue contrast makes MRI an ideal imaging modality for online ART. MRI-guided RT delivery systems that integrate MR scanners with radiation delivery machines are being introduced into the clinic (Mutic and Dempsey, 2014). For example, ViewRay system (Oakwood Village, OH) combines a 0.35 T MRI scanner with three 60Co sources with multi-leaf collimators (MLC).

Integration of a diagnostic MRI scanner with a Linac (MR-Linac) is also under development. The MR-Linac proposed by Lagendijk et al at the University Medical Center Utrecht (Lagendijk et al., 2014) that integrates a 1.5 T MRI scanner with a 6 MV Linac is being developed for commercialization (Lagendijk et al., 2008). With CT based IGRT, image quality adversely affects the CTV-to-PTV margins required for targeting and ART, mainly due to the residual uncertainties from the soft-tissue contrast for the image modality (Morrow et al., 2012). It is anticipated that the residual uncertainty with diagnostic quality MRI will be drastically smaller than those with CT or CBCT, allowing a smaller CTV-to-PTV margin.

The design of the MR-Linac system comprises a 6 MV Linac (Elekta Inc) mounted on a ring around a modified 1.5 T MRI scanner (Achieva, Philips Healthcare, Best, The Netherlands) and an online ART planning system (Lagendijk et al., 2008). The system is designed to be able to simultaneously image and irradiate the patient. The radiation beam is shaped by a 160-leaf MLC system and travels through the closed-bore MRI before it enters the patient. The accelerator and MRI are designed to be magnetically decoupled so that the MR images are not distorted by the presence of magnetized accelerator components, and the operation of the accelerator is not hampered by the magnetic field. A series of MR sequences can be scanned to produce pre-, during- and post-treatment images. Once the MR-Linac is fully developed, the pre- and post-treatment MRI can include both morphological (T1, T2...) and functional (DWI, DCE etc.) images. The during-treatment MRIs include cine MRI (2D), morphological 3D (e.g., T1, T2) and 4D images.

The online planning system integrated in the MR-Linac should be designed to generate an adaptive plan based on the pre-treatment MRI in the following steps: 1) deformably register the pre-treatment MRI with the planning images, 2) rapidly generate a plan by modifying or re-optimizing the original plan or by fast adaptive re-planning to account for the different anatomy based on the registered images, and 3) quickly perform a software-based QA check on the new plan. To be successful the system should complete this 3-step online process within 5 minutes while the patient is still lying on the couch. Then, the new adaptive plan is delivered simultaneously with the during-treatment images acquired.

The MR-Linac system is designed to able to track/monitor organ (e.g., prostate gland) motion in real-time on 2D (cine) MRI during the radiation delivery. Because of superior soft tissue contrast, this tracking should be very accurate and effective. The radiation beam can be paused, via the capability of exception gating, if prostate motion is detected outside a pre-defined range, and can be resumed if the prostate moves back to the range. Alternatively, it is anticipated that with technical enhancements, the radiation beam may be dynamically shaped to trace the prostate motion detected from the cine MRI acquired on the plane perpendicular to the beam orientation. Either way, the intra-fractional variations can be managed effectively, thus the margin required to account for intra-fraction variation can be reduced.

The superior soft tissue contrast along with function/physiological information with MRI will significantly improve the performance and implementation of the online ART strategy (e.g., improved target definition, image registration, auto-segmentation). In addition, with the availability of real-time MRI during RT delivery to measure and monitor intra-fraction motion, the motion

management techniques (gating or tracking) can be improved. With both inter- and intra-fractional variations being accounted for, the CTV-to-PTV margin may be safely reduced to ≤3 mm. Because the PTV often overlaps with rectum and bladder, such a drastic reduction in PTV margin should reduce toxicities or allow RT doses to be safely escalated to eradicate the tumour, thus improving treatment outcomes.

2.12 Conclusion

Extensive literature demonstrates that substantial inter- and intra-fractional variations occur in radiation therapy for prostate cancer. These variations include translational and rotational motions, deformations, and independent motions between the structures, and consist of both random and systematic components. While the current standard practice of IGRT based on CT or CBCT can only address translational motion, adaptive radiotherapy has the potential to fully account for these variations. The superior soft-tissue contrast and the continuous imaging capability of MRI are highly desirable for the management of inter- and intra-fraction variations. Integration of MRI radiotherapy delivery and ART capability, such as with the MR-Linac, holds the promise to optimize radiotherapy to the prostate. Using this approach the improved delineation of target and OARs in both planning and delivery, will mean inter- and intra-fractional variations may be confidently accounted for, permitting use of a decreased CTV-to-PTV margin.

Conflict of Interest:

Dr Tree has received funding from Elekta for a Research Fellow

Acknowledgements:

Dr van As and Dr Tree gratefully acknowledge the support of the Royal Marsden/Institute of Cancer NIHR Biomedical Research Centre.

Chapter 3: The potential role of interstitial points identified on high energy CT imaging to guide prostate MR and CT image registration

McPartlin AJ, Hosni A, Moseley J, Velec M, Lam T, Bayley A, Catton C, Warde P, Chung P, Menard C

3.1 Introduction and contribution of authors

Having established the benefit that MRI can bring to delineation of the prostate for radiotherapy planning and identification of inter and intra-fraction prostate motion, a significant consequent issue is the integration of MR and CT images. Currently CT imaging is required for radiotherapy planning due to the information on electron density, and therefore tissue attenuation, it provides. For MRI to be used as part of the planning process it must therefore be used in combination with CT images. This chapter addresses the challenges of registration of two image sets and investigates a novel method of performing registration, with potential benefits for patient comfort and treatment workflow.

I devised the design of this study. In part it utilised a set of prostate contours performed on high quality volumetric CT (HQVCT) and conventional CT by five staff radiation oncologists for a previous investigation of the effects of HQVCT on planning workflow. For the current study I recruited a fellow radiation oncology fellow to validate with me initial identification of interstitial points and two further radiotherapy planners to perform image registration, against which the new method would be compared. Summation of the previously generated prostate contours was performed by Joanne Moseley, Radiation Physicist, after discussion with me of the needs of the study. I performed the necessary preparation of data for this, moving files between pinnacle planning software and Morpheus deformable registration software package for analysis. I selected the appropriate statistical tests and carried out the statistical analysis. The distribution of data was assessed to enable selection of appropriate two-sided tests, with no assumption of superiority of the novel registration technique made.. All writing of this article was performed by me, with no review or corrections by any co-contributor.

3.2 Abstract

Background: Intra-prostatic structures may guide image registration but are challenging to identify on CT. HQVCT increases image resolution. We assessed whether HQVCT can improve identification of prostatic structures and image registration.

Methods: Nine men underwent conventional CT, HQVCT and MRI. Two operators attempted to identify prostate structures on CT and HQVCT, with three required for the image to be suitable for registration study. This was only possible with HQVCT. On HQVCT and MR images five experienced radiation oncologists (RO) delineated the prostate. Subsequently a second cohort of five patients underwent imaging with fiducial markers in-situ. All fourteen MR and HQVCT images were independently visually registered by two experienced radiotherapy planners. A single RO then identified interstitial points on each set of registered images and performed a further automated registration based upon these. Registration accuracy after each step was assessed by DSC coefficient of the average prostate contour or mean distance between fiducial markers centroid using the Wilcoxon signed rank test.

Results: It was possible to identify a minimum of three interstitial points on all HQVCT but only four of nine conventional CT. Repeat point based registration took an average of eight minutes (range 6 – 10) and achieved a significant 0.5 mm reduction ($p = 0.02$) in fiducial markers mean displacement and a significant 0.02 increase ($p = 0.01$) in mean DSC coefficient.

Conclusion: HQVCT improves the ability to identify prostatic structures. After visual registration the use of these for point based registration achieved a statistically improved match. Improvements on this method may remove the need for fiducial markers to guide registration.

3.3 Introduction

The use of MRI imaging has been shown to improve prostate delineation accuracy and reproducibility (Rasch et al., 1999a). In addition it allows identification of areas of high density disease within the prostate (Bauman et al., 2013). These characteristics allow for novel dose escalation strategies such as focal dose escalation and highly conformal stereotactic radiotherapy which may improve clinical outcomes. The use of MR imaging in combination with conventional CT based planning is therefore likely to increase.

Combining MR and CT scan datasets for planning requires their accurate registration. Due to the dynamic nature of bladder and rectum volumes over even a short time period, and consequent effect on prostate position, rigid registration of the prostate based on bony anatomy may be inaccurate and registration should be made to the prostate itself (McPartlin et al., 2016b). This is challenging due to the poor characterisation of the prostate anatomy on CT imaging. Intra-prostatic fiducial markers have been considered the gold standard to enable accurate registration, providing mutual points within prostate parenchyma on the two image sets on which to co-register independent of variation in nearby structures (Parker et al., 2003). The use of fiducial markers necessitates an invasive insertion procedure that is not without morbidity; around 1 in 40 patients required hospital admission for uro-sepsis in one series following insertion, consistent with rates experienced after prostate biopsy (Wagenlehner et al., 2014; Loh et al., 2015). The incidence of multi-drug resistant infection is also increasing, worsening the risk profile of this procedure. Without fiducial markers manual image registration is entirely operator dependent relying on the gestalt of a skilled clinician or radiation therapist to match the prostate boundary on the two image sets. A technique for accurate registration without the requirement for fiducial markers or dependent on operator expertise is therefore attractive.

Conventional CT imaging is not of sufficient resolution to allow for consistent identification of intra-prostatic structures with which to guide point registration. CT image resolution can be improved using high quality volume CT (HQVCT). Previously our group has completed a preliminary phantom study demonstrating that a tube current of 3600 mAs is able to enhance the contrast to noise ratio of the CT scan by a factor of 3.5 (Catton and Alasti, 2016). HQVCT can potentially provide rapid acquisition of images suitable for treatment planning with higher contrast and resolution than conventional CT imaging.

We report on the ability of HQVCT imaging to identify mutual interstitial structures with MR imaging. The value of performing point based registration based upon these identified structures after initial visual registration of images is assessed.

3.4 Materials and methods

3.4.1 *Study population*

Images taken as part of a prospective study assessing HQVCT imaging were used. Local ethical approval was obtained and all patients completed informed consent prior to enrolment. Eligible patients were ≥ 18 years old, planned to receive prostate EBRT and suitable for MRI. All patients

were subsequently treated with EBRT at Princess Margaret Cancer Centre. Two cohorts of patients were assessed. In the first cohort, patients without fiducial markers were imaged to remove the potential bias that their presence could introduce to operator manual matching and the degradation they introduce to both CT and MR image quality. A second cohort of patients had three fiducial markers inserted prior to planning imaging, as per local practice for their treatment, due to the potential benefit they could offer in assessing image registration accuracy.

3.4.2 *CT and MR Imaging*

A 320 slice volumetric CT scanner (Toshiba Aquillion 320 slice) was used. The wide coverage provided by the 16 cm-wide detector enabled volumetric image acquisition of the prostate gland in one rotation of 0.5 seconds. HDVCT used this volumetric approach to acquire multiple serial acquisitions of the same anatomy in 6 seconds. These images were averaged together to improve the signal to noise ratio of a final HDVCT image. The rapid acquisition of the 3D images resulted in minimal motion artefact, no increase in partial volume effects, and maintained continuity along the Z-axis. Conventional helical CCT was performed at 120kV, 350mAs and HDVCT at 120kV, 3300mAs. The CCT and HDVCT scans were performed consecutively in the same reference frame of the CT scanner. Subsequently a 3T MRI T2-weighted TSE axial planning scan (Field of view (FOV) 140 mm, slice thickness 2 mm, TR 2500 ms, TE 100 ms, matrix 320x320, in plane resolution 0.4 x 0.4 x 2.0 mm) was performed on the same day as CT imaging.

3.4.3 *Registration methods*

All rigid registrations had six degrees of freedom with three translational and three rotational planes of motion possible. The first stage of the study assessed the relative effectiveness of HQVCT in comparison to conventional CT in identifying mutual interstitial structures for registration. For each of the patients without fiducial markers two radiation oncologists (AM and AH) performed an operator guided rigid registration of MRI and CT imaging, visually matching prostate boundaries, before identifying mutual interstitial structures on MR and HQVCT images and then on conventional CT. Typically these structures were interstitial calcifications or cysts. A minimum of three shared interstitial structures, to allow for localisation in 3-D space, were required for a pair of image sets to be considered suitable for use in image fusion. At this point no further registration was attempted based on the structures identified.

Subsequently for the second stage of the study for all imaged patients two experienced radiation therapists (TL and MV) independently performed manual prostate boundary registration of prostate HQVCT and MR image sets (Boundary Matched BM). MV is a research radiation therapist with an interest in image registration, TL a radiation therapy planner with ≥ five years experience of pelvic CT and MR image registration. They were advised to not use fiducial markers when present to inform their matching. A single operator (AM) then identified interstitial points on each set of matched images and a further automated registration based upon these paired MR and HQVCT interstitial points (interstitial matching IM) was performed using Pinnacle planning software to minimize the root mean square distance between points.

3.4.4 *Registration Assessment*

The accuracy of the sequential registrations was assessed in two ways. For the patients with fiducial markers the displacement of their centroids on each image set was measured following registration using Pinnacle planning software. For each subject the mean displacement of the three fiducial markers was calculated and compared following each registration. Subsequently for images without fiducial markers five expert radiation oncologists delineated the prostate on each of the MR and CT image sets, blinded to patient identity and to existing contours. A schedule of contouring tasks was followed designed to limit memory bias with images from individual cases contoured only once in one session, with a minimum of a week between sessions. For each patient the delineated image sets for each modality underwent deformable registration using in house Morfeus software, which has previously been validated for prostate deformation (Brock et al., 2006). For each patient a mesh of the first contour was created and then deformed to each of the subsequent contours. The mean of the vector projections of the mesh deformation for each modality was taken to create a single volumetric assessment considered to represent the true prostate contour on MRI and CT. DICOM image files were transferred into MATLAB (the Mathworks, Natick MA). Assessment of the agreement of mean CT and MRI contours, with position of HQVCT relative to MRI adjusted based on registration parameters of the BM or IM method, was performed using DSC coefficient. The work flow is shown in Figure 3-1.

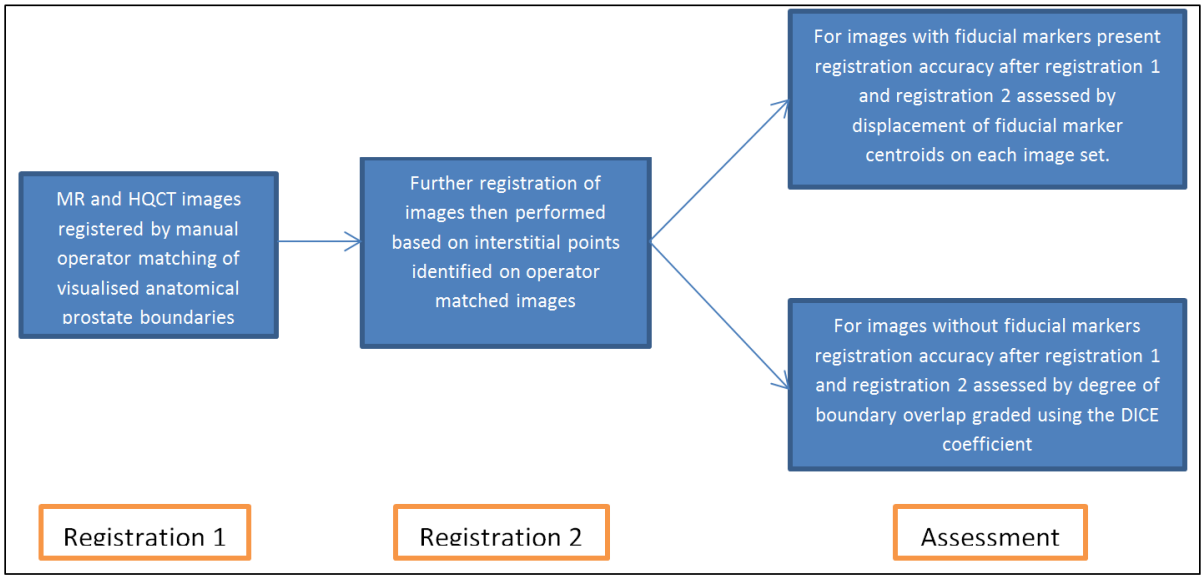

Figure 3-1: Schematic of registration and assessment process

3.4.5 *Statistics*

Distribution of displacements and DSC were assessed using the Shapiro- Wilks test and found to be non-normal. Following operator registration and then interstitial registration the displacement of the fiducial markers or the DSC coefficient for each process was compared using the non-parametric Wilcoxon signed rank test. All tests were two tailed. The tests were performed per operator and for all results to assess whether operator competency affected outcome.

3.5 Results

A total of 14 patients were considered for this analysis, nine without fiducial markers in situ and five with. All imaging was performed as planned without complication.

On imaging without fiducial markers in situ at least three mutual points were identified on all MR and HQVCT image pairs, mean 4.5 (range 3-6). Using conventional CT imaging a minimum of three mutual points were obtained for 4 patients without fiducial markers, mean 1.8 (1-5) ($p = 0.013$) (Figure 3-2).

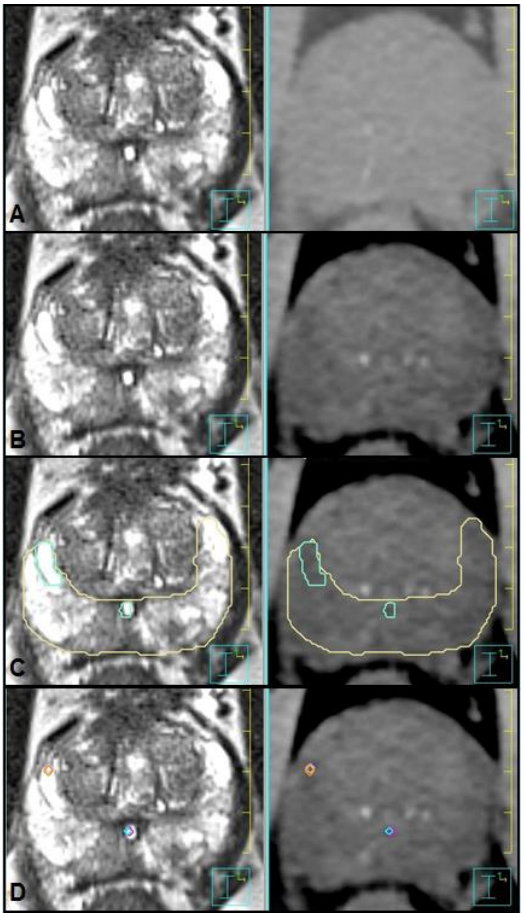

Figure 3-2: Images taken at the same level of the prostate after registration a) T2w MRI and conventional CT with no interstitial structures visible b) T2w MRI and high quality volumetric CT with shared interstitial features seen c) Interstitial contours segmented d) Points for registration picked out on segmented structures

The mean time for each operator to manually register MRI and HQVCT imaging using boundary matching was 25 minutes (range 15 –35 minutes). The mean time to perform repeat registration based on identified mutual interstitial points was 8 minutes (range 6-10 minutes).

The displacement of fiducial markers centroids after boundary registration and subsequent point registration for each operator is shown in (Table 3-1). Overall following point registration there was a significant reduction in the mean displacement distance of 19% ($p = 0.022$). Mean displacement distance was increased in three cases following secondary point registration. When analysed individually there was a significant reduction in mean displacement for operator 2 ($p = 0.007$) but not for operator 1 ($p = 0.45$). Table 3-2 shows DSC coefficient for nine patients without fiducial

markers after manual registration and then interstitial registration. Interstitial point registration performed after boundary registration was found to significantly improved DSC coefficient for operator 2 (p = 0.02), but not operator 1 (p = 0.30). Overall there was a significant mean DSC coefficient increased 0.02 (p = 0.01) following repeat interstitial based registration. In three of 18 instances repeat interstitial point registration caused a decline in DSC coefficient.

Table 3-1: Displacement of centroid of fiducial markers on MRI and HQVCT after (1) Operator registration of identified prostate boundary (2) subsequent further registration based on identified interstitial points

		Step 1: Boundary registration				Step 2: Interstitial registration				Change Mean (mm)	P value*	
		Displacement (mm)				Displacement (mm)						
		Inf FM	Mid FM	Sup FM	Mean	Inf FM	Mid FM	Sup FM	Mean			
Operator 1	Pt 1	3.8	2.0	1.1	2.3	4.4	4.0	1.8	3.4	1.1	0.45	0.022
	Pt 2	0.4	0.6	6.8	0.6	0.6	2.2	2.1	1.6	1.0		
	Pt 3	3.7	2.6	3.7	3.4	2.7	1.6	2.2	2.2	-1.2		
	Pt 4	1.3	1.9	2.5	1.9	1.2	0.9	1.6	1.2	-0.7		
	Pt 5	3.1	2.2	2.3	2.5	2.2	0.7	0.6	1.2	-1.3		
Operator 2	Pt 1	3.2	4.5	5.8	4.5	2.1	2.9	5.3	3.4	-1.1	0.007	
	Pt 2	2.7	2.0	2.3	2.3	2.0	3.4	2.6	2.7	0.4		
	Pt 3	3.6	3.9	5.0	4.2	0.26	0.25	2.9	2.6	-1.6		
	Pt 4	2.4	2.8	2.2	1.9	2.0	0.2	1.3	1.2	-0.7		
	Pt 5	1.7	2.0	2.4	2.0	1.0	1.7	1.6	1.4	-0.6		
*Wilcoxon signed-rank test; Inf, Inferior; Mid, Middle; Pt, Patient; Sup, Superior												

Table 3-2; DSC coefficient of prostate contours on MRI and HQVCT after (1) Operator registration of identified prostate boundary (2) subsequent further registration based on identified interstitial points

	Operator 1 (MV)			Operator 2 (TL)		
	DSC coefficient			DSC coefficient		
	Step 1: Boundary Registration	Step 2: Interstitial registration	Change in DSC coefficient	Step 1: Boundary Registration	Step 2: Interstitial registration	Change in DSC coefficient
Pt 1	0.899	0.914	0.015	0.902	0.907	0.005
Pt 2	0.844	0.855	0.011	0.849	0.854	0.005
Pt 3	0.856	0.830	-0.026	0.818	0.832	0.014
Pt 4	0.882	0.892	0.010	0.846	0.874	0.028
Pt 5	0.768	0.798	0.030	0.711	0.732	0.021
Pt 6	0.854	0.878	0.024	0.837	0.883	0.046
Pt 7	0.873	0.881	0.008	0.707	0.869	0.162
Pt 8	0.884	0.871	-0.013	0.837	0.828	-0.009
Pt 9	0.898	0.901	0.003	0.786	0.796	0.010
Average	0.862	0.869	0.007	0.810	0.842	0.031
P value*	Step 1 DSC vs Step 2 DSC = 0.301			Step 1 DSC vs Step 2 DSC = 0.020		
	Overall Step 1 DSC vs Step 2 DSC = 0.01					
*Wilcoxon signed-rank test, Pt, Patient						

3.6 Discussion

This study has assessed the potential use of common interstitial points identified on HQVCT to improve MR to CT registration. It has been demonstrated that the use of HQVCT imaging allows the consistent identification of interstitial structures which would not be possible using conventional CT imaging. The identification of interstitial structures and subsequent registration using these points was done in a timely manner, adding an average of eight minutes onto the registration workflow.

Using these identified structures it has been shown that a statistical improvement in registration measured by DSC coefficient ($p = 0.01$) can be achieved by repeat point based registration after expert boundary matched registration. When analysed individually this statistical benefit was seen for operator 2 ($p = 0.02$) but not operator 1 ($p = 0.3$). In addition a significant 19% reduction ($p = 0.022$) in the mean displacement of fiducial markers centroids was achieved by repeat registration using interstitial points. Again when analysed individually a statistically significant reduction was seen for operator 2 ($p = 0.007$) with repeat registration but not for operator 1 ($p = 0.45$). Of note operator 2, although experienced, had less expertise in image registration.

The improvement in mean displacement seen could have clinical significance; for operator 2 the improvement in accuracy of registration achieved, assuming the fiducial markers centroid to represent perfect registration appears to be in the order of 1-2 mm.

In the second portion of this study an alternative validation strategy was employed, using prostate contours delineated by five expert radiation oncologists to assess registration accuracy. The use of repeat interstitial point registration achieved a statistically significant improvement in DSC coefficient following one operator's boundary registration. The clinical significance of any improvement achieved is hard to quantify. An improvement in average DSC coefficient from 0.810 to 0.842 is unlikely to have any clinical significance, however but for the patients with largest increase in DSC the improvement in matching does appear clinically relevant (Figure 3-3).

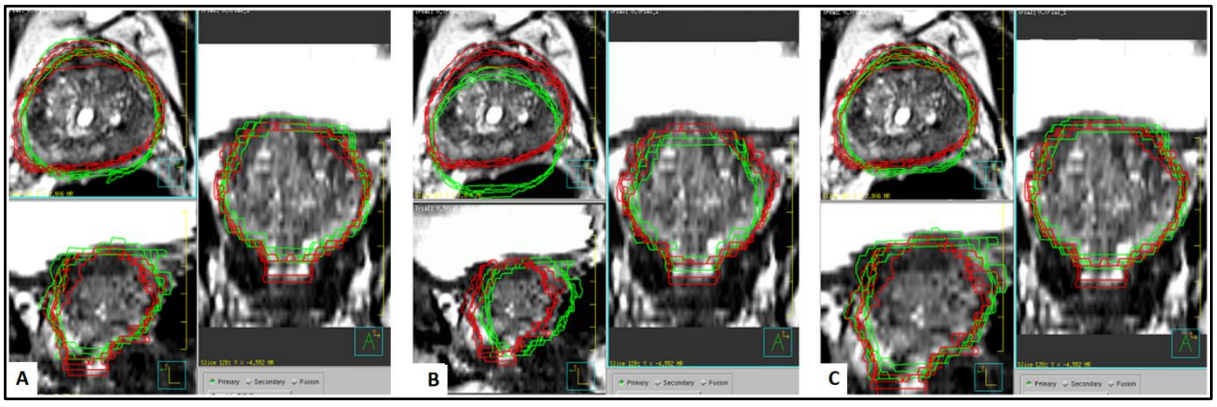

Figure 3-3: Comparison of contour position for patient seven with the contours of each clinician on CT and MR imaging shown (Red = MRI prostate contours, Green = High quality volumetric CT prostate contours) A) After operator 1 boundary registration (Dice Similarity Co-efficient (DSC) score 0.873) B) After operator 2 boundary registration (DSC score 0.707) (C) After repeat interstitial point registration for operator 2 (DSC score 0.869)

In a minority of cases, using both fiducial markers displacement and DSC coefficient for assessment, repeat point registration caused a small decline in registration accuracy. These patients were those in whom it was more challenging to identify mutual points and emphasises that HQVCT although an improvement over conventional CT imaging for identifying interstitial structures is an imperfect solution. Ongoing analysis is looking at the administration of intravenous contrast at the time of imaging to further improve visualisation of prostate parenchyma (Figure 3-4). This appears to enable more confident identification of intra-prostatic structures and will be the subject of future work.

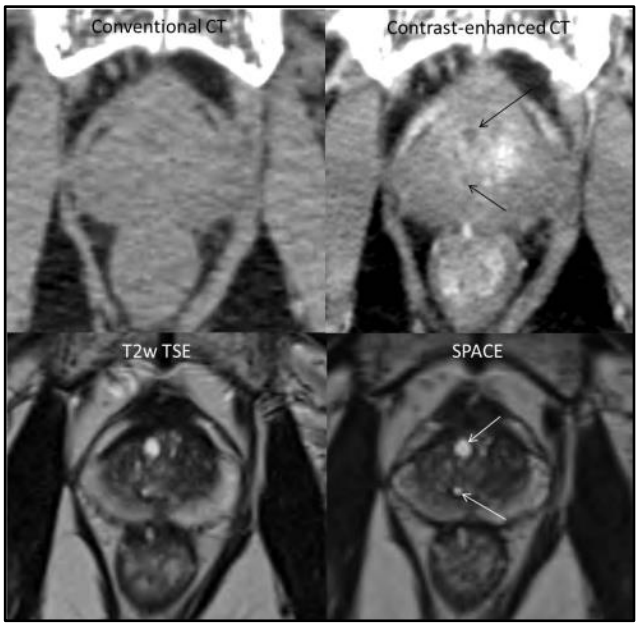

Figure 3-4: Comparison of prostate parenchyma visualised on various imaging modalities pre and post contrast

The study has shown a benefit to repeat point registration after operator controlled boundary registration. The repeatability of this outcome using different operators with different skill sets has not been demonstrated and is of interest. It is however acknowledged that the accuracy of matched interstitial points may be flawed due to the three dimensional nature of the structures which identified; finding an identical point on the structure on CT and MR images, when the gap between axial slices means the same points of the structure may not be seen on both scans, is unlikely. A better approach might be to contour the entire structure on both images and then register using an iterative approach, as has been used for fiducial markers previously, although image quality meant this would not be routinely possible with the current CT imaging technique (Huisman et al., 2005).

Conclusions regarding the potential improvements achieved using this additional registration technique are limited by the absence of a definitive registration with which to compare the two processes against. For the initial part of this study fiducial markers centroids were assumed to represent the optimal registration but this is not without issue. It is known that fiducial markers can shift following insertion during a course of radiotherapy (Delouya et al., 2010). By performing CT and MRI on the same day the risk of this was controlled for however some acute swelling of the

prostate following insertion or a shift of fiducial markers might have occurred. It is also known that gold fiducial markers introduce magnetic field distortion to MR imaging causing small deviations of < 1mm in imaged marker position relative to the actual position (Jonsson et al., 2012). An additional consideration is that the centroid of the fiducial markers on CT and MR was used assess registration of images rather than iterative closest point of the entire fiducial markers, which was not possible in this current study but has been shown to improve matching by around 1 mm (Huisman et al., 2005). Finally the use of 3mm thick axial HQVCT slices means any assessment of registration accuracy is limited by this resolution, making it impossible to identify the exact centroid of the fiducial markers. Taken in combination these potential sources of error make the variation between matching on fiducial markers and interstitial points harder to interpret and mean that registration based on them may not truly represent the optimal prostate fusion in this cohort. Following interstitial registration the fiducial markers centroids remained mismatched per patient by an average of > 1 mm in all dimensions and in the worst patient by > 3 mm, error which could easily be accounted for by the issues discussed.

The use of averaged contours to assess accuracy of registration is also problematic, relying on the assumption that they will most closely represent the true prostate boundary. It has been shown when contouring on CT imaging the anterior prostate is routinely over-contoured and posterior prostate under-contoured in comparison to MR imaging (Gao et al., 2007). In addition variation in the identification of prostate apex and base is greater on CT than MRI imaging and overall contoured prostate volume is consistently lower on MR than CT imaging (Tanaka et al., 2011b). As a consequence comparing CT and MR image delineations, which may effectively be contours of slightly different structures, will show an apparent registration error assessed using DSC even if the matching of the image sets is perfect. The DSC coefficient may not therefore represent accurately the quality of registration and the highest DSC score may not always be due to the best technique. These issues with variation of the identified prostate on MR and CT imaging are also what makes simple registration based on CT and MR prostate contours inaccurate and provides value to identifying interstitial points. Finally although a minimum of three structures were obtained in all cases the quality of interstitial imaging achieved with HQVCT varied, making it challenging in some cases to confidently identify matching points.

The future use of MR imaging to plan radiotherapy deliver, assigning “bulk densities” to tissue structures to mimic the electron density information provided by CT imaging, is of interest. It has been shown that dose differences of <2% in comparison to conventional CT planning can be achieved (Dowling et al., 2012). This approach would remove the necessity of MR/CT image fusion and may in future become common place. In the interval however improved methods of registration remain of interest.

In conclusion the use of interstitial points to guide fusion of MRI and HQVCT imaging shows promise as an alternative method to fiducial markers for accurate image registration, without its associated invasiveness and morbidity. For a proportion of patients identifying interstitial points is challenging but the use of IV contrast agents may improve this and is an area of ongoing investigation.

Chapter 4: Risk of Inadequate Sampling Despite MRI-Guided and Tumour-Targeted Prostate Biopsy

McPartlin AJ, Ghai S, Berlin A, Simeonov A, van der Kwast T, Catton C, Bristow R, Bayley A, Warde P, Gospodarowicz M, Chung P, Ménard C

4.1 Background and contribution of authors

A novel method for MR/CT image registration has been discussed in the previous chapter. Integrated MR/CT imaging allows the possibility of identification of areas of high density within the prostate on MP-MRI which would be impossible with CT imaging alone. As discussed in chapter 1 these areas may benefit from selective dose escalation to improve outcome for patients. The PIRADS scoring system is able to grade the likelihood that areas of disease identified on MP-MR contain disease. This chapter assesses whether lesions with a high probability of containing disease based on their PIRADS score should be biopsied prior to delivery of a focal boost to the region.

The analysis is based upon data generated from the ongoing TARGET study being carried out at Princess Margaret Cancer Centre. The idea for the analysis of biopsy outcome was from Cynthia Menard. I performed analysis of the data and statistical analysis, choosing appropriate statistical tests and carrying out all calculations. I wrote the entire report and discussion before minor revisions were suggested by Cynthia Menard

4.2 Abstract

Background: The merit of MR guided biopsies (MRGB) in patients with highly suspicious multi-parametric MRI (MP-MRI) prostate appearances is unclear.

Objective: Assess efficacy of in-bore MRGB via a trans-perineal template of PIRADS v2 4-5 lesions in patients with previously positive TRUS biopsy.

Design, Setting, and Participants: From 2012-2015 31 eligible men with biopsy proven prostate cancer participated in a single institution prospective study of selective dose escalation to a dominant intra-prostatic lesion. All underwent MP-MRI and in-bore trans-perineal MRBG of suspicious lesions prior to treatment. Results for PIRADS v2 4-5 targets are reported

Interventions: MP-MRI, in-bore trans-perineal MRGB.

Outcomes Measurements and Statistical Analysis: Distribution of disease, histology of biopsy results, location of needle relative to target (central/marginal). Characteristics of significant vs. non-significant or negative biopsies were compared using Mann Whitney, Fishers exact t-test, logistics regression and chi-squared.

Results and Limitations: In 30 men 84% (35) of 42 targeted lesions and 67% (58) of 84 core biopsies contained significant disease. Non-significant or no disease was reported in 16% (7) of lesions. Four negative lesions were confirmed to harbour significant disease on separate repeat biopsy. No significant difference in target location for positive vs. remainder was identified. All centrally sampled lesions yielded significant disease vs 59% of marginal ($p < 0.001$). Positive core involvement was greater following central sampling 66 vs 44% ($p = 0.005$). Marginal deflection occurred in 74% of cores. The study is limited by the lack of prostatectomy specimens to confirm disease location and characteristics.

Conclusions: Over 92% of lesions were ultimately confirmed to harbour significant disease and a 9% false negative rate was seen. Multiple targeted samples or confirmation of central sampling may mitigate this.

4.3 Introduction

Multi-parametric MRI is the gold standard imaging modality for detecting significant cancer within the prostate gland (Weinreb et al., 2016). Its use has been demonstrated to increase MRI performance in cancer detection (de Rooij et al., 2014a). Various methods for reporting MP-MRI have been proposed to standardise acquisition, interpretation and reporting with the Prostate Imaging Reporting and Data System (PIRADS) commonly used (Barentsz et al., 2012b; 2014) This method grades lesions with a 5 point Likert like scale from 1, highly unlikely to represent disease, to 5, highly likely. Targeting of a MP-MRI identified abnormality during diagnostic procedures is an area of promise; the use of MR guided biopsy (MRGB) appears to have similar efficacy to conventional TRUS biopsy to identify significant disease while identifying less non-significant disease and requiring less biopsy samples (Kasivisvanathan et al., 2013). The sensitivity and specificity of MRGB increases with higher risk PIRAD features on MR-imaging (Delongchamps et al., 2013). Lesions with score 4 or 5 appearance have been shown to correlate with incidence and location of significant disease in RP specimens and to yield significant disease in 86 and 93% of targeted biopsies respectively (Delongchamps et al., 2015a; Thompson et al., 2014).

MRGB may be performed via the rectal wall or perineum. Trans-perineal biopsies improve detection rates and reduce the risk of false negative results in comparison to conventional TRUS (Chang et al., 2013). Targeting may be performed within the magnet (in-bore), by use of registration of previous MR imaging fused with real time ultra-sound or with cognitive targeting combining US biopsy with clinicians prior knowledge of MR findings (Moore et al., 2013b). Each technique has merits in terms of speed, cost and accuracy. Trans-perineal in-bore MR-guided biopsies, first reported in 2001, allow for intra-procedure identification of needle and target lesion but remains an area of limited research (Hata et al., 2001). A prospective study reported last year showed this technique to be safe and effective at identifying disease (Penzkofer et al., 2015).

We performed direct in-bore MRGB in patients with known prostate cancer prior to dose-painted radiotherapy. Here we report diagnostic yield of this approach, and describe observed advantages and pitfalls. Reporting followed the Standards of Reporting for MRI-guided Biopsy Studies (START) work-group recommendations (Moore et al., 2013a).

4.4 Design and methods

4.4.1 *Study population*

Thirty-one patients were enrolled on a prospective registered clinical trial approved by our institutional research ethics board between 2013 and 2015 (Chung and Menard, 2012). None have been included in previously published biopsy cohorts.

Eligibility included patients with histologically proven prostate cancer, where low-risk patients were required to have > 50% of diagnostic biopsy cores involved with tumour, and all patients were required to have an overall risk of LN involvement by Roach formula of < 30%. All patients had an identifiable area of disease on screening MRI (Axial T2w TSE + DWI without endo-rectal coil).

A biopsy was considered to contain significant disease if containing ≥ 2 mm of malignant tissue and/or Gleason 4 disease (Goto et al., 1996).

4.4.2 *MRI guided biopsies*

Prior to dose-painted radiotherapy, a confirmation MRI-guided and tumour-targeted biopsy of all identified PIRADS score ≥ 4 lesions was performed using an integrated diagnostic and interventional MRI technique in a 3T Siemens Verio MRI scanner (IMRIS, Minnetonka, Minnesota, US) with endo-rectal coil system (Sentinelle, InVivo). A maximum of 6 cores per patient was permitted.

All patients were imaged and biopsied under propofol anaesthesia in frog-leg position. Trans-perineal biopsies were performed using an integrated trans-perineal template with online stereotactic navigation (Aegis, Hologic) (Figure 4-1). Biopsies were performed with the patient outside of the MRI bore before being returned for confirmation imaging.

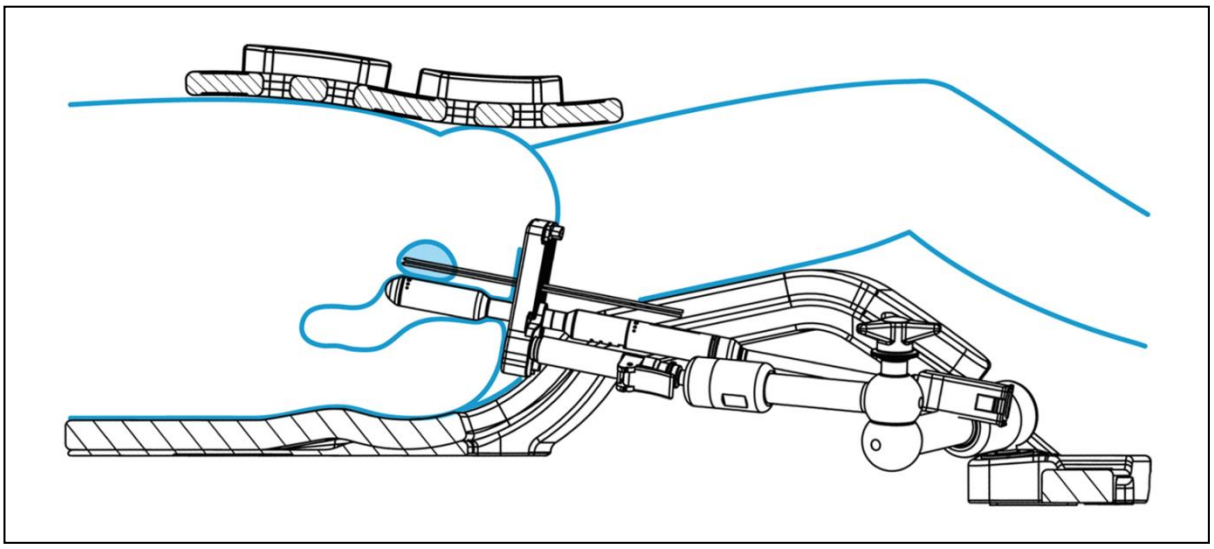

Figure 4-1: Trans-perineal MR guided intervention system

MP-MR images were acquired using an endorectal coil (ERC) and anterior surface coil. The protocol included high resolution T2-weighted TSE axial images (FOV 140 mm, slice thickness 2 mm, TR 2500ms, TE 100 ms, matrix 320x320, in plane resolution 0.4 x 0.4 x 2.0 mm); diffusion weighted imaging (DWI) (FOV 180 mm, slice thickness 3 mm, TR 6000ms, TE 83 ms, matrix 128x128, in plane resolution 1.4 x 1.4 x 3.0 mm, b = 0; 100; 600; 1000) and dynamic contrast-enhanced (DCE) (FOV 180 mm, slice thickness 3 mm, 3D FLASH, TE/TR=1.7/4.3ms, matrix 128x128, in plane resolution 1.4 x 1.4 x 3.0 mm, temporal resolution 5 s, scan time 5 min during bolus infusion of 0.1mmol/kg of gadolinium- DTPA at 4cc/s followed by a 20 cc saline flush). Axial TSE images (FOV 160 mm, slice thickness 3 mm, TR 1250ms, TE 11 ms, matrix 256x256, in plane resolution 0.6 x 0.6 x 3.0 mm) were acquired with co-axial needles (16g, InVivo, Philips) in situ to evaluate tumour-targeting accuracy.

4.4.3 *Data Analysis*

Scoring of lesions on MRI was independently performed by two experienced users with > 5 years reporting experience (CM, SG) using European Society of Urogenital Radiology (ESUR) guidelines

for PIRADS v2.0 (Weinreb et al., 2016). Clinical information was not used to aid decision making. Lesions scored 4 or 5 by both operators were considered in the current analysis. Multiple targets per patient were permissible with individual sites of disease required to be > 5 mm diameter.

Biopsies were considered centrally targeted if tumour features were identified circumferentially on needle-confirmation imaging. A repeat MRI-informed biopsy was performed for select patients with benign histology on MRI-guided biopsy if there was suspicion of false negative. Characteristics of significant vs. non-significant or negative biopsies were compared using Mann Whitney, Fishers exact t-test, logistical regression or the chi-squared test.

4.5 Results

Five biopsied lesions, and one patient, were excluded from analysis when found PIRADS v2.0 <4 by either observer. Ultimately 42 lesions in 30 patients were analysed. Patient characteristics at MRGB are shown in Table 4-1 with median age 68 (range 51-76), median PSA 7 (1.7- 29), 87% ≥ Gleason 7 (3+4) and all T1-T2 disease.

Table 4-1: Patient and disease characteristics

Patient age		68 (51-76)
PSA		7.0 (1.7-29)
Clinical stage	T1c	64%
	T2a	23%
	T2b	10%
	T2c	3%
TRUS Gleason score	3+3	13%
	3+4	64%
	4+3	10%
	4+4	13%
Prostate Volume (cm^3)		44 (24-85)

A median of one (range 1-3) PIRADS 4/5 lesions per patient were identified. Overall, 84 biopsy cores were sampled with a median number of biopsy cores per lesion of two (1-4). The distribution of target lesions is shown in Figure 4-2. The characteristics of positive and negative biopsy targets are shown in table 2. The median time per patient to complete imaging, biopsy, position confirmation and fiducial markers insertion was 2.0 hrs (range 1.5 – 3.3). Significant disease was identified in 69% (58) of MRGB and overall in 83% (35) of targeted lesions.

Six lesions (14%) were found negative for malignancy following MRGB and one further biopsied lesion (2%) contained non-significant disease. All biopsy needles for these seven lesions were identified at the peripheral margin of the tumour, which was not centrally sampled. Four of the seven lesions were confirmed to contain significant disease on a separate repeat biopsy.

All biopsy cores confirmed to be sampled at the centre of the lesion on MRI yielded significant disease. However, the majority of biopsy needles (74%) were deviated to the peripheral margin of the tumour despite central targeting. In lesions < 1 cm diameter > 90% of biopsies were marginal. The positive biopsy yield of cores sampled at the periphery of tumours was significantly lower at 59% ($p<0.001$). The % core-length involvement by malignancy was significantly higher in central vs. peripheral samples (66% vs 44%, $p= 0.005$). Gleason grade however did not significantly differ

between central and marginal cores (p=0.74) with a median score 6 (3+3) in both groups. Successful central tumour sampling was more common in larger lesions (mean diameter 1.6 cm vs. 1.1 cm, p=0.001). There was no significant difference in the PIRADS characteristics or location of disease in those target lesions which did, or did not, yield significant disease. In 3 patients (10%), Gleason grade was higher after tumour-targeted biopsy than at the time of enrolment.

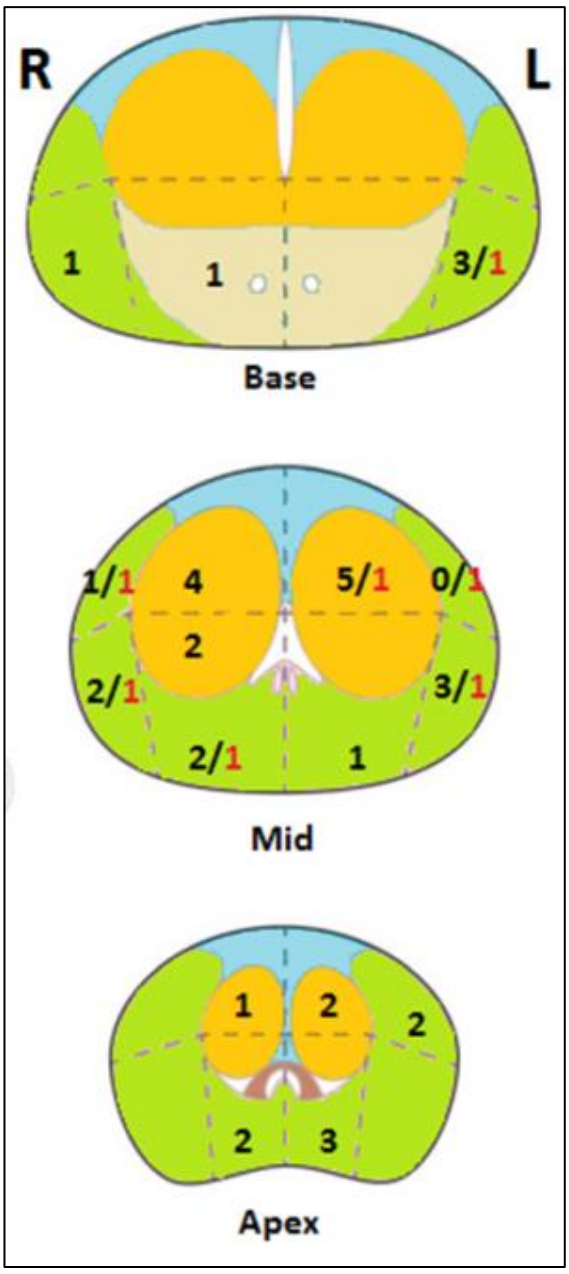

Figure 4-2: Distribution of targeted disease. First number (black) denotes number of positive targeted lesions in region, second number (red) denotes number of lesions having non-significant biopsy results

Table 4-2: Comparison of characteristics of targeted lesions stratified by presence of malignant disease on biopsy

		Significant disease	Non-significant disease	Negative	P-value*
Median target diameter (mm)		12	10	8.5	**0.016**[$]
Number or targets		35	1	6	
Number of biopsies per target	1	12	0	3	0.43* (1 biopsy vs > 1)
	2	15	1	1	
	3	5	0	1	
	4	3	0	1	
	Mean	2	2	2	
PIRADS	4/4	10	1	4	0.72[@]
	4/5	12	0	2	
	5/5	13	0	0	
Central biopsy		22	0	0	**0.0002**[+]
Marginal biopsy		38	2	24	
Area of gland biopsied	Apex	10	0	0	0.33*
	Mid	20	1	5	
	Base	5	0	1	
	Anterior	16	1	2	0.52[+]
	Posterior	19	0	4	

*All significant disease vs. remainder, [$]Mann Whitney [@]logistical regression testing*Chi x^2 test
[+]Fisher's exact test

4.6 Discussion

We report the results of a cohort of patients undergoing direct in-bore MRGB of PIRADS v2.0 score 4 and 5 lesions. This study has demonstrated that despite the use of in-bore MRI-guidance, there is around 10% risk of a false negative biopsy. Our data show that this is primarily due to needle deviation to the peripheral margin of tumours. Other groups have previously shown up to a third of patients with negative MRI guided biopsies have clinically significant prostate cancer, although explicit characterisation of MP-MRI appearance was not made (Sivaraman et al., 2015).

The majority biopsies performed were marginal. The cause of this needle displacement is of interest. Previously, we demonstrated a mean geometric needle placement error of 2.1mm employing this method (Susil et al., 2004), similar to other techniques (Wan et al., 2005; Fichtinger et al., 2006). Deflections seen in that study had a Rayleigh distribution with sigma 1.6 mm, suggesting the error seen was due to deflection within the tissue rather than targeting error. It was also greater than encountered previously in studies using gel phantoms suggesting the relative density of prostate tissues may have increased the effect.

It has been demonstrated that prostate cancer has increased stiffness, measured from viscosity parameter using sono-elastography, than surrounding prostate tissue (Hoyt et al., 2008). As a consequence malignant tissue may induce greater needle deflection than benign gland and would provide a mechanism for the results we observed. Despite targeting lesions with a median diameter of 1 cm 74% of biopsies in our study were identified at the periphery of tumours on confirmatory MRI. Even with in-bore MRGB samples were taken from the periphery of targeted disease and multiple attempts were necessary in some instances to obtain accurate tissue sampling (Figure 4-3).

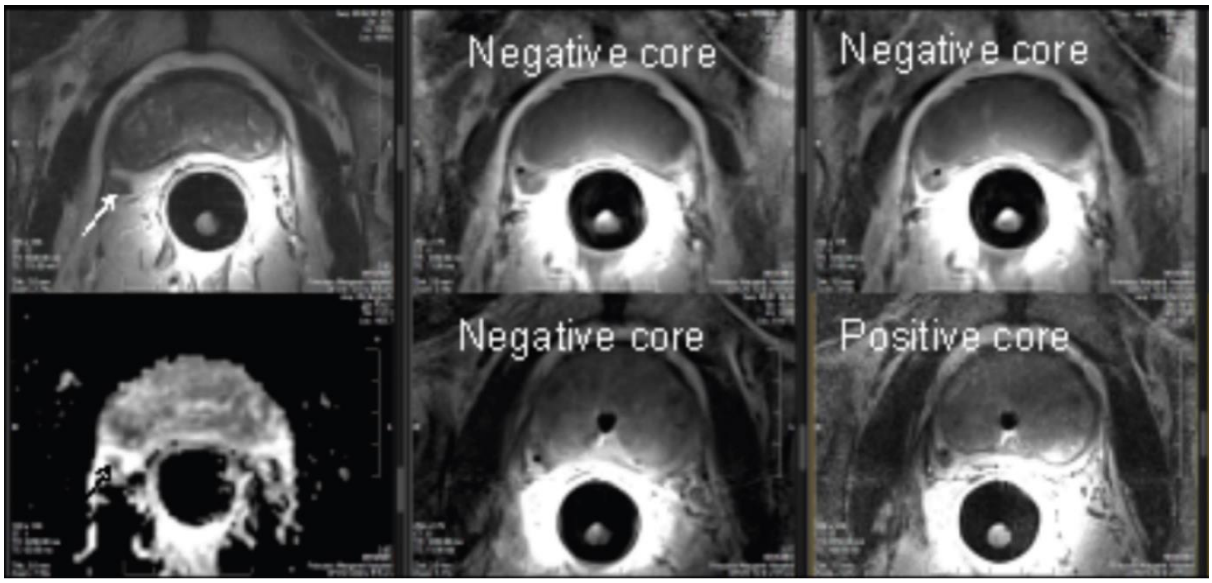

Figure 4-3: MR imaging of repeated sampling of targeted lesion. Four samples required before a centrally located sample, containing malignant tissue, was obtained

For smaller lesions this effect was even more pronounced with > 90% of biopsies targeted to lesions less than 1cm in size deviating to the peripheral tumour margin. We demonstrate that the positive yield of marginal biopsies is compromised compared with central sampling. Central sampling also achieves a more representative sample of tumour with higher percent core length involvement (66% v. 44%).

The primary limitation of this study is a lack of definitive gold-standard, as prostatectomy specimens were not available in this cohort of patients receiving radiotherapy. We attempted to address this limitation by restricting our analysis to lesions that were confirmed PIRADS v2.0 4/5 by two independent and experienced observers, and by carefully analysing the biopsy core location relative to visible tumours on MRI.

Using prostatectomy specimens and pre-operative MP-MRI one published series has demonstrated that 96% of those with PIRADS 4 and 100% of those with PIRADS 5 lesions harbour significant disease (Thompson et al., 2014). Another series using MP-MRI and trans-perineal template biopsies showed a PIRADS 5 score has a specificity of 96.5% for presence of malignancy (Grey et al., 2015). A recent study comparing the performance of systematic vs targeted trans-perineal biopsies, performing a minimum of two biopsies per target, identified 2 of 31 targeted PIRADS 5 lesions as giving false negative results and 2 achieving true negative (Radtke et al., 2015). Both PIRADS 4 and 5 scores were found to have a PPV of > 92 %.

We demonstrate a risk of inadequate sampling and false negative biopsy results in patients who have a visible lesion with high PIRADS score (4-5) even with the use of MR image guidance. Strategies to mitigate this problem could include more targeted sampled cores (4-6 per target). Alternatively, confirmation of central sampling using online MRI-guidance assures representative sampling despite limited core, reducing invasiveness.

Chapter 5: Comparison of dosimetry and toxicity for integrated VMAT or HDR boost treatment for prostate cancer

McPartlin AJ, Lee J, Craig T, Berlin A, Bayley A, Bristow R, Catton C, Chung P, Menard C.

5.1 Background and contribution of authors

This thesis has investigated methods for registering MRI in combination with CT imaging to identify areas of high density disease within the prostate and the necessity of biopsy of these prior to focal treatment intensification. In the introductory chapter the theoretical benefits of focal boosting were discussed with its potential to improve outcome for patients receiving treatment. The best method of delivering this boost, and the likely side effects profile, has not yet been established. This chapter fills some of this current gap in knowledge, investigating dosimetric and toxicity outcome for a cohort of patients receiving a HDR or EBRT focal boost to regions of high density disease identified on MRI.

This work is based upon the ongoing TARGET study being carried out at Princess Margaret Cancer Centre, Toronto (Chung and Menard, 2012). For analysis I identified patients treated on study with a minimum of six months follow up post therapy. I reviewed medical notes and trial information to record all acute and late toxicities experienced. I ensured conformity of contouring on all image sets and generated excel datasheets of DVH data for analysis from Pinnacle planning software. I produced all results seen in the report including DVH curves. The work includes a novel method of dose summation of brachytherapy and EBRT using deformable registration of radiotherapy dose maps. I was involved throughout the development process of this approach, liaising with the physics team. I made the choice of α/β ratio to apply to the deformable dose summation of brathytherapy and EBRT. The process of deformation registration was performed by Jenny Lee, after I had exported all appropriate patients into the Morfeus planning software and identified mutually shared points on CT and MR imaging, when required, to allow initial image registration.

I performed all reported statistical analysis of dosimetric and toxicity data from each arm of the study. I assessed the normality of data distribution and performed appropriate non-parametric tests based on its results. Due to the repeated statistical testing being performed a bonferroni correction was applied to reduce the risk of non-significant differences being identified in error (Moye, 1998).

I wrote the chapter in its entirety. Advice on the passage describing the method of dose summation was provided by Jenny Lee, Physician at Princess Margaret Cancer Centre. Minor revisions to the text were suggested by co-authors for the final draft.

5.2 Abstract:

Background: Focal dose escalation to an area of high disease burden within the prostate may improve outcome while minimising associated toxicity. This study reports dosimetric and early toxicity data from a phase II study of prostate EBRT with dose escalation to identifiable tumour (GTV) via integrated VMAT (VMAT-IB) or HDR brachytherapy (HDR-B) boost.

Methods: Patients with localised prostate cancer, low risk of LN involvement, and identifiable tumour on screening MRI were eligible. Participants received EBRT 76 Gy in 38 fractions to the prostate plus a 95 Gy VMAT-IB or 10 Gy HDR-B to the GTV, manually delineated on multi-parametric MRI. The CTV included the whole prostate gland plus up to 5 mm margin for 0microscopic extension beyond the GTV excluding OAR. CTV was expanded by 5 mm AP/ SI and 3 mm LR to form PTV76. VMAT-IB GTV was expanded by the same margins to form PTV(VMAT-IB). For HDR-B GTV was expanded 2 mm SI and 1 mm AP/RL, excluding OAR, to form the PTV(HDR-B). Penile bulb, urethra, rectum wall and bladder wall were contoured as OAR. Toxicity was recorded prospectively using CTCAE v4.0. For comparative analysis all dosimetry was converted to EQD2 assuming α/β 3 Gy for tumour and OAR. For the HDR-boost arm, the dose matrix for each therapy was combined using deformable registration to account for rectal distortion from an endo-rectal coil during brachytherapy delivery.

Results: From December 2012 to October 2015 26 and 20 patients were treated with VMAT-IB or HDR-B, respectively. There was no significant difference in patient or disease characteristics for either treatment. Median number of visible tumours treated per patient was 1 (1-3). GTV was significantly closer to rectum for HDR cohort. CTV and PTV76 dosimetry was similar. GTV D50 was significantly higher with HDR-B (160 Gy vs 111 Gy, (p=0.0001)). Rectal D0.5cc and D10-D30 was also significantly higher following HDR-B. Other OAR dosimetry was similar. There was no significant difference in acute or late GI and GU toxicity with either treatment.

Conclusions: Both VMAT-IB or HDR-B achieve comparable minimum GTV dose, but higher integral dose to the GTV following a HDR-B. Acute and late toxicity are comparable with either treatment. No episodes of urethral stricture occurred. Overall both approaches are well tolerated with limited toxicity consistent with other published series. Ongoing follow-up, including 3-year biopsy, will further determine long-term outcomes.

5.3 Introduction

Prostate cancer is the most common malignancy amongst men. It is known that dose-escalated radiotherapy improves biochemical control and may improve overall survival. It has been suggested that a dose response may be present up to 200 Gy BED (Crook et al., 2011). Dose escalation is, however, associated with increased treatment-related morbidity and treating the entire gland with EBRT to this level risks significant treatment side-effects (Ohri et al., 2012).

Multi-parametric MRI allows identification of areas of high density disease within the gland, identified as the GTV. Previously it has been shown that local recurrence of disease appears to occur predominantly within this region (Arrayeh et al., 2012; Cellini et al., 2002a). Recurrence rates of up to 60% have been reported in patients with tumour > 1cm visible on MRI prior to radiotherapy (Joseph et al., 2009a). Delivering a focal dose boost to the GTV may improve outcome whilst minimising associated increased toxicity. This escalation can be delivered as an integrated boost (IB) during external beam radiotherapy (EBRT) or using HDR brachytherapy. Limited data has been published assessing toxicity and outcome of either approach (Bauman et al., 2013). There is no prospective comparative data for these two approaches.

The Target study is an ongoing prospective phase II study assessing the use of a HDR boost (HDR-B) or integrated VMAT boost (VMAT-IB) for patients undergoing conventional EBRT with an identified GTV on MRI (Chung and Menard, 2012). This study reports dosimetric and early toxicity outcomes following delivery of a VMAT-IB or HDR-B in a cohort of prostate cancer patients from this study.

5.4 Methods and Materials

5.4.1 *Patients and treatment*

This study includes the first 46 patients enrolled and treated in a phase II prospective study delivering a VMAT-IB or HDR-B with EBRT for prostate cancer from 2012 to 2015. The study received ethical approval and all patients completed signed informed consent prior to enrolment. Choice of boost technique was at the discretion of patient and treating physician. Patients were required to have an identifiable and biopsy proven intra-prostatic lesion with >5 mm maximal diameter but with <33% of prostate volume on MP-MRI. All were ≥ 18 years old with ECOG performance status 0-1. All disease characteristics were permitted but those low risk (Gleason 6 and PSA < 10 and T1) were required to have > 50% of biopsy cores involved with tumor and all patients had risk LN involvement < 30% by Roach formula (=2/3*PSA((GS-6)*10)). Patients were ineligible if any diagnosis of non-skin cancer had been made within five years of enrolment or they had commenced hormone therapy > 2 weeks prior to enrolment. On study high risk patients were allowed up to six months of hormone therapy at the discretion of the treating physician. All had to be suitable for MRI and have no contraindication to an endorectal coil or sedation.

MRI was used to confirm eligibility prior to enrolment with either a diagnostic MRI (performed within three months of enrolment) or alternatively a screening MRI with T2-weighted FSE and DWI sequences.

5.4.2 *MR imaging*

Patients underwent MP-MRI using an integrated diagnostic and interventional MRI technique in a 3T Siemens Verio MRI scanner (IMRIS, Minnetonka, Minnesota, US) with endorectal coil system and body matrix (Sentinelle, InVivo). Three fiducial markers were inserted at time of MP-MRI at the region of suspected tumour burden, in the apex and in the base of gland to guide image fusion and treatment setup. At the time of fiducial markers insertion in-bore MR-guided biopsies were performed to confirm presence of malignant tissue. The requirement for histological confirmation was removed with evolving experience during the study due to likelihood of false negative biopsy (see Chapter 5). The imaging protocol included high resolution T2-weighted TSE axial images (FOV 140 mm, slice thickness 2 mm, TR 2500 ms, TE 100 ms, matrix 320x320, in plane resolution 0.4 x 0.4 x 2.0 mm); diffusion weighted imaging (DWI) (FOV 180 mm, slice thickness 3 mm, TR 6000 ms, TE 83 ms, matrix 128x128, in plane resolution 1.4 x 1.4 x 3.0 mm, b = 0; 100; 600; 1000) and dynamic contrast-enhanced (DCE) (FOV 180 mm, slice thickness 3 mm, 3D FLASH, TE/TR=1.7/4.3ms, matrix 128x128, in plane resolution 1.4 x 1.4 x 3.0 mm, temporal resolution 5 s, scan time 5 min during bolus infusion of 0.1mmol/kg of gadolinium- DTPA at 4cc/s followed by a 20 cc saline flush).

Subsequently a separate T2w MRI without ERC was performed in the treatment position immediately before or after CT simulation. For radiation planning, target lesions were identified on MP-MRI sequences and this information was combined with known histological diagnosis to contour the GTV on T2w-ERC image set Multi-parametric images were registered to non-ERC T2w and CT using interstitial points and fiducial markers for guidance. Localisation of GTV was determined by reviewing T2, ADC and DCE images. On both non-ERC and ERC T2w images the prostate was contoured and the GTV deformably registered onto the non-ERC T2w image set using in house software (Morpheus research group). Morfeus, a biomechanical-based deformable registration technique, has been previously described and validated for the prostate (Hensel et al., 2007). Contours were manually adjusted if required based on CT and non-ERC T2w images to ensure full coverage of target structures.

CTV76 was contoured on non-ERC T2w and included the entire prostate and a 5 mm uncertainty margin beyond the GTV, trimmed off muscle, bladder and rectum. PTV(CTV) was formed by expanding 5 mm anterior-posterior/superior-inferior and 3 mm left-right on CTV76. For VMAT boost the sum of GTVs, if multiple targets present, was considered CTV95. This was expanded 5 mm anterior-posterior/superior-inferior and 3 mm left-right to form PTV(VMAT-IB). For HDR-B the GTV was expanded 2 mm from GTV, except 1 mm left and right, excluding urethra, bladder and rectum and to a maximum of 1 mm beyond the CTV76 to form the PTV(HDR-B).

OAR contoured for planning were penile bulb, distal urethra, rectal wall, bladder wall and femoral heads. The rectal wall was contoured as a 3 mm thick cylindrical structure extending 18 mm cranial and caudal to the CTV76 volume. Bladder was contoured as a 3 mm thick structure contoured 18 mm superior to the CTV76.

Dose delivered via VMAT-IB or HDR-B was calculated to be biologically equivalent assuming α/β prostate = 1.5 Gy for dose equivalence calculations (Vogelius and Bentzen, 2013). All patients

received EBRT to the whole prostate gland (CTV) of 76 Gy in 38 fractions marginally reduced from our standard institutional practice of 78 Gy in 39 fractions. An equivalent 2 Gy per fraction (EQD2) dose of 109 Gy was then delivered to GTV using a VMAT-IB of 95 GY in 38 fractions or HDR-B of 10 Gy delivered in the week prior to EBRT. Dose constraints for EBRT treatment are shown in Table 5-1.

Table 5-1: External beam radiotherapy dose constraints

Volume of interest	Metric	HDR-B (Gy)	VMAT-IB (Gy)
PTV(VMAT-IB)	D99	-	≥ 90.2
	Max (1cc)	-	≤ 99.8
PTV76	D99	≥ 72.2	≥ 72.2
	Max (1cc)	≤ 79.8	-
Rectum Wall	D50	≤ 30	≤ 30
	D30	≤ 48	≤ 48
	Max (0.5cc)	-	≤ 90
Bladder Wall	D50	≤ 30	≤ 30
	D30	≤ 48	≤ 48
	Max (0.5cc)	-	≤ 90
L/R Femur	D5	≤ 42	≤ 42
Penile bulb	D30	≤ 54	≤ 54
Urethra	Max (0.1cc)	-	≤ 99.8

5.4.3 *Brachytherapy*

Prior to brachytherapy patients received light propofol sedation and were immobilised in the dorsal lithotomy position on the interventional MRI table (Hologic Inc). A sterile MRI-compatible perineal template and endorectal coil (Hologic Inc) was positioned and immobilised against the perineum (Figure 5-1).

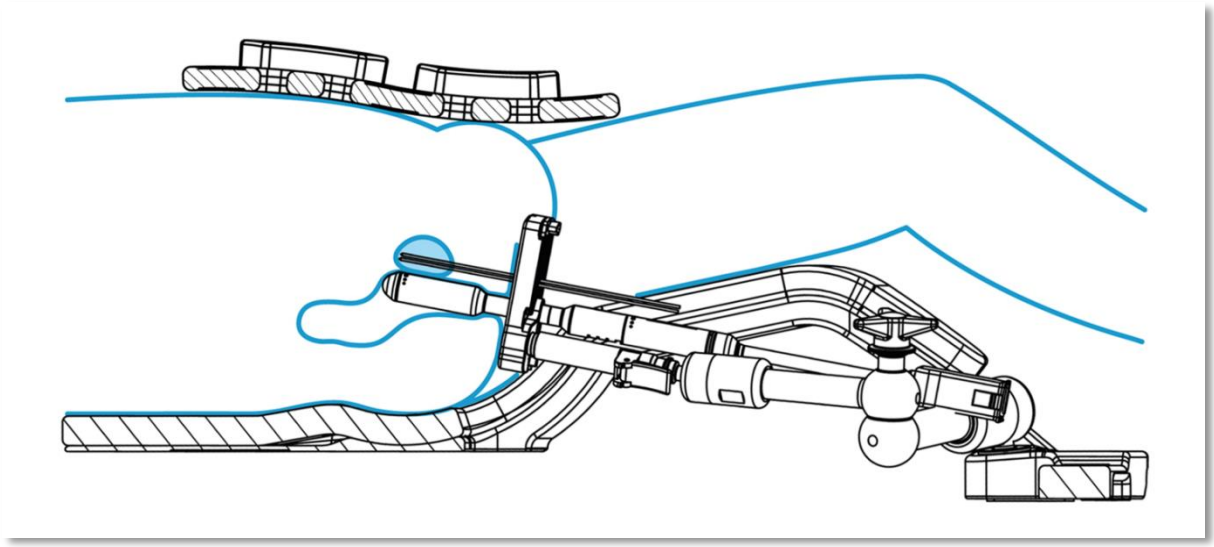

Figure 5-1: Trans-perineal biopsy template and endorectal coil

MR images were acquired for device registration and catheter target sites identified in targeting software (Aegis, Hologic Inc, ITA). MRI was obtained with catheters in position for treatment

planning and exported to treatment planning software (Oncentra, Nucletron). GTV and PTV(HDR-B) contours were deformably registered onto this MRI (Morpheus) and edited by treating physician as required. Patients were transferred to the HDR suite and verification x-rays were performed to assess for catheter displacement before delivery of a single 10 Gy HDR treatment. Dose constraints for HDR-B are shown in (Table 5-2).

Table 5-2: High dose rate brachytherapy organ at risk dose constraints

Volume	Dose constraint
GTV	V100 = 100%
PTV(HDR-B)	V100 > 98%
Rectum D 0.5cc	< 8 Gy
Urethra D 0.5cc	< 12 Gy
Bladder D 0.5cc	<12 Gy

5.4.4 *Scoring of toxicity, end points, analysed variables*

All patients were assessed at baseline, during and after completion of therapy using CTCAE v4.0 toxicity assessment (NICI, 2009). Follow up was scheduled at 1, 3, 6 months and 1, 2 and 3 years after therapy. Any toxicity occurring within the first 6 months of follow up was considered an acute toxicity. Any patient with follow-up greater than 6 months was assessed for late toxicity after this time-point.

5.4.5 *Dosimetric Analysis*

For dosimetric analysis EBRT dose data was extracted from PINNACLE planning software and converted to EQD2 equivalent assuming a conservative α/β 3 Gy for prostate and OAR, (Michalski et al., 2010; Brenner et al., 2002). Conversion was performed using:

$$EQD2 = n*d*(d + \alpha/\beta)/(2+ \alpha/\beta)$$

Where n is number of fractions, d is dose per fraction. This allowed for uniform conversion of the HDR_B dose matrix for treatment effect and late toxicity and summation in a single step with converted EBRT.

The distance of treated disease from rectal wall was measured using Pinnacle software and recorded as the minimum separation distance of any two points from each of the structures. For patients receiving a HDR brachytherapy boost the presence of the endorectal coil at time of brachytherapy delivery had the potential to cause rectal and prostate distortion, affecting dose received by these structures. Applying the HDR-B dose-grid to the previously acquired CT SIM would not account for this distortion. To prevent error being introduced by simple summation of treatment doses the brachytherapy dosimetry was therefore converted to EQD2 equivalent and deformably registered onto planning CT using MORPHEUS software. The brachytherapy treatment MRI (primary image to be registered) and the prostate non-ERC T2w (secondary image) were first bought closer together by point-based rigid registration. A guided surface projection was performed to map the primary surface of the prostate and rectum onto the corresponding surface generated from the secondary image. These surface displacements were applied as input to a

finite element model resulting in a deformation vector field that mapped the 3D dose distribution from brachytherapy treatment MR to non-ERC T2w.

The registration accuracy of deformable dose summation was measured as the signed error between the MORFEUS-predicted displacement and observed displacement of 3D common points (implanted markers or calcifications) within the prostate. Analysis was performed to assess for any clinically significant effect from the use of deformable dose summation in comparison to rigid summation. To account for the uncertain effect of ERC insertion a root mean squared analysis of the difference in dose to various rectal volumes for all patients was performed to look for areas of maximum discrepancy.

5.4.6 *Endpoints*

Comparative analysis of dosimetry for VMAT-IB and HDR-B and correlation with acute and late toxicity. Dosimetry was compared in 10 Gy bins for targets and OAR. D_{min} was considered at the minimum dose to 99.9% of a given volume.

5.4.7 *Statistical analysis*

Non-Gaussian distribution of data was confirmed using the D'Agostino-Pearson omnibus K2 test. The Wilcoxon signed-rank test was used to compare calculated rectal dose following rigid and deformed dose summation of external beam radiotherapy and HDR-B. Patient characteristics, target dosimetry and toxicity were compared using Mann Whitney U, Fishers Exact test and χ^2. For multiple comparisons of dosimetry and toxicity a Bonferroni correction was made (Moye, 1998).

5.5 Results

From August 2012 to June 2015 VMAT-IB was delivered to 27 patients and HDR-B to 20 patients. Median follow up was 11.9 months (range 0-35 months) and 17.7 months (range 2-35 months) following VMAT-IB and HDR-B respectively. The characteristics of the two cohorts are shown in Table 5-3. A median of 1 lesion (range 1- 3) was identified and boosted per patient. The mean volume of delineated GTV per patient was 2.9 cm^3 (range 0.6 - 9.0 cm^3) and 2.2 cm^3 (range 0.2 - 4.6 cm^3) for VMAT and HDR treatment respectively. The location of disease treated in both arms is shown in Figure 5-2.The median minimum distance of GTV targets to closest rectal wall was 11.5 mm (1-30 mm) and 4 mm (1-25 mm) ($p = 0.01$) for VMAT-IB and HDR-B respectively.

5.5.1 *Effect of deformable dose registration*

The mean (SD) signed error of common point registration was 0.3(1.5) mm, 0.8(2.3) mm and 0.5(2.5) mm in LR, AP, and SI respectively, over 63 markers for the 20 patients. In vector magnitude, the average (SD) error was 3.4 (1.8) mm. The registration accuracy was comparable to the largest dimension of the image resolution of 2 mm.

Comparison of mean DVH for rectal dose using deformable or rigid summation was performed for 18 of 20 patients receiving HDR-B. This did not identify a change in AUC with either approach (Figure 5-3). In particular there was not, on average, a significant increase in dose received to small volume of rectum following deformation ($D2_{rigid}$ 88.5 Gy vs $D2_{deformed}$ 85.7 Gy ($p = 0.686$).

Table 5-3: Patient characteristics

Characteristic		VMAT	HDR	p-value
Number of patient		26	20	-
Mean age years (range)		70.8 (51-82)	67.0 (58-77)	0.07*
Stage	T1c T2a T2b T2c T3a	16 7 2 0 1	12 5 1 2 0	0.476^
Median PSA		6.7	8.0	0.84*
Median(range) target lesions		1 (1-3)	1 (1-3)	0.4*
Location	Base Mid Apex	5 20 5	3 17 6	0.586^
Median sum GTV volume cm^3 (range)		2.9 (0.6-9.0)	2.2 (0.2-4.6)	0.31*
*Mann Whitney; ^ χ^2 test; GTV, Gross tumour volume; HDR, High dose rate; PSA, Prostate specific antigen; VMAT, volumetric arc therapy				

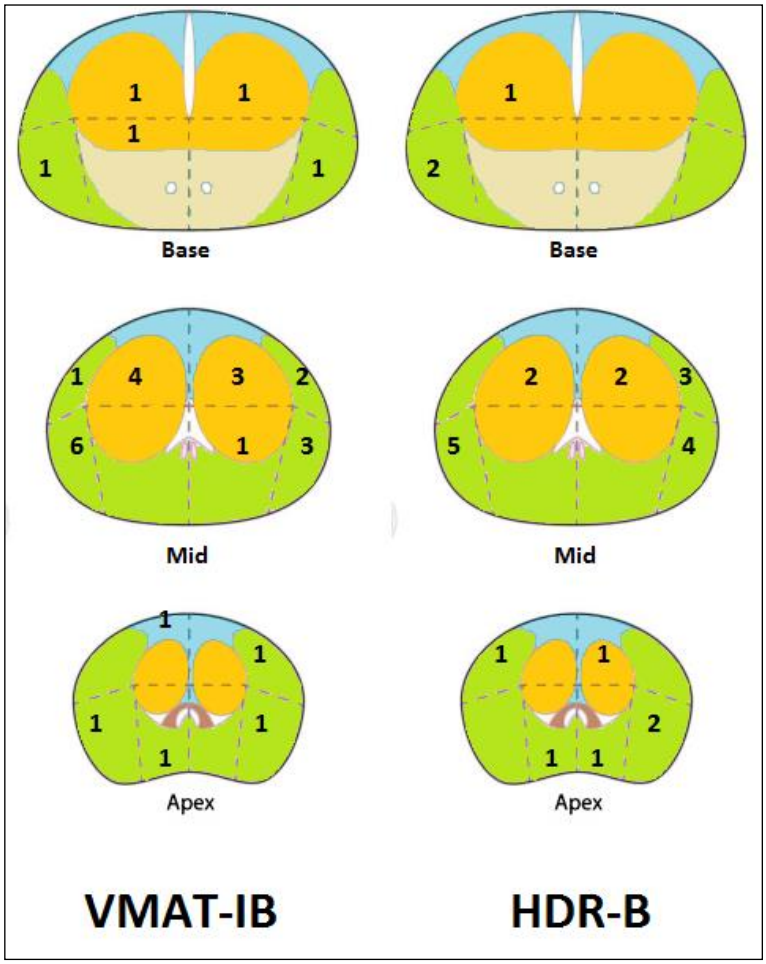

Figure 5-2: Disease location of patients undergoing Volumetric Arc Therapy Integrated Boost (VMAT-IB) or High Dose Rate Boost (HDR-B)

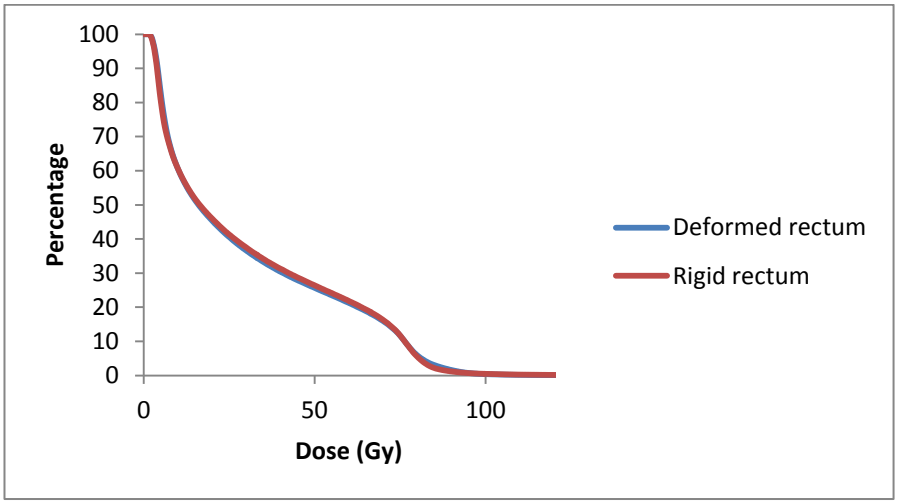

Figure 5-3: Dose volume histogram for rectum and deformed rectum

Further assessment of pre and post deformation structures in patients receiving HDR-B identified a proportion in which the introduction of an ERC caused a movement of the GTV away from, and not towards, the rectal wall. In this circumstance the rectal dose received from HDR would be overestimated if this were applied to the non-deformed CT-SIM rectal contour. In contrast for others the ERC pushed the rectal wall towards the GTV meaning the non-deformed rectal contour under-estimated delivered dose (Figure 5-4). This variable effect meant on average the difference in pre and post deformation dosimetry tended towards zero.

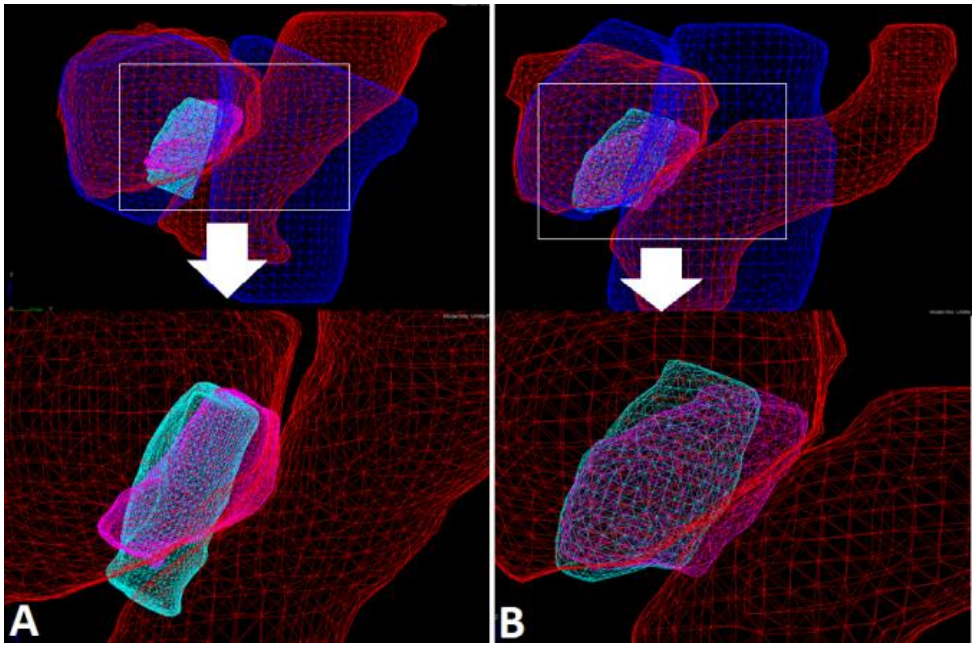

Figure 5-4: Prostate and rectum from original planning CT (red) and MRI taken at time of HDR (blue) for two patients (A + B). GTV after rigid registration (light blue) and after deformable registration (pink).

Root mean squared analysis of calculated rectal dose using deformed or rigid dose summation showed there to be two spikes in variation in volume calculated to receive a given dose, one at low dose and one from 75 - 110 Gy (Figure 5-5).

Despite the variation in calculated dose following deformed or rigid dose summation a Pearson correlation coefficient performed over the area of the DVH curve from 75 – 100 Gy using 1 Gy increments for data from all HDR patients showed strong correlation between the dosimetry of rigid or deformed summation ($r = 0.889$, $p < 0.001$). The dose received by 2% of rectal volume following rigid dose summation ($D2_{rigid}$), ranged per patient from 75.3 – 136.5 Gy, within the area of increased variation identified by RMS error analysis and therefore of particular interest. The upper range of $D2_{rigid}$ observed was greater than the EQD2 permissible if the maximum dose constraint to 0.5 cc for HDR and EBRT was met (max composite dose to 0.5cc 107 Gy). By contrast $D2_{deformed}$ ranged from 76.2 – 99.5 Gy, representative of the expected dose given for each treatment modality. The range in variation $D2_{rigid}$ vs $D2_{deformed}$ was -36% to 19% (Figure 5-6). As a consequence of this variation seen at high dose the more plausible deformed HDR dosimetry was used for all subsequent dosimetric analysis.

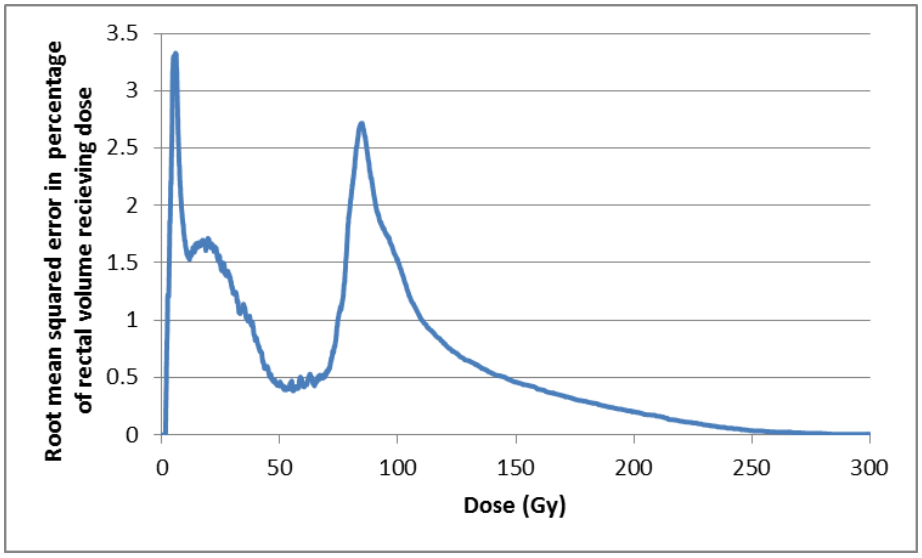

Figure 5-5: Root mean square (RMS) error analysis for 18 patients of variation in percentage volume receiving calculated dose to rectum following deformed or rigid dose summation of external beam radiotherapy and HDR boost

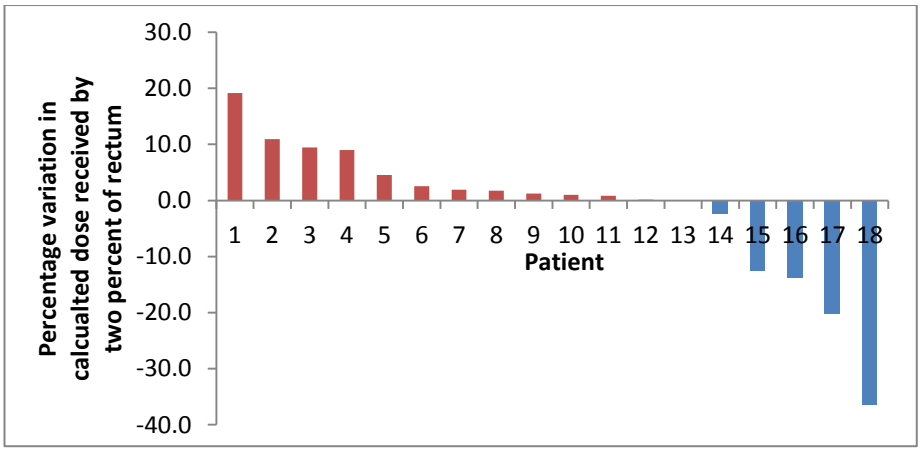

Figure 5-6: Per patient percentage change in calculated dose to two percent of rectal volume following rigid or deformable dose summation

5.5.2 *Dosimetric outcome*

All plans were prescribed within dose constraints. One patient did not complete EBRT following HDR at their request due to fatigue. All other plans were completed as prescribed. Mean target dosimetry for each treatment is shown in Table 5-4. A high dose tail with HDR therapy caused a significant variation ($p < 0.0001$) in D50 and D2 PTV(HDR-B) or PTV(VMAT-IB). The PTV(HDR-B) D_{min}, was significantly lower than PTV(VMAT-IB) (90.1 Gy SD +/- 5.4 Gy and 96.3 SD +/- 4.6 Gy ($p = 0.0004$)).

Table 5-4: Comparison between VMAT and HDR dosimetry

Structure	VMAT-IB Dose (Gy) (Median+/- SD)	HDR-B Dose (Gy) (Median+/- SD)	*Mann Whitney U (p)**
GTV Dmin	105.8 +/- 2.6	99.9 +/- 14.3	0.0085
GTV D98	106.5 +/- 2.3	106.5 +/- 16.2	0.908
GTV D50	109.5 +/- 1.4	159.4 +/- 28.4	**< 0.0001**
GTV D2	111.7 +/- 1.4	303.8 +/- 41.4	**< 0.0001**
PTV(GTV) Dmin	96.3 +/- 4.6	90.1 +/- 5.4	**0.0004**
PTV(GTV) D98	100.1 +/- 3.1	97.1 +/- 6.7	0.065
PTV(GTV) D50	107.3 +/- 1.4	146.4 +/-18.4	**< 0.0001**
PTV(GTV) D2	111.5 +/- 1.3	289.8 +/- 38.0	**< 0.0001**
PTV(CTV) Dmin	70.1 +/- 1.4	70.1 +/- 2.3	0.56
PTV(CTV) D98	72.3 +/- 1.0	73.0 +/- 1.0	0.031
PTV(CTV) D50	80.6 +/- 2.9	80.6 +/- 2.3	0.77
PTV(CTV) D2	109.6 +/- 1.5	183.1 +/- 30.0	**< 0.0001**
Significant results after Bonferroni correction highlighted in bold; GTV, Gross tumour volume; CTV, Clinical target volume; PTV, Planning target volume; D2, Dose to 2% of volume; VMAT, Volumetric Arc Therapy; HDR, High dose rate			

Median dose received by rectum, bladder and urethra with each treatment technique are shown in Table 5-5. There was no significant difference in dose to 0.5 cc of bladder wall following HDR-B or VMAT-IB, 77.5 Gy vs 77.2 Gy ($p= 0.518$). Rectal dose to 0.5 cc was increased, 82.4 Gy vs 78.8 Gy ($p =0.003$), with HDR therapy. In addition rectal D10 –D30 was also significantly increased with HDR-B, with D20 increasing on average by 5 Gy. For urethra and penile bulb there was no significant difference at any dose level.

DVH curves for PTV(GTV), PTV(CTV), GTV, urethra, bladder and rectum are shown in Figure 7 7. There was a significant variation in area under the curve of the DVH for PTV(HDR-B) and PTV(VMAT-IB) ($p < 0.0001$) and GTV ($p < 0.0001$) for VMAT-IB and HDR-B due to the high dose tail of HDR therapy, but not for PTV(CTV) or OAR structures.

Table 5-5: Organ at Risk dosimetry

	Rectal dose (Gy) (Median +/- SD)			Bladder dose (Gy) (Median+/- SD)			Urethral dose (Gy) (Median +/- SD)			Penile Bulb dose (Gy) (Median +/- SD)		
	VMAT	HDR	*p* Value*+	VMAT	HDR	*p* Value*+	VMAT	HDR	*p* Value*+	*VMAT*	*HDR*	*p Value**+
D0.5cc	78.8 +/14.6	82.4 +/-4.9	**0.003**	77.7 +/-16	77.5 +/-2.5	0.518	86.7 +/-7.1	81.6 +/-22.0	0.042	19.5 +/-20.2	26.4 +/-21.2	0.878
D2	81.0 +/-6.2	87.5 +/-6.2	0.011	79.6 +/-7.9	77.8 +/-2.8	0.137	99.0 +/-7.6	102.7 +/-60.5	0.610	37.5 +/-22.2	43.9 +/-22.4	0.968
D10	73.2 +/-3.8	76.1 +/-3.3	**0.0004**	73.2 +/-4.6	73.1+/- 3.3	0.697	96.1 +/-7.6	93.4 +/-43.8	0.934	29.1 +/- 19.0	37.7 20.6	0.520
D20	58.0 +/-5.3	63.0 +/-4.6	**0.0035**	55.4 +/-7.8	49.2 +/-8.0	0.344	91.8 +/-7.5	88.6 +/-31.1	0.755	13.1 +/-15.1	20.4 +/-17.4	0.365
D30	38.2 +/-4.8	41.6 +/-6.1	**0.0006**	36.4 +/-4.7	31.5 +/-6.9	0.149	89.9 +/-7.3	86.2 +/-21.7	0.542	8.2 +/-11.3	10.7 +/-14.8	0.347
D40	23.6 +/-3.6	24.8 +/-5.0	0.029	24.6 +/-3.4	21.6 +/-5.5	0.028	86.8 +/-7.2	85.4 +/-14.1	0.542	5.7 +/-9.0	8.7 +/-12.2	0.302
D50	15.4 +/-2.7	15.3 +/-4.1	0.318	18.8 +/-2.9	14.9 +/-4.4	0.03	85.6 +/-7.2	84.2 +/-11.6	0.571	4.5 +/-7.2	6.1 +/-10.9	0.296
D60	10.7 +/-2.0	9.5 +/-2.9	0.605	14.2 +/-2.7	10.9 +/-3.5	0.042	80.2 +/-7.4	82.3 +/-10.9	0.705	3.8 +/- 5.3	5.1 +/-9.0	0.251
D70	7.4 +/-1.2	6.7 +/-1.8	0.77	10.0 +/-2.3	8.1 +/-2.4	0.77	78.8 +/-12.9	80.9 +/-10.1	0.219	3.7 +/-3.9	4.0 +/-6.9	0.210
D80	5.7 +/-1.0	5.3 +/-1.1	0.620	7.2 +/-1.7	5.9 +/-1.7	0.186	77.1 +/-19.1	78.4 +/-9.4	0.278	3.4 +/-3.0	3.5 +/-5.6	0.260
D90	4.3 +/-0.8	4.3 +/-0.8	0.844	4.9 +/-1.0	4.4 +/-1.3	0.844	73.1 +/-29.2	75.6 +/-13.8	0.219	3.2 +/-2.2	3.2 +/-4.1	0.312
D98	2.8 +/-0.7	3.1 +/-0.6	0.827	3.0 +/-0.7	2.9 +/-0.9	0827	62.4 +/-29.2	60.9 +/-21.3	0.352	2.9 +/-1.6	2.9 +/-3.3	0.270
*Mann Whitney; +All significant values after bonferroni correction highlighted in bold D2, dose to 2% of volume; Gy, Gray; VMAT, Volumetric Arc Therapy; HDR, High dose rate; SD, Standard deviation												

There was no significant difference in dose to 0.5 cc of bladder wall following HDR-B or VMAT-IB, 77.5 Gy vs 77.2 Gy (p= 0.518). Rectal dose to 0.5 cc was increased, 82.4 Gy vs 78.8 Gy (p =0.003), with HDR therapy. In addition rectal D10 –D30 was also significantly increased with HDR-B, with D20 increasing on average by 5 Gy. For urethra and penile bulb there was no significant difference at any dose level.

DVH curves for PTV(GTV), PTV(CTV), GTV, urethra, bladder and rectum are shown in Figure 5-7. There was a significant variation in area under the curve of the DVH for PTV(HDR-B) and PTV(VMAT-IB) ($p < 0.0001$) and GTV ($p < 0.0001$) for VMAT-IB and HDR-B due to the high dose tail of HDR therapy, but not for PTV(CTV) or OAR structures.

5.5.3 *Toxicity and clinical outcome*

Two patients received six months hormone therapy. No acute ≥ G2 GI or late

G3 GI or GU toxicities were seen. Acute G2 GU toxicity was 30 % and 40% for IB-VMAT and HDR-boost respectively (p = 0.76) (Table 5-6)

Table 5-6: Prevalence of acute gastrointestinal and genitourinary toxicity following HDR or VMAT integrated boost

Acute toxicity		HDR (n = 20)			VMAT (n = 27)			none vs any toxicity (*p*-value)*+	Highest grade toxicity per patient (*p* value)^+
		G0	G1	G2	G0	G1	G2		
GI	Rectal pain	60% (12)	40% (8)	0%	93% (25)	7% (2)	0%	0.011	0.186
	BM Frequency	80% (16)	20% (4)	0%	74% (20)	26% (7)	0%	0.74	
	Bleed	90% (18)	10% (2)	0%	89% (24)	11% (3)	0%	> 0.99	
GU	Urinary frequency	0%	60% (12)	40% (8)	30% (8)	37% (10)	33% (9)	0.014	0.564
	Dysuria	65% (13)	35% (7)	0%	74% (20)	22% (6)	4% (1)	0.535	
	Retention	100%	0%	0%	96% (26)	0%	4% (1)	> 0.99	
	Haematuria	95% (19)	5% (1)	0%	100%	0%	0%	0.426	
	Erectile function	50% (10)	40% (8)	10% (2)	63% (17)	22% (6)	15% (4)	0.551	0.414

*Fishers Exact test; ^ $\chi 2$ test; + Significant values after Bonferonni correction shown in bold
BM, Bowel Motion; GI, Gastro-intestinal; GU, Genito-urinary; HDR, High dose rate; VMAT, Volumetric Arc Therapy;

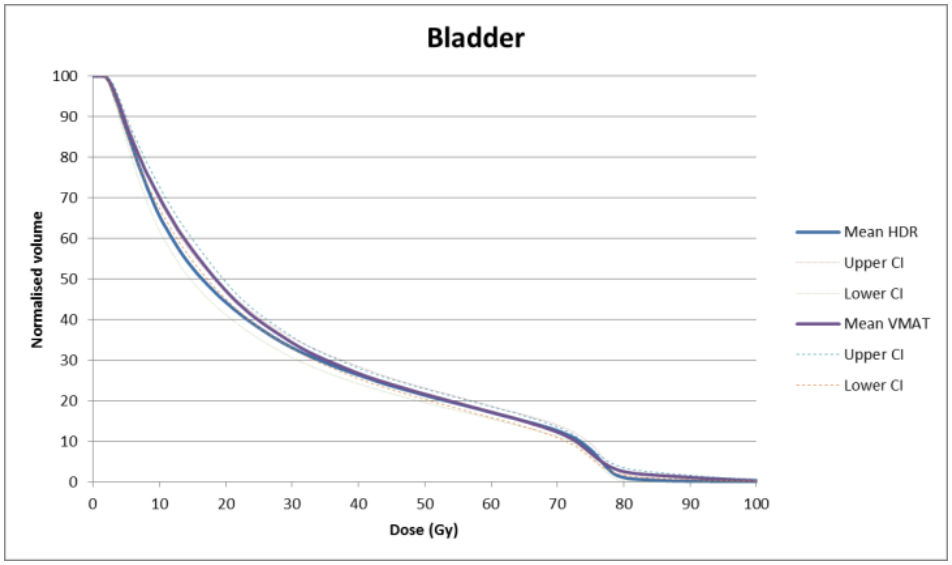

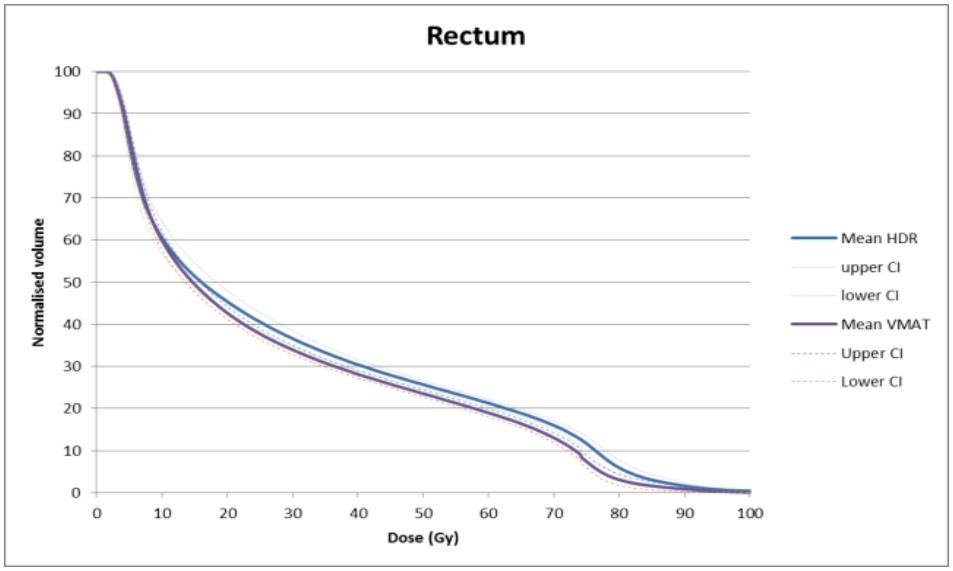

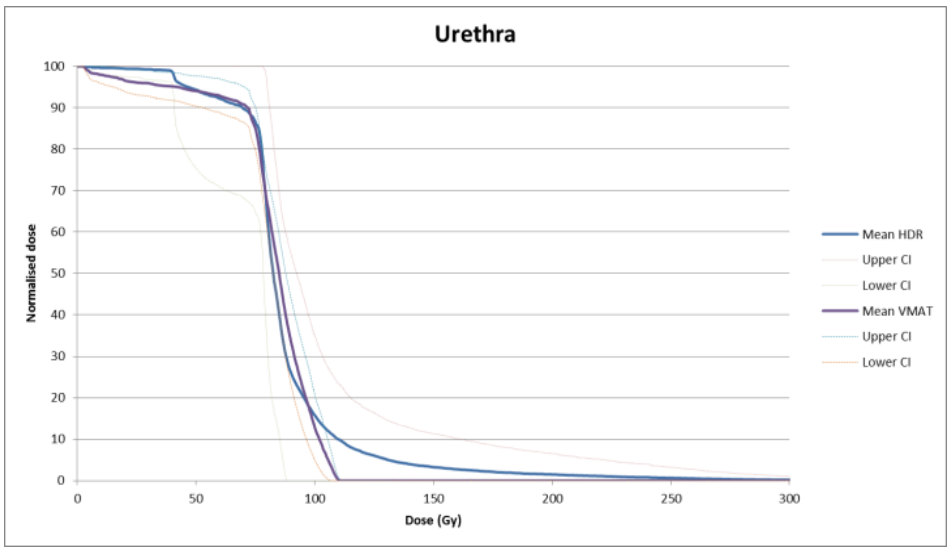

Figure 5-7: Cumulative dose volume histograms for VMAT integrated boost and HDR with 95% confidence intervals

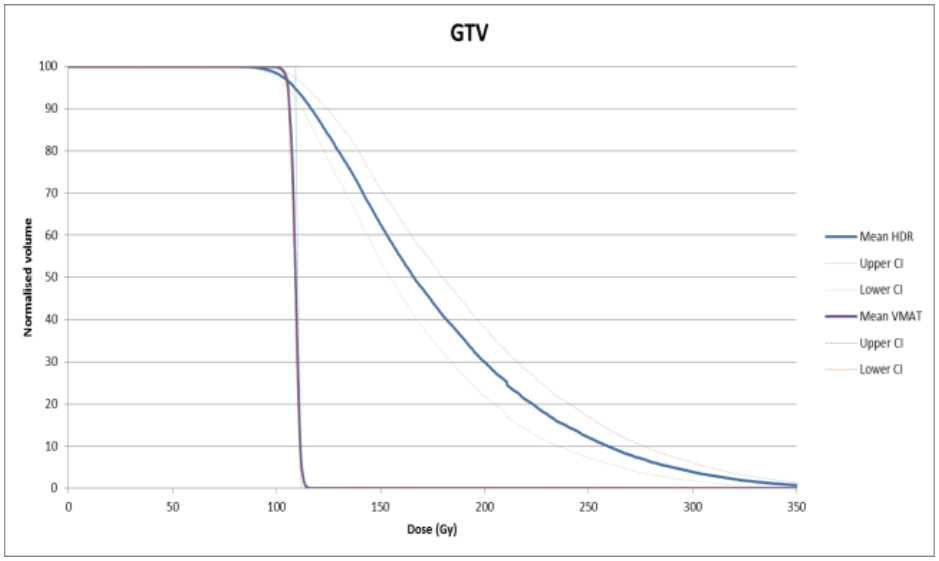

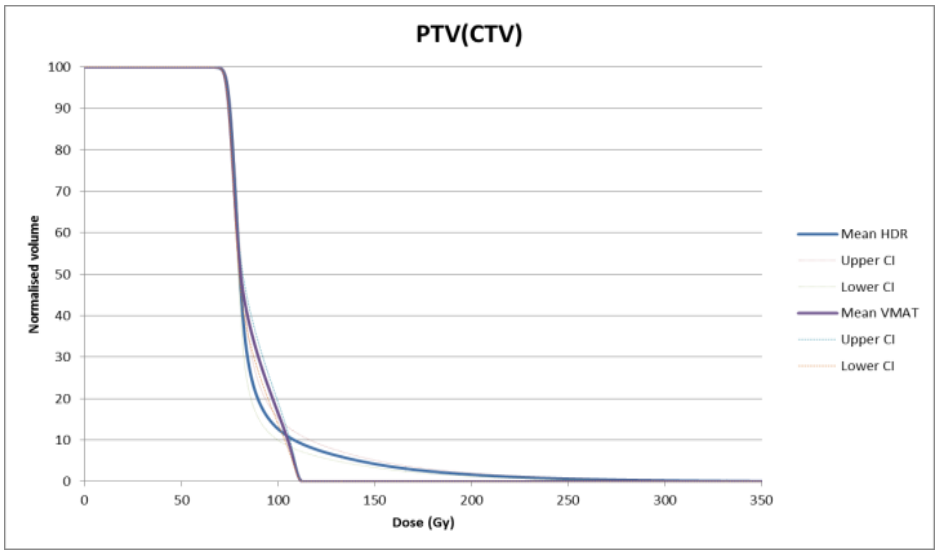

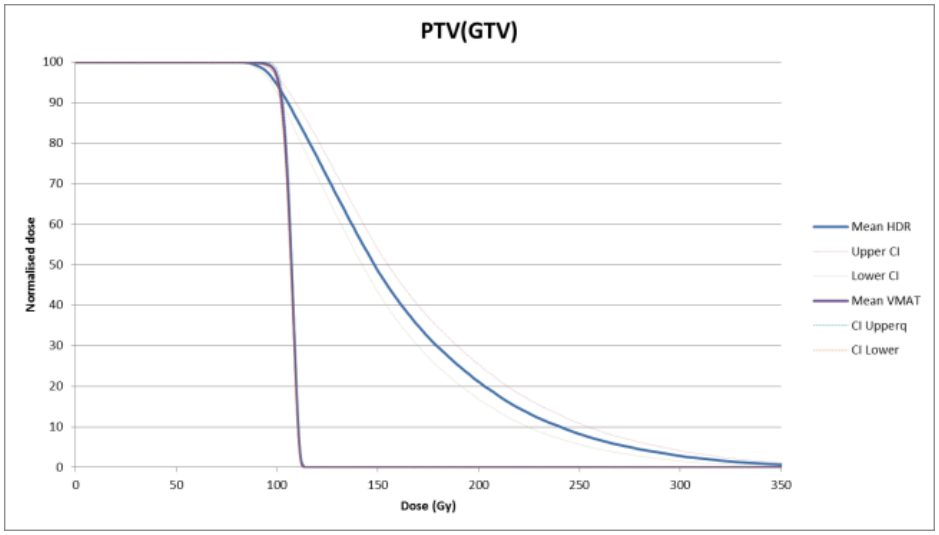

Figure 6-7: Cumulative dose volume histograms for VMAT integrated boost and HDR with 95% confidence intervals (Continued)

Follow up of ≥ 6 months was available for 34 men (18 HDR-B and 16 VMAT-IB) who were assessed for late toxicity (Table 5-7). The median follow up for this group following treatment was 20 months (range 6-35 months) for both HDR and VMAT groups. No significant difference was identified between rates of individual toxicity or severity of GI/GU/erectile toxicity. Nadir PSA for 25 patients with > 1 year follow up who did not receive HT was 0.69 ug/l (0.12- 1.6) and 1.05 ug/l (0.18-4.1) following IB-VMAT or HDR-boost (p = 0.92).

Table 5-7: Prevalence of late Gastrointestinal and Genitourinary toxicity

Late Toxicity		HDR (n = 18)			VMAT (n = 16)			None vs any toxicity (*p* value)	Highest grade GI/GU toxicity per patient (*p* value)
		G0	G1	G2	G0	G1	G2		
GI	rectal pain	94% (17)	6% (1)	0%	100% (16)	0%	0%	> 0.99*	0.354^
	BM frequency	100% (18)	0%	0%	75% (12)	25% (4)	0%	0.039*	
	Haemorrhoids	94% (17)	6% (1)	0%	100% (16)	0%	0%	> 0.99*	
	Haemorrhage	78% (14)	11% (2)	11% (2)	87% (14)	13% (2)	0%	0.658*	
GU	Urinary frequency	55% (10)	6% (1)	39% (7)	62% (10)	13% (2)	25% (4)	0.739*	0.595^
	Erectile dysfunction	50% (9)	28% (5)	22% (4)	38% (6)	31% (5)	31% (5)	0.510*	0.742^
*Fishers Exact test; ^ χ^2 test; BM, Bowel Motion; GI, Gastro-intestinal; GU, Genito-urinary; HDR, High dose rate; VMAT, Volumetric Arc Therapy;									

5.6 Discussion

Analysis is presented of prospective comparative dosimetric and toxicity data for patients receiving VMAT-EBRT with a HDR-B or VMAT-IB for prostate cancer. It has shown that both approaches offer similar OAR radiation exposure and associated levels of acute and late toxicity consistent with published literature, albeit with short follow up.

Previously meta-analysis showed that dose escalation is associated with a reduction in the risk of biochemical failure of approximately 1.8 % per 1 Gy increase and that overall survival may also be improved (Kalbasi et al., 2015; Viani et al., 2009). Randomised dose escalation studies of EBRT to 180 -200 Gy BED (assuming α/β 1.5 Gy for tumour) consistently show improved clinical outcome in intermediate and high risk groups. The use of optimal image guidance and IMRT has been shown to reduce toxicity associated with dose escalation but, despite this, further increases beyond these levels are limited by OAR tolerance (Wortel et al., 2016). Alternative escalation strategies using a form of a brachytherapy boost suggest that treating beyond 200 Gy BED may be associated with further improvements in local control and reduced incidence of biochemical failure, although this may not be identified with early follow-up (Zaorsky et al., 2015; Stone et al., 2010; Spratt et al., 2014). Early results from the ASCENDE-RT study have shown a significant reduction in biochemical failure when a whole gland low dose rate brachytherapy (LDR-BT) boost is administered after 46 Gy EBRT compared with 78 Gy EBRT alone (Rodda et al.). This dose escalation is however associated with a negative effect on health-related quality of life. The use of EBRT in combination with a single HDR boost also appears to an effective method of achieving

improved biochemical control in intermediate and high risk disease but is associated with around a 10% incidence of long term urethral stricture (Martinez et al., 2016; Grills et al., 2004; Denham et al., 2015).

Due to these associated toxicity from combination whole gland treatment a focal dose escalation is an attractive concept, allowing intensification of treatment for the area most likely to harbor resistant disease while minimising toxicity to normal structures. Emerging evidence supports the area of highest disease density within the prostate being the most likely site of recurrence and the source of metastatic spread (Pucar et al., 2007; Karavitakis et al., 2011). By combining a boost to this region with conventional therapy to the remaining prostate smaller multifocal satellite lesions, which have been shown can occur a median of 1cm from the GTV, are also treated (Hollmann et al., 2015). The volume of satellite lesions is generally small, however multiple dose escalated GTV targets, as used in the current study, are possible for more significant multifocal disease burden.

The use a HDR-B has enabled a higher dose to be delivered to a proportion of the GTV while maintaining OAR dose constraints. The median PTV(HDR-B) and PTV(VMAT-IB) D50 was 340 Gy BED and 247 Gy BED respectively. Studies of HDR monotherapy have commonly achieved >250 Gy BED with excellent biochemical control (Yoshioka et al., 2014). If a continued benefit is seen with dose escalation beyond 250 Gy BED the increased dose to PTV(HDR-B) may improve clinical outcome with longer follow up.

The PTV(HDR-B) D_{min} was 6 Gy lower than PTV(VMAT-IB) D_{min} ($p = 0.0004$). This is a consequence of the use of α/β 3 Gy for prostate when converting the HDR and VMAT dose to EQD2. The initial planning of the study used α/β 1.5 Gy to work out equivalent dosing for each arm; using this value would increase the calculated EQD2 HDR dose by around 6 Gy, removing the difference identified. Both values are theoretical, with data supporting an α/β of somewhere between 1.5 – 3 Gy, although meta-analysis suggests an $\alpha/\beta < 2$ Gy may be most accurate (Brenner et al., 2002; Fowler et al., 2013). The Target study incorporates repeat targeted biopsy three years after completion of therapy which may give an early indication of any difference in outcome between HDR-B and VMAT-IB and will be the subject of future reporting.

Avoiding the use of whole gland HDR-B is intended to minimise treatment related toxicity. Stricturing, a recognized complication of whole gland HDR treatment, has been shown most likely to occur within the bulbo-membranous urethra, suggesting increased dose sensitivity in this region (Hindson et al., 2013; Sullivan et al., 2009). By targeting a focal dose boost to a smaller GTV then dose escalation to the bulbo-membranous urethra may be minimised. The dose to penile bulb is a surrogate for this and in our series there was no significant difference in dose received following VMAT-IB or HDR-B, although the HDR-B D2, D10 and D20 were approximately 7 -8 Gy higher. Longer term follow up is needed to assess whether this ultimately translates into increased stricture incidence.

Overall the acute toxicity identified in both arms of the current study are similar to that seen with other reports of EBRT with an IMRT or HDR boost to GTV target, despite delivering a higher BED (Table 5-8). The degree of GU toxicity we report is higher than has been found by other groups

following optimal dose-escalated EBRT (Spratt et al., 2013). A partial explanation may be that the majority of G2 toxicity seen was a result of patients continuing on medical therapy for frequency or urgency which is then well controlled, and may over estimate toxicity in comparison to other groups. The levels reported are consistent with historic incidence and suggest either VMAT or HDR focal boost to a level of around 250 Gy BED may be safely achieved when performed appropriately.

With a median follow up of 20 months, late toxicity data is limited but reassuringly does not as yet show evidence of severe consequences of therapy. Toxicity between the two treatment arms is similar, with no statistically significant difference identified. Dosimetric analysis demonstrates the two treatment approaches to be well matched for OAR dose with the exception of high doses, D2-D30, received by the rectum for the HDR-B cohort. Previously it has been demonstrated that doses within this region may correlate with rectal bleeding and stool frequency (Peeters et al., 2006). An 11% incidence of G2 rectal bleeding occurred following HDR-B compared with no cases following VMAT-B. Longer follow is required to establish if this difference becomes statistically significant.

Analysis of GTV position demonstrated that this was significantly closer to the rectal wall in those receiving HDR-B than for those treated with VMAT-IB. Clinician selection bias, rather than any property of either boost technique may therefore be the reason for the variation in rectal dose seen and subsequent toxicity.

Dosimetric analysis in this report has employed a novel method of dose summation using deformable registration of HDR and EBRT dose gradients to account for variation in rectal position during brachytherapy delivery. Simple summation of HDR-B and EBRT generated composite doses incompatible with the individual prescriptions and were not an accurate reflection of the true dose delivered to rectal wall. By contrast the use of deformation generated plausible results and should be considered in future work. The Morpheus deformable registration method used has previously been validated for prostate deformation and other organs but not, as yet, for the rectum (Samavati et al., 2015). We have demonstrated a limited validation but further work will look to consolidate this although the lack of natural anatomical landmarks within the rectum makes a validation process challenging.

This analysis has limitations. The non-random allocation of treatment means there is significant variation in tumour location in the two treatment arms which will have affected OAR dosimetry, independent of boost delivery technique. This must be considered when assessing comparative analysis, which the study was not designed for. Despite this both cohorts represent real world patients and give an indication of likely dosimetry and toxicity for patients receiving either treatment. Toxicity assessment is limited by length of available follow up for assessment of late effects; it is possible in the longer term that increased GI complications related to increased rectal doses may be experienced by patients treated with HDR-B. Finally longer term PSA behavior and repeat targeted biopsy results are required to give some indication of the relative effectiveness of each approach.

Overall results are encouraging and provide preliminary evidence to support the use of focal dose escalation to achieve an improvement in the therapeutic ratio in patients undergoing radiotherapy for prostate cancer. Deformable dose summation of HDR and EBRT provides a plausible rectal dosimetry not achievable with summation of dose matrixes. The use of an HDR-B allows for increased dose delivery to GTV when compared to VMAT-IB without any variation in early toxicity and may improve long term clinical outcome.

Table 5-8: Studies reporting toxicity following an external beam or HDR GTV boost

Author	Pts	Lesion detection	Median GTV (cm3)	Median GTV distance to rectal wall (mm)	Expansion Margins		Dose PTV(GTV) (Gy)/ fraction	Dose PTV(CTV) (Gy)/ fraction	ADT use	Follow-up (mths)	Toxicity grading system	≥ G2 GI toxicity (%)	≥ G2 GU toxicity (%)
					PTV(GTV) (mm)	PTV(CTV) (mm)							
(De Meerleer et al., 2005)*	15	MRI	4	2	GTV	Prostate + 10 C/C 7 axial	80/NS BED NA	74/NS BED NA	87%	NS	Acute RTOG	20	47
(Singh et al., 2007)	3	MP-MRI	NS	NS	GTV + 3	Prostate+/- SV + 7	94.5/42 BED 245	75.6/42 BED 166	NS	3, 6, 18	Acute RTOG	0	66
(Fonteyne et al., 2008)*	118	MRI/MRSI	NS	NS	GTV + 8	Prostate + 4	81-82/38 BED 192	78/38 BED 185	78%	12	Acute RTOG	11	48
(Miralbell et al., 2010b)	50	MP-MRI	NS	NS	Involved lobe	Prostate + SV +/- PLN (expansion not specified)	64/32 + 10-16/2 BED 193-250	64/32 BED 149	66%	63	Acute RTOG Late RTOG	8 20	48 12
(Wong et al., 2011)	71	111Ln-Capromab SPECT	NS	NS	GTV	Prostate + 6	82/42 BED 189	75.6/42 BED 166	24%	66	Acute RTOG Late RTOG	45 21	55 44
(Schick et al., 2011)	20	MRI	NS	NS	Hemi-prostate	Prostate +/- SV +/- PLN	64/32 + 12-16/2 HDR-B	64/32	65%	62	Acute RTOG Late RTOG	0 15	0 30
(Ippolito et al., 2012)	40	MRI	NS	NS	GTV+ 15 (13 post)	Prostate + 10 (8 post)	80/40 BED 187	72/40 BED 158	100 %	19	Acute RTOG Late RTOG-EORTC	20 5	32.5 7.5
(Pinkawa et al., 2012)	46	F-choline PET	4	NS	GTV + 4 (3 post)	Prostate + base SV + 8 R/L/ant + 5 sup + 4 post	80/38 BED 192	76/38 BED 177	17%	19	EPID	"long term function did not differ from baseline"	

Table 5-8 (continued)

(Schild et al., 2014)	78	MP-MRI	2.2	NS	GTV (or post/ central prostate if not seen)	Prostate + SV + 3	83/43 BED 190	77.4/43 BED 170	41%	36	Acute RTOG	19	53
											Late RTOG	4	29
(Gomez-Iturriaga et al., 2016)	14	MP-MRI	1.4	NS	NS	NS	37.5/15 + 18.75HDR BED 353 (possible in 14/15 planned)	37.5/15 + 15 HDR BED 265	29%	18	Acute CTCAE	13	20
											Late CTCAE		7
(Sundahl et al., 2016)*	225	MP-MRI/ MRI	6.6	NS	GTV	Prostate + 7	82/38 BED 198	78/38 BED 185	94%	72	Acute RTOG/LENT-SOMA	20	45
											Late RTOG/LENT-SOMA	8	29
Current study	26	MP-MRI	2.9	11	GTV + 5 (3 L/R)	Prostate + 5 (3 L/R)	95/38 BED 253	76/38 BED 177	4%	12	Acute CTCAE	0	41
											Late CTCAE	0	25
	20	MP-MRI	2.2	4	GTV + 2 (1 L/R)	Prostate + 5mm (3 L/R)	76/38 + 10/1 BED 253	76/38 BED 177	5%	18	Acute CTCAE	0	40
											Late CTCAE	11	39

*Results from same centre of different reported patient cohorts

ADT, Androgen Deprivation Therapy; Ant, Anterior; BED, Biological Equivalent Dose (calculated for α/β= 1.5 Gy); C/C, Craniocaudal; CTCAE, Common Terminology Criteria for Adverse Events; HDR-B, High Dose Rate Boost; GTV, Gross Tumour Volume; L, Left; MP-MRI, Multi-parametric Magnetic Resonance Imaging; MRI, Magnetic Resonance Imaging; PET, Positron Emission Tomography; Post, Posterior; Pts, Patients; PLN, Pelvic lymph nodes; PTV, Planned Target Volume; R, Right; RTOG, Radiation Therapy Oncology Group; SPECT, Single Photon Emission Computerised Tomography; Sup, Superior; SV, Seminal Vesicle

Chapter 6: **Changes in prostate ADC values and volume during a course of EBRT after neo-adjuvant hormones in a cohort of prostate cancer patients**

McPartlin AJ, Kershaw LE, McWilliam A, Taylor B, van Herk M, Choudhury A

6.1 Background and contribution of authors

In the preceding chapter it was demonstrated that a focal boost can be delivered to an area of the prostate within a realistic workflow and with an acceptable side effects profile. With limited late follow up it was shown however that significant variation in late rectal bleeding, for example, may be seen depending on boost technique used. This finding highlights that any treatment intensification carries with it a risk of increased morbidity. In this final research chapter the possibility of using MRI to identify those patients who might benefit most from treatment intensification, avoiding this potential toxicity in those who will not benefit, is investigated.

The results of a 15 patient study of multi-parametric MRI changes during and after radiotherapy are reported and analysed. I devised this study, developed its protocol, applied for and obtained ethical approval and recruited the 15 patients investigated, ensuring imaging was performed at the specified time points during treatment and supervising all interventions. The imaging sequences used were selected by Lucy Kershaw, MR Physicist at Christie NHS Foundation Trust, who performed subsequent analysis of image data to obtain desired parameters. I performed analysis of the obtained information and carried out appropriate statistical tests with support from Lucy Kershaw who generated figures 7.1-7.4. I wrote this chapter in its entirety including the discussion of results and review of current literature. Lucy Kershaw and Ananya Choudhury provided suggestions on improvements to its structure.

6.2 Abstract

Background: Diffusion-weighted imaging (DWI) and Dynamic Contrast Enhancement (DCE) MRI are functional imaging techniques allowing quantification of physiological properties during hormone therapy (HT) or radiotherapy (RT). This study assessed changes following neo adjuvant (NA)-HT during RT of biopsy proven prostate cancer and normal gland to investigate any variation in response between the two. Volume changes during therapy were measured to inform margin expansion.

Methods: Fifteen patients with biopsy proven intermediate or high risk prostate cancer, due to receive NA-HT and subsequent four weeks of RT, were prospectively recruited. All underwent DWI and DCE-MRI at three time points; pre-RT, in week 3 of RT and 8 weeks post-RT. Pre-HT MRI if available was considered for volume analysis. Quantitative ADC analysis of normal prostate and tumour was performed at 1.5 T with b values = 100, 400, 800 s/mm^2 and the adiabatic approximation to the tissue homogeneity model applied on a voxel by voxel basis to calculate plasma flow (Fp) and permeability surface area product (PS). Mann Whitney U, Wilcoxon signed rank and tests and spearman correlation coefficient were applied.

Results: Pre-HT imaging was available for 12 patients, two patients did not complete all three study scans. Pre-RT there was a significant difference between median tumour and normal gland ADC ($p < 0.05$), which disappeared during and after RT. Tumour ADC values did not significantly alter during RT. An increase in Fp and PS was seen early in treatment which reduced following treatment but not did not reach pre-RT levels. There was a correlation between relative ADC and FP changes between scan 1 and 2 ($r = -0.74$, $p = 0.003$). Volume changes during NA-HT inversely correlated with volume change during RT (r -0.755, p=0.01).

Conclusions: No significant changes ADC during or after RT post NA-HT were shown but early changes were found to correlate with variation in Fp. Further analysis with larger cohorts and mature outcome data will further inform interpretation. Volume changes during NA-HT may have implications for IGRT and margin rationalisation.

6.3 Introduction

Dose-escalated radiotherapy has been shown to improve outcome for prostate cancer (Kalbasi et al., 2015). This comes at the cost of increased treatment-associated toxicity (Kuban et al., 2003). Early identification during treatment of those whose disease is poorly radio-responsive would allow targeted treatment intensification through an adaptive radiotherapy approach. This would minimise unnecessary side effects. Local changes within the treatment field identified on functional imaging may provide a non-invasive method of obtaining this information.

Variation in tissue functional characteristics during radiotherapy can be quantified using multi-parametric MRI (MP-MRI). Diffusion-weighted imaging (DWI) provides information on the random motion of water molecules which is affected by cellular density and thus provides quantitative data on variation in tumour micro-environment. The Apparent Diffusion Coefficient (ADC), derived from DWI, has been shown to vary during and after radiotherapy in different sites such as liver, brain and cervix and may predict for response (Eccles et al., 2009; Harry et al., 2008; Hamstra et al., 2008). Changes during prostate radiotherapy have also been demonstrated but using this variation to predict for ultimate outcome has not been shown (Decker et al., 2014).

Dynamic contrast-enhanced (DCE) MRI enables non-invasive characterisation of tissue microvasculature. It has been shown to have a prognostic value for the response to radiotherapy of some tumour types (Loncaster et al., 2002; Petrillo et al., 2015). It has emerged a component of validated structured reporting scheme for the presence of prostate tumour using MP-MRI and DCE-MRI quantitative parameters appear to correlate with tumour grade (Rothke et al., 2013; Vos et al., 2013). DCE-MRI parameter changes pre- and post-radiotherapy have been demonstrated but have not been shown to correlate with treatment response (Franiel et al., 2009).

DCE-MRI is commonly analysed using a tracer kinetic model to estimate the transfer constant, K^{trans} (Tofts et al., 1999). This reflects a combination of perfusion and microvascular permeability. The more complex adiabatic approximation to the tissue homogeneity (AATH) model permits these two factors to be estimated separately (St Lawrence and Lee, 1998). Reproducibility of this model has previously been demonstrated at our centre in a cohort of patients with benign prostatic hypertrophy (Kershaw et al., 2009).

The use of pre-radiation hormone therapy (NA-HT) is standard of care for high risk and some intermediate risk patients receiving radiotherapy (see Chapter 8: Appendix A); the groups which might be expected to most benefit from the use of dose escalation. It is known that NA-HT induces significant changes in DCE, DWI and associated ADC parameters but what subsequent effect this has on tissue characteristics during radiotherapy is unclear (Barrett et al., 2012; Hotker et al., 2015).

Animal studies have suggested the combination of ADC, DCE, change in prostate tumour volume and prostate specific antigen (PSA) may predict for response to hormone therapy and radiotherapy allowing for identification of poor response to therapy (Roe et al., 2011). Comparative studies in humans have not been reported.

Radiation and hormone therapies induce changes in prostate volume through cell shrinkage and apoptosis (Nichol et al., 2007; Whittington et al., 1999). The changes in prostate volume that occur during radiotherapy after NA-HT are poorly described but may have implications for image guidance and margin expansions- being able to predict the likely change in prostate volume during RT might allow for margin reduction as treatment progresses, reducing dose to nearby normal structures.

We report outcomes from MP-MRI performed before, during and after a course of radical radiotherapy following NA-HT. This work was designed as a feasibility study to quantify changes in ADC, DCE and tumour volume as a potential early biomarker for prostate cancer response. Additionally prostate volume changes during treatment were assessed for their potential significance for future IGRT and margin planning.

6.4 Materials and methods

6.4.1 *Patients*

This prospective study received ethical approval with participants providing written informed consent. Eligible patients were required to have biopsy-proven prostate cancer with at least clinical T2c disease and to be receiving treatment with definitive radiotherapy plus three months NA-HT as standard of care. A total HT duration from 6 months to two years at the treating clinician's discretion was allowed. Study protocol was for each patient to receive three multi-parametric (mp)-MRI scans; in the week before EBRT commenced, in the third week of EBRT and eight weeks after its completion. Exclusion criteria were performance status (PS) >1, contraindication to MRI or any previous malignancy excluding skin cancer. PSA levels were monitored prior to commencing hormones and at routine follow up after completion of EBRT as standard of care.

6.4.2 *Radiotherapy*

EBRT was delivered using volumetric arc therapy (VMAT) at 3 Gy per fraction in 20 fractions over four weeks at 6 MV via a linear accelerator. Target volumes followed the previously described CHHIP study protocol with treatment delivered using an integrated simultaneous boost technique to a dose of 48 Gy to prostate and base or all of seminal vesicles plus a uniform 1 cm margin; a dose of 57.6 Gy for prostate plus a 1 cm margin except 0.5 cm posteriorly; and 60 Gy to prostate plus a 0.5 cm margin except no expansion posteriorly (Dearnaley et al., 2012). No EBRT was given to the pelvic nodes.

6.4.3 *MR imaging protocol*

Patients were imaged at 1.5 T (Achieva, Philips Medical Systems, Best, The Netherlands) using a cardiac coil with a flat perspex table top (made in-house) to match the radiotherapy treatment position. The MR examination began with high resolution T2w imaging (TSE, TR/TE=4800/120 ms, matrix 560 x 560 x 20),then DWI (EPI with TR/TE 8000/70 ms, matrix 176x176x20, SENSE factor 2 LR, b = 100, 400, 800 s/mm^2). All subsequent images were acquired with matrix 176x176x20 (over-contiguous slices) and SENSE factor 2.5 in the PE (LR) direction. Inversion-recovery turbo field echo (IRTFE) was used to measure T1 (TR/TE/α=2.38/0.77 ms/12°, shot interval 4 s, ETL=51, TI = 64, 250, 1000, 2500, 3900 ms), and was followed by DCE-MRI images (turbo field echo TR/TE/α

=2.47/0.86 ms/30°, temporal resolution 1.2 s for 260 time points) acquired during injection of 0.2 ml/kg gadoterate meglumine at 2 ml/s followed by a saline chaser.

6.4.4 *Image analysis*

ADC maps were processed offline (ADCmap ver. 1.6 for Osirix) using b-values 100, 400, 800. The arterial input function was extracted from the external iliac artery at each visit, T1 was estimated from fitting to the inversion recovery turbo field echo data, signal-intensity vs time curves were converted to contrast agent concentration vs time curves and finally the AATH model was fitted on a voxel-wise basis using in house software (Python 3.4)(St Lawrence and Lee, 1998). Haematocrit was assumed to be 0.4.

ADC and DCE-MRI maps were registered to the high resolution T_2w images using Worldmatch software (van Herk et al., 2000). Regions of interest were contoured on high-resolution T_2w images using registered ADC maps and DCE-MRI to aid identification. Reference was made to MP-MRI imaging acquired at referring centres before ADT commencement where available. The tumour, peripheral zone (PZ) and central zone (CZ) were identified by a genito-urinary radiologist (BT) with 6 years' experience of reporting MP-MRI and an oncologist with an interest in prostate MP-MRI (AM). With reference to previous images where available to aid localisation, visible tumour was also manually contoured at each time point by a radiologist (BT) on the T2w image set, using DCE-MRI and ADC to inform contouring. When this was not possible tumour contours were manually copied from pre-radiotherapy imaging to subsequent mid- and post-treatment data sets using local anatomical landmarks to aid accuracy. PZ and CZ regions were outlined for each visit without reference to other image sets. Volumes of regions of interest were generated from the 3-D delineated structures on each image set.The median ADC value was then calculated along with the microvascular parameters in each ROI after isotropic erosion by one pixel to minimise partial voluming effect.

For patients with pre-HT MR imaging performed locally prior to recruitment, prostate volume changes during RT were analysed with volume pre-HT, pre-RT and after three weeks of RT assessed. These images were not used to assess pre-HT multi-parametric values since wide variation in local imaging protocols and differing MR scanners employed made it impossible to assess the changes induced by HT, rather than a consequence of differing image acquisition techniques.

6.4.5 *Statistical analysis*

A power analysis for this study was performed based upon the pre-clinical study by Roe et al in 32 mice with human prostate xenografts treated with a combination of androgen deprivation and/or radiotherapy (Roe et al., 2012). In that study DWI and DCE data was acquired pre-radiotherapy and on days one and nine following treatment with K^{trans} and ADC recorded for tumour. Treatment response was measured as tumour volume 30 days after completion of radiotherapy (v). A power calculation for the combination of v, ADC and K^{trans} was performed using the data from this study. Using a 95% significance level and 80% power with three co-variates assuming R = 0.7 would require a cohort group of 15 to identify the presence of a predictive model.

In the current study ADC and DCE data were assessed using the Shapiro-Wilks test and found to have a non-normal distribution. Comparison of DCE values and ADC values in malignant and normal tissue at each time point was performed using the non-parametric Mann Whitney U-test (GraphPad Prism software, version 6, La Jolla, California USA). The Wilcoxon-signed ranks test was used to compare ADC and DCE parameter values for each structure at each time point and the differences between regions were assessed with the Mann-Whitney U test.

Statistical analysis of prostate volume was performed using Spearman correlation, the Mann-Whitney U test for comparison of volume response to RT after dichotomised response to NA-HT and Wilcoxon signed-rank test for repeated testing of volumes during treatment. Due to multiple testing for all tests a two tailed p-value of less than 0.01 was considered to indicate significance.

6.5 Results

Between September and December 2014, 15 patients met inclusion criteria and were enrolled in the study (median age 68.3 years, range 57-78). Patient characteristics are show in Table 6-1. Median Gleason score was 7 (6-9) and median PSA at diagnosis 14 (3-197) ng/ml. Median interval from biopsy to first study MR scan was 116 (91- 449) days. Median period of HT prior to first study MR scan was 96 (69 – 115) days.

Table 6-1: Patient characteristics

Patient	Age	Gleason Score	Stage	PSA pre hormones (ng/ml)	Dominant lesion size cm^3
1	70	6 (3+3)	T3a	12	0.39
2	78	8 (4+4)	T4	21	1.40
3	71	9 (4+5)	T2c	17	0.42
4	58	9 (4+5)	T3b	16	5.46
5	68	7 (3+4)	T2c	9	2.55
6	76	7 (3+4)	T3a	18	0.72
7	76	7 (3+4)	T2c	197	0.18
8	68	7 (3+4)	T2c	6.1	0.54
9	60	9 (5+4)	T2c	22	0.43
10	62	7 (3+4)	T2c	7	0.14
11	65	7 (3+4)	T3a	14	1.24
12	68	9 (4+5)	T2c	3	15.48
13	72	7 (3+4)	T2c	6.5	1.06
14	76	8 (4+4)	T3a	10	1.5
15	57	7 (3+4)	T3a	46	1.26
Median	68	7 (3+4)	T2C	14	1.06

Median follow up from the first day of radiotherapy is 13 months (range 7 – 18 months). One patient has died from metastatic lung cancer eight months after completion of treatment and one patient has developed metastatic disease six months after radiotherapy, likely a result of occult metastases at time of treatment. For the remaining 13 patients, seven of who remain on adjuvant hormone therapy, no biochemical failures have occurred with a median PSA at last review of < 0.1 ng/ml (range <0.1 – 0.2 ng/ml).

6.5.1 *Identification of disease*

Pre-HT MP-MRI was available for 12 patients to assist in tumour delineation with disease identified in all cases. For the remaining three patients the likely site of disease was identified using post-

hormone study imaging in combination with pathology reports, with it being impossible to confidently identify disease in all three cases. Thirteen patients completed all MRI intended with one patient withdrawn from the study after one scan due to identification of an undisclosed historic episode of vasculitis and a second patient not attending their final imaging visit. One patient's tumour burden was such that normal values from the PZ and CZ could not be calculated. All patients received radiotherapy and hormone treatment as prescribed.

Disease could not confidently be identified from benign prostate parenchyma on any repeat imaging during or after completion of radiotherapy. Analysis of tumour volume changes was therefore not possible.

6.5.2 *Changes in ADC*

Figure 6-1 shows box plots of ADC values for tumour, PZ and CZ at the three time points. After NA-HT, during radiotherapy and post treatment the median tumour ADC was 1.19 x 10^{-3} mm^2/s (interquartile range (x 10-3 mm^2/s), 1.29 (IQR 0.18 x 10-3 mm^2/s) then 1.31 x 10^{-3} mm^2/s (IQR 0.16 x 10-3 mm^2/s) respectively. There was no significant change in tumour ADC between any time points. Pre-RT median ADC in PZ and CG was 1.40 x 10-3 mm^2/s (IQR 0.26 x 10-3 mm^2/s) and 1.34 x 10^{-3} mm^2/s (IQR 0.19 x 10^{-3} mm^2/s) respectively. There was a significant difference between median tumour and PZ ADC (p=0.006) but not median tumour and CG ADC (p=0.029) at this time point. This variation was not significant at later time points. The median ADC values of benign tissue in the peripheral and central gland experienced no significant change during or after therapy, with no significant difference between PZ and CG at any time point. Changes in ADC for the 14 identified tumours with repeat imaging during treatment are shown in Figure 6-2. Gleason score did not correlate with ADC values.

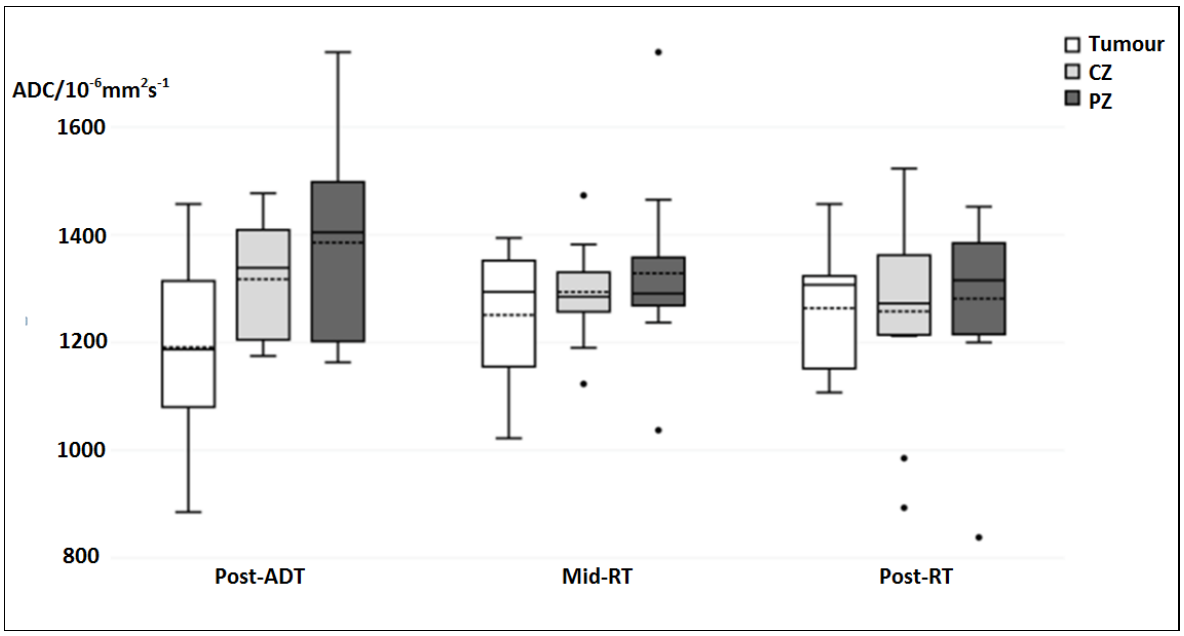

Figure 6-1: Box plots showing ADC values in tumour, central zone (CZ) and peripheral zone (PZ) for the three visits: post androgen deprivation therapy (post-ADT), in the middle of radiotherapy (mid-RT) and after radiotherapy (post-RT). Boxes show mean (dashed line), median, lower quartile and upper quartiles. Whiskers show 1.5*interquartile range, outliers shown by dots.

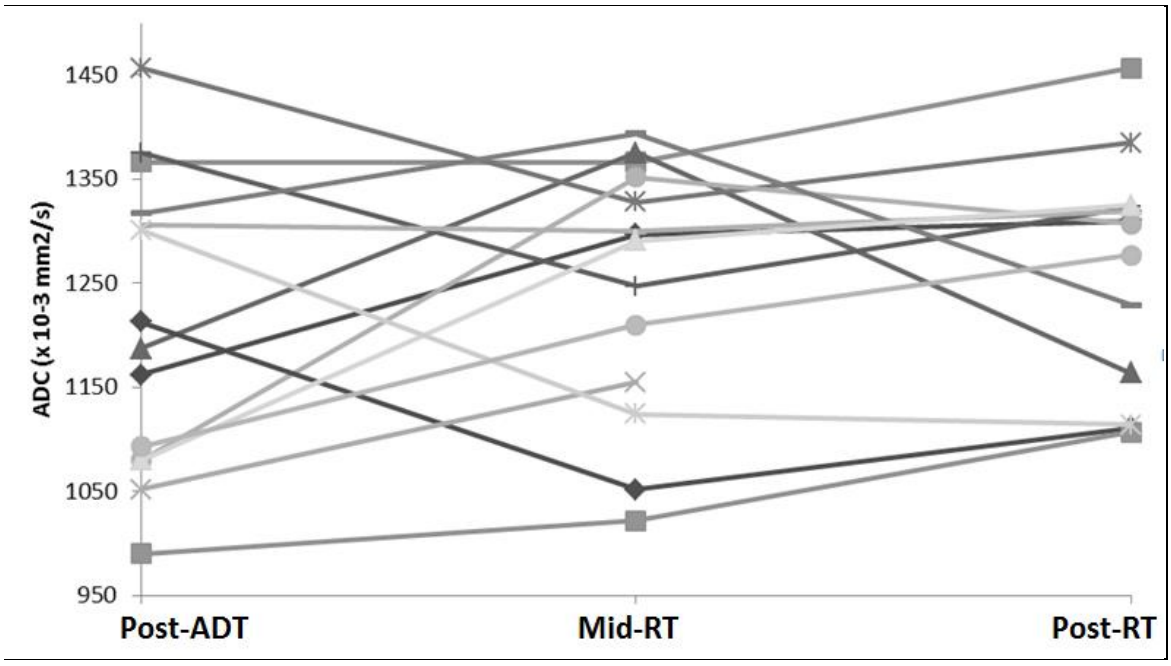

Figure 6-2: Graph of changes in apparent diffusion coefficient (ADC) values in 14 prostate cancers (1) before (post ADT), (2) after three weeks of radiotherapy (mid RT) and (3) eight weeks after completion of radiotherapy (post RT)

6.5.3 *Change in DCE-MRI parameters*

Box plots for plasma flow (Fp) (

Figure 6-3) and permeability surface area product (PS) (Figure 6-4) are shown for tumour, CZ, and PZ for each of the three scans. P-values for paired tests between visits and Mann-Whitney U tests between regions at each visit are shown in Table 6-2 and Table 6-3. A significant rise then fall in Fp of tumour was seen. The PS of tumour experienced a significant rise is the first three weeks of radiotherapy but did not significantly alter after this time. Post treatment Fp, but not PS, values remained significantly higher than pre-treatment. No correlation with Gleason score was identified.

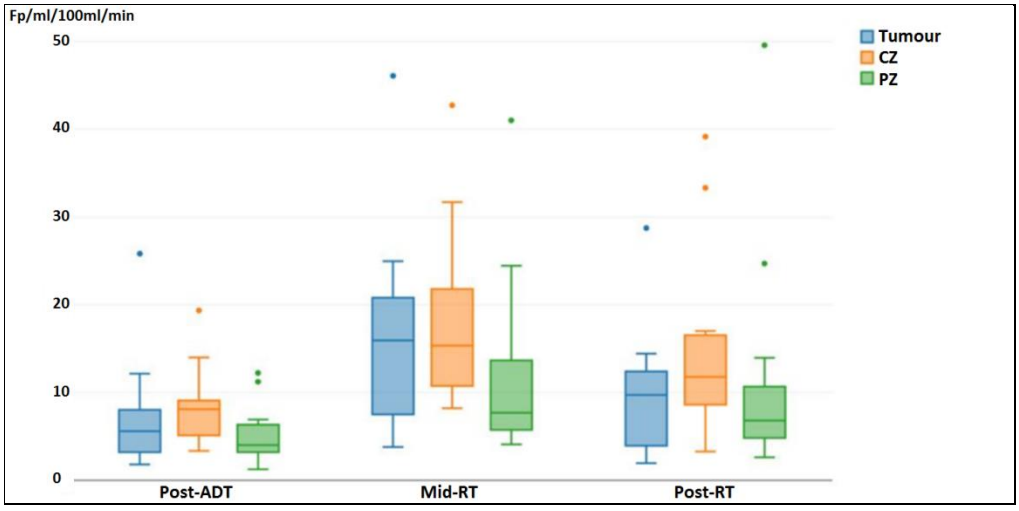

Figure 6-3: Box plot showing median, interquartile range and outliers for plasma flow (Fp) measured in prostate tumour, central zone (CZ) and peripheral zone (PZ) before, in the third of four weeks, and eight weeks after completion of radiotherapy with neo-adjuvant and concurrent hormone therapy

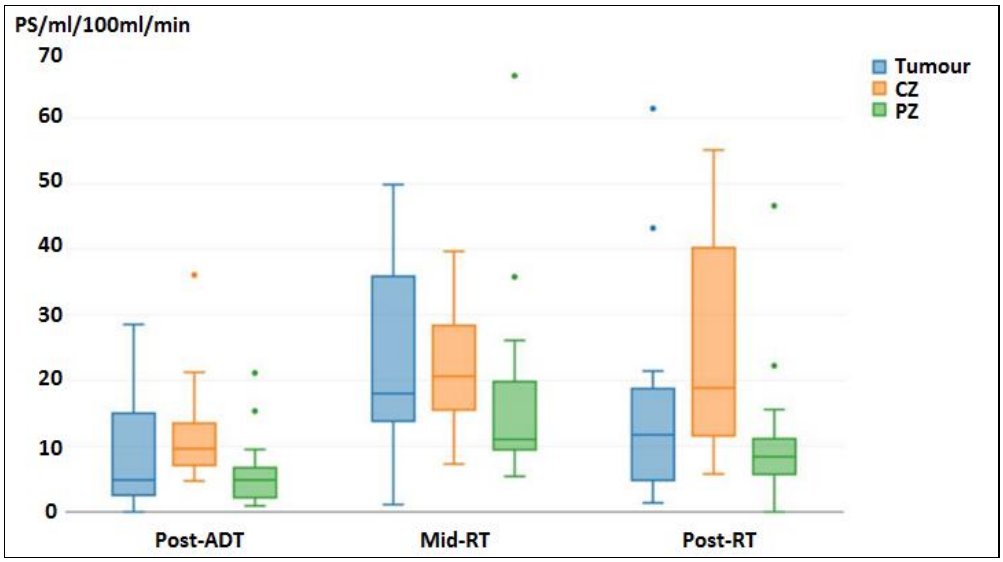

Figure 6-4: Box plot showing median, interquartile range and outliers for permeability surface-area product (PS) measured in prostate tumour, central zone and peripheral zone before, in the third of four weeks, and eight weeks after completion of radiotherapy with neo-adjuvant and concurrent hormone therapy

Table 6-2: p-values for different parameters comparing regions between time point.

Wilcoxon signed ranks			
	Plasma Flow (Fp)		
Visit	Tumour	Central zone	Peripheral zone
1 vs 2	**0.001**	**<0.001**	**0.002**
2 vs 3	**0.001**	0.03	0.06
1 vs 3	**0.001**	**0.004**	0.03
	Permeability surface area product (PS)		
1 vs 2	**<0.001**	**<0.001**	**<0.001**
2 vs 3	0.07	0.2	**0.01**
1 vs 3	0.02	**0.001**	0.03
Visit 1, Pre-radiotherapy; Visit 2; In third of four weeks of radiotherapy; Visit 3, Eight weeks after completion of radiotherapy			

Table 6-3: p-values for different parameters comparing different regions at each time point.

Mann-Whitney U significance test			
	Plasma flow (Fp)		
Region	Visit 1	Visit 2	Visit 3
Tumour vs CZ	0.02	0.3	0.06
Tumour vs PZ	0.3	0.06	0.5
CZ vs PZ	**0.004**	**0.009**	0.05
	Permeability surface-area product (PS)		
Tumour vs CZ	0.05	0.339	0.07
Tumour vs PZ	0.3	0.06	0.3
CZ vs PZ	**0.002**	0.03	0.03
CZ, Central Zone; PZ, Peripheral Zone; Visit 1, Pre-radiotherapy; Visit 2; In third of four weeks of radiotherapy; Visit 3, Eight weeks after completion of radiotherapy			

6.5.4 *Correlation of ADC and DCE*

No correlation between baseline ADC, PS or Fp values were found after NA-HT. Both relative and absolute ADC and Fp changes between scan 1 and 2 were found to be correlated, ($r = -0.74$, $p = 0.0034$)(Figure 6-5) and ($r = -0.64$, $p = 0.016$). No other correlation was identified.

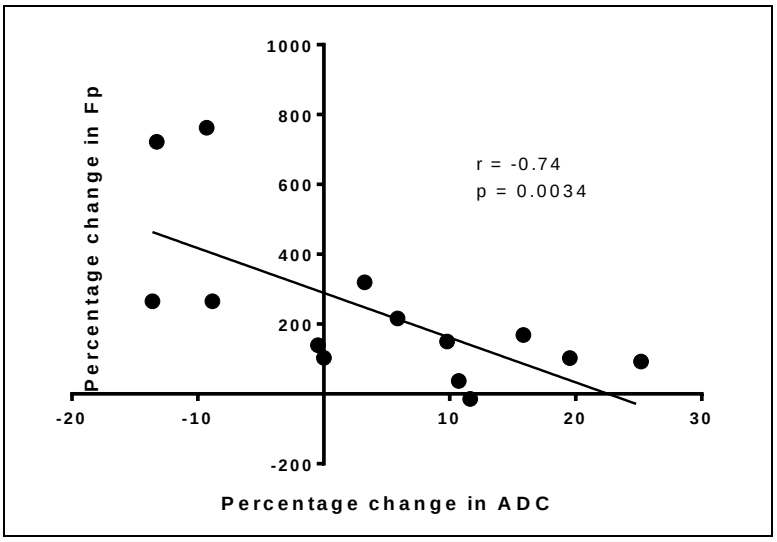

Figure 6-5: Scatterplot of percentage change in ADC plotted against percentage change in Plasma Flow (Fp) between pre-radiotherapy and week three of treatment

6.5.5 *Volumetric Analysis*

Imaging to assess initial volume and subsequent changes during NA-HT and RT was available for 11 patients (Table 6-4). NA-HT induced a significant mean prostate volume reduction of 47% (range -27% to -64%) (p = 0.001). The volume changes identified during NA-HT inversely correlated with volume change during the first three weeks of RT (r -0.72, p=0.014) (Figure 6-6). Patients with ≥ 50% vs < 50% reduction during NA-HT experienced significantly different responses to RT with +29% vs -11% (p=0.01) mean volume changes respectively from pre-RT size by week three. On average there was a mean increase of 7.5% in volume during RT. Absolute volume pre-NA-HT (r = 0.18, p = 0.604)) or pre-RT (r=-0.19, p = 0.57) did not correlate with subsequent relative volume change. No correlation was seen between relative volume change and ADC characteristics.

Table 6-4: Prostate volume changes during neoadjuvant hormone therapy and radiotherapy

	Pt 1	Pt 2	Pt 3	Pt 4	Pt 5	Pt 6	Pt 7	Pt 8	Pt 9	Pt 10	Pt 11	Mean
Initial volume (cm^3)	25.4	30.8	41.8	13.9	41.2	27.8	33.9	43.9	57.3	14.9	29.2	32.2
% volume change during hormone therapy	-27	-28	-39	-40	-44	-45	-50	-60	-62	.-63	-64	-47
% volume change by week 3 of radiotherapy	-5	0	-21	-17	12	-33	0	38	25	36	48	7.5

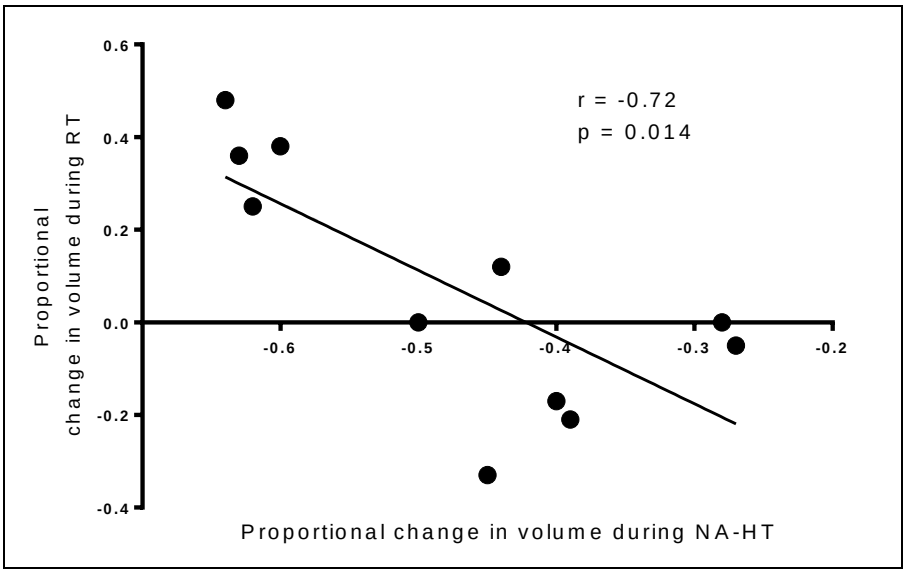

Figure 6-6: Scatterplot of changes in prostate volume during neoadjuvant hormone therapy (NA-HT) plotted against subsequent prostate volume changes between week one and three of radiotherapy (RT)

6.6 Discussion

This is the first study to report prospective data on changes of ADC and DCE in prostate tumour during radiotherapy after NA-HT. This pilot study was intended to assess these changes in combination with variation in tumor volume as a possible predictive tool for outcome following combination therapy. At the time of analysis one treatment failure has occurred, likely due to occult metastatic disease at the time of treatment, and one patient has died of unrelated causes.

The study has found that identification of disease in this cohort of patients was not possible after three weeks of radiotherapy and previous NA-HT. Tumour volume changes could not therefore be used an early surrogate for response in this cohort.

In this study at time point 1 after 3 months NA-HT tumour ADC was 12.5% lower than normal peripheral zone ($p < 0.01$). No difference between structures was seen at later time points and no significant change in ADC parameters during and after treatment was identified.

Variation in ADC values are a result of differences in diffusion restriction, thought to reflect relative cellular density and therefore of interest in assessing tumour response to therapy. ADC has been demonstrated to be lower in prostate cancer tissues than normal structures and to correlate with tumour grade and density (Langer et al., 2008; Tamada et al., 2008). HT appears to have a differential effect on ADC values in malignant and normal prostate tissue. Previous work has shown that in the former it induces cell shrinkage, atrophy and apoptosis, with associated marked reduction in tumour volume, density and capsule penetration which appears to cause overall ADC values to remain static or rise (Bullock et al., 2002; Hotker et al., 2015; Barrett et al., 2012). In contrast HT induces a significant reduction in the ADC values of normal prostatic structures, possibly due to induced atrophy of acini with associated fibrosis, basal cell hyperplasia and reduced gland volume causing increased diffusion restriction (Roznovanu et al., 2005; Patterson et al.,

2008). The reduction in prostate volume and contrasting responses in ADC values between malignant and normal tissue during NA-HT make tumour identification after its completion challenging (Groenendaal et al., 2012b; Riches et al., 2014). In the current study this issue was mitigated by having pre-hormone MP-MRI available to aid tumour delineation in most cases. In the three cases where there was no pre-hormone MRI, areas of low ADC and previous biopsy results were used to guide delineation. However benign BPH nodules have similar characteristics on imaging making confident disease identification in this context challenging.

The differing responses of tumour and normal tissue to HT provide some explanation for the smaller range of ADC values pre-radiotherapy presented here compared with previous work without NA-HT. The differences at baseline between normal gland and tumour in previous studies assessing ADC changes during EBRT without NA-ADT has ranged from 29.5%- 51.3% (Decker et al., 2014; Foltz et al., 2013; Song et al., 2010; Takayama et al., 2008). One retrospective study has assessed ADC after NA-HT of up to two years and found a difference of -29% persisting between tumour and normal gland, higher than in the current study, but this is confounded by analysis only assessing tumour visible after HT, which was present in 14 of 44 patients (Iraha et al., 2012). These were likely to be of higher grade, which may have reduced the average malignant ADC value and artificially increased the difference between tumour and normal tissue. In another study assessing the effect of HT the relative difference in ADC fell from 41.2% to 28.6% following three months treatment (Hotker et al., 2015). Patients in that study had on average a higher grade of disease at diagnosis than in our study which may have contributed to the preservation of more marked variation. Our results suggest that the use of HT reduces the difference in ADC between normal and malignant prostate tissue.

Malignant and benign prostate tissue did not experience a significant change in median ADC value during the first three weeks of RT. However a significant difference between the two present prior to starting RT was not seen at subsequent time points and the study may have been underpowered to detect subtle variations after NA-ADT. When imaging was performed eight weeks after completion of treatment a significant rise in median tumour ADC was not seen, in contrast with the findings of other groups. A possible mechanism for the rise that others have seen may be continuing cell apoptosis and tumour necrosis as cells experience ongoing mitotic catastrophe in the weeks after treatment as a consequence of irreversible RT-induced DNA damage (Endlich et al., 2000). It may be that this tumour response after NA-ADT, as measured by ADC, is attentuated.

There was marked variation of ADC changes in different tumours. Four of thirteen evaluable patients experienced an early and persistent decline in tumour ADC. Two of these were patients in whom pre-HT MP-MRI was not available to guide tumour identification, raising the possibility of inadvertent measuring of normal tissue attenuating the treatment response. Alternatively a decline in prostate tumour ADC has been associated with poor outcome, with one study finding patients who suffered subsequent local failure following RT did not experience a rise in tumour ADC after completion of treatment (Liu et al., 2014a). It may be that the decline seen in some of our cohort represents a similar poor response to therapy. With one year of follow up one patient in our cohort has experienced biochemical failure with widespread metastasis, suggesting occult disease at presentation rather than local failure. This patient did not experience a decline in ADC during

therapy. One patient has died without biochemical failure and the remainder continue to experience biochemical response. Further long term follow up may allow correlation of biochemical failures with ADC changes seen during therapy.

Multiple small studies of prostate tumour ADC during and after radiotherapy have now demonstrated a degree of uniformity in outcome despite wide variation in imaging protocols, timing, treatment received and patient characteristics (Table 6-5,Figure 6-7) (Hotker et al., 2015; Park et al., 2012c; Decker et al., 2014; Liu et al., 2014b; Iraha et al., 2012; Song et al., 2010; Takayama et al., 2008; Barrett et al., 2012; Foltz et al., 2013). Due to the ADC being dependent on b-values used, likely because low b-value DWI can be heavily contaminated by perfusion and high values by increased signal noise, direct comparison between studies is not possible but trends may be identified (Thörmer et al., 2012; Peng et al., 2014). In combination they raise the prospect that ADC changes during treatment may predict for ultimate outcome but this has not yet been demonstrated. If ADC rise within tumour is indeed a result of tumour necrosis then it is logical that patients experiencing the most significant rise might be least likely to experience treatment failure. Recent studies identifying a predictive variation in ADC following therapy in those ultimately destined to suffer poor PSA response or biochemical failure are encouraging but would not guide treatment intensification (Liu et al., 2014b; Qi et al., 2016).

Table 6-5: Summary of imaging protocol and scheduling for studies assessing effects of hormone therapy and radiotherapy of prostate cancer ADC

						MR Imaging timing						
	Author	No	Imaging	RT Length (weeks)	HT	Pre-HT	Pre-RT	Early RT	Mid RT	Late RT	End RT	Post RT
[1]	(Barrett et al., 2012)	23	3T, b-values 100,200 500,800,1000	-	Yes	Yes	After 3 mths HT	-	-	-	-	-
[2]	(Hotker et al., 2015)	27	1.5 – 3 T* b-values 0,700 or 1000	-	Yes	Yes	After 3 mths HT	-	-	-	-	-
[3]	(Park et al., 2012b)	8	3T b-values 0,100,1000	7	No	-	Yes	Week 2	-	Week 4	-	1 mth post
[4]	(Foltz et al., 2013)	17	1.5T b-values 0,600,1200	8	No	-	Yes	Week 2	Week 4	Week 6	Week 8	-
[5]	(Decker et al., 2014)	13	3T b-values 0,50,800	7	No	-	yes	-	Week 4	-	1-4 days post	3 mths post
[6]	(Song et al., 2010)	49	3T b-values 0,1000	7	No	-	Yes	-	-	-	-	1-5 mths post
[7]	(Takayama et al., 2008)	9	1.5T b-values 0,700	NS (carbon ion RT)	45%	-	Yes	-	-	-	-	3-9 mths post
[8]	Current study	15	1.5T b-values 100,400,800	4	Yes	-	After 3 mths HT	-	-	Week 3	-	2 mths post
[9]	(Liu et al., 2014a)	78	3T b-values 0,800	5	Yes with RT	-	yes	-	-	-	-	1-5 mths post
[10]	(Iraha et al., 2012)	44	1.5T b-values 0,800,2000	7-8	Yes	-	After 2 mths HT	-	-	-	-	3-4 mths post

*12 pts had pre/post imaging at different magnetic strengths
Mth, Month; RT, Radiotherapy; HT, Hormone Therapy;

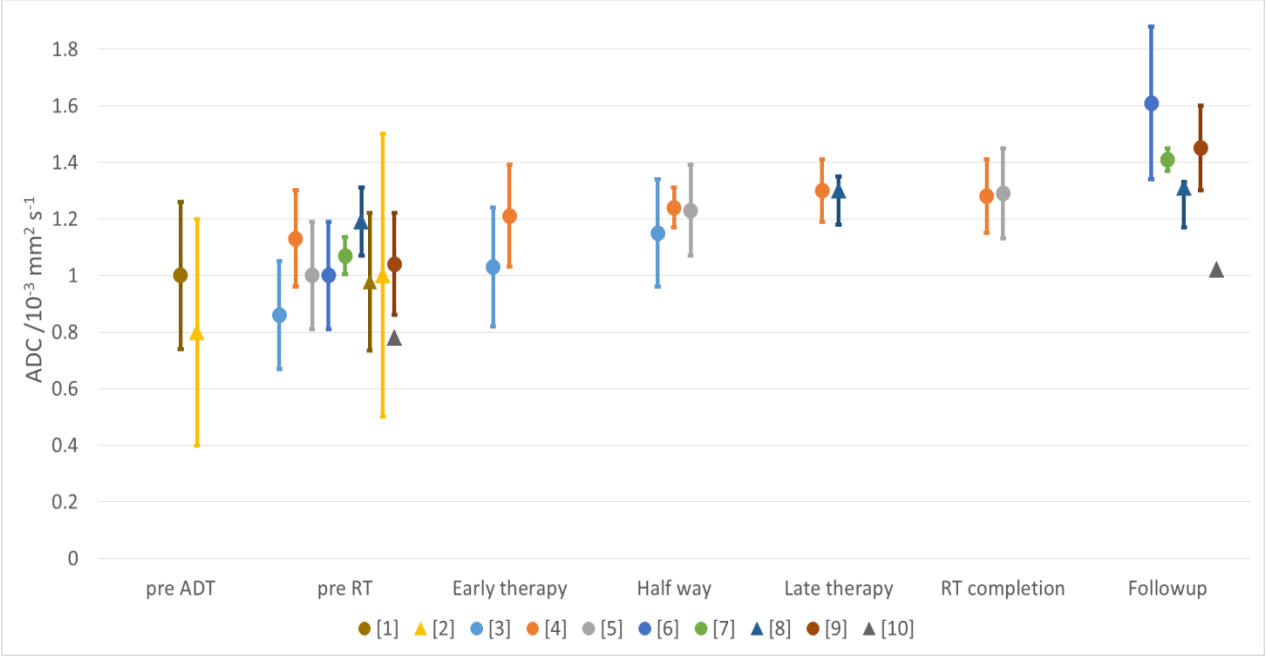

Figure 6-7: Summary of identified changes in Apparent Diffusion Co-efficient during neoadjuvant hormone therapy and radiotherapy (studies referenced in Table 6-5)

The use of ADC in combination with other markers may allow for early response assessment. The present study demonstrates that following NA-HT no significant difference can be identified between tumour and normal gland Fp or PS at any of the three time points. This is consistent with previous findings that HT induces a significant reduction in tumour DCE-MRI parameters making it indistinguishable from normal tissue (Barrett et al., 2012; Hotker et al., 2015). During treatment there was a significant rise in tumour Fp and PS. Eight weeks after treatment was completed the Fp, but not PS, had experienced a significant decline. The Fp at this point remained significantly higher than pre-radiotherapy. Other groups have also demonstrated a rise in tumour and normal gland perfusion during radiotherapy followed by a subsequent continuing decline at three and twelve months (Franiel et al., 2009; Harvey et al., 2001). This initial increase in perfusion appears due to an acute hyperemic response to radiotherapy. Improved oxygenation of tumours may improve radiosensitivity, reducing the radiation dose required to kill more hypoxic cells (Nahum et al., 2003). There appears to be a correlation between DCE-MRI changes and PSA decline following radiotherapy; it may therefore correspond with long term outcome (Low et al., 2011).

In the current study changes in Fp between the beginning of radiotherapy and at week three have been show to negatively correlate with variation in ADC. The relationship of these two variables is not well described. ADC has been shown to weakly correlate with K^{trans} in 34 treatment naïve patients with squamous cell carcinoma of the head and neck but not in 21 treatment naïve patients with renal cell carcinoma (Han et al., 2015; Ahn et al., 2013). In addition in a study of eight patients changes in Fp and PS did not correlate with change in ADC during chemo-radiotherapy for squamous cell carcinoma of the head and neck (Subesinghe et al., 2015). A relationship between the loss of cell density and reduced perfusion in a tumour responding to therapy would seem possible. This might explain a correlation in the current study due to treatment induced necrosis within the tumour reducing thevascular supply and cell density of this region of non-viable tissue. If

this is the case then those tumours with reducing ADC and rising Fp during radiotherapy might be most likely to have poor treatment response and to benefit from dose intensification. The use of the two values in combination may improve sensitivity for early response identification.

Volumetric analysis of patients treated on the current study revealed a correlation between volume changes during NA-HT and subsequent variation with RT. In this cohort an increase in prostate volume during RT was seen in patients with > 50% prostate shrinkage due to NA-HT. Conversely for patients with prostate shrinkage of < 50% on NA-HT a mean prostate volume decrease by week three of RT was seen. This finding is consistent with other groups who have shown a variable volume response to radiotherapy alone and also following NA-HT (Budiharto et al., 2009; Kasaova et al., 2011; Frank et al., 2010). It is the first time to our knowledge that a possible predictive value of response to NA-HT for subsequent volume changes during RT has been proposed. The mechanism for this may relate to variable fibrosis and reductions in cellular volume during NA-HT attenuating any subsequent volume response to RT. The changes seen in the current study during RT would be equivalent to an increase of up to 4 mm for an initial diameter of 40mm. In case of small treatment margins, an adjustment of expansions to account for these changes might be necessary.

Given the challenges found in identification of disease and attenuation of changes in ADC values during RT after NA-HT it is is likely predictive changes will be more easily identified in patients who are not previously exposed to androgen deprivation. Unfortunately it is clear that for high risk patients HT, even with dose escalation, has a significant benefit on disease control. Further for intermediate risk disease recent data suggests that this group experiences benefit from HT administration with dose escalated radiotherapy (See Chapter 8:Appendix A). The identification of predictive MP-MR changes after NA-HT therefore remains a necessary objective.

Our study has several limitations. First the use of manual matching of tumour contours from initial imaging to subsequent scans introduces potential error in ADC and DCE-MRI parameter measurement in tumour and normal tissue, although anatomical landmarks were identified to inform contouring and mitigate this effect. Second MRI at 1.5 T without an endorectal coil has a lower signal to noise ratio than 3.0 T imaging and delineation accuracy may be further impaired by reduced image resolution. Of note however a previous consensus statement has included 1.5 T imaging as a reasonable method of tumour identification. It is possible with the use of an endorectal coil or 3T scanner than identification of tumour at later time points to assess volume response would have been possible. Third our study assessed response during and after a four week course of hypo-fractionated radiotherapy and its findings may not be applicable to a longer course of conventional fractionation. Given recent trial outcomes it is likely that the use of hypo-fractionated therapy will remain a significant treatment option in future, and the results are therefore of interest (Dearnaley, 2015). Fourth since patients did not undergo surgery we were unable to obtain histopathological specimens to compare with MP-MRI findings. Fifth we did not have a control group with repeat imaging to assess the repeatability of our method, although the general repeatability of DWI values has been confirmed and we have previously demonstrated the repeatability of the DCE method (Gibbs et al., 2007; Kershaw et al., 2009). Finally the follow up

period is not long enough to assess any relationship between functional response and subsequent disease relapse. Longer term follow up data will be collected and reported.

Due to multiple statistical tests being performed a lower p-value of <0.01 was chosen to be considered significant. A bonferroni correction, sometimes applied in this context, would give a lower p-value but tends to be overly conservative and may miss significant relationships (Bender and Lange, 1999). Given this is an exploratory study designed to identify possible areas for future work it was felt appropriate to be more generous when setting a level of significance whilst acknowledging the risks of false positive results with multiple testing.

In conclusion this work has demonstrated that differences in ADC and DCE parameters of normal and malignant tissue are attenuated by prior NA-HT. Despite this a significant change in Fp during radiotherapy that negatively correlates with ADC variation has been shown. The predictive value of this will be informed by longer clinical follow up. Changes in prostate volume during NA-HT in this cohort predicted for subsequent changes during RT and may help inform highly conformal treatment and individualised margin expansions in future work.

Chapter 7: Discussion

The systemic treatment of cancer continues to evolve with recent promising developments in targeted agents and modulation of the immune-response (Garon et al., 2015; Melero et al., 2015; Chapman et al., 2011). For prostate cancer sufferers in particular in the last decade prolific progress in the systemic treatment of advanced disease has occurred (Valenca et al., 2015). During this period prostate cancer radiotherapy has also become increasingly sophisticated and its use as a curative treatment option seems likely to persist for the foreseeable future (Baumann et al., 2016). As a consequence novel methods to further improve outcome and reduce treatment related toxicity through adaptive approaches are desired. The use of radiotherapy for prostate cancer has evolved and diversified with research underpinning this progress; it is needed for future improvements and MRI will be a crucial modality in these developments.

This thesis has quantified through a systematic review of the literature the dynamic motion and deformation of the prostate as a consequence of the behaviour of nearby structures. MRI, with its ability to differentiate soft tissue structures, has been shown to be highly effective at identifying this behaviour, both during planning and delivery of RT. Already, using cobalt sources integrated with a MR scanner, the use of online MR imaging to support adaptive RT has been demonstrated (Mutic and Dempsey, 2014). With other commercial MR-Linac solutions due to become available in the near future the use of this technology will grow, enabling margin reduction and further safe dose escalation. Future research will have to investigate the safe integration of these developments into every day practice, building on two decades of analysis of prostate behaviour and applying the data in novel ways with innovative technology.

For effective use of MR and CT imaging in combination the images must be accurately registered to one another. Chapter 3 has shown that registration of CT and MR images can be improved by the use of interstitial points identified on CT imaging after an initial visual registration. With continued refinement, such as the addition of a contrast medium previously discussed, this technique may negate the need for fiducial markers to guide registration. It does not however address the benefit fiducial markers currently offer for image guidance. Daily treatment set-up using cone beam imaging is challenging due to poor identification of prostate boundaries. In the absence of clearly visualised soft tissue structures fiducial markers have been shown to significantly improve this process (Moseley et al., 2007). On treatment MRI will allow clear identification of the prostate boundary and interstitium, ultimately removing this indication. A commercial MR-Linac permits this and will consequently reduce uncertainty in image guidance and treatment volumes. Quantifying this benefit and its clinical implications will need to be some of the first studies performed with this technology, allowing for rationalised treatment decisions.

Registration of MR and CT imaging allows for identification of high density disease within the prostate and has results in multiple studies delivering focal treatment boosts to these regions. The findings of Chapter 4 suggest limited utility of in-bore MRI-guided biopsy of areas with concerning

features on MP-MRI prior to focal dose escalation. The ongoing phase III FLAME trial of focal dose escalation does not mandate biopsy of the focal boost target and, as a consequence of the analysis of Chapter 4, neither now does the TARGET study (Lips et al., 2011; Chung and Menard, 2016). Whilst sparing patients the morbidity of an additional interventional procedure, this has implications for research. It is known that the genetic make-up of multi-focal disease within the prostate is heterogeneous but it is less clear how variation occurs within individual dominant areas of disease (Boutros et al., 2015). Analysis of the genetic signature of tumours receiving treatment and correlation of this with patient outcomes will help inform an understanding of treatment response and a move towards personalised patient therapy. Both the PIRADS and Gleason score are imperfect systems to categorise disease, and tumours indistinguishable using these classifications may have markedly different outcomes following identical treatment. The genetic information provided by targeted biopsies therefore may have prognostic and predictive value, even if a high PIRADS score alone appears able to confirm the presence of disease.

If a biopsy of a targeted lesion was felt necessary, then even using in-bore MR-guidance multiple samples are likely to be required to obtain malignant tissue. Multiple positive samples may then be needed to obtain representative tissue sampling of heterogeneity within the target lesion, if this is indeed present. The use of robotic needle guidance trans-perineal biopsy device appears to improve accuracy of sampling and may partially mitigate this issue (Tilak et al., 2015). A future study using optimal technology to perform multiple samples per lesion with genetic sequencing of each biopsy correlated with full mount histology following radical prostatectomy would inform focal dose escalation studies.

Analysis of focal dose escalation demonstrates, reassuringly, that doses up to 250 Gy BED may be delivered with either a VMAT-IB or HDR-B with acceptable toxicity. The dosimetric analysis of the TARGET study performed in Chapter 5 however identified two findings which may have implications for long term outcome. First HDR-B delivers a much higher dose to a large proportion of the GTV than is achievable with VMAT-IB. Second, in the cohort analysed, a HDR-B results in a significantly smaller PTV(GTV) minimum dose than VMAT-IB, with the median value some 6 Gy lower, although this finding is influenced by the choice of α/β ratio used to combine dosimetry. Which of these factors will have more significance for ultimate disease response is of interest. Previously the importance of optimal HDR whole gland boost dosimetry for long term outcome has been shown and it may be that a similar effect is seen with focal boosts (Hoskin et al., 2014). Biopsies performed at three years post therapy will provide some information but if small areas of viable tissue persist due to PTV under-dosing they may be missed and it is only with data on longer term biochemical failure rates that a fuller picture will emerge. Given the strong evidence supporting a benefit from dose escalation then this data supports the development of further randomised phase III studies assessing the effectiveness and toxicity of these treatments in comparison with standard of care EBRT and EBRT with whole gland HDR boost. The ongoing FLAME study is currently recruiting 566 patients to investigate whether a 10% improvement in biochemical control can be achieved from the addition of a 95 Gy focal boost to whole gland 77 Gy EBRT. Data from other phase III studies would help validate any findings.

Even using a focal boost technique the associated toxicity remains of concern; a method of delivering treatment intensification to those who benefit most is desirable. Unfortunately a predictive radiomic signature for prostate cancer patients based on changes in functional characteristics during radiotherapy remains challenging. Multiple studies have now been performed, both in patients receiving RT alone, and now in those receiving combination RT with HT, which all shown trends in the changes in ADC during treatment. However, even when assessed sometime after completion of treatment, there remains a marked degree of overlap between the individual ADC values of those destined to relapse or remain free from biochemical failure after treatment; it therefore remains a crude predictive tool (Liu et al., 2014a). Chapter 6 again showed this variation during and after radiotherapy; longer clinical follow up is required to correlate this with biochemical outcome in this group. DCE-MRI parameters have also been shown to widely vary during radiotherapy, in both normal and malignant tissue, and for the first time a correlation between ADC and Fp changes has been suggested. It may be that the use of these sequences in combination with larger study cohorts and longer follow-up demonstrates a predictive ability but additional factors could also inform response monitoring. Assessment of changes in tumour volume, when performed at 1.5T without an endorectal coil, has not proved to be possible. As an alternative information on the genetic make-up of an individual's disease in combination with functional changes during treatment may improve predictive performance (Dewhirst and Chi, 2013). To allow for increased cohort size a consensus amongst members of the MR-Linac consortium on a common imaging protocol, allowing comparison after calibration of results from different centres, is being sought. A future study using a large pool of functional data in combination with genetic information would be an informative next step.

7.1 The future

This thesis has assessed the future role of MRI in radical prostate radiotherapy and it seems probable it will contribute to improvements in every stage of prostate treatment delivery, breaking down into four broad areas.

Firstly MRI is likely to play an increasingly prominent role in the planning process of radiotherapy delivery. As described in Chapter 2 its superb soft tissue imaging improves the accuracy and consistency of prostate contouring and as treatment conformality improves this will increase in importance. The challenges of registration of MR and CT images, discussed in detail in this thesis, may ultimately be rendered irrelevant by the advent of MR planning. For MRI to be used in isolation the information provided by CT must accounted for. MRI does not provide the direct measure of electron density achieved by CT, which is required for calculation of radiation attenuation. It has however been demonstrated that applying known bulk electron densities to tissue structures on MRI allows for generation of radiotherapy plans with differences in dose distribution of < 2% compared with conventional CT planning, removing the necessity for performing and registering two image sets (Jonsson et al., 2010). For MRI to be used without CT other significant challenges will also need to be overcome. These include performing MRI in the radiotherapy treatment position which may compromise the acquisition of high quality images, and the risk of image distortion away from the centre of the magnetic field. These problems potentially impair the accuracy of MRI planning in comparison to the fidelity of CT anatomy but methods to mitigate them have been

proposed. Resolution of these issues to allow the routine adoption of this technology into daily practice will be the challenge for future work over the coming years (Greer et al., 2011).

Secondly the use of MRI for planning will allow for the identification of interstitial high density disease to which a focal treatment boost may be targeted. The dosimetry and toxicity data reported in Chapter 5 provide reassurance that this can be delivered safely to patients. The results of the previously discussed FLAME and TARGET studies are awaited but if these do show a benefit in biochemical control for focal dose escalation with an acceptable toxicity profile then its use is likely to become routine for some patients. In particular the use of a VMAT integrated boost for patients not suitable for a brachytherapy could be incorporated into a MRI planning protocol with minimal disruption. This VMAT boost could be delivered with conventional fractionation to the prostate or as part of a hypofractionated stereotactic treatment, minimising inconvenience and toxicity to the patient while optimising outcome (Tree et al., 2013).

Thirdly the excellent soft tissue definition achieved with on treatment MRI will improve IGRT by allowing for more accurate identification of prostate position, reducing residual set-up uncertainty. The development of Linacs with integrated MR imaging capacity will, in the first instance, facilitate a reduction in radiotherapy expansion margins required to account for inter-fraction motion uncertainty (Lagendijk et al., 2014). In the longer term routine MR imaging during radiotherapy delivery is achievable. This will allow for accurate assessment of individual intra-fraction motion and over a course of conventionally fractionated radiotherapy would permit the generation of personalised expansion margins (Boye et al., 2013). In addition confidence in the accuracy of delivery of SBRT (shortened treatment courses of up to six fractions delivering large doses per fraction) would be improved by MRI for tracking of set up and prostate motion. The use of real time cine-MRI for gating, with treatment delivered only when the prostate is within the predefined target field, or with the radiation beam dynamically shaped to trace prostate motion during treatment, would allow for even larger reductions in PTV expansion margins (Yun et al., 2013). Although the delivery of treatment within an magnetic field may have dosimetric effects, particularly on secondary electrons, it appears that this can be compensated for in the planning process (Menten et al., 2016). Ultimately it may even prove possible to use the presence of a magnetic field to improve electron beam dose profiles opening up exciting opportunities for future research (Chen et al., 2005).

Finally the use of MP-MRI may play a role in adaptive treatment and surveillance. Already it has been demonstrated that ADC changes during and after treatment correspond with ultimate treatment outcome (Liu et al., 2014b). This information would allow a rationalised follow schedule, with repeat biopsy or MP-MRI in those at highest risk of relapse. It has not yet been shown that predictive MP-MRI changes can in isolation be identified during treatment. It seems possible however that the use of combinations of different MP-MRI sequences (ADC plus DCE for example as discussed in Chapter 7, or Blood Oxygen Level Dependent (BOLD) sequences) or in combination with other potential prognostic identifiers, such as radiomic, hypoxic or genomic signatures, will overcome this hurdle (Gong et al., 2015; Hill et al., 2015; Stoyanova et al., 2016). The development of a prognostic tool would allow the routine use of MP-MRI during treatment to

inform the need for dose boosting of resistant disease, minimising treatment related toxicity while maximising local control of disease.

In conclusion, MRI has an important and expanding role to play in future advancements in all aspects of technical radiotherapy for prostate cancer. MRI has the potential to improve planning and delivery through optimised IGRT and personalise treatment through predictive imaging and targeted treatment intensification. MRI guided focal dose escalation shows promise in minimising treatment related toxicity from treatment intensification while improving clinical outcome. The adoption of these novel approaches will be dependent on effective integration of MRI into routine prostate planning practice and the imminent arrival of the first commercial MR-Linacs will facilitate this.

Chapter 8: **Appendix A: PMH 9907- Long term outcomes of a randomized phase III study of short term bicalutamide hormonal therapy and dose escalated external beam radiation therapy for localized prostate cancer**

McPartlin AJ, Glicksman R, Pintilie M, Tsuji D, Mok G, Bayley A, Chung P, Bristow RG, Gospodarowicz M, Catton C, Milosevic M, Warde P

8.1 Introduction and contribution of authors

As highlighted in chapter 5 the use of NA-HT has implications for the visibility of tumour on MP-MRI. It is harder to confidently identify disease after this treatment and the variations in multi-parametric values between normal and malignant tissue during radiotherapy appears attenuated. The ability of MP-MRI to provide predictive information during radiotherapy may therefore be impaired by the administration of NA-HT.

While it appears clear that NA-HT improves outcome for patients with high risk disease, its role in those with intermediate risk with dose escalated radiotherapy is less clear. If its use could be avoided in this group then creating a method for early identification of response to therapy may be simplified. In this appendix I perform an analysis of a phase III study looking at the role of bicalutamide, an anti-androgen therapy, with dose escalated radiotherapy in predominantly intermediate risk disease. The original study was devised and led by Padraig Warde at Princess Margaret Cancer Centre in the late 1990's and prospective data subsequently collected by the trials team there. For this chapter I verified the collected data and formatted it for analysis. I liaised with the Melania Pintilie at the Princess Margaret statistical department who used this data for her analysis. The unplanned post hoc analysis of intermediate risk divided into favourable and unfavourable was my initiative as was assessing response by dose received as it varied over the trial recruitment period.

I interpreted the statistical analysis and wrote the entire paper, excluding the description of statistical methods employed. Major suggestions to revision of format were provided by Padraig Warde. The other co-authors all provided minor revisions to the final manuscript. I submitted the paper for publication, responded to amendments requested by reviewers. It was ultimately accepted for publication in Cancer (McPartlin et al., 2016a).

8.2 Abstract

Background: The role of hormone therapy (HT) with dose-escalated external beam radiotherapy (DE-EBRT) in intermediate risk prostate cancer (IRPC) remains controversial. We report the long term outcome of a phase III study of DE-EBRT with or without HT for patients with localized prostate cancer (LPC).

Methods: From 1999-2006 252 of an intended 338 patients with LPC were randomized to DE-EBRT +/- five months neo-adjuvant and concurrent bicalutamide 150mg OD. The study was closed early due to contemporary concerns surrounding bicalutamide. Primary outcome was biochemical failure (BF) incidence with overall survival (OS), local control (LC) and quality of life (QoL) as secondary endpoints. BF and OS rates were estimated using Cumulative Incidence Function and Kaplan-Meier and compared with Gray's test and log rank test.

Results: 11 patients were excluded from analysis. Characteristics were well balanced in each treatment arm. 95% of patients had IRPC. Prescribed dose increased from 75.6Gy in 42 fractions to 78Gy in 39 fractions over the period. At a median follow up of 9.1 years 98 BF have occurred with no significant effect of HT vs none on BF, 40 vs 47% ($p = 0.32$), OS, 82 vs 86 % ($p = 0.37$), LC, 52% vs 48 % ($p=0.32$) or QoL in the minority of patients completing questionnaires. Dose escalation, 75.6Gy vs > 75.6Gy, reduced BF by 26% ($p=0.004$).

Conclusion: For predominantly IRPC patients the addition of HT to DE-EBRT did not significantly affect BF, OS or LC. Bicalutamide appeared well tolerated. Conclusions are limited by incomplete recruitment.

8.3 Introduction

Prostate cancer is responsible globally for over 300000 deaths annually(2014). External beam radiotherapy (EBRT) is an effective treatment modality but a significant proportion of men will relapse. The addition of hormone therapy (HT) to EBRT has been shown in laboratory studies to reduce the required lethal dose to prostate tumour and in clinical studies to increase overall survival (Bolla et al., 2002; Zietman et al., 1997b).

The benefit of dual therapy is most clearly seen in high risk prostate cancer; its role in intermediate risk disease is less certain. Two prospective clinical studies, treating predominantly intermediate risk patients, have shown a significant disease specific survival benefit at five to ten years from the addition of four to six months HT starting two months prior, versus EBRT alone (D'Amico et al., 2008; Jones et al., 2011). Both of these studies administered HT with standard dose EBRT (66.6 – 70Gy) which has been shown to achieve inferior biochemical control to dose escalated (DE) EBRT (Kalbasi et al., 2015). The evidence of benefit from its addition to DE-EBRT in intermediate risk disease is mixed with recent prospective data supporting its efficacy (Nabid A, 2015; Dubray et al., 2011b; Bolla et al., 2016).

PMH 9907 was devised in the late 1990's to assess the benefit of HT with DE-EBRT. At that time the optimal form of HT to employ was unclear. It was known that luteinizing hormone releasing hormone (LHRH) agonists were associated with significant loss of sexual function and bone density (Decensi et al., 1993). Early data suggested that use of an androgen receptor blocker such as bicalutamide might be as effective without such significant side effects; it was therefore chosen for this study (Sieber et al., 2004; Iversen et al., 2000). Although subsequent evidence has implied the relative clinical effectiveness may be inferior to LHRH agonists it has been suggested that 150mg daily of bicalutamide improves overall survival compared to EBRT alone in locally advanced disease (Kunath et al., 2014; See et al., 2006); its effectiveness with DE-EBRT is therefore of interest

We report the mature outcome data of a randomized phase III study looking at the role of bicalutamide with DE-EBRT for localized prostate cancer. Unplanned post hoc analysis has been performed to assess sub-classification of intermediate risk disease into favourable and unfavourable categories, and the effect of further dose escalation through the study period as local practice evolved.

8.4 Materials and methods

8.4.1 *Eligibility and study design*

This study assessed the effect of bicalutamide 150mg OD with DE-EBRT of 75.6Gy to 79.8Gy in 42 fractions or 78Gy in 39 fractions for the treatment of localized prostate cancer. GUROC consensus guidelines were published in 2001 and, as a result, stratification in the study allowed for inclusion of disease which would not be considered intermediate risk by current standards (Lukka et al., 2001). Eligible patients had T1b-T2, Gleason 6-8, and PSA ≤20ng/ml disease. Patients with

clinical stage T1b/T2a and Gleason 6 required a PSA of 10-20 ng/ml. Central review of all pathology was performed. All patients with PSA >10 ng/ml had a negative bone scan within 12 months of study entry. CT staging was not required. No previous hormonal or cytotoxic therapy was permitted prior to entry. All patients were ECOG performance status ≤ 2, aged ≤ 80 years and without contraindication to DE-EBRT.

A stratified randomization was carried out according to initial PSA (< 10 ng/ml versus ≥ 10 ng/ml), Gleason score <7 versus 7 or 8, T1 versus T2 staging. Patients were randomized 1:1 to receive radiotherapy with or without five months of neoadjuvant and adjuvant bicalutamide starting three months prior to radiotherapy.

Ethical approval was obtained for the study and all patients gave informed signed consent prior to enrolment.

8.4.2 *Radiotherapy*

The clinical target volume (CTV) was defined as the prostate, plus seminal vesicles if risk of involvement was >15% by Partin table (Partin et al., 1997). The CTV was expanded 10 mm isotropically except 7 mm posteriorly to form the planned target volume. Pelvic lymph nodes were not treated. Patients were planned and treated with empty rectum and full bladder. Prior to therapy all patients had fiducial markers inserted under trans-rectal ultrasound guidance. Radiotherapy was given using six coplanar equally weighted 18 MV beams, or IMRT, with daily EPID imaging and set up verification using fiducial markers. From 1999-2001 patients received 75.6Gy in 42 fractions over 8.5 weeks. After this time the dose was increased up to 79.8Gy in 42 fractions then 78Gy in 39 fractions as experience with DE-EBRT increased.

8.4.3 *Quality of life assessment*

Quality of life (QoL) and treatment related toxicity was measured prospectively using QLQ-C30+3 and prostate cancer checklist, the International Index of Erectile Function (IIEF) and RTOG acute and late toxicity scales (Aaronson NK, 1993; Cox et al., 1995; Rosen et al., 2002).

8.4.4 *Study endpoints*

The primary end point of the study was biochemical failure (BF), defined using the Phoenix criteria of a rise ≥ 2ng/ml above nadir PSA (Roach et al., 2006). Secondary endpoints were local tumour control as assessed by repeat trans-rectal prostate biopsy two years after completion of RT, QoL and OS of patients.

8.4.5 *Statistical methods*

The study assumed a 35% 5-year BF incidence for RT alone and was powered for a one-sided 5% level test to detect a 15% decrease with 90% power. This required a sample size of 338 with 85 expected events

Due to inter-current deaths before BF this was analysed using competing risks specific techniques. The probability of BF was calculated using cumulative incidence method and the effect of treatment unadjusted or adjusted for other factors was tested using the Gray test and the Fine and Gray

model, respectively (Fine and Gray, 1999; Gray, 1988; Kalbfleisch and Prentice, 2002). The time to death was calculated from the date of randomization. The survival probabilities were calculated using Kaplan-Meier technique and the effect of treatment was tested using the log rank test and Cox proportional hazards model. The analyses for BF and OS were performed as intent to treat analysis. Logistical regression was used to compare the findings of post-radiotherapy biopsies between the treatment arms

For IIEF scores were categorized in 5 classes: Severe dysfunction, Moderate dysfunction, Mild-moderate dysfunction, Mild dysfunction, No dysfunction. These were further dichotomized in Severe/Moderate/Mild-Moderate vs. Mild/No dysfunction. For each time point the percentages of patients in each category were calculated.

For the EORTC questionnaire the scores for all the functions and toxicity items were calculated as averages of the relevant questions. The missing values were treated as recommended by the EORTC guidelines (Fayers et al., 2001). If a patient answered ≥ 50% of questions pertaining to an item then then score was the average of the answered questions, otherwise the score for that particular item was considered missing. The percentages 'with problems' were calculated at each time point.

Comparison of outcome for increasing radiotherapy doses was complicated by differing follow up as practice changed over time. To verify the robustness of comparison we generated a censoring time for patients receiving 75.6Gy which was similar to the censoring time for those receiving higher doses. An event was preserved in the low dose group only if the newly generated censoring time was larger than the observed event. Otherwise the observation was considered censored at the generated censored time. The observed times and events remained unchanged for the high dose group. The comparison was performed with the outcome defined as described above. This process was repeated 1000 times.

8.5 Results

A total of 252 patients were recruited from 1999-2006. The study was closed early after suspension from 2005 due to concerns related to contemporary data showing a statistically insignificant trend towards survival deficit from the addition of bicalutamide therapy to watchful waiting (McLeod et al., 2006).

Median follow up for surviving patients was 9.1 years (range 0.1-14.8). Eleven patients were excluded from analysis; eight were found to be ineligible after randomization following central review of pathology, one withdrew and two had no follow up data after treatment (Figure 8-1). Distribution of analysed patients by pre-treatment and prognostic factors was balanced between the two arms ($p>0.05$) with the exception of pre-radiotherapy PSA (Table 8-1). There were 14 (5.8%) protocol violations. Due to patient choice six randomized to bicalutamide received radiotherapy alone and one randomized to radiotherapy alone received bicalutamide. In addition a total of 10 patients received doses of less than 75.6Gy. In three cases this was due to failure to complete treatment, the remainder were prescribed a dose of between 66-72Gy due to concerns about toxicity from large treatment volumes.

A dose of 75.6Gy in 42 fractions was received by 76 patients and 79.8Gy in 42 fractions or 78 Gy in 39 fractions by 155. Randomization between treatment arms was matched at each dose level.

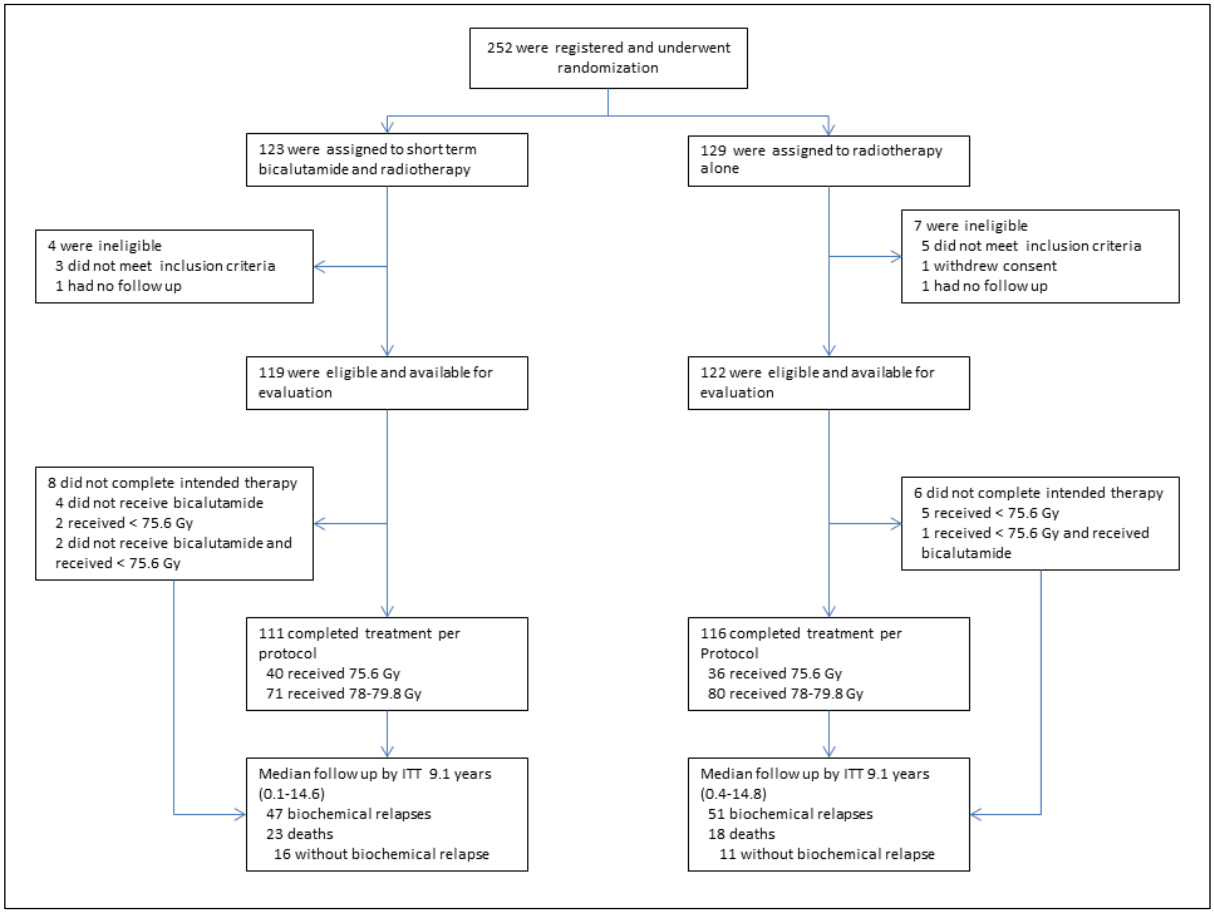

Figure 8-1: Modified consort diagram

8.5.1 *Outcomes*

At the time of analysis 98 biochemical failures and 41 deaths have occurred. Men who received bicalutamide had a non-statistically significant 7% reduction in BF rate at five years, 17% (95% CI 11%-25%) vs 24% (95% CI 17%-33%) which remained at nine years follow up, 40% (95% CI 31% - 51%) vs 47% (95% CI 37% – 58%) (p = 0.32) (Figure 8-2). Overall survival was also not significantly different in those who did or did not receive bicalutamide, 82% (95% CI 75% – 90%) vs 86% (95% CI 80% - 94%) (p = 0.37) at nine years (Figure 8-3). Biopsy results were available within four years of completing treatment for 94 patients (38%), 50 following radiotherapy alone and 44 after combination therapy. At the time of biopsy 51 (54%) had experienced at least two preceding consecutive rises in PSA and 11 (12%) had suffered BF. Biopsies identified malignant disease in 58% after radiotherapy and 48% after combined treatment (p=0.32, OR = 0.66, 95% CI 0.29-1.49). Ultimately 68% of patients with positive biopsies and 42% with negative biopsies went on to experience BF. Further HT had been received after relapse by 30 (63.8%) patients randomized to dual treatment and 34 (66.6%) of the remainder. Five patients received local salvage therapy and eight went on to palliative chemotherapy. Distant metastases were ultimately

identified in 24 (51.0%) of patients failing after dual therapy and 35 (68.6%) failing after radiotherapy alone.

Table 8-1: Patient characteristics

		Radiotherapy plus bicalutamide (n=119)	Radiotherapy alone (n=122)	p-value*
Age	Median(range)	71.4(57.6-79.4)	70.9(55.3-79.5)	0.41†
Gleason score	3+3	13(10.9%)	17(13.9%)	0.51
	3+4	67(56.3%)	71(58.2%)	
	4+3	34(28.6%)	26(21.3%)	
	3+5	1(0.8%)	2(1.6%)	
	4+4	4(3.4%)	5(4.1%)	
	5+3	0(0%)	1(0.8%)	
Stage	T1B-2A	96(80.7%)	91(74.6%)	0.28
	T2B-2C	23(19.3%)	31(25.4%)	
Percent positive cores	Median(range)	50(8-100)	50(7-100)	0.36†
	Missing	6	5	
PSA at randomization	Median(range)	8.3(1.2-19.6)	7.6(1.1-20)	0.49†
PSA at radiotherapy	Median(range)	2.6(0.1-20.4)	7.6(0.4-22.3)	< 0.001†
Radiotherapy dose	75.6 Gy	40(33.6%)	36(29.5%)	0.58^
	78-79.8 Gy	75(63.0%)	80(66.4%)	
	< 75.6 Gy	4 (3.4%)	6(4.9%)	
Risk group	Unclassified intermediate	1(0.8%)	3(2.5%)	
	Favourable intermediate	29(24.4%)	28(23.0%)	> 0.99#
	Unfavourable intermediate	84(70.6%)	83(68.0%)	
	High	5(4.2%)	8(6.5%)	

ADT, androgen deprivation therapy; Gy, Gray; PSA, prostate specific antigen; RT, radiotherapy
* Fisher exact test unless otherwise indicated, † Mann-Whitney test, # 75.6 Gy vs 78-79.8 Gy, ‡Favorable vs unfavorable

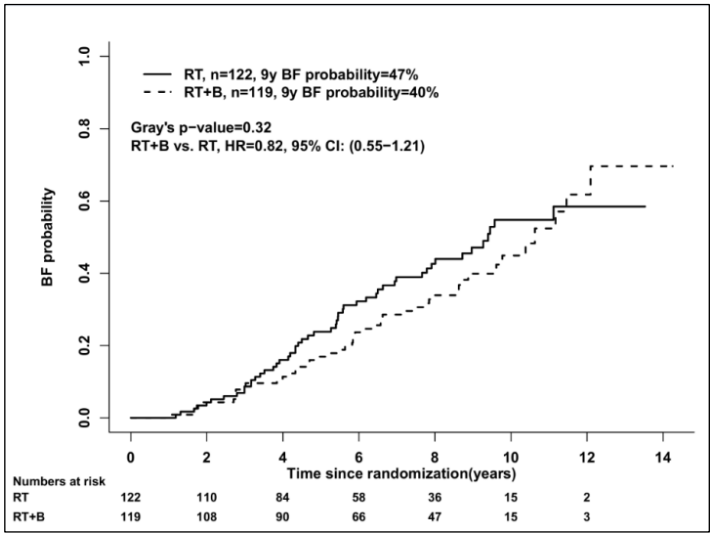

Figure 8-2: Cumulative incidence of Biochemical Failure for those receiving bicalutamide plus radiotherapy or radiotherapy alone. (RT = Radiotherapy, B = Bicalutamide, BF = Biochemical Failure)

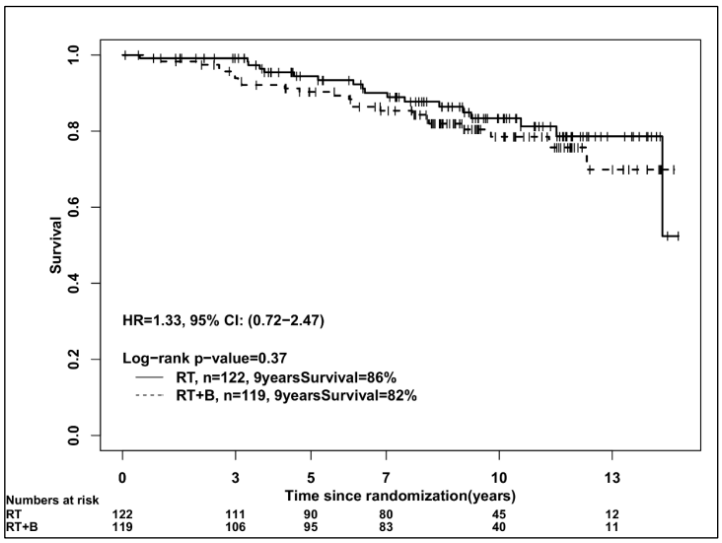

Figure 8-3: Kaplan-Meier survival probability curve for those receiving bicalutamide plus radiotherapy, or radiotherapy alone (RT = Radiotherapy, B = Bicalutamide)

8.5.2 *Toxicity and Quality of life*

Bicalutamide therapy was stopped prematurely in five patients (4.3%). In three cases this was due to gynecomastia, once due to peri-orbital pain of unclear aetiology and once for unspecified reasons. The addition of bicalutamide had no effect on acute or late genito-urinary (GU) and gastro-intestinal (GI) toxicity. Use of IMRT increase over time with none receiving 75.6 Gy and 57% receiving 78-79.8 Gy treated with this method. When analysed by radiotherapy dose those receiving 78-79.8Gy experienced higher acute grade ≥ 2 GU toxicity, 38.7% vs 14.5% ($p < 0.001$), and late grade 2 ≥ GI toxicity, 5.8% vs 0% ($p = 0.033$). No significant difference in QoL assessment was found between dose levels. The erectile dysfunction (ED) and EORTC-30 questionnaires were considered at various time points; baseline, baseline- 6m, 6m-1yr, 1-2yr, 2-4yr and >4yr. A minority of patients completed questionnaires within each given time point from a maximum of 79 responses at baseline. There was almost no long term change in erectile dysfunction in either group although there were marked levels of impairment at baseline. There was deterioration in intercourse satisfaction and sexual desire in both arms during follow up but no clear change from baseline in overall satisfaction four years after treatment in either group (Figure 8-4).

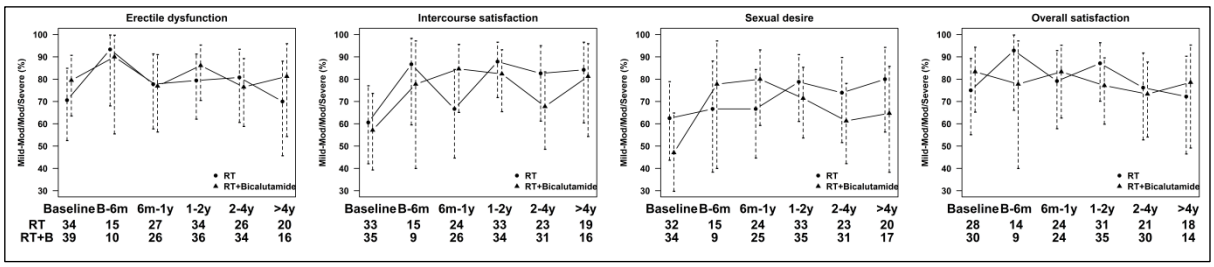

Figure 8-4: Sexual health at various time-points following treatment with bicalutamide plus radiotherapy or radiotherapy alone (RT = Radiotherapy).

Table 8-2: RTOG Acute and late toxicity for those receiving bicalutamide plus radiotherapy or radiotherapy alone

	Toxicity grade	Radiotherapy alone (n=122)	Radiotherapy plus bicalutamide (n=119)	p-value*	Treated to 75.6 Gy	Treated to 78-79.8 Gy	p-value*
Acute GI toxicity	G2	11 (9%)	11 (10%)	0.83	5(7%)	16(10%)	0.47
	G3	0	0		0	0	
Acute GU toxicity	G2	38 (30%)	33(28.9%)	>0.99	11(15%)	60(40%)	**0.00027**
	G3	0	2(1.8%)		1(1%)	1(1%)	
Late GI toxicity	G2	6(5 %)	4(3.5%)	0.55	0	9(6%)	**0.033**
	G3	1(1%)	0		0	1(1%)	
Late GU toxicity	G2	7(6%)	11(10%)	0.41	5(7%)	13(8%)	>0.99
	G3	14(11%)	13(11%)		9(12%)	15(10%)	

ADT, androgen deprivation therapy; GI, gastro-intestinal; GU, genito-urinary; Gy, Gray,
*Fisher exact test reflecting association between grade 2/3 vs 0/1 and treatment given (bicalutamide or radiotherapy dose)

The EORTC-30 questionnaire similarly identified no marked effect of the addition of bicalutamide, with stable overall quality of life in both groups through the treatment period.

8.5.3 *Exploratory stratification of disease and dose received*

Patient risk group was defined as proposed by Zumsteg et al, with unfavourable intermediate risk including patients with at least one of predominant Gleason 4, ≥50% positive cores or ≥2 intermediate risk factors (Zumsteg et al., 2013a). Stratification of intermediate risk appeared predictive with an 18% higher incidence of BF in unfavourable risk disease although this did reach statistical significance (p = 0.052). There remained no statistically significant benefit from the addition of HT following stratification.

Further dose escalation during this study from 75.6 Gy to 78 or 79.8 Gy had a significant effect on the risk of BF with a reduction in incidence at 9 years, from 61% to 35%, for those receiving the higher doses (HR 0.54, CI 0.36-0.8). Median follow up was 11.2 years (1.4-14.8) for those receiving 75.6 Gy and 8.9 years (0.4-13.3) for those receiving 78-79.8 Gy. The p-value was significant (<0.05) in 99.4% instances when repeat testing was performed to account for follow up variation. There was no significant difference in any disease characteristic between patients receiving the lower or higher doses (p > 0.2). There remained no significant reduction in BF from the addition of bicalutamide when stratified by dose received.

Differences in outcome identified between study arms were maintained on multivariate analysis.

8.6 Discussion

This study reports mature prospective outcome data on the addition of HT to DE-EBRT in intermediate risk prostate cancer. Bicalutamide has not been demonstrated to provide a significant effect on BF at a median of 9.1 years follow-up for patients with intermediate risk prostate cancer, the primary end point of this trial. There was however a trend towards benefit with a 7% decrease in BF, from 47% to 40%, for those receiving HT. The study was not powered to detect this level of difference, and failed to reach its accrual target, raising the possibility of a false negative

conclusion. Previously a larger study of 1065 patients by the Early Prostate Cancer (EPC) Trialists' Group demonstrated that ongoing bicalutamide 150mg in addition to median dose of 64Gy EBRT made a significant difference to BF, but not OS, at a median follow up of 7.2 years in a group with T1-2 N0 disease (See et al., 2006). In that study BF decreased from 47.2% to 41.1% for patients treated with bicalutamide; the current study has achieved a similar benefit despite higher radiotherapy doses and shorter HT duration. Of note, the EPC study demonstrated in a further 305 patients with locally advanced disease that the addition of bicalutamide had a more pronounced benefit on BF, reducing it from 59.7% to 41.0% (HR 0.56, 0.4-0.78), and also improved OS (HR 0.65, 0.44-0.95), consistent with the survival benefit seen from the addition of LHRH agonists in high risk disease.

Although anti-androgen monotherapy may be inferior to medical castration in advanced disease its relative merits with DE-EBRT in IRPC remain unclear(Kunath et al., 2014). By way of comparison the EORTC 22991 study has reported outcome for 819 patients, 74.8% with intermediate risk disease and 25.2% high risk, who received 70 – 78 Gy with or without 6 months of LHRH-agonist therapy (Bolla et al., 2016). At a median f/u of 7.2 years the addition of HT reduced BF from 49.1% to 28.8% (HR 0.52, CI 0.41-0.66). The increased benefit seen in comparison the present study may in part be due to the increased proportion of high risk disease and an increased efficacy of LHRH-agonists.

It is known that intermediate risk prostate cancer represents a heterogeneous disease. The Zumsteg et al proposed sub-categorization of unfavourable intermediate risk disease has been suggested to be prognostic (Zumsteg et al., 2013a; Keane et al., 2014). Retrospective analysis by other groups has identified that a benefit from HT with DE-EBRT may only be seen in unfavourable intermediate patients, although the definition of this varied (Castle et al., 2013; Bian et al., 2012). No significant effect on BF from the addition of HT in favourable or unfavourable intermediate risk disease was seen in our current study.

The overall results achieved in both arms in our study are lower than those that have been described elsewhere. The cause of this may be multifactorial. Firstly by sub-group analysis 76% of patients in the current study had unfavourable-intermediate or high risk disease. These two risk groups have been shown in the prostate cancer risk stratification (ProCaRS) project, classified as unfavourable-intermediate risk if PSA >=10 and either T2b/2c or Gleason 7 disease, to have a similar BF rate that is significantly worse than favourable-intermediate risk disease (Rodrigues et al., 2013). Further, a subgroup analysis of DFCI 95096 looked at 206 patients with intermediate or high risk disease who received 70Gy with or without six months HT at 14.3 years follow up. This found that the risk of dying from prostate cancer was not significantly different, adjusting for variables, for unfavourable-intermediate or high risk disease, 13 vs 17%. By contrast in those with favourable-intermediate risk disease there was no disease specific mortality (Keane et al., 2014).

Secondly the degree of dose escalation employed in our study was initially modest due to evolving experience. A dose of 75.6Gy at 1.8Gy per fraction, received by around a third of participants, has an EQD2 of 72.6Gy, assuming an α/β_{tumor} of 3Gy, which would not be considered effective dose escalation by current standards. With no difference in baseline disease characteristics the

incidence of positive biopsy was reduced from 63% (29 of 46 biopsies) in those receiving 75.6Gy to 46% (21 of 46 biopsies) in those receiving 78-79.8Gy (p = 0.14). Patients who underwent biopsy, regardless of finding, were more likely to experience BF than those who were not biopsied, 62% vs 40% (p = 0.001), suggesting a possible selection bias contributing to the high positive biopsy rate. Of relevance an MSKCC retrospective review of patients who received RT with or without HT and underwent repeat biopsies at two years identified a 18% reduction in positive findings, from 33% to 15%, with dose escalation from 75.6Gy to ≥ 81 Gy (p = 0.05) (Zelefsky et al., 2008b).

Dose escalation during the study period was associated with a significant reduction in BF. This was driven by a reduction from 63% to 39% (HR 0.53, CI 0.33-0.84) at nine years in those with unfavourable intermediate disease, compared with a decrease from 28% to 27% (HR 0.88, CI 0.33-2.35) in favourable. Higher doses were also associated with a rise in acute G2 GU and late G2 GI toxicity, despite increasing IMRT use over time. These findings are consistent with published data and highlight that ultimately more accurate predictive tools utilizing novel predictive genomic and proteomic biomarkers are needed if dose escalation, with associated increased toxicity, is to be targeted better at those who will benefit most (Bostrom et al., 2015; Shipitsin et al., 2014; Kuban et al., 2003).

Bicalutamide therapy was found to be well tolerated with only 4.6% failing to complete therapy as prescribed. Sexual function, assessed by the IIEF questionnaire, was not significantly different in each of the five questionnaire categories in either treatment arm. There were an increased proportion of patients in both arms who complained of more severe symptoms after treatment but this was not worsened by the addition of bicalutamide, with the exception of sexual desire. Only intercourse satisfaction and sexual desire experienced persistent worsening in both arms when assessed more than four years after treatment. Conclusions are limited due to the numbers of patients assessed within each time point, with possible selection bias, but the results suggest the additive effects of bicalutamide with radiotherapy on sexual function are limited. Previous work has shown patients taking bicalutamide 150mg OD are significantly more likely to retain sexual interest than those undergoing medical castration and the benefit appears to be retained with radiotherapy in this current study (Iversen et al., 2001).

8.7 Conclusion

This study has failed to show a significant benefit from the addition of bicalutamide to DE-EBRT for a group of patients with predominantly intermediate risk prostate cancer. A trend towards a reduction in BF following combination therapy was seen and conclusions are limited by failure to complete accrual.

Bicalutamide was well tolerated and appeared in this cohort to have no significant adverse effect on sexual function.

Conflict of interest Statement

None

Financial Disclosure

Small unrestricted educational grant from Astra-Zeneca

Chapter 9: **References**

Aaronson NK, A. S., Bergman B, Bullinger M, Cull A, Duez NJ, Filiberti A, Flechtner H, Fleishman SB, de Haes JCJM. (1993) The European Organisation for Research and Treatment of Cancer QLQ-C30: A quality-of-life instrument for use in international clinical trials in oncology. *Journal of the National Cancer Institute,* 85**,** 365-376.

Adamson, J. & Wu, Q. (2009) Inferences about prostate intrafraction motion from pre- and posttreatment volumetric imaging. *Int. J. Radiat. Oncol. Biol. Phys.,* 75(1)**,** 260-7.

Adamson, J. & Wu, Q. (2010) Prostate intrafraction motion assessed by simultaneous kV fluoroscopy at MV delivery II: adaptive strategies. *International journal of radiation oncology, biology, physics,* 78(5)**,** 1323-30.

Ahmed, H. U., Hu, Y., Carter, T., Arumainayagam, N., Lecornet, E., et al. (2011) Characterizing clinically significant prostate cancer using template prostate mapping biopsy. *J. Urol.,* 186(2)**,** 458-64.

Ahn, S. J., Park, M. S., Kim, K. A., Park, J. Y., Kim, I., et al. (2013) (1)(8)F-FDG PET metabolic parameters and MRI perfusion and diffusion parameters in hepatocellular carcinoma: a preliminary study. *PLoS One,* 8(8)**,** e71571.

Ahunbay, E. E., Peng, C., Chen, G. P., Narayanan, S., Yu, C., et al. (2008) An on-line replanning scheme for interfractional variations. *Med. Phys.,* 35(8)**,** 3607-15.

Ahunbay, E. E., Peng, C., Holmes, S., Godley, A., Lawton, C., et al. (2010) Online adaptive replanning method for prostate radiotherapy. *International journal of radiation oncology, biology, physics,* 77(5)**,** 1561-72.

Akimoto, T., Katoh, H., Kitamoto, Y., Tamaki, T., Harada, K., et al. (2006) Rectal bleeding after high-dose-rate brachytherapy combined with hypofractionated external-beam radiotherapy for localized prostate cancer: impact of rectal dose in high-dose-rate brachytherapy on occurrence of grade 2 or worse rectal bleeding. *Int. J. Radiat. Oncol. Biol. Phys.,* 65(2)**,** 364-70.

Al-Mamgani, A., Heemsbergen, W. D., Levendag, P. C. & Lebesque, J. V. (2010) Subgroup analysis of patients with localized prostate cancer treated within the Dutch-randomized dose escalation trial. *Radiother. Oncol.,* 96(1)**,** 13-8.

Albertsen, P. C., Hanley, J. A. & Fine, J. (2005) 20-year outcomes following conservative management of clinically localized prostate cancer. *Jama,* 293(17)**,** 2095-101.

Ali, K., Gunnar, A., Jan-Erik, D., Hans, L., Pär, L., et al. (2007) PSA doubling time predicts the outcome after active surveillance in screening-detected prostate cancer: Results from the European randomized study of screening for prostate cancer, Sweden section. *International Journal of Cancer,* 120(1)**,** 170-174.

Alonzi, R., Padhani, A. R., Taylor, N. J., Collins, D. J., D'Arcy, J. A., et al. (2011) Antivascular effects of neoadjuvant androgen deprivation for prostate cancer: an in vivo human study using susceptibility and relaxivity dynamic MRI. *Int. J. Radiat. Oncol. Biol. Phys.,* 80(3)**,** 721-7.

Amro, H., Hamstra, D. A., McShan, D. L., Sandler, H., Vineberg, K., et al. (2013) The dosimetric impact of prostate rotations during electromagnetically guided external-beam radiation therapy. *Int. J. Radiat. Oncol. Biol. Phys.,* 85(1)**,** 230-6.

Andriole, G. L., Crawford, E. D., Grubb, R. L., 3rd, Buys, S. S., Chia, D., et al. (2009) Mortality results from a randomized prostate-cancer screening trial. *The New England journal of medicine,* 360(13)**,** 1310-9.

Antolak, J. A., Rosen, II, Childress, C. H., Zagars, G. K. & Pollack, A. (1998) Prostate target volume variations during a course of radiotherapy. *International journal of radiation oncology, biology, physics,* 42(3)**,** 661-72.

Arrayeh, E., Westphalen, A. C., Kurhanewicz, J., Roach, M., 3rd, Jung, A. J., et al. (2012) Does local recurrence of prostate cancer after radiation therapy occur at the site of primary tumor? Results of a longitudinal MRI and MRSI study. *Int. J. Radiat. Oncol. Biol. Phys.,* 82(5)**,** e787-93.

Arsov, C., Rabenalt, R., Blondin, D., Quentin, M., Hiester, A., et al. (2015) Prospective randomized trial comparing magnetic resonance imaging (MRI)-guided in-bore biopsy to MRI-ultrasound fusion and transrectal ultrasound-guided prostate biopsy in patients with prior negative biopsies. *Eur. Urol.,* 68(4)**,** 713-20.

Aubry, J. F., Beaulieu, L., Girouard, L. M., Aubin, S., Tremblay, D., et al. (2004) Measurements of intrafraction motion and interfraction and intrafraction rotation of prostate by three-dimensional analysis of daily portal imaging with radiopaque markers. *International journal of radiation oncology, biology, physics,* 60(1)**,** 30-9.

Azzeroni, R., Maggio, A., Fiorino, C., Mangili, P., Cozzarini, C., et al. (2013) Biological optimization of simultaneous boost on intra-prostatic lesions (DILs): Sensitivity to TCP parameters. *Physica Medica,* 29(6)**,** 592-598.

Badakhshi, H., Wust, P., Budach, V. & Graf, R. (2013) Image-guided radiotherapy with implanted markers and kilovoltage imaging and 6-dimensional position corrections for intrafractional motion of the prostate. *Anticancer Res,* 33(9)**,** 4117-21.

Ballhausen, H., Li, M., Hegemann, N. S., Ganswindt, U. & Belka, C. (2015) Intra-fraction motion of the prostate is a random walk. *Phys. Med. Biol.,* 60(2)**,** 549-63.

Barentsz, J. O., Richenberg, J., Clements, R., Choyke, P., Verma, S., et al. (2012a) ESUR prostate MR guidelines 2012. *Eur. Radiol.,* 22(4)**,** 746-757.

Barentsz, J. O., Richenberg, J., Clements, R., Choyke, P., Verma, S., et al. (2012b) ESUR prostate MR guidelines 2012. *Eur. Radiol.,* 22(4)**,** 746-57.

Barentsz, J. O., Weinreb, J. C., Verma, S., Thoeny, H. C., Tempany, C. M., et al. (2016) Synopsis of the PI-RADS v2 Guidelines for Multiparametric Prostate Magnetic Resonance Imaging and Recommendations for Use. *Eur. Urol.,* 69(1)**,** 41-9.

Barrett, T., Gill, A. B., Kataoka, M. Y., Priest, A. N., Joubert, I., et al. (2012) DCE and DW MRI in monitoring response to androgen deprivation therapy in patients with prostate cancer: a feasibility study. *Magn. Reson. Med.,* 67(3)**,** 778-85.

Bastian, P. J., Mangold, L. A., Epstein, J. I. & Partin, A. W. (2004) Characteristics of insignificant clinical T1c prostate tumors: A contemporary analysis. *Cancer,* 101(9)**,** 2001-2005.

Bauman, G., Haider, M., Van der Heide, U. A. & Menard, C. (2013) Boosting imaging defined dominant prostatic tumors: a systematic review. *Radiother. Oncol.,* 107(3)**,** 274-81.

Baumann, M., Krause, M., Overgaard, J., Debus, J., Bentzen, S. M., et al. (2016) Radiation oncology in the era of precision medicine. *Nat. Rev. Cancer,* 16(4)**,** 234-249.

Baur, A. D., Maxeiner, A., Franiel, T., Kilic, E., Huppertz, A., et al. (2014) Evaluation of the prostate imaging reporting and data system for the detection of prostate cancer by the results of targeted biopsy of the prostate. *Invest. Radiol.,* 49(6)**,** 411-20.

Beard, C. J., Kijewski, P., Bussiere, M., Gelman, R., Gladstone, D., et al. (1996) Analysis of prostate and seminal vesicle motion: implications for treatment planning. *International journal of radiation oncology, biology, physics,* 34(2)**,** 451-8.

Beckendorf, V., Guerif, S., Le Prise, E., Cosset, J. M., Lefloch, O., et al. (2004) The GETUG 70 Gy vs. 80 Gy randomized trial for localized prostate cancer: feasibility and acute toxicity. *International journal of radiation oncology, biology, physics,* 60(4)**,** 1056-65.

Beltran, C., Herman, M. G. & Davis, B. J. (2008) Planning target margin calculations for prostate radiotherapy based on intrafraction and interfraction motion using four localization methods. *International journal of radiation oncology, biology, physics,* 70(1)**,** 289-95.

Bender, R. & Lange, S. (1999) Multiple test procedures other than Bonferroni's deserve wider use. *Bmj,* 318(7183)**,** 600-1.

Besl, P. & McKay, D. (1992) A Method for Registration of 3-D Shapes. *IEEE Transactions on Pattern analysis and machine intelligence,* 14(2)**,** 239-255.

Bian, S. X., Kuban, D. A., Levy, L. B., Oh, J., Castle, K. O., et al. (2012) Addition of short-term androgen deprivation therapy to dose-escalated radiation therapy improves failure-free survival for select men with intermediate-risk prostate cancer. *Ann. Oncol.,* 23(9)**,** 2346-52.

Bill-Axelson, A., Holmberg, L., Ruutu, M., Garmo, H., Stark, J. R., et al. (2011) Radical prostatectomy versus watchful waiting in early prostate cancer. *The New England journal of medicine,* 364(18)**,** 1708-17.

Birkner, M., Yan, D., Alber, M., Liang, J. & Nusslin, F. (2003) Adapting inverse planning to patient and organ geometrical variation: algorithm and implementation. *Med Phys,* 30(10)**,** 2822-31.

Boda-Heggemann, J., Kohler, F., Wertz, H., Welzel, G., Riesenacker, N., et al. (2007) Fiducial-based quantification of prostate tilt using cone beam computer tomography (CBCT). *Radiother. Oncol.,* 85(2)**,** 247-50.

Bolla, M., Collette, L., Blank, L., Warde, P., Dubois, J. B., et al. (2002) Long-term results with immediate androgen suppression and external irradiation in patients with locally advanced prostate cancer (an EORTC study): a phase III randomised trial. *Lancet,* 360(9327)**,** 103-6.

Bolla, M., de Reijke, T. M., Van Tienhoven, G., Van den Bergh, A. C., Oddens, J., et al. (2009) Duration of androgen suppression in the treatment of prostate cancer. *The New England journal of medicine,* 360(24)**,** 2516-27.

Bolla, M., Maingon, P., Carrie, C., Villa, S., Kitsios, P., et al. (2016) Short Androgen Suppression and Radiation Dose Escalation for Intermediate- and High-Risk Localized Prostate Cancer: Results of EORTC Trial 22991. *J. Clin. Oncol.,* 34(15)**,** 1748-56.

Bolla, M., van Poppel, H., Tombal, B., Vekemans, K., Da Pozzo, L., et al. (2012) Postoperative radiotherapy after radical prostatectomy for high-risk prostate cancer: long-term results of a randomised controlled trial (EORTC trial 22911). *Lancet,* 380(9858)**,** 2018-27.

Boorjian, S. A., Karnes, R. J., Rangel, L. J., Bergstralh, E. J. & Blute, M. L. (2008) Mayo Clinic validation of the D'amico risk group classification for predicting survival following radical prostatectomy. *The Journal of urology,* 179(4)**,** 1354-60; discussion 1360-1.

Boorjian, S. A., Karnes, R. J., Viterbo, R., Rangel, L. J., Bergstralh, E. J., et al. (2011) Long-term survival after radical prostatectomy versus external-beam radiotherapy for patients with high-risk prostate cancer. *Cancer,* 117(13)**,** 2883-2891.

Borren, A., Moman, M. R., Groenendaal, G., Boeken Kruger, A. E., van Diest, P. J., et al. (2013) Why prostate tumour delineation based on apparent diffusion coefficient is challenging: an exploration of the tissue microanatomy. *Acta Oncol.,* 52(8)**,** 1629-36.

Bostrom, P. J., Bjartell, A. S., Catto, J. W., Eggener, S. E., Lilja, H., et al. (2015) Genomic Predictors of Outcome in Prostate Cancer. *European urology*.

Boutros, P. C., Fraser, M., Harding, N. J., de Borja, R., Trudel, D., et al. (2015) Spatial genomic heterogeneity within localized, multifocal prostate cancer. *Nat Genet,* 47(7)**,** 736-45.

Boye, D., Lomax, T. & Knopf, A. (2013) Mapping motion from 4D-MRI to 3D-CT for use in 4D dose calculations: a technical feasibility study. *Med Phys,* 40(6)**,** 061702.

Bray, F., Lortet-Tieulent, J., Ferlay, J., Forman, D. & Auvinen, A. (2010) Prostate cancer incidence and mortality trends in 37 European countries: an overview. *Eur J Cancer,* 46(17)**,** 3040-52.

Brenner, D. J. (2004) Fractionation and late rectal toxicity. *Int. J. Radiat. Oncol. Biol. Phys.,* 60(4)**,** 1013-5.

Brenner, D. J., Martinez, A. A., Edmundson, G. K., Mitchell, C., Thames, H. D., et al. (2002) Direct evidence that prostate tumors show high sensitivity to fractionation (low alpha/beta ratio), similar to late-responding normal tissue. *Int. J. Radiat. Oncol. Biol. Phys.,* 52(1)**,** 6-13.

Briganti, A., Karnes, R. J., Joniau, S., Boorjian, S. A., Cozzarini, C., et al. (2014) Prediction of Outcome Following Early Salvage Radiotherapy Among Patients with Biochemical Recurrence After Radical Prostatectomy. *European urology,* 66(3)**,** 479-486.

Brock, K. K., Ménard, C., Hensel, J. & Jaffray, D. A. (Year) A multi-organ biomechanical model to analyze prostate deformation due to large deformation of the rectum. *In*, 2006. 614312-614312-10.

Budiharto, T., Slagmolen, P., Hermans, J., Maes, F., Verstraete, J., et al. (2009) A semi-automated 2D/3D marker-based registration algorithm modelling prostate shrinkage during radiotherapy for prostate cancer. *Radiother Oncol,* 90(3)**,** 331-6.

Bullock, M. J., Srigley, J. R., Klotz, L. H. & Goldenberg, S. L. (2002) Pathologic effects of neoadjuvant cyproterone acetate on nonneoplastic prostate, prostatic intraepithelial neoplasia, and adenocarcinoma: a detailed analysis of radical prostatectomy specimens from a randomized trial. *The American journal of surgical pathology,* 26(11)**,** 1400-13.

Butler, W. M., Merrick, G. S., Reed, J. L., Murray, B. C. & Kurko, B. S. (2013) Intrafraction displacement of prone versus supine prostate positioning monitored by real-time electromagnetic tracking. *Journal of applied clinical medical physics / American College of Medical Physics,* 14(2)**,** 4141.

Bylund, K. C., Bayouth, J. E., Smith, M. C., Hass, A. C., Bhatia, S. K., et al. (2008) Analysis of interfraction prostate motion using megavoltage cone beam computed tomography. *International journal of radiation oncology, biology, physics,* 72(3)**,** 949-56.

Byrne, T. E. (2005) A review of prostate motion with considerations for the treatment of prostate cancer. *Med Dosim,* 30(3)**,** 155-61.

Caldwell, C. B., Mah, K., Ung, Y. C., Danjoux, C. E., Balogh, J. M., et al. (2001) Observer variation in contouring gross tumor volume in patients with poorly defined non-small-cell lung tumors on CT: The impact of 18FDG-hybrid PET fusion. *International Journal of Radiation Oncology Biology Physics,* 51(4)**,** 923-931.

Cancer, N. C. C. f. (2014) *Prostate Cancer- Diagnosis and treatment* [Online]. Available: https://www.nice.org.uk/guidance/cg175/evidence/full-guideline-191710765 [Accessed 19/6/16 2016].

Capitanio, U., Briganti, A., Gallina, A., Suardi, N., Karakiewicz, P. I., et al. (2010) Predictive models before and after radical prostatectomy. *The Prostate,* 70(12)**,** 1371-8.

Carrie, C., Hasbini, A., de Laroche, G., Richaud, P., Guerif, S., et al. Salvage radiotherapy with or without short-term hormone therapy for rising prostate-specific antigen concentration after radical prostatectomy (GETUG-AFU 16): a randomised, multicentre, open-label phase 3 trial. *The Lancet Oncology*.

Castle, K. O., Hoffman, K. E., Levy, L. B., Lee, A. K., Choi, S., et al. (2013) Is androgen deprivation therapy necessary in all intermediate-risk prostate cancer patients treated in the dose escalation era? *International journal of radiation oncology, biology, physics,* 85(3)**,** 693-9.

Catton, C. & Alasti, H. (2016) *Prostate Delineation During Radiation Treatment Planning for Prostate Cancer: Comparison of High Quality Volume Computerized Tomography with Conventional Tomography and Magnetic Resonance Imaging* [Online]. Available: https://clinicaltrials.gov/ct2/show/NCT01878773 [Accessed 12th March 2016].

Cazzaniga, L. F., Marinoni, M. A., Bossi, A., Bianchi, E., Cagna, E., et al. (1998a) Interphysician variability in defining the planning target volume in the irradiation of prostate and seminal vesicles. *Radiotherapy and Oncology,* 47(3)**,** 293-296.

Cazzaniga, L. F., Marinoni, M. A., Bossi, A., Bianchi, E., Cagna, E., et al. (1998b) Interphysician variability in defining the planning target volume in the irradiation of prostate and seminal vesicles. *Radiother Oncol,* 47(3)**,** 293-6.

Cellini, N., Morganti, A. G., Mattiucci, G. C., Valentini, V., Leone, M., et al. (2002a) Analysis of intraprostatic failures in patients treated with hormonal therapy and radiotherapy: implications for conformal therapy planning. *Int. J. Radiat. Oncol. Biol. Phys.,* 53(3)**,** 595-9.

Cellini, N., Morganti, A. G., Mattiucci, G. C., Valentini, V., Leone, M., et al. (2002b) Analysis of intraprostatic failures in patients treated with hormonal therapy and radiotherapy: implications for conformal therapy planning. *International Journal of Radiation Oncology*Biology*Physics,* 53(3)**,** 595-599.

Chang, D. T., Challacombe, B. & Lawrentschuk, N. (2013) Transperineal biopsy of the prostate--is this the future? *Nat Rev Urol,* 10(12)**,** 690-702.

Chapman , P. B., Hauschild , A., Robert , C., Haanen , J. B., Ascierto , P., et al. (2011) Improved Survival with Vemurafenib in Melanoma with BRAF V600E Mutation. *N. Engl. J. Med.,* 364(26)**,** 2507-2516.

Charnley, N., Morgan, A., Thomas, E., Wilson, S., Bacon, S., et al. (2005) The use of CT-MR image registration to define target volumes in pelvic radiotherapy in the presence of bilateral hip replacements. *Br J Radiol,* 78(931)**,** 634-6.

Chavaudra, J. & Bridier, A. (2001) [Definition of volumes in external radiotherapy: ICRU reports 50 and 62]. *Cancer radiotherapie : journal de la Societe francaise de radiotherapie oncologique,* 5(5)**,** 472-8.

Chen, Y., Bielajew, A. F., Litzenberg, D. W., Moran, J. M. & Becchetti, F. D. (2005) Magnetic confinement of electron and photon radiotherapy dose: a Monte Carlo simulation with a nonuniform longitudinal magnetic field. *Med Phys,* 32(12)**,** 3810-8.

Choi, Y., Kwak, D. W., Lee, H. S., Hur, W. J., Cho, W. Y., et al. (2015) Effect of rectal enema on intrafraction prostate movement during image-guided radiotherapy. *Journal of medical imaging and radiation oncology,* 59(2)**,** 236-42.

Chung, P. & Menard, C. (2012) *Tumour TARGET prostate cancer* [Online]. Available: https://clinicaltrials.gov/ct2/show/NCT01802242 [Accessed 25th April 2016].

Chung, P. & Menard, C. (2016) *Tumor TARGET Prostate Cancer* [Online]. Available: https://clinicaltrials.gov/ct2/show/NCT01802242 [Accessed 8th June 2016].

Ciezki, J. P., Klein, E. A., Angermeier, K., Ulchaker, J., Chehade, N., et al. (2004) A retrospective comparison of androgen deprivation (AD) vs. no AD among low-risk and intermediate-risk prostate cancer patients treated with brachytherapy, external beam radiotherapy, or radical prostatectomy. *International journal of radiation oncology, biology, physics,* 60(5)**,** 1347-50.

Cookson, M. S., Aus, G., Burnett, A. L., Canby-Hagino, E. D., D'Amico, A. V., et al. (2007) Variation in the definition of biochemical recurrence in patients treated for localized prostate cancer: the American Urological Association Prostate Guidelines for Localized Prostate Cancer Update Panel report and recommendations for a standard in the reporting of surgical outcomes. *The Journal of urology,* 177(2)**,** 540-5.

Court, L. E., Dong, L., Lee, A. K., Cheung, R., Bonnen, M. D., et al. (2005) An automatic CT-guided adaptive radiation therapy technique by online modification of multileaf collimator leaf positions for prostate cancer. *International journal of radiation oncology, biology, physics,* 62(1)**,** 154-63.

Cox, J. A., Zagoria, R. J. & Raben, M. (1994) Prostate cancer: Comparison of retrograde urethrography and computed tomography in radiotherapy planning. *International Journal of Radiation Oncology Biology Physics,* 29(5)**,** 1119-1123.

Cox, J. D., Stetz, J. & Pajak, T. F. (1995) Toxicity criteria of the Radiation Therapy Oncology Group (RTOG) and the European Organization for Research and Treatment of Cancer (EORTC). *International journal of radiation oncology, biology, physics,* 31(5)**,** 1341-6.

Cramer, A. K., Haile, A. G., Ognjenovic, S., Doshi, T. S., Reilly, W. M., et al. (2013) Real-time prostate motion assessment: image-guidance and the temporal dependence of intra-fraction motion. *BMC medical physics,* 13(1)**,** 4.

Creak, A., Hall, E., Horwich, A., Eeles, R., Khoo, V., et al. (2013) Randomised pilot study of dose escalation using conformal radiotherapy in prostate cancer: long-term follow-up. *Br. J. Cancer,* 109(3)**,** 651-7.

Crook, J., Borg, J., Evans, A., Toi, A., Saibishkumar, E. P., et al. (2011) 10-year experience with I-125 prostate brachytherapy at the Princess Margaret Hospital: results for 1,100 patients. *International journal of radiation oncology, biology, physics,* 80(5)**,** 1323-9.

Crook, J., Ots, A., Gaztañaga, M., Schmid, M., Araujo, C., et al. (2014) Ultrasound-planned high-dose-rate prostate brachytherapy: Dose painting to the dominant intraprostatic lesion. *Brachytherapy,* 13(5)**,** 433-441.

Crook, J. M., Raymond, Y., Salhani, D., Yang, H. & Esche, B. (1995) Prostate motion during standard radiotherapy as assessed by fiducial markers. *Radiother Oncol,* 37(1)**,** 35-42.

CRUK. (2016) *Average Number of new cases per year and Age-Specific Incidence Rates, Males, UK, 2011-2013* [Online]. Available: http://www.cancerresearchuk.org/health-professional/cancer-statistics/statistics-by-cancer-type/prostate-cancer/incidence#heading-One [Accessed 1st December 2014].

CRUK. & UK, N. C. I. N. a. C. R. (2009) Cancer Incidence and Survival by Major Ethnic Group. England 2002-2006.

Crum, W. R., Camara, O. & Hill, D. L. G. (2006) Generalized Overlap Measures for Evaluation and Validation in Medical Image Analysis. *IEEE Trans. Med. Imaging,* 25(11)**,** 1451-1461.

Curtis, W., Khan, M., Magnelli, A., Stephans, K., Tendulkar, R., et al. (2013) Relationship of imaging frequency and planning margin to account for intrafraction prostate motion: analysis based on real-time monitoring data. *International journal of radiation oncology, biology, physics,* 85(3)**,** 700-6.

Cyran, C. C., Paprottka, P. M., Schwarz, B., Sourbron, S., Ingrisch, M., et al. (2012) Perfusion MRI for monitoring the effect of sorafenib on experimental prostate carcinoma: a validation study. *AJR Am J Roentgenol,* 198(2)**,** 384-91.

D'Amico, A. V., Chen, M. H., Renshaw, A. A., Loffredo, M. & Kantoff, P. W. (2008) Androgen suppression and radiation vs radiation alone for prostate cancer: a randomized trial. *JAMA,* 299(3)**,** 289-95.

D'Amico, A. V., Whittington, R., Malkowicz, S. & et al. (1998) BIochemical outcome after radical prostatectomy, external beam radiation therapy, or interstitial radiation therapy for clinically localized prostate cancer. *JAMA,* 280(11)**,** 969-974.

Daly, P. E., Dunne, M. T., O'Shea, C. M., Finn, M. A. & Armstrong, J. G. (2012) The effect of short term neo-adjuvant androgen deprivation on erectile function in patients treated with external beam radiotherapy for localised prostate cancer: an analysis of the 4- versus 8-month randomised trial (Irish Clinical Oncology Research Group 97-01). *Radiother Oncol,* 104(1)**,** 96-102.

Dawson, L. A., Mah, K., Franssen, E. & Morton, G. (1998) Target position variability throughout prostate radiotherapy. *Int. J. Radiat. Oncol. Biol. Phys.,* 42(5)**,** 1155-61.

de Boer, H. C., van Os, M. J., Jansen, P. P. & Heijmen, B. J. (2005) Application of the No Action Level (NAL) protocol to correct for prostate motion based on electronic portal imaging of implanted markers. *International journal of radiation oncology, biology, physics,* 61(4)**,** 969-83.

de Boer, J., Wolf, A. L., Szeto, Y. Z., van Herk, M. & Sonke, J. J. (2015) Dynamic collimator angle adjustments during volumetric modulated arc therapy to account for prostate rotations. *Int. J. Radiat. Oncol. Biol. Phys.,* 91(5)**,** 1009-16.

de Crevoisier, R., Tucker, S. L., Dong, L., Mohan, R., Cheung, R., et al. (2005) Increased risk of biochemical and local failure in patients with distended rectum on the planning CT for prostate cancer radiotherapy. *Int. J. Radiat. Oncol. Biol. Phys.,* 62(4)**,** 965-73.

De Meerleer, G., Villeirs, G., Bral, S., Paelinck, L., De Gersem, W., et al. (2005) The magnetic resonance detected intraprostatic lesion in prostate cancer: planning and delivery of intensity-modulated radiotherapy. *Radiother. Oncol.,* 75(3)**,** 325-33.

de Rooij, M., Hamoen, E. H., Futterer, J. J., Barentsz, J. O. & Rovers, M. M. (2014a) Accuracy of multiparametric MRI for prostate cancer detection: a meta-analysis. *AJR Am. J. Roentgenol.,* 202(2)**,** 343-51.

de Rooij, M., Hamoen, E. H. J., Fütterer, J. J., Barentsz, J. O. & Rovers, M. M. (2014b) Accuracy of Multiparametric MRI for Prostate Cancer Detection: A Meta-Analysis. *American Journal of Roentgenology,* 202(2)**,** 343-351.

Dearnaley, D., Syndikus, I., Sumo, G., Bidmead, M., Bloomfield, D., et al. (2012) Conventional versus hypofractionated high-dose intensity-modulated radiotherapy for prostate cancer: preliminary safety results from the CHHiP randomised controlled trial. *The Lancet. Oncology,* 13(1)**,** 43-54.

Dearnaley, D. P. (2015) Hypofractionated radiotherapy in prostate cancer. *Lancet Oncol.,* 16(3)**,** 237-8.

Dearnaley, D. P., Jovic, G., Syndikus, I., Khoo, V., Cowan, R. A., et al. (2014) Escalated-dose versus control-dose conformal radiotherapy for prostate cancer: long-term results from the MRC RT01 randomised controlled trial. *The Lancet Oncology,* 15(4)**,** 464-473.

Dearnaley, D. P., Khoo, V. S., Norman, A. R., Meyer, L., Nahum, A., et al. (1999) Comparison of radiation side-effects of conformal and conventional radiotherapy in prostate cancer: a randomised trial. *The Lancet,* 353(9149)**,** 267-272.

Debois, M., Oyen, R., Maes, F., Verswijvel, G., Gatti, G., et al. (1999) The contribution of magnetic resonance imaging to the three-dimensional treatment planning of localized prostate cancer. *Int. J. Radiat. Oncol. Biol. Phys.,* 45(4)**,** 857-65.

Decensi, A., Torrisi, R., Fontana, V., Marroni, P., Padovani, P., et al. (1993) Long-term endocrine effects of administration of either a non-steroidal antiandrogen or a luteinizing hormone-releasing hormone agonist in men with prostate cancer. *Acta endocrinologica,* 129(4)**,** 315-21.

Decker, G., Murtz, P., Gieseke, J., Traber, F., Block, W., et al. (2014) Intensity-modulated radiotherapy of the prostate: dynamic ADC monitoring by DWI at 3.0 T. *Radiother Oncol,* 113(1)**,** 115-20.

Decker, G., Mürtz, P., Gieseke, J., Träber, F., Block, W., et al. Intensity-modulated radiotherapy of the prostate: Dynamic ADC monitoring by DWI at 3.0 T. *Radiotherapy and Oncology,* (0).

Delongchamps, N. B., Escourou, C. & Cornud, F. (2015a) Integrated US-MR fusion images and MR targeted biopsies. What are their role and value in the detection and follow-up of prostate cancer. *Arch Esp Urol,* 68(3)**,** 349-53.

Delongchamps, N. B., Lefevre, A., Bouazza, N., Beuvon, F., Legman, P., et al. (2015b) Detection of significant prostate cancer with magnetic resonance targeted biopsies--should transrectal ultrasound-magnetic resonance imaging fusion guided biopsies alone be a standard of care? *The Journal of urology,* 193(4)**,** 1198-204.

Delongchamps, N. B., Peyromaure, M., Schull, A., Beuvon, F., Bouazza, N., et al. (2013) Prebiopsy magnetic resonance imaging and prostate cancer detection: comparison of random and targeted biopsies. *J. Urol.,* 189(2)**,** 493-9.

Delongchamps, N. B., Rouanne, M., Flam, T., Beuvon, F., Liberatore, M., et al. (2011) Multiparametric magnetic resonance imaging for the detection and localization of prostate cancer: combination of T2-weighted, dynamic contrast-enhanced and diffusion-weighted imaging. *BJU Int.,* 107(9)**,** 1411-8.

Delouya, G., Carrier, J. F., Beliveau-Nadeau, D., Donath, D. & Taussky, D. (2010) Migration of intraprostatic fiducial markers and its influence on the matching quality in external beam radiation therapy for prostate cancer. *Radiother. Oncol.,* 96(1)**,** 43-7.

Denham, J. W., Steigler, A., Joseph, D., Lamb, D. S., Spry, N. A., et al. (2015) Radiation dose escalation or longer androgen suppression for locally advanced prostate cancer? Data from the TROG 03.04 RADAR trial. *Radiother. Oncol.,* 115(3)**,** 301-307.

Deurloo, K. E., Steenbakkers, R. J., Zijp, L. J., de Bois, J. A., Nowak, P. J., et al. (2005) Quantification of shape variation of prostate and seminal vesicles during external beam radiotherapy. *International journal of radiation oncology, biology, physics,* 61(1)**,** 228-38.

Dewhirst, M. W. & Chi, J. T. (2013) Understanding the tumor microenvironment and radioresistance by combining functional imaging with global gene expression. *Semin. Radiat. Oncol.,* 23(4)**,** 296-305.

Dickinson, L., Ahmed, H. U., Allen, C., Barentsz, J. O., Carey, B., et al. (2011) Magnetic resonance imaging for the detection, localisation, and characterisation of prostate cancer: recommendations from a European consensus meeting. *Eur. Urol.,* 59(4)**,** 477-94.

Dinkel, J., Thieke, C., Plathow, C., Zamecnik, P., Prum, H., et al. (2011) Respiratory-induced prostate motion: characterization and quantification in dynamic MRI. *Strahlenther. Onkol.,* 187(7)**,** 426-32.

Disler, D. G., Marr, D. S. & Rosentahl, D. I. (1994) Accuracy of volume measurements of computed tomography and magnetic resonance imaging phantoms by three-dimensional reconstruction and preliminary clinical application. *Investigative radiology,* 29(8)**,** 739-745.

Djavan, B. O. B., Ravery, V., Zlotta, A., Dobronski, P., Dobrovits, M., et al. (2001) PROSPECTIVE EVALUATION OF PROSTATE CANCER DETECTED ON BIOPSIES 1, 2, 3 AND 4: WHEN SHOULD WE STOP? *The Journal of urology,* 166(5)**,** 1679-1683.

Dowling, J. A., Lambert, J., Parker, J., Salvado, O., Fripp, J., et al. (2012) An atlas-based electron density mapping method for magnetic resonance imaging (MRI)-alone treatment planning and adaptive MRI-based prostate radiation therapy. *International journal of radiation oncology, biology, physics,* 83(1)**,** e5-11.

dubray, B. M., Beckendorf, V. & Guerif S, e. a. (2011a) Does short-term androgen depletion add to high-dose radiotherapy (80 Gy) in localized intermediate-risk prostate cancer-Intermediary analysis of GETUG 14 randomized trial. *J. Clin. Oncol.,* 29(suppl)**,** 4521.

Dubray, B. M., Beckendorf, V., Guerif, S., Le Prise, E., Reynaud-Bougnoux, A., et al. (2011b) Does short term androgen depletion add to high-dose radiotherapy (80 Gy) in localized intermediate-risk prostate cancer: intermediary analysisi of GETUG 14 randomized trial (EU-20503/NCT00104741). *Journal of Clinical Oncology,* 29 (suppl)**,** 4521.

Eade, T. N., Hanlon, A. L., Horwitz, E. M., Buyyounouski, M. K., Hanks, G. E., et al. (2007) What dose of external-beam radiation is high enough for prostate cancer? *International journal of radiation oncology, biology, physics,* 68(3)**,** 682-9.

Eccles, C. L., Haider, E. A., Haider, M. A., Fung, S., Lockwood, G., et al. (2009) Change in diffusion weighted MRI during liver cancer radiotherapy: preliminary observations. *Acta Oncol.,* 48(7)**,** 1034-43.

Edge, S. B., DR; Compton, CC; Fitz, AG; Greene, FL; Trotti, A. (2010) *AJCC Cancer Staging Manual* (7th Edition ed.). New York, NY: Springer.

Eeles, R., Goh, C., Castro, E., Bancroft, E., Guy, M., et al. (2014) The genetic epidemiology of prostate cancer and its clinical implications. *Nat Rev Urol,* 11(1)**,** 18-31.

Eifler, J. B., Feng, Z., Lin, B. M., Partin, M. T., Humphreys, E. B., et al. (2013a) An updated prostate cancer staging nomogram (Partin tables) based on cases from 2006 to 2011. *BJU international,* 111(1)**,** 22-9.

Eifler, J. B., Feng, Z., Lin, B. M., Partin, M. T., Humphreys, E. B., et al. (2013b) An updated prostate cancer staging nomogram (Partin tables) based on cases from 2006 to 2011. *BJU international,* 111(1)**,** 22-29.

Ellis, J. H., Tempany, C., Sarin, M. S., Gatsonis, C., Rifkin, M. D., et al. (1994) MR imaging and sonography of early prostatic cancer: pathologic and imaging features that influence identification and diagnosis. *AJR Am J Roentgenol,* 162(4)**,** 865-72.

Endlich, B., Radford, I. R., Forrester, H. B. & Dewey, W. C. (2000) Computerized video time-lapse microscopy studies of ionizing radiation-induced rapid-interphase and mitosis-related apoptosis in lymphoid cells. *Radiat. Res.,* 153(1)**,** 36-48.

Engels, B., Soete, G., Verellen, D. & Storme, G. (2009a) Conformal Arc Radiotherapy for Prostate Cancer: Increased Biochemical Failure in Patients With Distended Rectum on the Planning Computed Tomogram Despite Image Guidance by Implanted Markers. *International Journal of Radiation Oncology*Biology*Physics,* 74(2)**,** 388-391.

Engels, B., Tournel, K., Soete, G. & Storme, G. (2009b) Assessment of rectal distention in radiotherapy of prostate cancer using daily megavoltage CT image guidance. *Radiother Oncol,* 90(3)**,** 377-81.

Epstein, J. I., Walsh, P. C., Carmichael, M. & Brendler, C. B. (1994) Pathologic and clinical findings to predict tumor extent of nonpalpable (stage T1c) prostate cancer. *Jama,* 271(5)**,** 368-74.

Fayers, P., Aaronson, N., Bjordal, K., Groenvold, M., Curran, D., et al. (2001) *EORTC QLQ-C30 Scoring Manual (3rd edition)* [Online]. Brussels: EORTC. [Accessed].

Fichtinger, G., Burdette, E. C., Tanacs, A., Patriciu, A., Mazilu, D., et al. (2006) Robotically assisted prostate brachytherapy with transrectal ultrasound guidance--Phantom experiments. *Brachytherapy,* 5(1)**,** 14-26.

Fine, J. P. & Gray, R. J. (1999) A proportional hazards model for the sub-distribution of a competing risk. *Journal of the American Statistical Association,* 94(446)**,** 496-509.

Fine, S. W., Amin, M. B., Berney, D. M., Bjartell, A., Egevad, L., et al. (2012) A contemporary update on pathology reporting for prostate cancer: biopsy and radical prostatectomy specimens. *Eur. Urol.,* 62(1)**,** 20-39.

Fiorino, C., Di Muzio, N., Broggi, S., Cozzarini, C., Maggiulli, E., et al. (2008) Evidence of limited motion of the prostate by carefully emptying the rectum as assessed by daily MVCT image guidance with helical tomotherapy. *International journal of radiation oncology, biology, physics,* 71(2)**,** 611-7.

Fiorino, C., Reni, M., Bolognesi, A., Cattaneo, G. M. & Calandrino, R. (1998a) Intra- and inter-observer variability in contouring prostate and seminal vesicles: implications for conformal treatment planning. *Radiother Oncol,* 47(3)**,** 285-92.

Fiorino, C., Reni, M., Bolognesi, A., Cattaneo, G. M. & Calandrino, R. (1998b) Intra- and inter-observer variability in contouring prostate and seminal vesicles: Implications for conformal treatment planning. *Radiotherapy and Oncology,* 47(3)**,** 285-292.

Fleshner, N. E., O'Sullivan, M., Premdass, C. & Fair, W. R. (1999) Clinical significance of small (less than 0.2 cm3) hypoechoic lesions in men with normal digital rectal examinations and prostate-specific antigen levels less than 10 ng/mL. *Urology,* 53(2)**,** 356-8.

Foltz, W. D., Wu, A., Chung, P., Catton, C., Bayley, A., et al. (2013) Changes in apparent diffusion coefficient and T2 relaxation during radiotherapy for prostate cancer. *J. Magn. Reson. Imaging,* 37(4)**,** 909-16.

Fonteyne, V., Villeirs, G., Speleers, B., De Neve, W., De Wagter, C., et al. (2008) Intensity-Modulated Radiotherapy as Primary Therapy for Prostate Cancer: Report on Acute Toxicity After Dose Escalation With Simultaneous Integrated Boost to Intraprostatic Lesion. *International Journal of Radiation Oncology*Biology*Physics,* 72(3)**,** 799-807.

Fowler, J. F., Toma-Dasu, I. & Dasu, A. (2013) Is the alpha/beta ratio for prostate tumours really low and does it vary with the level of risk at diagnosis? *Anticancer Res.,* 33(3)**,** 1009-11.

Franiel, T., Ludemann, L., Taupitz, M., Bohmer, D. & Beyersdorff, D. (2009) MRI before and after external beam intensity-modulated radiotherapy of patients with prostate cancer: the feasibility of monitoring of radiation-induced tissue changes using a dynamic contrast-enhanced inversion-prepared dual-contrast gradient echo sequence. *Radiother Oncol,* 93(2)**,** 241-5.

Frank, S. J., Dong, L., Kudchadker, R. J., De Crevoisier, R., Lee, A. K., et al. (2008) Quantification of prostate and seminal vesicle interfraction variation during IMRT. *Int. J. Radiat. Oncol. Biol. Phys.,* 71(3)**,** 813-20.

Frank, S. J., Kudchadker, R. J., Kuban, D. A., De Crevoisier, R., Lee, A. K., et al. (2010) A volumetric trend analysis of the prostate and seminal vesicles during a course of intensity-modulated radiation therapy. *Am. J. Clin. Oncol.,* 33(2)**,** 173-5.

Freedland, S. J., Aronson, W. J., Terris, M. K., Kane, C. J., Amling, C. L., et al. (2003) The percentage of prostate needle biopsy cores with carcinoma from the more involved side of the biopsy as a predictor of prostate specific antigen recurrence after radical prostatectomy: results from the Shared Equal Access Regional Cancer Hospital (SEARCH) database. *Cancer,* 98(11)**,** 2344-50.

Futterer, J. J., Briganti, A., De Visschere, P., Emberton, M., Giannarini, G., et al. (2015) Can Clinically Significant Prostate Cancer Be Detected with Multiparametric Magnetic Resonance Imaging? A Systematic Review of the Literature. *Eur. Urol.,* 68(6)**,** 1045-53.

Gao, Z., Wilkins, D., Eapen, L., Morash, C., Wassef, Y., et al. (2007) A study of prostate delineation referenced against a gold standard created from the visible human data. *Radiotherapy and Oncology,* 85(2)**,** 239-246.

Garon, E. B., Rizvi, N. A., Hui, R., Leighl, N., Balmanoukian, A. S., et al. (2015) Pembrolizumab for the Treatment of Non–Small-Cell Lung Cancer. *N. Engl. J. Med.,* 372(21)**,** 2018-2028.

Geets, X., Daisne, J.-F., Arcangeli, S., Coche, E., Poel, M. D., et al. (2005) Inter-observer variability in the delineation of pharyngo-laryngeal tumor, parotid glands and cervical spinal cord: Comparison between CT-scan and MRI. *Radiotherapy and Oncology,* 77(1)**,** 25-31.

Ghilezan, M., Yan, D. & Martinez, A. (2010) Adaptive radiation therapy for prostate cancer. *Semin Radiat Oncol,* 20(2)**,** 130-7.

Ghilezan, M. J., Jaffray, D. A., Siewerdsen, J. H., Van Herk, M., Shetty, A., et al. (2005) Prostate gland motion assessed with cine-magnetic resonance imaging (cine-MRI). *Int. J. Radiat. Oncol. Biol. Phys.,* 62(2)**,** 406-17.

Gibbs, P., Pickles, M. D. & Turnbull, L. W. (2007) Repeatability of echo-planar-based diffusion measurements of the human prostate at 3 T. *Magnetic resonance imaging,* 25(10)**,** 1423-9.

Gill, S., Dang, K., Fox, C., Bressel, M., Kron, T., et al. (2014) Seminal vesicle intrafraction motion analysed with cinematic magnetic resonance imaging. *Radiat. Oncol.,* 9**,** 174.

Giordano, S. H., Lee, A., Kuo, Y. F., Freeman, J. & Goodwin, J. S. (2006) Late gastrointestinal toxicity after radiation for prostate cancer. *Cancer,* 107(2)**,** 423-32.

Goldgar, D. E., Easton, D. F., Cannon-Albright, L. A. & Skolnick, M. H. (1994) Systematic population-based assessment of cancer risk in first-degree relatives of cancer probands. *Journal of the National Cancer Institute,* 86(21)**,** 1600-8.

Gomez-Iturriaga, A., Casquero, F., Urresola, A., Ezquerro, A., Lopez, J. I., et al. (2016) Dose escalation to dominant intraprostatic lesions with MRI-transrectal ultrasound fusion High-Dose-Rate prostate brachytherapy. Prospective phase II trial. *Radiother. Oncol.,* 119(1)**,** 91-6.

Gong, P., Zhang, T., He, D. & Hsieh, J. T. (2015) MicroRNA-145 Modulates Tumor Sensitivity to Radiation in Prostate Cancer. *Radiat Res,* 184(6)**,** 630-8.

Goto, Y., Ohori, M., Arakawa, A., Kattan, M. W., Wheeler, T. M., et al. (1996) Distinguishing clinically important from unimportant prostate cancers before treatment: value of systematic biopsies. *J. Urol.,* 156(3)**,** 1059-63.

Graham, J., Kirkbride, P., Cann, K., Hasler, E. & Prettyjohns, M. (2014) Prostate cancer: summary of updated NICE guidance. *Bmj,* 348**,** f7524.

Gray, R. J. (1988) A class of K-sample tests for comparing the cumulative incidence of competing risk. *Annals of Statistics,* 16(3)**,** 1141-1154.

Greer, P. B., Dowling, J. A., Lambert, J. A., Fripp, J., Parker, J., et al. (2011) A magnetic resonance imaging-based workflow for planning radiation therapy for prostate cancer. *The Medical journal of Australia,* 194(4)**,** S24-7.

Grey, A. D., Chana, M. S., Popert, R., Wolfe, K., Liyanage, S. H., et al. (2015) Diagnostic accuracy of magnetic resonance imaging (MRI) prostate imaging reporting and data system (PI-RADS) scoring in a transperineal prostate biopsy setting. *BJU Int.,* 115(5)**,** 728-35.

Grills, I. S., Martinez, A. A., Hollander, M., Huang, R., Goldman, K., et al. (2004) High dose rate brachytherapy as prostate cancer monotherapy reduces toxicity compared to low dose rate palladium seeds. *J. Urol.,* 171(3)**,** 1098-104.

Groenendaal, G., Borren, A., Moman, M. R., Monninkhof, E., van Diest, P. J., et al. (2012a) Pathologic validation of a model based on diffusion-weighted imaging and dynamic contrast-enhanced magnetic resonance imaging for tumor delineation in the prostate peripheral zone. *Int. J. Radiat. Oncol. Biol. Phys.,* 82(3)**,** e537-44.

Groenendaal, G., Moman, M. R., Korporaal, J. G., van Diest, P. J., van Vulpen, M., et al. (2010a) Validation of functional imaging with pathology for tumor delineation in the prostate. *Radiother. Oncol.,* 94(2)**,** 145-50.

Groenendaal, G., van den Berg, C. A., Korporaal, J. G., Philippens, M. E., Luijten, P. R., et al. (2010b) Simultaneous MRI diffusion and perfusion imaging for tumor delineation in prostate cancer patients. *Radiother. Oncol.,* 95(2)**,** 185-90.

Groenendaal, G., van Vulpen, M., Pereboom, S. R., Poelma-Tap, D., Korporaal, J. G., et al. (2012b) The effect of hormonal treatment on conspicuity of prostate cancer: implications for focal boosting radiotherapy. *Radiother. Oncol.,* 103(2)**,** 233-8.

Haas, G. P., Delongchamps, N., Brawley, O. W., Wang, C. Y. & de la Roza, G. (2008) The worldwide epidemiology of prostate cancer: perspectives from autopsy studies. *The Canadian journal of urology,* 15(1)**,** 3866-71.

Haider, M. A., van der Kwast, T. H., Tanguay, J., Evans, A. J., Hashmi, A. T., et al. (2007) Combined T2-weighted and diffusion-weighted MRI for localization of prostate cancer. *AJR Am J Roentgenol,* 189(2)**,** 323-8.

Hambrock, T., Hoeks, C., Hulsbergen-van de Kaa, C., Scheenen, T., Futterer, J., et al. (2012) Prospective assessment of prostate cancer aggressiveness using 3-T diffusion-weighted magnetic resonance imaging-guided biopsies versus a systematic 10-core transrectal ultrasound prostate biopsy cohort. *Eur. Urol.,* 61(1)**,** 177-84.

Hambrock, T., Somford, D. M., Huisman, H. J., van Oort, I. M., Witjes, J. A., et al. (2011) Relationship between Apparent Diffusion Coefficients at 3.0-T MR Imaging and Gleason Grade in Peripheral Zone Prostate Cancer. *Radiology,* 259(2)**,** 453-461.

Hamoen, E. H., de Rooij, M., Witjes, J. A., Barentsz, J. O. & Rovers, M. M. (2015) Use of the Prostate Imaging Reporting and Data System (PI-RADS) for Prostate Cancer Detection with Multiparametric Magnetic Resonance Imaging: A Diagnostic Meta-analysis. *Eur. Urol.,* 67(6)**,** 1112-21.

Hamstra, D. A., Chenevert, T. L., Moffat, B. A., Johnson, T. D., Meyer, C. R., et al. (2005) Evaluation of the functional diffusion map as an early biomarker of time-to-progression and overall survival in high-grade glioma. *Proceedings of the National Academy of Sciences of the United States of America,* 102(46)**,** 16759-64.

Hamstra, D. A., Galban, C. J., Meyer, C. R., Johnson, T. D., Sundgren, P. C., et al. (2008) Functional diffusion map as an early imaging biomarker for high-grade glioma: correlation with conventional radiologic response and overall survival. *J. Clin. Oncol.,* 26(20)**,** 3387-94.

Han, M., Kim, S. Y., Lee, S. J. & Choi, J. W. (2015) The Correlations Between MRI Perfusion, Diffusion Parameters, and 18F-FDG PET Metabolic Parameters in Primary Head-and-Neck Cancer: A Cross-Sectional Analysis in Single Institute. *Medicine (Baltimore),* 94(47)**,** e2141.

Hara, N., Okuizumi, M., Koike, H., Kawaguchi, M. & Bilim, V. (2005) Dynamic contrast-enhanced magnetic resonance imaging (DCE-MRI) is a useful modality for the precise detection and staging of early prostate cancer. *Prostate,* 62(2)**,** 140-7.

Harry, V. N., Semple, S. I., Gilbert, F. J. & Parkin, D. E. (2008) Diffusion-weighted magnetic resonance imaging in the early detection of response to chemoradiation in cervical cancer. *Gynecol. Oncol.,* 111(2)**,** 213-20.

Harvey, C. J., Blomley, M. J., Dawson, P., Morgan, J. A., Dooher, A., et al. (2001) Functional CT imaging of the acute hyperemic response to radiation therapy of the prostate gland: early experience. *J. Comput. Assist. Tomogr.,* 25(1)**,** 43-9.

Hashimoto, Y., Akimoto, T., Iizuka, J., Tanabe, K. & Mitsuhashi, N. (2015) Correlation between the changes in the EPIC QOL scores and the dose-volume histogram parameters in high-dose-rate brachytherapy combined with hypofractionated external beam radiation therapy for prostate cancer. *Jpn. J. Clin. Oncol.,* 45(1)**,** 81-7.

Hata, N., Jinzaki, M., Kacher, D., Cormak, R., Gering, D., et al. (2001) MR imaging-guided prostate biopsy with surgical navigation software: device validation and feasibility. *Radiology,* 220(1)**,** 263-8.

Heemsbergen, W. D., Al-Mamgani, A., Slot, A., Dielwart, M. F. H. & Lebesque, J. V. (2014) Long-term results of the Dutch randomized prostate cancer trial: Impact of dose-escalation on local, biochemical, clinical failure, and survival. *Radiotherapy and Oncology,* 110(1)**,** 104-109.

Heemsbergen, W. D., Hoogeman, M. S., Witte, M. G., Peeters, S. T., Incrocci, L., et al. (2007) Increased risk of biochemical and clinical failure for prostate patients with a large rectum at radiotherapy planning: results from the Dutch trial of 68 GY versus 78 Gy. *Int. J. Radiat. Oncol. Biol. Phys.,* 67(5)**,** 1418-24.

Heijmink, S. W., Scheenen, T. W., van Lin, E. N., Visser, A. G., Kiemeney, L. A., et al. (2009) Changes in prostate shape and volume and their implications for radiotherapy after introduction of endorectal balloon as determined by MRI at 3T. *Int. J. Radiat. Oncol. Biol. Phys.,* 73(5)**,** 1446-53.

Hensel, J. M., Menard, C., Chung, P. W., Milosevic, M. F., Kirilova, A., et al. (2007) Development of multiorgan finite element-based prostate deformation model enabling registration of endorectal coil magnetic resonance imaging for radiotherapy planning. *Int. J. Radiat. Oncol. Biol. Phys.,* 68(5)**,** 1522-8.

Hentschel, B., Oehler, W., Strauß, D., Ulrich, A. & Malich, A. (2011a) Definition of the CTV Prostate in CT and MRI by Using CT–MRI Image Fusion in IMRT Planning for Prostate Cancer. *Strahlentherapie und Onkologie : Organ der Deutschen Rontgengesellschaft ... [et al],* 187(3)**,** 183-190.

Hentschel, B., Oehler, W., Strauss, D., Ulrich, A. & Malich, A. (2011b) Definition of the CTV prostate in CT and MRI by using CT-MRI image fusion in IMRT planning for prostate cancer. *Strahlenther. Onkol.,* 187(3)**,** 183-90.

Hill, R. P., Bristow, R. G., Fyles, A., Koritzinsky, M., Milosevic, M., et al. (2015) Hypoxia and Predicting Radiation Response. *Semin Radiat Oncol,* 25(4)**,** 260-72.

Hindson, B. R., Millar, J. L. & Matheson, B. (2013) Urethral strictures following high-dose-rate brachytherapy for prostate cancer: analysis of risk factors. *Brachytherapy,* 12(1)**,** 50-5.

Hollmann, B. G., van Triest, B., Ghobadi, G., Groenendaal, G., de Jong, J., et al. (2015) Gross tumor volume and clinical target volume in prostate cancer: How do satellites relate to the index lesion. *Radiother. Oncol.,* 115(1)**,** 96-100.

Hoogeman, M. S., van Herk, M., de Bois, J. & Lebesque, J. V. (2005) Strategies to reduce the systematic error due to tumor and rectum motion in radiotherapy of prostate cancer. *Radiother. Oncol.,* 74(2)**,** 177-85.

Horwitz, E. M., Bae, K., Hanks, G. E., Porter, A., Grignon, D. J., et al. (2008) Ten-year follow-up of radiation therapy oncology group protocol 92-02: a phase III trial of the duration of elective androgen deprivation in locally advanced prostate cancer. *J. Clin. Oncol.,* 26(15)**,** 2497-504.

Hoskin, P. J., Rojas, A. M., Ostler, P. J., Hughes, R., Bryant, L., et al. (2014) Dosimetric predictors of biochemical control of prostate cancer in patients randomised to external beam radiotherapy with a boost of high dose rate brachytherapy. *Radiother. Oncol.,* 110(1)**,** 110-3.

Hotker, A. M., Mazaheri, Y., Zheng, J., Moskowitz, C. S., Berkowitz, J., et al. (2015) Prostate Cancer: assessing the effects of androgen-deprivation therapy using quantitative diffusion-weighted and dynamic contrast-enhanced MRI. *Eur. Radiol.,* 25(9)**,** 2665-72.

Housri, N., Ning, H., Ondos, J., Choyke, P., Camphausen, K., et al. (2011) Parameters favorable to intraprostatic radiation dose escalation in men with localized prostate cancer. *Int. J. Radiat. Oncol. Biol. Phys.,* 80(2)**,** 614-20.

Hoyt, K., Castaneda, B., Zhang, M., Nigwekar, P., di Sant'agnese, P. A., et al. (2008) Tissue elasticity properties as biomarkers for prostate cancer. *Cancer Biomark.,* 4(4-5)**,** 213-25.

Huang, C. Y., Tehrani, J. N., Ng, J. A., Booth, J. & Keall, P. (2015) Six degrees-of-freedom prostate and lung tumor motion measurements using kilovoltage intrafraction monitoring. *Int. J. Radiat. Oncol. Biol. Phys.,* 91(2)**,** 368-75.

Huang, E., Dong, L., Chandra, A., Kuban, D. A., Rosen, II, et al. (2002) Intrafraction prostate motion during IMRT for prostate cancer. *Int. J. Radiat. Oncol. Biol. Phys.,* 53(2)**,** 261-8.

Huisman, H. J., Futterer, J. J., van Lin, E. N., Welmers, A., Scheenen, T. W., et al. (2005) Prostate cancer: precision of integrating functional MR imaging with radiation therapy treatment by using fiducial gold markers. *Radiology,* 236(1)**,** 311-7.

Hurkmans, C. W., Borger, J. H., Pieters, B. R., Russell, N. S., Jansen, E. P. M., et al. (2001) Variability in target volume delineation on CT scans of the breast. *International Journal of Radiation Oncology Biology Physics,* 50(5)**,** 1366-1372.

Huttenlocher, D. P., Klanderman, G. A. & Rucklidge, W. J. (1993) Comparing images using the Hausdorff distance. *IEEE Transactions on Pattern Analysis and Machine Intelligence,* 15(9)**,** 850-863.

Ippolito, E., Mantini, G., Morganti, A. G., Mazzeo, E., Padula, G. D., et al. (2012) Intensity-modulated radiotherapy with simultaneous integrated boost to dominant intraprostatic lesion: preliminary report on toxicity. *Am. J. Clin. Oncol.,* 35(2)**,** 158-62.

Iraha, Y., Murayama, S., Kamiya, A., Iraha, S. & Ogawa, K. (2012) Diffusion-weighted MRI and PSA correlations in patients with prostate cancer treated with radiation and hormonal therapy. *Anticancer Res.,* 32(10)**,** 4467-71.

Isebaert, S., Van den Bergh, L., Haustermans, K., Joniau, S., Lerut, E., et al. (2013) Multiparametric MRI for prostate cancer localization in correlation to whole-mount histopathology. *J. Magn. Reson. Imaging,* 37(6)**,** 1392-401.

Issa, B. (2002) In vivo measurement of the apparent diffusion coefficient in normal and malignant prostatic tissues using echo-planar imaging. *Journal of magnetic resonance imaging : JMRI,* 16(2)**,** 196-200.

Iversen, P., Melezinek, I. & Schmidt, A. (2001) Nonsteroidal antiandrogens: a therapeutic option for patients with advanced prostate cancer who wish to retain sexual interest and function. *BJU Int.,* 87(1)**,** 47-56.

Iversen, P., Tyrrell, C. J., Kaisary, A. V., Anderson, J. B., Van Poppel, H., et al. (2000) Bicalutamide monotherapy compared with castration in patients with nonmetastatic locally advanced prostate cancer: 6.3 years of followup. *J. Urol.,* 164(5)**,** 1579-82.

Jackson, A. S., Reinsberg, S. A., Sohaib, S. A., Charles-Edwards, E. M., Mangar, S. A., et al. (2007a) Distortion-corrected T2 weighted MRI: a novel approach to prostate radiotherapy planning. *Br J Radiol,* 80(959)**,** 926-33.

Jackson, A. S. N., Reinsberg, S. A., Sohaib, S. A., Charles-Edwards, E. M., Mangar, S. A., et al. (2007b) Distortion-corrected T2 weighted MRI: a novel approach to prostate radiotherapy planning. *The British journal of radiology,* 80(959)**,** 926-933.

Jeldres, C., Suardi, N., Walz, J., Hutterer, G. C., Ahyai, S., et al. (2008) Validation of the Contemporary Epstein Criteria for Insignificant Prostate Cancer in European Men. *European urology,* 54(6)**,** 1306-1313.

Jemal, A., Bray, F., Center, M. M., Ferlay, J., Ward, E., et al. (2011) Global cancer statistics. *CA: a cancer journal for clinicians,* 61(2)**,** 69-90.

Jeong, C. W., Park, H. K., Hong, S. K., Byun, S. S., Lee, H. J., et al. (2008) Comparison of prostate volume measured by transrectal ultrasonography and MRI with the actual prostate volume measured after radical prostatectomy. *Urol. Int.,* 81(2)**,** 179-85.

Johnson, L. M., Turkbey, B., Figg, W. D. & Choyke, P. L. (2014) Multiparametric MRI in prostate cancer management. *Nature reviews. Clinical oncology,* 11(6)**,** 346-53.

Jones, C. U., Hunt, D., McGowan, D. G., Amin, M. B., Chetner, M. P., et al. (2011) Radiotherapy and short-term androgen deprivation for localized prostate cancer. *N. Engl. J. Med.,* 365(2)**,** 107-18.

Jonsson, J. H., Garpebring, A., Karlsson, M. G. & Nyholm, T. (2012) Internal fiducial markers and susceptibility effects in MRI-simulation and measurement of spatial accuracy. *Int. J. Radiat. Oncol. Biol. Phys.,* 82(5)**,** 1612-8.

Jonsson, J. H., Karlsson, M. G., Karlsson, M. & Nyholm, T. (2010) Treatment planning using MRI data: an analysis of the dose calculation accuracy for different treatment regions. *Radiat Oncol,* 5**,** 62.

Joseph, S., Moazami, N., Cupps, B. P., Howells, A., Craddock, H., et al. (2009a) Magnetic resonance imaging-based multiparametric systolic strain analysis and regional contractile heterogeneity in patients with dilated cardiomyopathy. *J. Heart Lung Transplant.,* 28(4)**,** 388-94.

Joseph, T., McKenna, D. A., Westphalen, A. C., Coakley, F. V., Zhao, S., et al. (2009b) Pretreatment endorectal magnetic resonance imaging and magnetic resonance spectroscopic imaging features of prostate cancer as predictors of response to external beam radiotherapy. *Int. J. Radiat. Oncol. Biol. Phys.,* 73(3)**,** 665-71.

Kagawa, K., Lee, W. R., Schultheiss, T. E., Hunt, M. A., Shaer, A. H., et al. (1997) Initial clinical assessment of CT-MRI image fusion software in localization of the prostate for 3D conformal radiation therapy. *Int. J. Radiat. Oncol. Biol. Phys.,* 38(2)**,** 319-25.

Kalbasi, A., Li, J., Berman, A., Swisher-McClure, S., Smaldone, M., et al. (2015) Dose-Escalated Irradiation and Overall Survival in Men With Nonmetastatic Prostate Cancer. *JAMA Oncol,* 1(7)**,** 897-906.

Kalbfleisch, J. D. & Prentice, R. L. (2002) *The statistical Analysis of Failure Time Data*: Wiley.

Karavitakis, M., Ahmed, H. U., Abel, P. D., Hazell, S. & Winkler, M. H. (2011) Tumor focality in prostate cancer: implications for focal therapy. *Nat. Rev. Clin. Oncol.,* 8(1)**,** 48-55.

Kasaova, L., Sirak, I., Jansa, J., Paluska, P. & Petera, J. (2011) Daily prostate volume and position monitoring using implanted gold markers and on-board imaging during radiotherapy. *Acta Medica (Hradec Kralove),* 54(4)**,** 149-52.

Kasivisvanathan, V., Dufour, R., Moore, C. M., Ahmed, H. U., Abd-Alazeez, M., et al. (2013) Transperineal magnetic resonance image targeted prostate biopsy versus transperineal template prostate biopsy in the detection of clinically significant prostate cancer. *J. Urol.,* 189(3)**,** 860-6.

Kattan, M. W., Zelefsky, M. J., Kupelian, P. A., Scardino, P. T., Fuks, Z., et al. (2000) Pretreatment nomogram for predicting the outcome of three-dimensional conformal radiotherapy in prostate cancer. *J. Clin. Oncol.,* 18(19)**,** 3352-9.

Kava, B. R. (2014) To treat or not to treat with testosterone replacement therapy: a contemporary review of management of late-onset hypogonadism and critical issues related to prostate cancer. *Current urology reports,* 15(7)**,** 422.

Keane, F. K., Chen, M. H., Zhang, D., Loffredo, M. J., Kantoff, P. W., et al. (2014) The likelihood of death from prostate cancer in men with favorable or unfavorable intermediate-risk disease. *Cancer,* 120(12)**,** 1787-93.

Kerkhof, E. M., van der Put, R. W., Raaymakers, B. W., van der Heide, U. A., van Vulpen, M., et al. (2008) Variation in target and rectum dose due to prostate deformation: an assessment by repeated MR imaging and treatment planning. *Phys. Med. Biol.,* 53(20)**,** 5623-34.

Kershaw, L. E., Hutchinson, C. E. & Buckley, D. L. (2009) Benign prostatic hyperplasia: evaluation of T1, T2, and microvascular characteristics with T1-weighted dynamic contrast-enhanced MRI. *Journal of magnetic resonance imaging : JMRI,* 29(3)**,** 641-8.

Kershaw, L. E., Logue, J. P., Hutchinson, C. E., Clarke, N. W. & Buckley, D. L. (2008) Late tissue effects following radiotherapy and neoadjuvant hormone therapy of the prostate measured with quantitative magnetic resonance imaging. *Radiother Oncol,* 88(1)**,** 127-34.

Kestin, L., Goldstein, N., Vicini, F., Yan, D., Korman, H., et al. (2002) Treatment of prostate cancer with radiotherapy: should the entire seminal vesicles be included in the clinical target volume? *Int. J. Radiat. Oncol. Biol. Phys.,* 54(3)**,** 686-97.

Khoo, E. L., Schick, K., Plank, A. W., Poulsen, M., Wong, W. W., et al. (2012) Prostate contouring variation: can it be fixed? *Int. J. Radiat. Oncol. Biol. Phys.,* 82(5)**,** 1923-9.

Khoo, V. S., Bedford, J. L., Padhani, A. R., Leach, M., Husband, J. E., et al. (2002) Prostate and rectal deformation assessed using cine magnetic resonance imaging (MRI) during a course of radical prostate radiotherapy. *Radiother. Oncol.,* 64(Sup1)**,** S285.

Kim, C. K., Park, B. K. & Kim, B. (2010) High-b-value diffusion-weighted imaging at 3 T to detect prostate cancer: comparisons between b values of 1,000 and 2,000 s/mm2. *AJR Am J Roentgenol,* 194(1)**,** W33-7.

Kim, H., Huq, M. S., Houser, C., Beriwal, S. & Michalski, D. (2014) Mapping of dose distribution from IMRT onto MRI-guided high dose rate brachytherapy using deformable image registration for cervical cancer treatments: preliminary study with commercially available software. *J Contemp Brachytherapy,* 6(2)**,** 178-84.

Kim, S., Loevner, L., Quon, H., Sherman, E., Weinstein, G., et al. (2009a) Diffusion-weighted magnetic resonance imaging for predicting and detecting early response to chemoradiation therapy of squamous cell carcinomas of the head and neck. *Clinical cancer research : an official journal of the American Association for Cancer Research,* 15(3)**,** 986-94.

Kim, S., Shen, S., Moore, D. F., Shih, W., Lin, Y., et al. (2011) Late gastrointestinal toxicities following radiation therapy for prostate cancer. *European urology,* 60(5)**,** 908-16.

Kim, S. H., Lee, J. M., Hong, S. H., Kim, G. H., Lee, J. Y., et al. (2009b) Locally advanced rectal cancer: added value of diffusion-weighted MR imaging in the evaluation of tumor response to neoadjuvant chemo- and radiation therapy. *Radiology,* 253(1)**,** 116-25.

King, C. R. & Long, J. P. (2000) Prostate biopsy grading errors: a sampling problem? *Int J Cancer,* 90(6)**,** 326-30.

Kirkham, A. P., Emberton, M. & Allen, C. (2006) How good is MRI at detecting and characterising cancer within the prostate? *Eur. Urol.,* 50(6)**,** 1163-74; discussion 1175.

Kitajima, K., Takahashi, S., Ueno, Y., Yoshikawa, T., Ohno, Y., et al. (2012) Clinical utility of apparent diffusion coefficient values obtained using high b-value when diagnosing prostate cancer using 3 tesla MRI: comparison between ultra-high b-value (2000 s/mm(2)) and standard high b-value (1000 s/mm(2)). *J. Magn. Reson. Imaging,* 36(1)**,** 198-205.

Kitamura, K., Shirato, H., Shimizu, S., Shinohara, N., Harabayashi, T., et al. (2002) Registration accuracy and possible migration of internal fiducial gold marker implanted in prostate and liver treated with real-time tumor-tracking radiation therapy (RTRT). *Radiother. Oncol.,* 62(3)**,** 275-81.

Klotz, L., Vesprini, D., Sethukavalan, P., Jethava, V., Zhang, L., et al. (2015) Long-term follow-up of a large active surveillance cohort of patients with prostate cancer. *J. Clin. Oncol.,* 33(3)**,** 272-7.

Kotte, A. N., Hofman, P., Lagendijk, J. J., van Vulpen, M. & van der Heide, U. A. (2007) Intrafraction motion of the prostate during external-beam radiation therapy: analysis of 427 patients with implanted fiducial markers. *Int. J. Radiat. Oncol. Biol. Phys.,* 69(2)**,** 419-25.

Krauss, D., Kestin, L., Ye, H., Brabbins, D., Ghilezan, M., et al. (2011) Lack of benefit for the addition of androgen deprivation therapy to dose-escalated radiotherapy in the treatment of intermediate- and high-risk prostate cancer. *Int. J. Radiat. Oncol. Biol. Phys.,* 80(4)**,** 1064-71.

Kron, T., Thomas, J., Fox, C., Thompson, A., Owen, R., et al. (2010) Intra-fraction prostate displacement in radiotherapy estimated from pre- and post-treatment imaging of patients with implanted fiducial markers. *Radiother. Oncol.,* 95(2)**,** 191-7.

Kuban, D., Pollack, A., Huang, E., Levy, L., Dong, L., et al. (2003) Hazards of dose escalation in prostate cancer radiotherapy. *Int. J. Radiat. Oncol. Biol. Phys.,* 57(5)**,** 1260-8.

Kuban, D. A., Tucker, S. L., Dong, L., Starkschall, G., Huang, E. H., et al. (2008) Long-term results of the M. D. Anderson randomized dose-escalation trial for prostate cancer. *Int. J. Radiat. Oncol. Biol. Phys.,* 70(1)**,** 67-74.

Kunath, F., Grobe, H. R., Rucker, G., Motschall, E., Antes, G., et al. (2014) Non-steroidal antiandrogen monotherapy compared with luteinising hormone-releasing hormone agonists or surgical castration monotherapy for advanced prostate cancer. *The Cochrane database of systematic reviews,* 6**,** CD009266.

Kupelian, P. & Meyer, J. L. (2011) Image-guided, adaptive radiotherapy of prostate cancer: toward new standards of radiotherapy practice. *Front. Radiat. Ther. Oncol.,* 43**,** 344-68.

Lagendijk, J. J., Raaymakers, B. W., Raaijmakers, A. J., Overweg, J., Brown, K. J., et al. (2008) MRI/linac integration. *Radiother Oncol,* 86(1)**,** 25-9.

Lagendijk, J. J., Raaymakers, B. W. & van Vulpen, M. (2014) The magnetic resonance imaging-linac system. *Semin Radiat Oncol,* 24(3)**,** 207-9.

Lambrecht, M., Vandecaveye, V., De Keyzer, F., Roels, S., Penninckx, F., et al. (2012) Value of diffusion-weighted magnetic resonance imaging for prediction and early assessment of response to neoadjuvant radiochemotherapy in rectal cancer: preliminary results. *International journal of radiation oncology, biology, physics,* 82(2)**,** 863-70.

Lane, J. A., Hamdy, F. C., Martin, R. M., Turner, E. L., Neal, D. E., et al. (2010) Latest results from the UK trials evaluating prostate cancer screening and treatment: the CAP and ProtecT studies. *Eur J Cancer,* 46(17)**,** 3095-101.

Lange, D., Zappavigna, C., Hamidizadeh, R., Goldenberg, S. L., Paterson, R. F., et al. (2009) Bacterial sepsis after prostate biopsy--a new perspective. *Urology,* 74(6)**,** 1200-5.

Langen, K. M., Willoughby, T. R., Meeks, S. L., Santhanam, A., Cunningham, A., et al. (2008) Observations on real-time prostate gland motion using electromagnetic tracking. *Int. J. Radiat. Oncol. Biol. Phys.,* 71(4)**,** 1084-90.

Langer, D. L., van der Kwast, T. H., Evans, A. J., Sun, L., Yaffe, M. J., et al. (2008) Intermixed normal tissue within prostate cancer: effect on MR imaging measurements of apparent diffusion coefficient and T2--sparse versus dense cancers. *Radiology,* 249(3)**,** 900-8.

Langer, D. L., van der Kwast, T. H., Evans, A. J., Trachtenberg, J., Wilson, B. C., et al. (2009) Prostate cancer detection with multi-parametric MRI: logistic regression analysis of

quantitative T2, diffusion-weighted imaging, and dynamic contrast-enhanced MRI. *Journal of magnetic resonance imaging : JMRI,* 30(2)**,** 327-34.

Le, J. D., Tan, N., Shkolyar, E., Lu, D. Y., Kwan, L., et al. (2014) Multifocality and Prostate Cancer Detection by Multiparametric Magnetic Resonance Imaging: Correlation with Whole-mount Histopathology. *European urology*.

Lee, C. H., Akin-Olugbade, O. & Kirschenbaum, A. (2011) Overview of Prostate Anatomy, Histology, and Pathology. *Endocrinology and Metabolism Clinics of North America,* 40(3)**,** 565-575.

Lee, J., Demissie, K., Lu, S. E. & Rhoads, G. G. (2007) Cancer incidence among Korean-American immigrants in the United States and native Koreans in South Korea. *Cancer control : journal of the Moffitt Cancer Center,* 14(1)**,** 78-85.

Leongamornlert, D., Mahmud, N., Tymrakiewicz, M., Saunders, E., Dadaev, T., et al. (2012) Germline BRCA1 mutations increase prostate cancer risk. *British journal of cancer,* 106(10)**,** 1697-701.

Letourneau, D., Martinez, A. A., Lockman, D., Yan, D., Vargas, C., et al. (2005) Assessment of residual error for online cone-beam CT-guided treatment of prostate cancer patients. *International journal of radiation oncology, biology, physics,* 62(4)**,** 1239-46.

Li, J. S., Jin, L., Pollack, A., Horwitz, E. M., Buyyounouski, M. K., et al. (2009) Gains from real-time tracking of prostate motion during external beam radiation therapy. *International journal of radiation oncology, biology, physics,* 75(5)**,** 1613-20.

Li, J. S., Lin, M. H., Buyyounouski, M. K., Horwitz, E. M. & Ma, C. M. (2013a) Reduction of prostate intrafractional motion from shortening the treatment time. *Phys. Med. Biol.,* 58(14)**,** 4921-32.

Li, X., Quan, E. M., Li, Y., Pan, X., Zhou, Y., et al. (2013b) A fully automated method for CT-on-rails-guided online adaptive planning for prostate cancer intensity modulated radiation therapy. *International journal of radiation oncology, biology, physics,* 86(5)**,** 835-41.

LI, X. A. (2011) *Adaptive Radiation Therapy*: CRC Press.

Li, X. A., Wu, Q. & Orton, C. G. (2014) Point/Counterpoint. Online adaptive planning for prostate cancer radiotherapy is necessary and ready now. *Med. Phys.,* 41(8)**,** 080601.

Liang, J., Wu, Q. & Yan, D. (2009) The role of seminal vesicle motion in target margin assessment for online image-guided radiotherapy for prostate cancer. *International journal of radiation oncology, biology, physics,* 73(3)**,** 935-43.

Lichtenstein, P., Holm, N. V., Verkasalo, P. K., Iliadou, A., Kaprio, J., et al. (2000) Environmental and heritable factors in the causation of cancer--analyses of cohorts of twins from Sweden, Denmark, and Finland. *N. Engl. J. Med.,* 343(2)**,** 78-85.

Lin, Y., Liu, T., Yang, W., Yang, X. & Khan, M. K. (2013) The non-Gaussian nature of prostate motion based on real-time intrafraction tracking. *Int. J. Radiat. Oncol. Biol. Phys.,* 87(2)**,** 363-9.

Lips, I. M., van der Heide, U. A., Haustermans, K., van Lin, E. N., Pos, F., et al. (2011) Single blind randomized phase III trial to investigate the benefit of a focal lesion ablative microboost in prostate cancer (FLAME-trial): study protocol for a randomized controlled trial. *Trials,* 12**,** 255.

Litzenberg, D. W., Balter, J. M., Hadley, S. W., Sandler, H. M., Willoughby, T. R., et al. (2006) Influence of intrafraction motion on margins for prostate radiotherapy. *Int. J. Radiat. Oncol. Biol. Phys.,* 65(2)**,** 548-53.

Liu, L., Wu, N., Ouyang, H., Dai, J. R. & Wang, W. H. (2014a) Diffusion-Weighted MR Imaging in Early Assessment of Tumor Response to Radiotherapy in high-risk Prostate Cancer. *Br. J. Radiol.***,** 20140359.

Liu, L., Wu, N., Ouyang, H., Dai, J. R. & Wang, W. H. (2014b) Diffusion-weighted MRI in early assessment of tumour response to radiotherapy in high-risk prostate cancer. *Br. J. Radiol.,* 87(1043)**,** 20140359.

Loh, J., Baker, K., Sridharan, S., Greer, P., Wratten, C., et al. (2015) Infections after fiducial marker implantation for prostate radiotherapy: are we underestimating the risks? *Radiat Oncol,* 10**,** 38.

Loncaster, J. A., Carrington, B. M., Sykes, J. R., Jones, A. P., Todd, S. M., et al. (2002) Prediction of radiotherapy outcome using dynamic contrast enhanced MRI of carcinoma of the cervix. *Int. J. Radiat. Oncol. Biol. Phys.,* 54(3)**,** 759-67.

Low, R. N., Fuller, D. B. & Muradyan, N. (2011) Dynamic gadolinium-enhanced perfusion MRI of prostate cancer: assessment of response to hypofractionated robotic stereotactic body radiation therapy. *AJR Am. J. Roentgenol.,* 197(4)**,** 907-15.

Ludlum, E., Mu, G., Weinberg, V., Roach, M., 3rd, Verhey, L. J., et al. (2007) An algorithm for shifting MLC shapes to adjust for daily prostate movement during concurrent treatment with pelvic lymph nodes. *Med. Phys.,* 34(12)**,** 4750-6.

Lukka, H., Warde, P., Pickles, T., Morton, G., Brundage, M., et al. (2001) Controversies in prostate cancer radiotherapy: consensus development. *The Canadian journal of urology,* 8(4)**,** 1314-22.

Mah, D., Freedman, G., Milestone, B., Hanlon, A., Palacio, E., et al. (2002) Measurement of intrafractional prostate motion using magnetic resonance imaging. *Int. J. Radiat. Oncol. Biol. Phys.,* 54(2)**,** 568-75.

Maintz, J. B. & Viergever, M. A. (1998) A survey of medical image registration. *Medical image analysis,* 2(1)**,** 1-36.

Mak, D., Gill, S., Paul, R., Stillie, A., Haworth, A., et al. (2012) Seminal vesicle interfraction displacement and margins in image guided radiotherapy for prostate cancer. *Radiat Oncol,* 7**,** 139.

Mansson Haska, T., Honore, H., Muren, L. P., Hoyer, M. & Poulsen, P. R. (2008) Intrafraction changes of prostate position and geometrical errors studied by continuous electronic portal imaging. *Acta oncologica,* 47(7)**,** 1351-7.

Marks, L., Young, S. & Natarajan, S. (2013) MRI-ultrasound fusion for guidance of targeted prostate biopsy. *Curr Opin Urol,* 23(1)**,** 43-50.

Martinez, A. A., Gonzalez, J., Ye, H., Ghilezan, M., Shetty, S., et al. (2011) Dose escalation improves cancer-related events at 10 years for intermediate- and high-risk prostate cancer patients treated with hypofractionated high-dose-rate boost and external beam radiotherapy. *Int. J. Radiat. Oncol. Biol. Phys.,* 79(2)**,** 363-70.

Martinez, A. A., Shah, C., Mohammed, N., Demanes, D. J., Galalae, R., et al. (2016) Ten-year outcomes for prostate cancer patients with Gleason 8 through 10 treated with external beam radiation and high-dose-rate brachytherapy boost in the PSA era. *Journal of Radiation Oncology,* 5(1)**,** 87-93.

Mayyas, E., Chetty, I. J., Chetvertkov, M., Wen, N., Neicu, T., et al. (2013) Evaluation of multiple image-based modalities for image-guided radiation therapy (IGRT) of prostate carcinoma: A prospective study. *Medical Physics,* 40(4)**,** -.

Mayyas, E., Kim, J., Kumar, S., Liu, C., Wen, N., et al. (2014) A novel approach for evaluation of prostate deformation and associated dosimetric implications in IGRT of the prostate. *Med. Phys.,* 41(9)**,** 091709.

Mazaheri, Y., Hricak, H., Fine, S. W., Akin, O., Shukla-Dave, A., et al. (2009) Prostate Tumor Volume Measurement with Combined T2-weighted Imaging and Diffusion-weighted MR: Correlation with Pathologic Tumor Volume. *Radiology,* 252(2)**,** 449-457.

McLeod, D. G., Iversen, P., See, W. A., Morris, T., Armstrong, J., et al. (2006) Bicalutamide 150 mg plus standard care vs standard care alone for early prostate cancer. *BJU Int.,* 97(2)**,** 247-54.

McNair, H. A., Hansen, V. N., Parker, C. C., Evans, P. M., Norman, A., et al. (2008) A comparison of the use of bony anatomy and internal markers for offline verification and an evaluation of the potential benefit of online and offline verification protocols for prostate radiotherapy. *Int. J. Radiat. Oncol. Biol. Phys.,* 71(1)**,** 41-50.

McNair, H. A., Wedlake, L., Lips, I. M., Andreyev, J., Van Vulpen, M., et al. (2014) A systematic review: effectiveness of rectal emptying preparation in prostate cancer patients. *Practical radiation oncology,* 4(6)**,** 437-47.

McNeal, J. E. (1992) The Pathobiology of Prostate Cancer-Part 1Cancer volume and site of origin of adenocarcinoma in the prostate: Relationship to local and distant spread. *Hum. Pathol.,* 23(3)**,** 258-266.

McPartlin, A. J., Glicksman, R., Pintilie, M., Tsuji, D., Mok, G., et al. (2016a) PMH 9907: Long-term outcomes of a randomized phase 3 study of short-term bicalutamide hormone therapy and dose-escalated external-beam radiation therapy for localized prostate cancer. *Cancer*.

McPartlin, A. J., Li, X. A., Kershaw, L. E., Heide, U., Kerkmeijer, L., et al. (2016b) MRI-guided prostate adaptive radiotherapy - A systematic review. *Radiother. Oncol.*

McPartlin, A. J., Li, X. A., Kershaw, L. E., Heide, U., Kerkmeijer, L., et al. (2016c) MRI-guided prostate adaptive radiotherapy - A systematic review. *Radiother Oncol,* 119(3)**,** 371-80.

Melero, I., Berman, D. M., Aznar, M. A., Korman, A. J., Gracia, J. L. P., et al. (2015) Evolving synergistic combinations of targeted immunotherapies to combat cancer. *Nat. Rev. Cancer,* 15(8)**,** 457-472.

Melian, E., Mageras, G. S., Fuks, Z., Leibel, S. A., Niehaus, A., et al. (1997) Variation in prostate position quantitation and implications for three-dimensional conformal treatment planning. *Int. J. Radiat. Oncol. Biol. Phys.,* 38(1)**,** 73-81.

Menten, M. J., Fast, M. F., Nill, S., Kamerling, C. P., McDonald, F., et al. (2016) Lung stereotactic body radiotherapy with an MR-linac - Quantifying the impact of the magnetic field and real-time tumor tracking. *Radiother Oncol,* 119(3)**,** 461-6.

Merrick, G. S., Taubenslag, W., Andreini, H., Brammer, S., Butler, W. M., et al. (2008) The morbidity of transperineal template-guided prostate mapping biopsy. *BJU Int.,* 101(12)**,** 1524-9.

Michalski, J. M., Gay, H., Jackson, A., Tucker, S. L. & Deasy, J. O. (2010) Radiation dose-volume effects in radiation-induced rectal injury. *Int. J. Radiat. Oncol. Biol. Phys.,* 76(3 Suppl)**,** S123-9.

Miralbell, R., Moll, M., Rouzaud, M., Hidalgo, A., Toscas, J. I., et al. (2010a) Hypofractionated boost to the dominant tumor region with intensity modulated stereotactic radiotherapy for prostate cancer: A sequential dose escalation pilot study. *International Journal of Radiation Oncology Biology Physics,* 78(1)**,** 50-57.

Miralbell, R., Molla, M., Rouzaud, M., Hidalgo, A., Toscas, J. I., et al. (2010b) Hypofractionated boost to the dominant tumor region with intensity modulated stereotactic radiotherapy for prostate cancer: a sequential dose escalation pilot study. *Int. J. Radiat. Oncol. Biol. Phys.,* 78(1)**,** 50-7.

Mohan, R., Zhang, X., Wang, H., Kang, Y., Wang, X., et al. (2005) Use of deformed intensity distributions for on-line modification of image-guided IMRT to account for interfractional anatomic changes. *Int. J. Radiat. Oncol. Biol. Phys.,* 61(4)**,** 1258-66.

Moiseenko, V., Liu, M., Kristensen, S., Gelowitz, G. & Berthelet, E. (2007) Effect of bladder filling on doses to prostate and organs at risk: a treatment planning study. *Journal of Applied Clinical Medical Physics; Vol 8, No 1 (2007)*.

Moore, C. M., Kasivisvanathan, V., Eggener, S., Emberton, M., Futterer, J. J., et al. (2013a) Standards of reporting for MRI-targeted biopsy studies (START) of the prostate: recommendations from an International Working Group. *European urology,* 64(4)**,** 544-52.

Moore, C. M., Robertson, N. L., Arsanious, N., Middleton, T., Villers, A., et al. (2013b) Image-guided prostate biopsy using magnetic resonance imaging-derived targets: a systematic review. *Eur. Urol.,* 63(1)**,** 125-40.

Morrow, N. V., Lawton, C. A., Qi, X. S. & Li, X. A. (2012) Impact of computed tomography image quality on image-guided radiation therapy based on soft tissue registration. *Int. J. Radiat. Oncol. Biol. Phys.,* 82(5)**,** e733-8.

Moseley, D. J., White, E. A., Wiltshire, K. L., Rosewall, T., Sharpe, M. B., et al. (2007) Comparison of localization performance with implanted fiducial markers and cone-beam computed tomography for on-line image-guided radiotherapy of the prostate. *International Journal of Radiation Oncology*Biology*Physics,* 67(3)**,** 942-953.

Moulton, C. R., House, M. J., Lye, V., Tang, C. I., Krawiec, M., et al. (2015) Registering prostate external beam radiotherapy with a boost from high-dose-rate brachytherapy: a comparative evaluation of deformable registration algorithms. *Radiat. Oncol.,* 10**,** 254.

Moye, L. A. (1998) P-value interpretation and alpha allocation in clinical trials. *Ann. Epidemiol.,* 8(6)**,** 351-7.

Muller, B. G., Fütterer, J. J., Gupta, R. T., Katz, A., Kirkham, A., et al. (2014) The role of magnetic resonance imaging (MRI) in focal therapy for prostate cancer: recommendations from a consensus panel. *BJU Int.,* 113(2)**,** 218-227.

Mullerad, M., Hricak, H., Kuroiwa, K., Pucar, D., Chen, H.-N., et al. (2005) COMPARISON OF ENDORECTAL MAGNETIC RESONANCE IMAGING, GUIDED PROSTATE BIOPSY AND DIGITAL RECTAL EXAMINATION IN THE PREOPERATIVE ANATOMICAL LOCALIZATION OF PROSTATE CANCER. *The Journal of urology,* 174(6)**,** 2158-2163.

Mullins, J. K., Feng, Z., Trock, B. J., Epstein, J. I., Walsh, P. C., et al. (2012) The impact of anatomical radical retropubic prostatectomy on cancer control: the 30-year anniversary. *The Journal of urology,* 188(6)**,** 2219-24.

Mutanga, T. F., de Boer, H. C., Rajan, V., Dirkx, M. L., Incrocci, L., et al. (2012) Day-to-day reproducibility of prostate intrafraction motion assessed by multiple kV and MV imaging of implanted markers during treatment. *Int. J. Radiat. Oncol. Biol. Phys.,* 83(1)**,** 400-7.

Mutanga, T. F., de Boer, H. C., van der Wielen, G. J., Wentzler, D., Barnhoorn, J., et al. (2008) Stereographic targeting in prostate radiotherapy: speed and precision by daily automatic positioning corrections using kilovoltage/megavoltage image pairs. *International journal of radiation oncology, biology, physics,* 71(4)**,** 1074-83.

Mutic, S. & Dempsey, J. F. (2014) The ViewRay system: magnetic resonance-guided and controlled radiotherapy. *Seminars in radiation oncology,* 24(3)**,** 196-9.

Nabid A, C. N., Vigneault E, Souhami L, Lemaire C, Brassard MA, Bahoric B, Archambault R, Vincent F, Nguyen-Huynh TV. (2015) Place of short-term androgen deprivation therapy in intermediate-risk prostate cancer treated with radiotherapy: A phase III trial. *Journal of Clinical Oncology,* 33(7 (suppl))**,** abstr 5.

Nahum, A. E., Movsas, B., Horwitz, E. M., Stobbe, C. C. & Chapman, J. D. (2003) Incorporating clinical measurements of hypoxia into tumor local control modeling of prostate cancer: implications for the alpha/beta ratio. *International journal of radiation oncology, biology, physics,* 57(2)**,** 391-401.

Nederveen, A. J., van der Heide, U. A., Dehnad, H., van Moorselaar, R. J., Hofman, P., et al. (2002) Measurements and clinical consequences of prostate motion during a radiotherapy fraction. *Int. J. Radiat. Oncol. Biol. Phys.,* 53(1)**,** 206-14.

Nguyen, P. L., Schultz, D., Renshaw, A. A., Vollmer, R. T., Welch, W. R., et al. (2004) The impact of pathology review on treatment recommendations for patients with adenocarcinoma of the prostate. *Urol. Oncol.,* 22(4)**,** 295-9.

NICE. (2014) Prostate cancer: diagnosis and management. National Institute for Health and Care Excellence.

Nichol, A. M., Brock, K. K., Lockwood, G. A., Moseley, D. J., Rosewall, T., et al. (2007) A magnetic resonance imaging study of prostate deformation relative to implanted gold fiducial markers. *Int. J. Radiat. Oncol. Biol. Phys.,* 67(1)**,** 48-56.

NICI, N., DHHS. (2009) *Common Terminology Criteria for Adverse Events v4.0*: NIH Publication #09-7473.

Nicolae, A., Davidson, M., Easton, H., Helou, J., Musunuru, H., et al. (2015) Clinical evaluation of an endorectal immobilization system for use in prostate hypofractionated Stereotactic Ablative Body Radiotherapy (SABR). *Radiat. Oncol.,* 10(1)**,** 122.

Nijkamp, J., De Haas-Kock, D. F. M., Beukema, J. C., Neelis, K. J., Woutersen, D., et al. (2012) Target volume delineation variation in radiotherapy for early stage rectal cancer in the Netherlands. *Radiotherapy and Oncology,* 102(1)**,** 14-21.

Nijkamp, J., Pos, F. J., Nuver, T. T., de Jong, R., Remeijer, P., et al. (2008) Adaptive radiotherapy for prostate cancer using kilovoltage cone-beam computed tomography: first clinical results. *International journal of radiation oncology, biology, physics,* 70(1)**,** 75-82.

Noguchi, M., Stamey, T. A., McNeal, J. E. & Nolley, R. (2003) Prognostic factors for multifocal prostate cancer in radical prostatectomy specimens: lack of significance of secondary cancers. *J. Urol.,* 170(2 Pt 1)**,** 459-63.

O'Daniel, J. C., Dong, L., Zhang, L., de Crevoisier, R., Wang, H., et al. (2006) Dosimetric comparison of four target alignment methods for prostate cancer radiotherapy. *Int. J. Radiat. Oncol. Biol. Phys.,* 66(3)**,** 883-91.

Oates, R., Gill, S., Foroudi, F., Joon, M. L., Schneider, M., et al. (2015) What benefit could be derived from on-line adaptive prostate radiotherapy using rectal diameter as a predictor of motion? *Journal of medical physics / Association of Medical Physicists of India,* 40(1)**,** 18-23.

Oehler, C., Lang, S., Dimmerling, P., Bolesch, C., Kloeck, S., et al. (2014) PTV margin definition in hypofractionated IGRT of localized prostate cancer using cone beam CT and orthogonal image pairs with fiducial markers. *Radiat. Oncol.,* 9**,** 229.

Oesterling, J. E., Jacobsen, S. J., Chute, C. G., Guess, H. A., Girman, C. J., et al. (1993) Serum prostate-specific antigen in a community-based population of healthy men. Establishment of age-specific reference ranges. *JAMA,* 270(7)**,** 860-4.

Ogino, I., Kaneko, T., Suzuki, R., Matsui, T., Takebayashi, S., et al. (2011) Rectal content and intrafractional prostate gland motion assessed by magnetic resonance imaging. *J Radiat Res,* 52(2)**,** 199-207.

Oh, Y. K., Baek, J. G., Kim, O. B. & Kim, J. H. (2014) Assessment of setup uncertainties for various tumor sites when using daily CBCT for more than 2200 VMAT treatments. *J. Appl. Clin. Med. Phys.,* 15(2)**,** 4418.

Ohri, N., Dicker, A. P. & Showalter, T. N. (2012) Late toxicity rates following definitive radiotherapy for prostate cancer. *The Canadian journal of urology,* 19(4)**,** 6373-80.

Okamoto, M., Ishikawa, H., Ebara, T., Kato, H., Tamaki, T., et al. (2012) Rectal Bleeding After High-Dose-Rate Brachytherapy Combined With Hypofractionated External-Beam Radiotherapy for Localized Prostate Cancer: The Relationship Between Dose-Volume Histogram Parameters and the Occurrence Rate. *International Journal of Radiation Oncology*Biology*Physics,* 82(2)**,** e211-e217.

Onal, C., Sonmez, S., Erbay, G., Guler, O. C. & Arslan, G. (2014) Simultaneous integrated boost to intraprostatic lesions using different energy levels of intensity-modulated radiotherapy and volumetric-arc therapy. *The British journal of radiology,* 87(1034)**,** 20130617.

Osugi, K., Tanimoto, A., Nakashima, J., Shinoda, K., Hashiguchi, A., et al. (2013) What is the most effective tool for detecting prostate cancer using a standard MR scanner? *Magn. Reson. Med. Sci.,* 12(4)**,** 271-80.

Padhani, A. R., Khoo, V. S., Suckling, J., Husband, J. E., Leach, M. O., et al. (1999) Evaluating the effect of rectal distension and rectal movement on prostate gland position using cine MRI. *Int. J. Radiat. Oncol. Biol. Phys.,* 44(3)**,** 525-33.

Panigrahy, A., Caruthers, S. D., Krejza, J., Barnes, P. D., Faddoul, S. G., et al. (2000) Registration of Three-Dimensional MR and CT Studies of the Cervical Spine. *American Journal of Neuroradiology,* 21(2)**,** 282-289.

Park, S. S., Yan, D., McGrath, S., Dilworth, J. T., Liang, J., et al. (2012a) Adaptive image-guided radiotherapy (IGRT) eliminates the risk of biochemical failure caused by the bias of rectal distension in prostate cancer treatment planning: clinical evidence. *International journal of radiation oncology, biology, physics,* 83(3)**,** 947-52.

Park, S. Y., Kim, C. K., Park, B. K., Park, W., Park, H. C., et al. (2012b) Early changes in apparent diffusion coefficient from diffusion-weighted MR imaging during radiotherapy for prostate cancer. *International Journal of Radiation Oncology Biology Physics,* 83(2)**,** 749-755.

Park, S. Y., Kim, C. K., Park, B. K., Park, W., Park, H. C., et al. (2012c) Early changes in apparent diffusion coefficient from diffusion-weighted MR imaging during radiotherapy for prostate cancer. *Int. J. Radiat. Oncol. Biol. Phys.,* 83(2)**,** 749-55.

Parker, C. C., Damyanovich, A., Haycocks, T., Haider, M., Bayley, A., et al. (2003) Magnetic resonance imaging in the radiation treatment planning of localized prostate cancer using

intra-prostatic fiducial markers for computed tomography co-registration. *Radiother. Oncol.,* 66(2)**,** 217-24.

Partin, A. W., Kattan, M. W., Subong, E. N., Walsh, P. C., Wojno, K. J., et al. (1997) Combination of prostate-specific antigen, clinical stage, and Gleason score to predict pathological stage of localized prostate cancer. A multi-institutional update. *JAMA,* 277(18)**,** 1445-51.

Patterson, D. M., Padhani, A. R. & Collins, D. J. (2008) Technology insight: water diffusion MRI--a potential new biomarker of response to cancer therapy. *Nat. Clin. Pract. Oncol.,* 5(4)**,** 220-33.

Peeters, S. T., Lebesque, J. V., Heemsbergen, W. D., van Putten, W. L., Slot, A., et al. (2006) Localized volume effects for late rectal and anal toxicity after radiotherapy for prostate cancer. *Int. J. Radiat. Oncol. Biol. Phys.,* 64(4)**,** 1151-61.

Peng, Y., Jiang, Y., Antic, T., Sethi, I., Schmid-Tannwald, C., et al. (2014) Apparent diffusion coefficient for prostate cancer imaging: impact of B values. *AJR Am J Roentgenol,* 202(3)**,** W247-53.

Penzkofer, T., Tuncali, K., Fedorov, A., Song, S. E., Tokuda, J., et al. (2015) Transperineal in-bore 3-T MR imaging-guided prostate biopsy: a prospective clinical observational study. *Radiology,* 274(1)**,** 170-80.

Petrillo, M., Fusco, R., Catalano, O., Sansone, M., Avallone, A., et al. (2015) MRI for Assessing Response to Neoadjuvant Therapy in Locally Advanced Rectal Cancer Using DCE-MR and DW-MR Data Sets: A Preliminary Report. *BioMed Research International,* 2015**,** 8.

Pickett, B., Vigneault, E., Kurhanewicz, J., Verhey, L. & Roach, M. (1999) Static field intensity modulation to treat a dominant intra-prostatic lesion to 90 Gy compared to seven field 3-dimensional radiotherapy. *International Journal of Radiation Oncology*Biology*Physics,* 44(4)**,** 921-929.

Pilepich, M. V., Asbell, S. O., Krall, J. M., Baerwald, W. H., Sause, W. T., et al. (1987) Correlation of radiotherapeutic parameters and treatment related morbidity--analysis of RTOG Study 77-06. *International journal of radiation oncology, biology, physics,* 13(7)**,** 1007-12.

Pinkawa, M., Asadpour, B., Gagel, B., Piroth, M. D., Holy, R., et al. (2006a) Prostate position variability and dose-volume histograms in radiotherapy for prostate cancer with full and empty bladder. *Int. J. Radiat. Oncol. Biol. Phys.,* 64(3)**,** 856-61.

Pinkawa, M., Piroth, M. D., Holy, R., Klotz, J., Djukic, V., et al. (2012) Dose-escalation using intensity-modulated radiotherapy for prostate cancer - evaluation of quality of life with and without (18)F-choline PET-CT detected simultaneous integrated boost. *Radiat. Oncol.,* 7**,** 14.

Pinkawa, M., Siluschek, J., Gagel, B., Demirel, C., Asadpour, B., et al. (2006b) Influence of the initial rectal distension on posterior margins in primary and postoperative radiotherapy for prostate cancer. *Radiother Oncol,* 81(3)**,** 284-90.

Pisansky, T. M., Hunt, D., Gomella, L. G., Amin, M. B., Balogh, A. G., et al. (2015) Duration of androgen suppression before radiotherapy for localized prostate cancer: radiation therapy oncology group randomized clinical trial 9910. *J. Clin. Oncol.,* 33(4)**,** 332-9.

Polat, B., Guenther, I., Wilbert, J., Goebel, J., Sweeney, R. A., et al. (2008) Intra-fractional uncertainties in image-guided intensity-modulated radiotherapy (IMRT) of prostate cancer. *Strahlenther Onkol,* 184(12)**,** 668-73.

Potter, R., Haie-Meder, C., Van Limbergen, E., Barillot, I., De Brabandere, M., et al. (2006) Recommendations from gynaecological (GYN) GEC ESTRO working group (II): concepts and terms in 3D image-based treatment planning in cervix cancer brachytherapy-3D dose volume parameters and aspects of 3D image-based anatomy, radiation physics, radiobiology. *Radiother. Oncol.,* 78(1)**,** 67-77.

Pucar, D., Hricak, H., Shukla-Dave, A., Kuroiwa, K., Drobnjak, M., et al. (2007) Clinically significant prostate cancer local recurrence after radiation therapy occurs at the site of primary tumor: magnetic resonance imaging and step-section pathology evidence. *Int. J. Radiat. Oncol. Biol. Phys.,* 69(1)**,** 62-9.

Puech, P., Potiron, E., Lemaitre, L., Leroy, X., Haber, G.-P., et al. (2009) Dynamic Contrast-enhanced–magnetic Resonance Imaging Evaluation of Intraprostatic Prostate Cancer: Correlation with Radical Prostatectomy Specimens. *Urology,* 74(5)**,** 1094-1099.

Qi, W. X., Zhang, Q., Li, P., Zhang, X. M., Zhang, G. Y., et al. (2016) The predictive role of ADC values in prostate cancer patients treated with carbon-ion radiotherapy: initial clinical experience at Shanghai Proton and Heavy Ion Center (SPHIC). *J. Cancer Res. Clin. Oncol.,* 142(6)**,** 1361-7.

Qian, J., Wollan, P. & Bostwick, D. G. (1997) The extent and multicentricity of high-grade prostatic intraepithelial neoplasia in clinically localized prostatic adenocarcinoma. *Human pathology,* 28(2)**,** 143-8.

Qin, A., Sun, Y., Liang, J. & Yan, D. (2015) Evaluation of online/offline image guidance/adaptation approaches for prostate cancer radiation therapy. *Int. J. Radiat. Oncol. Biol. Phys.,* 91(5)**,** 1026-33.

Quon, H., Loblaw, D. A., Cheung, P. C., Holden, L., Tang, C., et al. (2012) Intra-fraction motion during extreme hypofractionated radiotherapy of the prostate using pre- and post-treatment imaging. *Clinical oncology,* 24(9)**,** 640-5.

Radtke, J. P., Kuru, T. H., Boxler, S., Alt, C. D., Popeneciu, I. V., et al. (2015) Comparative analysis of transperineal template saturation prostate biopsy versus magnetic resonance imaging targeted biopsy with magnetic resonance imaging-ultrasound fusion guidance. *J. Urol.,* 193(1)**,** 87-94.

Rasch, C., Barillot, I., Remeijer, P., Touw, A., van Herk, M., et al. (1999a) Definition of the prostate in CT and MRI: a multi-observer study. *Int. J. Radiat. Oncol. Biol. Phys.,* 43(1)**,** 57-66.

Rasch, C., Remeijer, P., Koper, P. C. M., Meijer, G. J., Stroom, J. C., et al. (1999b) Comparison of prostate cancer treatment in two institutions: A quality control study. *International Journal of Radiation Oncology Biology Physics,* 45(4)**,** 1055-1062.

Reggiori, G., Mancosu, P., Tozzi, A., Cantone, M. C., Castiglioni, S., et al. (2011) Cone beam CT pre- and post-daily treatment for assessing geometrical and dosimetric intrafraction variability during radiotherapy of prostate cancer. *Journal of applied clinical medical physics / American College of Medical Physics,* 12(1)**,** 3371.

Resnick, M. J., Koyama, T., Fan, K. H., Albertsen, P. C., Goodman, M., et al. (2013) Long-term functional outcomes after treatment for localized prostate cancer. *The New England journal of medicine,* 368(5)**,** 436-45.

Riches SF, M. V., Payne GS, Dearnley D, deSouza N. (2007) Diffusion weighted imaging of androgen deivation hormone therapy prostate cancer patients. *Proceedings of the Internation Society of Magnetic Resonance in Medicine***,** 793.

Riches, S. F., Payne, G. S., Desouza, N. M., Dearnaley, D., Morgan, V. A., et al. (2014) Effect on therapeutic ratio of planning a boosted radiotherapy dose to the dominant intraprostatic tumour lesion within the prostate based on multifunctional MR parameters. *Br. J. Radiol.,* 87(1037)**,** 20130813.

Rischke, H. C., Nestle, U., Fechter, T., Doll, C., Volegova-Neher, N., et al. (2013) 3 Tesla multiparametric MRI for GTV-definition of Dominant Intraprostatic Lesions in patients with Prostate Cancer--an interobserver variability study. *Radiat. Oncol.,* 8**,** 183.

Roach Iii, M., Faillace-Akazawa, P., Malfatti, C., Holland, J. & Hricak, H. (1996) Prostate volumes defined by magnetic resonance imaging and computerized tomographic scans for three-dimensional conformal radiotherapy. *International Journal of Radiation Oncology Biology Physics,* 35(5)**,** 1011-1018.

Roach, M., 3rd, Hanks, G., Thames, H., Jr., Schellhammer, P., Shipley, W. U., et al. (2006) Defining biochemical failure following radiotherapy with or without hormonal therapy in men with clinically localized prostate cancer: recommendations of the RTOG-ASTRO Phoenix Consensus Conference. *International journal of radiation oncology, biology, physics,* 65(4)**,** 965-74.

Robertson, N. L., Emberton, M. & Moore, C. M. (2013) MRI-targeted prostate biopsy: a review of technique and results. *Nat Rev Urol,* 10(10)**,** 589-97.

Rodda, S. L., Duncan, G., Hamm, J. & Morris, W. J. Quality of Life Outcomes: ASCENDE-RT a Multicenter Randomized Trial of Radiation Therapy for Prostate Cancer. *International Journal of Radiation Oncology • Biology • Physics,* 93(3)**,** S2.

Rodrigues, G., Lukka, H., Warde, P., Brundage, M., Souhami, L., et al. (2013) The prostate cancer risk stratification (ProCaRS) project: recursive partitioning risk stratification analysis. *Radiother Oncol,* 109(2)**,** 204-10.

Roe, K., Kakar, M., Seierstad, T., Ree, A. H. & Olsen, D. R. (2011) Early prediction of response to radiotherapy and androgen-deprivation therapy in prostate cancer by repeated functional MRI: a preclinical study. *Radiat. Oncol.,* 6**,** 65.

Roe, K., Mikalsen, L. T., van der Kogel, A. J., Bussink, J., Lyng, H., et al. (2012) Vascular responses to radiotherapy and androgen-deprivation therapy in experimental prostate cancer. *Radiat. Oncol.,* 7**,** 75.

Roeske, J. C., Forman, J. D., Mesina, C. F., He, T., Pelizzari, C. A., et al. (1995) Evaluation of changes in the size and location of the prostate, seminal vesicles, bladder, and rectum during a course of external beam radiation therapy. *Int. J. Radiat. Oncol. Biol. Phys.,* 33(5)**,** 1321-9.

Rosen, R. C., Cappelleri, J. C. & Gendrano, N. (2002) The Internation Index of Erectile Function (IIEF): a state -of-the-science review. *International journal of impotence research,* 14(4)**,** 226-244.

Rosenkrantz, A. B., Kim, S., Lim, R. P., Hindman, N., Deng, F. M., et al. (2013) Prostate cancer localization using multiparametric MR imaging: comparison of Prostate Imaging Reporting and Data System (PI-RADS) and Likert scales. *Radiology,* 269(2)**,** 482-92.

Rosewall, T., Kong, V., Vesprini, D., Catton, C., Chung, P., et al. (2009) Prostate delineation using CT and MRI for radiotherapy patients with bilateral hip prostheses. *Radiother. Oncol.,* 90(3)**,** 325-30.

Rothke, M., Blondin, D., Schlemmer, H. P. & Franiel, T. (2013) [PI-RADS classification: structured reporting for MRI of the prostate]. *RoFo : Fortschritte auf dem Gebiete der Rontgenstrahlen und der Nuklearmedizin,* 185(3)**,** 253-61.

Roznovanu, S. L., Radulescu, D., Novac, C. & Stolnicu, S. (2005) The morphologic changes induced by hormone and radiation therapy on prostate carcinoma. *Revista medico-chirurgicala a Societatii de Medici si Naturalisti din Iasi,* 109(2)**,** 337-42.

Russo, F., Regge, D., Armando, E., Giannini, V., Vignati, A., et al. (2015) Detection of prostate cancer index lesions with multiparametric magnetic resonance imaging (mp-MRI) using whole-mount histological sections as the reference standard. *BJU Int.*

Saman, D. M., Lemieux, A. M., Nawal Lutfiyya, M. & Lipsky, M. S. (2014) A review of the current epidemiology and treatment options for prostate cancer. *Dis. Mon.,* 60(4)**,** 150-4.

Samavati, N., McGrath, D. M., Jewett, M. A., van der Kwast, T., Menard, C., et al. (2015) Effect of material property heterogeneity on biomechanical modeling of prostate under deformation. *Physics in medicine and biology,* 60(1)**,** 195-209.

Sanda, M. G., Dunn, R. L., Michalski, J., Sandler, H. M., Northouse, L., et al. (2008) Quality of life and satisfaction with outcome among prostate-cancer survivors. *N. Engl. J. Med.,* 358(12)**,** 1250-61.

Sannazzari, G. L., Ragona, R., Ruo Redda, M. G., Giglioli, F. R., Isolato, G., et al. (2002) CT-MRI image fusion for delineation of volumes in three-dimensional conformal radiation therapy in the treatment of localized prostate cancer. *Br. J. Radiol.,* 75(895)**,** 603-7.

Satoh, T., Matsumoto, K., Fujita, T., Tabata, K., Okusa, H., et al. (2005) Cancer core distribution in patients diagnosed by extended transperineal prostate biopsy. *Urology,* 66(1)**,** 114-8.

Schallenkamp, J. M., Herman, M. G., Kruse, J. J. & Pisansky, T. M. (2005) Prostate position relative to pelvic bony anatomy based on intraprostatic gold markers and electronic portal imaging. *Int. J. Radiat. Oncol. Biol. Phys.,* 63(3)**,** 800-11.

Scheenen, T. W. J., Heijmink, S., Roell, S. A., Hulsbergen-Van de Kaa, C. A., Knipscheer, B. C., et al. (2007) Three-dimensional proton MR spectroscopy of human prostate at 3 T without endorectal coil: Feasibility. *Radiology,* 245(2)**,** 507-516.

Schick, U., Popowski, Y., Nouet, P., Bieri, S., Rouzaud, M., et al. (2011) High-dose-rate brachytherapy boost to the dominant intra-prostatic tumor region: hemi-irradiation of prostate cancer. *The Prostate,* 71(12)**,** 1309-16.

Schild, M. H., Schild, S. E., Wong, W. W., Vora, S. A., Silva, A. C., et al. (2014) Early Outcome of Prostate Intensity Modulated Radiation Therapy (IMRT) Incorporating a Simultaneous Intra-Prostatic MRI Directed Boost. *OMICS journal of radiology,* 3(4).

Schild, S. E., Casale, H. E. & Bellefontaine, L. P. (1993) Movements of the prostate due to rectal and bladder distension: implications for radiotherapy. *Med. Dosim.,* 18(1)**,** 13-5.

Schimmoller, L., Quentin, M., Arsov, C., Lanzman, R. S., Hiester, A., et al. (2013) Inter-reader agreement of the ESUR score for prostate MRI using in-bore MRI-guided biopsies as the reference standard. *European radiology,* 23(11)**,** 3185-90.

Schmidt, H., DeAngelis, G., Eltze, E., Gockel, I., Semjonow, A., et al. (2006) Asynchronous growth of prostate cancer is reflected by circulating tumor cells delivered from distinct, even small foci, harboring loss of heterozygosity of the PTEN gene. *Cancer Res,* 66(18)**,** 8959-65.

Schmuecking, M., Boltze, C., Geyer, H., Salz, H., Schilling, B., et al. (2009) Dynamic MRI and CAD vs. choline MRS: where is the detection level for a lesion characterisation in prostate cancer? *Int. J. Radiat. Biol.,* 85(9)**,** 814-24.

Schoots, I. G., Roobol, M. J., Nieboer, D., Bangma, C. H., Steyerberg, E. W., et al. (2015) Magnetic resonance imaging-targeted biopsy may enhance the diagnostic accuracy of significant prostate cancer detection compared to standard transrectal ultrasound-guided biopsy: a systematic review and meta-analysis. *Eur. Urol.,* 68(3)**,** 438-50.

Schreiber, D., Rineer, J., Surapaneni, A., Navo, E., Agarwal, M., et al. (2014a) Dose-escalated radiation therapy with and without short-course androgen deprivation for intermediate-risk prostate cancer. *Anticancer Res,* 34(8)**,** 4189-93.

Schreiber, D., Rineer, J. M., Safdieh, J., Weiner, J., Weiss, J. P., et al. (2014b) Comparative Effectiveness of Radical Prostatectomy Versus Dose Escalated Radiation Therapy in a Predominantly African American Population. *International Journal of Radiation Oncology • Biology • Physics,* 90(1)**,** S583-S584.

Schroder, F. H., Hugosson, J., Roobol, M. J., Tammela, T. L., Ciatto, S., et al. (2009) Screening and prostate-cancer mortality in a randomized European study. *The New England journal of medicine,* 360(13)**,** 1320-8.

Schröder, F. H., Kruger, A. B., Rietbergen, J., Kranse, R., Maas, P. v. d., et al. (1998) Evaluation of the Digital Rectal Examination as a Screening Test for Prostate Cancer. *Journal of the National Cancer Institute,* 90(23)**,** 1817-1823.

See, W. A., Tyrrell, C. J. & Group, C. E. P. C. T. (2006) The addition of bicalutamide 150 mg to radiotherapy significantly improves overall survival in men with locally advanced prostate cancer. *J. Cancer Res. Clin. Oncol.,* 132 Suppl 1**,** S7-16.

Shaffer, R., Morris, W. J., Moiseenko, V., Welsh, M., Crumley, C., et al. (2009) Volumetric Modulated Arc Therapy and Conventional Intensity-modulated Radiotherapy for Simultaneous Maximal Intraprostatic Boost: a Planning Comparison Study. *Clinical oncology,* 21(5)**,** 401-407.

Shelton, J., Rossi, P. J., Chen, H., Liu, Y., Master, V. A., et al. (2011) Observations on prostate intrafraction motion and the effect of reduced treatment time using volumetric modulated arc therapy. *Practical radiation oncology,* 1(4)**,** 243-50.

Shimizu, S., Osaka, Y., Shinohara, N., Sazawa, A., Nishioka, K., et al. (2011) Use of implanted markers and interportal adjustment with real-time tracking radiotherapy system to reduce intrafraction prostate motion. *International journal of radiation oncology, biology, physics,* 81(4)**,** e393-9.

Shipitsin, M., Small, C., Choudhury, S., Giladi, E., Friedlander, S., et al. (2014) Identification of proteomic biomarkers predicting prostate cancer aggressiveness and lethality despite biopsy-sampling error. *British journal of cancer,* 111(6)**,** 1201-12.

Shipley, W. U., Seiferheld, W., Lukka, H., Major, P., Heney, N. M., et al. Report of NRG Oncology/RTOG 9601, A Phase 3 Trial in Prostate Cancer: Anti-androgen Therapy (AAT) With Bicalutamide During and After Radiation Therapy (RT) in Patients Following Radical

Prostatectomy (RP) With pT2-3pN0 Disease and an Elevated PSA. *International Journal of Radiation Oncology • Biology • Physics,* 94(1)**,** 3.

Shipley, W. U., Thames, H. D., Sandler, H. M. & et al. (1999) Radiation therapy for clinically localized prostate cancer: A multi-institutional pooled analysis. *JAMA,* 281(17)**,** 1598-1604.

Sieber, P. R., Keiller, D. L., Kahnoski, R. J., Gallo, J. & McFadden, S. (2004) Bicalutamide 150 mg maintains bone mineral density during monotherapy for localized or locally advanced prostate cancer. *J. Urol.,* 171(6 Pt 1)**,** 2272-6, quiz 2435.

Singh, A. K., Guion, P., Sears-Crouse, N., Ullman, K., Smith, S., et al. (2007) Simultaneous integrated boost of biopsy proven, MRI defined dominant intra-prostatic lesions to 95 Gray with IMRT: early results of a phase I NCI study. *Radiat. Oncol.,* 2**,** 36.

Sinha, R., Park, Y., Graubard, B. I., Leitzmann, M. F., Hollenbeck, A., et al. (2009) Meat and meat-related compounds and risk of prostate cancer in a large prospective cohort study in the United States. *Am. J. Epidemiol.,* 170(9)**,** 1165-77.

Sivaraman, A., Sanchez-Salas, R., Ahmed, H. U., Barret, E., Cathala, N., et al. (2015) Clinical utility of transperineal template-guided mapping biopsy of the prostate after negative magnetic resonance imaging-guided transrectal biopsy. *Urol. Oncol.,* 33(7)**,** 329 e7-11.

Sjoerd, C. & Bas, R. (2014) From static to dynamic 1.5T MRI-linac prototype: impact of gantry position related magnetic field variation on image fidelity. *Phys. Med. Biol.,* 59(13)**,** 3241.

Soete, G., De Cock, M., Verellen, D., Michielsen, D., Keuppens, F., et al. (2007) X-ray–assisted positioning of patients treated by conformal arc radiotherapy for prostate cancer: Comparison of setup accuracy using implanted markers versus bony structures. *International Journal of Radiation Oncology*Biology*Physics,* 67(3)**,** 823-827.

Song, I., Kim, C. K., Park, B. K. & Park, W. (2010) Assessment of Response to Radiotherapy for Prostate Cancer: Value of Diffusion-Weighted MRI at 3 T. *American Journal of Roentgenology,* 194(6)**,** W477-W482.

Sosna, J., Rofsky, N. M., Gaston, S. M., DeWolf, W. C. & Lenkinski, R. E. (2003) Determinations of prostate volume at 3-tesla using an external phased array coil: Comparison to pathologic specimens1. *Academic radiology,* 10(8)**,** 846-853.

Spratt, D. E., Pei, X., Yamada, J., Kollmeier, M. A., Cox, B., et al. (2013) Long-term survival and toxicity in patients treated with high-dose intensity modulated radiation therapy for localized prostate cancer. *Int. J. Radiat. Oncol. Biol. Phys.,* 85(3)**,** 686-92.

Spratt, D. E., Zumsteg, Z. S., Ghadjar, P., Kollmeier, M. A., Pei, X., et al. (2014) Comparison of high-dose (86.4 Gy) IMRT vs combined brachytherapy plus IMRT for intermediate-risk prostate cancer. *BJU Int.,* 114(3)**,** 360-7.

St Lawrence, K. S. & Lee, T. Y. (1998) An adiabatic approximation to the tissue homogeneity model for water exchange in the brain: I. Theoretical derivation. *J. Cereb. Blood Flow Metab.,* 18(12)**,** 1365-77.

Stanley, K., Eade, T., Kneebone, A. & Booth, J. T. (2015) Investigation of an adaptive treatment regime for prostate radiation therapy. *Pract. Radiat. Oncol.,* 5(1)**,** e23-9.

Steenbakkers, R. J. H. M., Deurloo, K. E. I., Nowak, P. J. C. M., Lebesque, J. V., van Herk, M., et al. (2003) Reduction of dose delivered to the rectum and bulb of the penis using MRI delineation for radiotherapy of the prostate. *International Journal of Radiation Oncology*Biology*Physics,* 57(5)**,** 1269-1279.

Steenbergen, P., Haustermans, K., Lerut, E., Oyen, R., De Wever, L., et al. (2015) Prostate tumor delineation using multiparametric magnetic resonance imaging: Inter-observer variability and pathology validation. *Radiother. Oncol.,* 115(2)**,** 186-90.

Steiner, E., Georg, D., Goldner, G. & Stock, M. (2013) Prostate and patient intrafraction motion: impact on treatment time-dependent planning margins for patients with endorectal balloon. *International journal of radiation oncology, biology, physics,* 86(4)**,** 755-61.

Stenmark, M. H., Vineberg, K., Ten Haken, R. K., Hamstra, D. A. & Feng, M. (2012) Dosimetric implications of residual seminal vesicle motion in fiducial-guided intensity-modulated radiotherapy for prostate cancer. *Med Dosim,* 37(3)**,** 240-4.

Stephenson, A. J., Scardino, P. T., Kattan, M. W., Pisansky, T. M., Slawin, K. M., et al. (2007) Predicting the outcome of salvage radiation therapy for recurrent prostate cancer after radical prostatectomy. *J Clin Oncol,* 25(15)**,** 2035-41.

Stone, N. N., Stock, R. G., Cesaretti, J. A. & Unger, P. (2010) Local control following permanent prostate brachytherapy: effect of high biologically effective dose on biopsy results and oncologic outcomes. *International journal of radiation oncology, biology, physics,* 76(2)**,** 355-60.

Stoyanova, R., Takhar, M., Tschudi, Y., Ford, J. C., Solórzano, G., et al. (2016) Prostate cancer radiomics and the promise of radiogenomics. *Translational Cancer Research,* 5(4)**,** 432-447.

Stroom, J. C., Koper, P. C., Korevaar, G. A., van Os, M., Janssen, M., et al. (1999) Internal organ motion in prostate cancer patients treated in prone and supine treatment position. *Radiother Oncol,* 51(3)**,** 237-48.

Su, Z., Zhang, L., Murphy, M. & Williamson, J. (2011) Analysis of prostate patient setup and tracking data: potential intervention strategies. *International journal of radiation oncology, biology, physics,* 81(3)**,** 880-7.

Subesinghe, M., Scarsbrook, A. F., Sourbron, S., Wilson, D. J., McDermott, G., et al. (2015) Alterations in anatomic and functional imaging parameters with repeated FDG PET-CT and MRI during radiotherapy for head and neck cancer: a pilot study. *BMC Cancer,* 15**,** 137.

Sullivan, L., Williams, S. G., Tai, K. H., Foroudi, F., Cleeve, L., et al. (2009) Urethral stricture following high dose rate brachytherapy for prostate cancer. *Radiother. Oncol.,* 91(2)**,** 232-6.

Sundahl, N., De Meerleer, G., Villeirs, G., Ost, P., De Neve, W., et al. (2016) Combining high dose external beam radiotherapy with a simultaneous integrated boost to the dominant intraprostatic lesion: Analysis of genito-urinary and rectal toxicity. *Radiother. Oncol.*

Susil, R. C., Camphausen, K., Choyke, P., McVeigh, E. R., Gustafson, G. S., et al. (2004) System for prostate brachytherapy and biopsy in a standard 1.5 T MRI scanner. *Magn. Reson. Med.,* 52(3)**,** 683-7.

Takayama, Y., Kishimoto, R., Hanaoka, S., Nonaka, H., Kandatsu, S., et al. (2008) ADC value and diffusion tensor imaging of prostate cancer: Changes in carbon-ion radiotherapy. *Journal of Magnetic Resonance Imaging,* 27(6)**,** 1331-1335.

Tamada, T., Sone, T., Jo, Y., Toshimitsu, S., Yamashita, T., et al. (2008) Apparent diffusion coefficient values in peripheral and transition zones of the prostate: comparison between normal and malignant prostatic tissues and correlation with histologic grade. *Journal of magnetic resonance imaging : JMRI,* 28(3)**,** 720-6.

Tanaka, H., Hayashi, S., Ohtakara, K., Hoshi, H. & Iida, T. (2011a) Usefulness of CT-MRI Fusion in Radiotherapy Planning for Localized Prostate Cancer. *J. Radiat. Res. (Tokyo),* 52(6)**,** 782-788.

Tanaka, H., Hayashi, S., Ohtakara, K., Hoshi, H. & Iida, T. (2011b) Usefulness of CT-MRI fusion in radiotherapy planning for localized prostate cancer. *Journal of radiation research,* 52(6)**,** 782-8.

Tanyi, J. A., He, T., Summers, P. A., Mburu, R. G., Kato, C. M., et al. (2010) Assessment of planning target volume margins for intensity-modulated radiotherapy of the prostate gland: role of daily inter- and intrafraction motion. *International journal of radiation oncology, biology, physics,* 78(5)**,** 1579-85.

Ten Haken, R. K., Forman, J. D., Heimburger, D. K., Gerhardsson, A., McShan, D. L., et al. (1991) Treatment planning issues related to prostate movement in response to differential filling of the rectum and bladder. *International journal of radiation oncology, biology, physics,* 20(6)**,** 1317-24.

Terashima, K., Nakamura, K., Shioyama, Y., Sasaki, T., Ohga, S., et al. (2013) Can a belly board reduce respiratory-induced prostate motion in the prone position?--assessed by cine-magnetic resonance imaging. *Technol. Cancer Res. Treat.,* 12(5)**,** 447-53.

Thompson, J. E., Moses, D., Shnier, R., Brenner, P., Delprado, W., et al. (2014) Multiparametric magnetic resonance imaging guided diagnostic biopsy detects significant prostate cancer

and could reduce unnecessary biopsies and over detection: a prospective study. *J. Urol.,* 192(1)**,** 67-74.

Thörmer, G., Otto, J., Reiss-Zimmermann, M., Seiwerts, M., Moche, M., et al. (2012) Diagnostic value of ADC in patients with prostate cancer: influence of the choice of b values. *Eur. Radiol.,* 22(8)**,** 1820-1828.

Tilak, G., Tuncali, K., Song, S. E., Tokuda, J., Olubiyi, O., et al. (2015) 3T MR-guided in-bore transperineal prostate biopsy: A comparison of robotic and manual needle-guidance templates. *J. Magn. Reson. Imaging,* 42(1)**,** 63-71.

Tinger, A., Michalski, J. M., Cheng, A., Low, D. A., Zhu, R., et al. (1998) A critical evaluation of the planning target volume for 3-D conformal radiotherapy of prostate cancer. *Int. J. Radiat. Oncol. Biol. Phys.,* 42(1)**,** 213-21.

Tofts, P. S., Brix, G., Buckley, D. L., Evelhoch, J. L., Henderson, E., et al. (1999) Estimating kinetic parameters from dynamic contrast-enhanced T(1)-weighted MRI of a diffusable tracer: standardized quantities and symbols. *J. Magn. Reson. Imaging,* 10(3)**,** 223-32.

Tong, X., Chen, X., Li, J., Xu, Q., Lin, M. H., et al. (2015) Intrafractional prostate motion during external beam radiotherapy monitored by a real-time target localization system. *Journal of applied clinical medical physics / American College of Medical Physics,* 16(2)**,** 5013.

Tree, A., Jones, C., Sohaib, A., Khoo, V. & van As, N. (2013) Prostate stereotactic body radiotherapy with simultaneous integrated boost: which is the best planning method? *Radiat Oncol,* 8**,** 228.

Turkbey, B., Pinto, P. A., Mani, H., Bernardo, M., Pang, Y., et al. (2010) Prostate cancer: value of multiparametric MR imaging at 3 T for detection--histopathologic correlation. *Radiology,* 255(1)**,** 89-99.

Ueno, Y., Kitajima, K., Sugimura, K., Kawakami, F., Miyake, H., et al. (2013) Ultra-high b-value diffusion-weighted MRI for the detection of prostate cancer with 3-T MRI. *J. Magn. Reson. Imaging,* 38(1)**,** 154-60.

Valenca, L. B., Sweeney, C. J. & Pomerantz, M. M. (2015) Sequencing current therapies in the treatment of metastatic prostate cancer. *Cancer Treat. Rev.,* 41(4)**,** 332-340.

Valicenti, R. K., Bae, K., Michalski, J., Sandler, H., Shipley, W., et al. (2011) Does hormone therapy reduce disease recurrence in prostate cancer patients receiving dose-escalated radiation therapy? An analysis of Radiation Therapy Oncology Group 94-06. *Int. J. Radiat. Oncol. Biol. Phys.,* 79(5)**,** 1323-9.

Van de Steene, J., Linthout, N., de Mey, J., Vinh-Hung, V., Claassens, C., et al. (2002) Definition of gross tumor volume in lung cancer: inter-observer variability. *Radiotherapy and Oncology,* 62(1)**,** 37-49.

van de Water, S., Valli, L., Aluwini, S., Lanconelli, N., Heijmen, B., et al. (2014) Intrafraction prostate translations and rotations during hypofractionated robotic radiation surgery: dosimetric impact of correction strategies and margins. *Int. J. Radiat. Oncol. Biol. Phys.,* 88(5)**,** 1154-60.

van den Elsen, P. A., Pol, E. J. D. & Viergever, M. A. (1993) Medical image matching-a review with classification. *Engineering in Medicine and Biology Magazine, IEEE,* 12(1)**,** 26-39.

Van den Heuvel, F., Fugazzi, J., Seppi, E. & Forman, J. D. (2006) Clinical application of a repositioning scheme, using gold markers and electronic portal imaging. *Radiother. Oncol.,* 79(1)**,** 94-100.

van der Burgt, M., Bergsma, L., de Vries, J., Pos, F. J., Kalisvaart, R., et al. (2015) Impact of tumour invasion on seminal vesicles mobility in radiotherapy of prostate cancer. *Radiother. Oncol.*

van der Heide, U. A., Korporaal, J. G., Groenendaal, G., Franken, S. & van Vulpen, M. (2011) Functional MRI for tumor delineation in prostate radiation therapy. *Imaging Med.,* 3(2)**,** 219-231.

van der Heide, U. A., Kotte, A. N., Dehnad, H., Hofman, P., Lagenijk, J. J., et al. (2007) Analysis of fiducial marker-based position verification in the external beam radiotherapy of patients with prostate cancer. *Radiother. Oncol.,* 82(1)**,** 38-45.

van der Wielen, G. J., Mutanga, T. F., Incrocci, L., Kirkels, W. J., Vasquez Osorio, E. M., et al. (2008) Deformation of prostate and seminal vesicles relative to intraprostatic fiducial markers. *Int. J. Radiat. Oncol. Biol. Phys.,* 72(5)**,** 1604-1611 e3.

van der Wielen, G. J., van Putten, W. L. & Incrocci, L. (2007) Sexual function after three-dimensional conformal radiotherapy for prostate cancer: results from a dose-escalation trial. *Int. J. Radiat. Oncol. Biol. Phys.,* 68(2)**,** 479-84.

van Herk, M. (2004) Errors and margins in radiotherapy. *Seminars in Radiation Oncology,* 14(1)**,** 52-64.

van Herk, M., Bruce, A., Kroes, A. P., Shouman, T., Touw, A., et al. (1995) Quantification of organ motion during conformal radiotherapy of the prostate by three dimensional image registration. *International journal of radiation oncology, biology, physics,* 33(5)**,** 1311-20.

van Herk, M., De Jaeger, K., de Munck, J., Hoogeman, M., Meinders, J., et al. (2000) A delineation system for N modalities — software aspects. *In:* Schlegel, W. & Bortfeld, T. (eds.) *The Use of Computers in Radiation Therapy: XIIIth International Conference Heidelberg, Germany May 22–25, 2000.* Berlin, Heidelberg: Springer Berlin Heidelberg.

van Lin, E. N., Futterer, J. J., Heijmink, S. W., van der Vight, L. P., Hoffmann, A. L., et al. (2006) IMRT boost dose planning on dominant intraprostatic lesions: gold marker-based three-dimensional fusion of CT with dynamic contrast-enhanced and 1H-spectroscopic MRI. *Int. J. Radiat. Oncol. Biol. Phys.,* 65(1)**,** 291-303.

Vargas, C., Saito, A. I., Hsi, W. C., Indelicato, D., Falchook, A., et al. (2010) Cine-magnetic resonance imaging assessment of intrafraction motion for prostate cancer patients supine or prone with and without a rectal balloon. *Am. J. Clin. Oncol.,* 33(1)**,** 11-6.

Vargas, H. A., Akin, O., Franiel, T., Mazaheri, Y., Zheng, J., et al. (2011) Diffusion-weighted endorectal MR imaging at 3 T for prostate cancer: tumor detection and assessment of aggressiveness. *Radiology,* 259(3)**,** 775-84.

Verma, S., Rajesh, A., Futterer, J. J., Turkbey, B., Scheenen, T. W., et al. (2010) Prostate MRI and 3D MR spectroscopy: how we do it. *AJR Am. J. Roentgenol.,* 194(6)**,** 1414-26.

Viani, G. A., Stefano, E. J. & Afonso, S. L. (2009) Higher-Than-Conventional Radiation Doses in Localized Prostate Cancer Treatment: A Meta-analysis of Randomized, Controlled Trials. *International Journal of Radiation Oncology*Biology*Physics,* 74(5)**,** 1405-1418.

Villeirs, G. M., De Meerleer, G. O., Verstraete, K. L. & De Neve, W. J. (2004) Magnetic resonance assessment of prostate localization variability in intensity-modulated radiotherapy for prostate cancer. *Int. J. Radiat. Oncol. Biol. Phys.,* 60(5)**,** 1611-21.

Villeirs, G. M., K, L. V., De Neve, W. J. & De Meerleer, G. O. (2005) Magnetic resonance imaging anatomy of the prostate and periprostatic area: a guide for radiotherapists. *Radiother. Oncol.,* 76(1)**,** 99-106.

Villers, A., McNeal, J. E., Freiha, F. S. & Stamey, T. A. (1992) Multiple cancers in the prostate. Morphologic features of clinically recognized versus incidental tumors. *Cancer,* 70(9)**,** 2313-8.

Villers, A., Puech, P., Mouton, D., Leroy, X., Ballereau, C., et al. (2006) Dynamic Contrast Enhanced, Pelvic Phased Array Magnetic Resonance Imaging of Localized Prostate Cancer for Predicting Tumor Volume: Correlation With Radical Prostatectomy Findings. *The Journal of urology,* 176(6)**,** 2432-2437.

Vogelius, I. R. & Bentzen, S. M. (2013) Meta-analysis of the alpha/beta ratio for prostate cancer in the presence of an overall time factor: bad news, good news, or no news? *Int. J. Radiat. Oncol. Biol. Phys.,* 85(1)**,** 89-94.

Vos, E. K., Litjens, G. J., Kobus, T., Hambrock, T., Hulsbergen-van de Kaa, C. A., et al. (2013) Assessment of prostate cancer aggressiveness using dynamic contrast-enhanced magnetic resonance imaging at 3 T. *Eur. Urol.,* 64(3)**,** 448-55.

Wagenlehner, F. M., Pilatz, A., Waliszewski, P., Weidner, W. & Johansen, T. E. (2014) Reducing infection rates after prostate biopsy. *Nat Rev Urol,* 11(2)**,** 80-6.

Wagner, M., Rief, M., Busch, J., Scheurig, C., Taupitz, M., et al. (2010) Effect of butylscopolamine on image quality in MRI of the prostate. *Clin Radiol,* 65(6)**,** 460-4.

Wan, G., Wei, Z., Gardi, L., Downey, D. B. & Fenster, A. (2005) Brachytherapy needle deflection evaluation and correction. *Med. Phys.,* 32(4)**,** 902-9.

Weinreb, J. C., Barentsz, J. O., Choyke, P. L., Cornud, F., Haider, M. A., et al. (2016) PI-RADS Prostate Imaging - Reporting and Data System: 2015, Version 2. *Eur. Urol.,* 69(1)**,** 16-40.

Westphalen, A. C., Koff, W. J., Coakley, F. V., Muglia, V. F., Neuhaus, J. M., et al. (2011) Prostate cancer: prediction of biochemical failure after external-beam radiation therapy--Kattan nomogram and endorectal MR imaging estimation of tumor volume. *Radiology,* 261(2)**,** 477-86.

Whittington, R., Broderick, G. A., Arger, P., Malkowicz, S. B., Epperson, R. D., et al. (1999) The effect of androgen deprivation on the early changes in prostate volume following transperineal ultrasound guided interstitial therapy for localized carcinoma of the prostate. *International journal of radiation oncology, biology, physics,* 44(5)**,** 1107-10.

WHO.;. (2014) *World Cancer Report*: International Agency for Research on Cancer, World Health Organization.

Wilt, T. J., Brawer, M. K., Jones, K. M., Barry, M. J., Aronson, W. J., et al. (2012) Radical prostatectomy versus observation for localized prostate cancer. *N. Engl. J. Med.,* 367(3)**,** 203-13.

Wo, J. Y. & Zietman, A. L. (2008) Why does androgen deprivation enhance the results of radiation therapy? *Urologic Oncology: Seminars and Original Investigations,* 26(5)**,** 522-529.

Wong, W. W., Schild, S. E., Vora, S. A., Ezzell, G. A., Nguyen, B. D., et al. (2011) Image-guided radiotherapy for prostate cancer: a prospective trial of concomitant boost using indium-111-capromab pendetide (ProstaScint) imaging. *Int. J. Radiat. Oncol. Biol. Phys.,* 81(4)**,** e423-9.

Wortel, R. C., Incrocci, L., Pos, F. J., Lebesque, J. V., Witte, M. G., et al. (2015) Acute toxicity after image-guided intensity modulated radiation therapy compared to 3D conformal radiation therapy in prostate cancer patients. *Int. J. Radiat. Oncol. Biol. Phys.,* 91(4)**,** 737-44.

Wortel, R. C., Incrocci, L., Pos, F. J., van der Heide, U. A., Lebesque, J. V., et al. (2016) Late Side Effects After Image Guided Intensity Modulated Radiation Therapy Compared to 3D-Conformal Radiation Therapy for Prostate Cancer: Results From 2 Prospective Cohorts. *Int. J. Radiat. Oncol. Biol. Phys.,* 95(2)**,** 680-9.

Wu, L.-M., Xu, J.-R., Ye, Y.-Q., Lu, Q. & Hu, J.-N. (2012a) The Clinical Value of Diffusion-Weighted Imaging in Combination With T2-Weighted Imaging in Diagnosing Prostate Carcinoma: A Systematic Review and Meta-Analysis. *American Journal of Roentgenology,* 199(1)**,** 103-110.

Wu, L. M., Xu, J. R., Gu, H. Y., Hua, J., Chen, J., et al. (2012b) Usefulness of diffusion-weighted magnetic resonance imaging in the diagnosis of prostate cancer. *Academic radiology,* 19(10)**,** 1215-24.

Xia, P., Pickett, B., Vigneault, E., Verhey, L. J. & Roach Iii, M. (2001) Forward or inversely planned segmental multileaf collimator IMRT and sequential tomotherapy to treat multiple dominant intraprostatic lesions of prostate cancer to 90 Gy. *International Journal of Radiation Oncology*Biology*Physics,* 51(1)**,** 244-254.

Xie, Y., Djajaputra, D., King, C. R., Hossain, S., Ma, L., et al. (2008) Intrafractional motion of the prostate during hypofractionated radiotherapy. *International journal of radiation oncology, biology, physics,* 72(1)**,** 236-46.

Yan, D., Lockman, D., Brabbins, D., Tyburski, L. & Martinez, A. (2000) An off-line strategy for constructing a patient-specific planning target volume in adaptive treatment process for prostate cancer. *Int. J. Radiat. Oncol. Biol. Phys.,* 48(1)**,** 289-302.

Yan, D., Lockman, D., Martinez, A., Wong, J., Brabbins, D., et al. (2005) Computed tomography guided management of interfractional patient variation. *Semin. Radiat. Oncol.,* 15(3)**,** 168-79.

Yoshioka, Y., Suzuki, O., Otani, Y., Yoshida, K., Nose, T., et al. (2014) High-dose-rate brachytherapy as monotherapy for prostate cancer: technique, rationale and perspective. *J Contemp Brachytherapy,* 6(1)**,** 91-8.

Yoshizako, T., Wada, A., Hayashi, T., Uchida, K., Sumura, M., et al. (2008) Usefulness of diffusion-weighted imaging and dynamic contrast-enhanced magnetic resonance imaging in the diagnosis of prostate transition-zone cancer. *Acta Radiol.,* 49(10)**,** 1207-13.

Yun, J., Wachowicz, K., Mackenzie, M., Rathee, S., Robinson, D., et al. (2013) First demonstration of intrafractional tumor-tracked irradiation using 2D phantom MR images on a prototype linac-MR. *Med Phys,* 40(5)**,** 051718.

Zakian, K. L., Sircar, K., Hricak, H., Chen, H.-N., Shukla-Dave, A., et al. (2005) Correlation of Proton MR Spectroscopic Imaging with Gleason Score Based on Step-Section Pathologic Analysis after Radical Prostatectomy. *Radiology,* 234(3)**,** 804-814.

Zaorsky, N. G., Palmer, J. D., Hurwitz, M. D., Keith, S. W., Dicker, A. P., et al. (2015) What is the ideal radiotherapy dose to treat prostate cancer? A meta-analysis of biologically equivalent dose escalation. *Radiother. Oncol.,* 115(3)**,** 295-300.

Zapatero, A., Guerrero, A., Maldonado, X., Alvarez, A., Gonzalez San Segundo, C., et al. (2015) High-dose radiotherapy with short-term or long-term androgen deprivation in localised prostate cancer (DART01/05 GICOR): a randomised, controlled, phase 3 trial. *Lancet Oncol.,* 16(3)**,** 320-7.

Zelefsky, M. J., Crean, D., Mageras, G. S., Lyass, O., Happersett, L., et al. (1999a) Quantification and predictors of prostate position variability in 50 patients evaluated with multiple CT scans during conformal radiotherapy. *Radiotherapy and Oncology,* 50(2)**,** 225-234.

Zelefsky, M. J., Crean, D., Mageras, G. S., Lyass, O., Happersett, L., et al. (1999b) Quantification and predictors of prostate position variability in 50 patients evaluated with multiple CT scans during conformal radiotherapy. *Radiother. Oncol.,* 50(2)**,** 225-34.

Zelefsky, M. J., Levin, E. J., Hunt, M., Yamada, Y., Shippy, A. M., et al. (2008a) Incidence of Late Rectal and Urinary Toxicities After Three-Dimensional Conformal Radiotherapy and Intensity-Modulated Radiotherapy for Localized Prostate Cancer. *International Journal of Radiation Oncology*Biology*Physics,* 70(4)**,** 1124-1129.

Zelefsky, M. J., Pei, X., Chou, J. F., Schechter, M., Kollmeier, M., et al. (2011) Dose escalation for prostate cancer radiotherapy: predictors of long-term biochemical tumor control and distant metastases-free survival outcomes. *European urology,* 60(6)**,** 1133-9.

Zelefsky, M. J., Reuter, V. E., Fuks, Z., Scardino, P. & Shippy, A. (2008b) Influence of local tumor control on distant metastases and cancer related mortality after external beam radiotherapy for prostate cancer. *J. Urol.,* 179(4)**,** 1368-73; discussion 1373.

Zelefsky, M. J., Yamada, Y., Fuks, Z., Zhang, Z., Hunt, M., et al. (2008c) Long-term results of conformal radiotherapy for prostate cancer: impact of dose escalation on biochemical tumor control and distant metastases-free survival outcomes. *Int. J. Radiat. Oncol. Biol. Phys.,* 71(4)**,** 1028-33.

Zelhof, B., Pickles, M., Liney, G., Gibbs, P., Rodrigues, G., et al. (2009) Correlation of diffusion-weighted magnetic resonance data with cellularity in prostate cancer. *BJU Int.,* 103(7)**,** 883-8.

Zietman, A. L., Bae, K., Slater, J. D., Shipley, W. U., Efstathiou, J. A., et al. (2010) Randomized Trial Comparing Conventional-Dose With High-Dose Conformal Radiation Therapy in Early-Stage Adenocarcinoma of the Prostate: Long-Term Results From Proton Radiation Oncology Group/American College of Radiology 95-09. *Journal of Clinical Oncology,* 28(7)**,** 1106-1111.

Zietman, A. L., Coen, J. J., Dallow, K. C. & Shipley, W. U. (1995) The treatment of prostate cancer by conventional radiation therapy: an analysis of long-term outcome. *International journal of radiation oncology, biology, physics,* 32(2)**,** 287-92.

Zietman, A. L., Prince, E. A., Nakfoor, B. M. & Park, J. J. (1997a) Androgen deprivation and radiation therapy: sequencing studies using the Shionogi in vivo tumor system. *International journal of radiation oncology, biology, physics,* 38(5)**,** 1067-70.

Zietman, A. L., Prince, E. A., Nakfoor, B. M. & Shipley, W. U. (1997b) Neoadjuvant androgen suppression with radiation in the management of locally advanced adenocarcinoma of the prostate: experimental and clinical results. *Urology,* 49(3A Suppl)**,** 74-83.

Zou, K. H., Warfield, S. K., Bharatha, A., Tempany, C. M. C., Kaus, M. R., et al. (2004) Statistical validation of image segmentation quality based on a spatial overlap index1: scientific reports. *Acad. Radiol.,* 11(2)**,** 178-189.

Zu, K., Mucci, L., Rosner, B. A., Clinton, S. K., Loda, M., et al. (2014) Dietary lycopene, angiogenesis, and prostate cancer: a prospective study in the prostate-specific antigen era. *J. Natl. Cancer Inst.,* 106(2)**,** djt430.

Zumsteg, Z. S., Spratt, D. E., Pei, I., Zhang, Z., Yamada, Y., et al. (2013a) A new risk classification system for therapeutic decision making with intermediate-risk prostate cancer patients undergoing dose-escalated external-beam radiation therapy. *Eur. Urol.,* 64(6)**,** 895-902.

Zumsteg, Z. S., Spratt, D. E., Pei, X., Yamada, Y., Kalikstein, A., et al. (2013b) Short-term androgen-deprivation therapy improves prostate cancer-specific mortality in intermediate-risk prostate cancer patients undergoing dose-escalated external beam radiation therapy. *Int. J. Radiat. Oncol. Biol. Phys.,* 85(4)**,** 1012-7.

Zumsteg, Z. S. & Zelefsky, M. J. (2013) Improved survival with surgery in prostate cancer patients without medical comorbidity: a self-fulfilling prophecy? *Eur. Urol.,* 64(3)**,** 381-3.